THE UNIVERSITY OF CHICAGO

MACROEVOLUTIONARY PATTERNS AND DIETARY ADAPTATIONS IN EARLY CLADOTHERIAN MAMMALS

A DISSERTATION SUBMITTED TO

THE FACULTY OF THE DIVISION OF THE BIOLOGICAL SCIENCES

AND THE PRITZKER SCHOOL OF MEDICINE

IN CANDIDACY FOR THE DEGREE OF

DOCTOR OF PHILOSOPHY

COMMITTEE ON EVOLUTIONARY BIOLOGY

BY

DAVID MARK GROSSNICKLE

CHICAGO, ILLINOIS

MARCH 2018

In memory of my grandmothers, Jane Grossnickle and Edith Sankey.

TABLE OF CONTENTS

LIST OF FIGURES

LIST OF TABLES

ACKNOWLEDGEMENTS

I am extremely fortunate to have been guided by knowledgeable and generous faculty during my dissertation work. My co-advisors, Zhe-Xi Luo and Kenneth Angielczyk, have been particularly supportive. Luo has an encyclopedic knowledge of early mammals, and I frequently rely on him for information and discussions on numerous aspects of early mammal evolution. He is also an unrelenting optimist and supporter. I thank him for his constant encouragement, which was much more important to my progress and frame of mind than he probably realizes. Ken has been my chief strategist in Chicago. Graduate school is often daunting, and Ken helped me navigate academia and prioritize my research and classroom efforts. He also provided a considerable amount of feedback on manuscripts, abstracts, and applications, which greatly enhanced my work and improved my scientific writing skills. I am very grateful for his thoughtful advice, and I promise him that one day I will remember that "data" is plural.

I thank my remaining dissertation committee members for assistance with various aspects of my research. Conversations with Callum Ross provided me with much of my background knowledge on jaw biomechanics. Graham Slater taught me phylogenetic comparative methods, an especially valuable research tool that I will certainly continue to use. Finally, Michael Coates has been my quality control specialist, challenging me to perform and present clear, thought-out analyses. These committee members and numerous additional faculty at The University of Chicago have had a significant, positive influence on my dissertation.

My doctorate studies would not have been possible without generous assistance from my master's degree advisors at Indiana University, P. David Polly and Jackson Njau. Jackson provided me with a place in his lab, opening the door to graduate school for me. I will forever be

grateful for the opportunity. David's lectures, conversations, and publications have influenced almost every aspect of my research, and I continue to rely on him for advice. He is my academic role model, and I cannot thank him enough for his help and guidance.

My dissertation is built upon data obtained from museum specimens, and I thank numerous museum staff for assistance and access to specimens. I am especially grateful to those at the Field Museum of Natural History, including Bruce Patterson, Lawrence Heaney, Bill Stanley, Adam Ferguson, and William Simpson. The museum work was made possible by funding assistance from the Field Museum (Brown Graduate Fellowship), Committee on Evolutionary Biology (Henry Hinds Fund), the University of California Museum of Paleontology (Doris O. and Samuel P. Welles Research Fund), and the University of Chicago (William Rainey Harper Fellowship).

Many friends, colleagues, and lab mates discussed or commented on portions of this dissertation, greatly enhancing the quality and scope of the projects. I thank all of them. Those who made an especially large impact include Julia Schultz, David Reed, Jose Iriarte-Diaz, Aaron Olson, Courtney Orsbon, Peter Makovicky, Ali Nabavizadeh, Susumu Tomiya, Brian Rankin, Dallas Krentzel, Bhart-Anjan S. Bhullar, Christine Janis, Gregory Wilson, Jonathan Mitchell, Peter Smits, Alfred Crompton, Kenneth-Dieter Benton, Carrie Vrabel, Wesley Vermillion, and several anonymous reviewers of manuscripts. In addition, my Luo/Angielczyk lab mates, Jackie Lungmus and Robert Burroughs, have been reliable sounding boards for my rambling research ideas.

I cannot put into words how lucky I am to have my incredible family in my life. My parents, Bruce and Jeanne Grossnickle, have been a constant source for support and encouragement, no matter how convoluted my career path(s). My siblings, Mark Grossnickle and

Jaimie Cunningham, have inspired me to pursue a career in which I am passionate. I thank them for their love and support.

About a decade ago my sister gave me the book *Your Inner Fish* by Neil Shubin as a gift. I was teaching high school biology at the time and contemplating returning to college for graduate school. The book re-ignited my childhood fascination of paleontology and solidified my decision to attend graduate school to study paleontology/evolutionary biology. At Indiana University, I chose to focus on early mammal evolution for my master's thesis because David Polly sparked my interest with a presentation on Zhe-Xi Luo's research. This led me to The University of Chicago to work with Luo for my doctorate, and I ended up in the same buildings and classes that Neil discusses in *Your Inner Fish*. I am still a bit in awe at how it all played out, and I am forever thankful to those who helped me along my fortuitous path, including Jaimie, Neil, David, and Luo.

Finally, I thank my partner and best friend, Allison Bormet. She makes me laugh every day, most of the time on purpose. She is a constant source of support, and I cannot thank her enough for the tremendous amount of help with all aspects of life, including this dissertation. Allison, you are my favorite.

ABSTRACT

Therian mammals experienced an immense evolutionary radiation and now represent one of the most ecologically diverse clades on Earth. However, therians and their closest relatives (i.e., cladotherians) were primarily small insectivores for the first half of their history, a period from approximately 165 to 80 million years ago, suggesting that this radiation was delayed or suppressed during this period. Although research has often examined phylogenetic relationships and morphological evolution of early cladotherians, little work has been devoted to analyzing their ecological diversity and biomechanical functions. Thus, questions remain about the adaptive nature of early evolutionary changes and the timing of the ecomorphological radiation of cladotherians. In this dissertation, I address these topics by examining jaw and molar morphologies, which are associated with diet and biomechanical function. I investigate two evolutionary events in particular. First, I analyze changes to jaw morphologies that accompanied the evolution of the tribosphenic molar (and its precursors). Biomechanical analyses of musculoskeletal configurations support the hypothesis that changes to jaw, molar, and ear morphologies in cladotherians are associated with increased transverse movement via yaw rotation during mastication. These changes may have been especially important prerequisites for the evolution of the tribosphenic molar morphology, an evolutionary innovation that likely assisted in the longterm survival and diversification of therians. In addition, the evolution of a posteriorly positioned angular process (and accompanying changes to masticatory muscles) may have been crucial for the development of yaw rotation, and the functional significance of the angular process is further supported by analyses that demonstrate that its size and position is a strong correlate of diet. Second, I use molar and jaw morphologies to examine the

ecomorphological patterns of therians in the Cretaceous and early Cenozoic. I find evidence that the adaptive radiation of therians began in the latest Cretaceous, a period in which angiosperms, social insects, and non-therian mammals (e.g., multituberculates) are also diversifying. This suggests that the macroevolutionary patterns of mammals in the Cretaceous were an interplay of functional adaptations (e.g., evolution of tribosphenic molars) and evolutionary patterns in likely food sources (i.e., plants and insects). Further, the molar data indicate that mammals experienced a selective extinction at the Cretaceous-Paleogene (K-Pg) boundary, and jaw morphologies show evidence for a multi-step radiation of mammals between 80 and 50 million years ago. I conclude by proposing that the evolutionary adaptations of therians were not only important to their ecomorphological diversification, but they may have also been critical to their survival during periods of major environmental perturbations such as the K-Pg mass extinction event.

CHAPTER 1
The early evolution of cladotherian mammals

1.1 INTRODUCTION

The fossil record provides considerable insight into the origins and evolutionary histories of clades, often supplying information that cannot be inferred from modern taxa. Detailed morphological analyses of fossils allow for extinct lineages to be differentiated, permitting the development of phylogenetic hypotheses. From these data, macroevolutionary patterns can be further analyzed, such as by calculating taxonomic diversity, morphological disparity, and rates of evolutionary change.

However, morphological and phylogenetic data are not the only information that can be extracted from fossils—ecological and biomechanical traits can also be inferred from anatomy. The importance of these inferences is apparent when considering major evolutionary events such as adaptive radiations and origins of key innovations. For instance, adaptive radiations involve invasions into distinct ecological niches, and therefore testing for this type of diversification necessitates collection of ecological information. Ecological evidence also helps inform our understanding of the tempo in which lineages evolve to produce adaptive changes on broad time scales (i.e., millions of years), which cannot be adequately revealed by modern ecological studies that only span years or decades. Further, this evidence can be especially important in formulating evolutionary hypotheses about the differential origination and extinction rates of various clades.

However, obtaining ecological and biomechanical data from fossils can be challenging. It often requires examination of morphological correlates of ecological traits in modern analogs (Fig. 1.1) or building models for biomechanical analyses. Thus, in comparison to morphological and taxonomic data, it is less common for ecological and functional data to be incorporated into quantitative paleontological studies. This hinders our ability to recognize critical evolutionary events such as adaptive radiations and the appearance of key innovations, and it limits our ability to examine potential influences on macroevolutionary patterns.

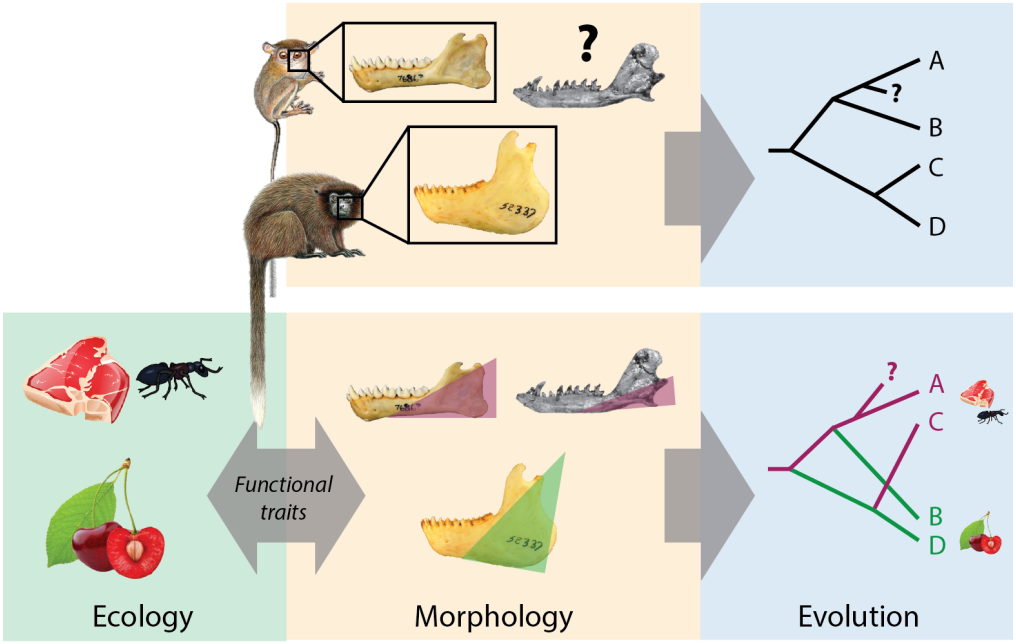

Figure 1.1. A schematic illustration of the interactions between ecology, morphology, and evolution. Morphology alone can provide valuable evolutionary information (top), but incorporation of ecological information (e.g., diets) allows for additional considerations such as adaptive evolutionary changes (bottom). Functional traits (e.g., jaw correlates of diet as shown here; see Chapter 3) can serve as the link between ecology and morphology. Identification of functional traits can be applied to fossil taxa (e.g., gray jaw and question marks in the phylogenies). Jaws are of *Tarsius bancanus* (FMNH 76863), *Callicebus personatus* (FMNH 52337), and the fossil *Sasayamamylos kawaii* (Kusuhashi et al., 2013). Primate illustrations are by Stephen D. Nash and reproduced from Mittermeier et al. (2007) and Byrne et al. (2016).

Early cladotherian mammals offer a unique opportunity to integrate ecomorphological and biomechanical information into macroevolutionary analyses. From small insectivores in the Jurassic and Early Cretaceous, cladotherians (led by therians) have diversified into an immense array of ecological niches and now comprise all but three modern mammal genera (Fig. 1.2). Cladotheria includes tribosphenidans (therians and closely related taxa with tribosphenic molars), peramurids, amphitheriids, and dryolestoids, and a diagnostic apomorphy of Cladotheria is the talonid (shelf or basin) of the posterior portion of molars. Although the early cladotherian fossil record is limited (especially due to a scarcity of postcranial elements), it includes a considerable number of teeth and jaws, and these can be compared to modern analogs for which ecological and biomechanical information is known. Further, there is special interest in the early evolution of the clade because there remains contentious debate over the timing of the early therian radiation.

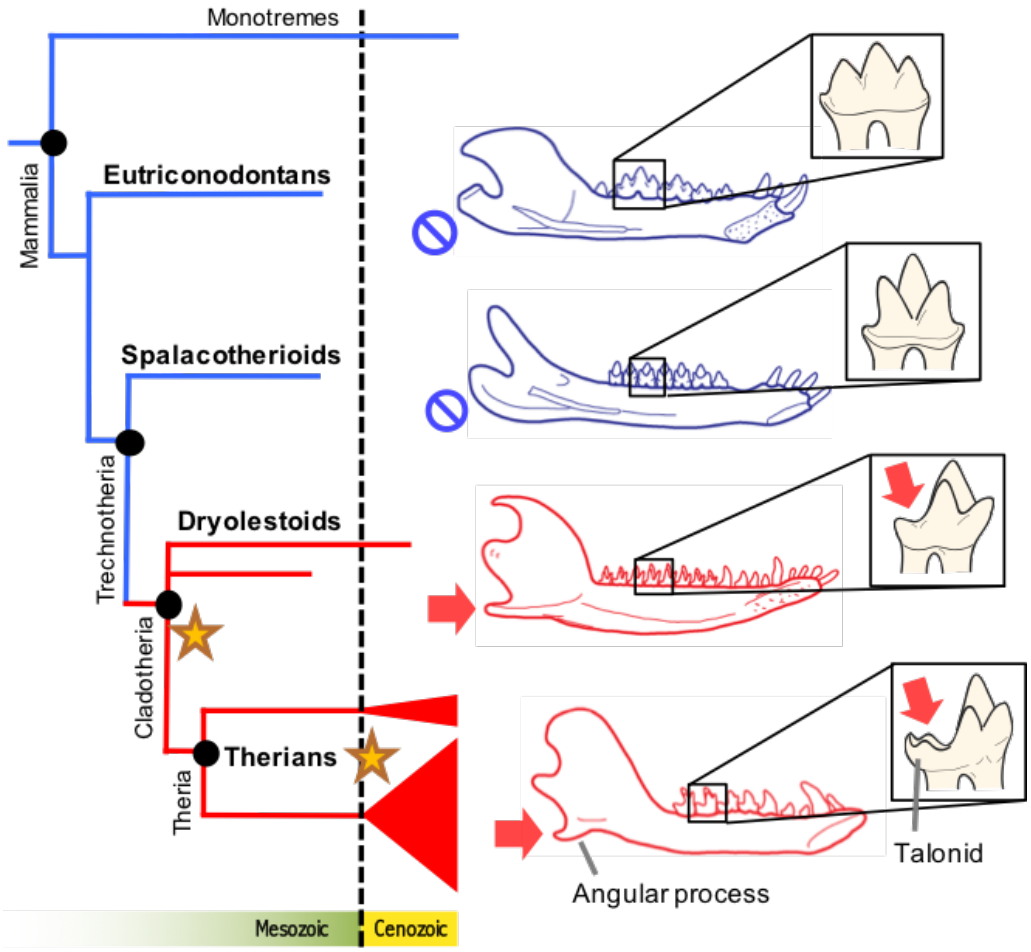

Figure 1.2. Early mammal clades that are examined in this dissertation, with images of example jaws and molars to emphasize morphological differences among groups. Red arrows highlight the concurrent appearance of a talonid and posteriorly-positioned angular process at the cladotherian node (left star), which is the focus of Chapter 2. Therians now comprise all living mammals besides three monotreme genera, and it is often hypothesized that the Cretaceous-Paleogene mass extinction event 66 million years ago (dashed line) catalyzed their radiation (right star). The timing and dynamics of the early stages of this radiation are the focus of Chapters 3 and 4. The smaller therian radiation represents metatherians (i.e., stem and crown marsupials) and the larger radiation represents eutherians (i.e., stem and crown placentals). See Chapter 2 for source and taxon information for jaw and molar images.

In this dissertation, I specifically examine morphological traits of mandibles and molars that are correlated with dietary preferences or biomechanical properties, providing novel insight into the early history of Cladotheria and the origins of modern mammalian biodiversity. I use

results to develop new hypotheses on the origins of the therian masticatory apparatus and challenge the long-held view that the therian radiation was a product of the extinction of non-avian dinosaurs. I further posit that early changes to the jaws and molars of cladotherians were critical to the long-term survival and diversification of the clade.

1.2 EARLY CLADOTHERIAN MAMMALS

I investigate the early history and macroevolutionary patterns of cladotherian mammals, which include therians (i.e., eutherians and metatherians) and their close relatives (Fig. 1.2). Paleontologists and evolutionary biologists have long been interested in the early history of the clade, often using early cladotherians to examine key evolutionary concepts. This includes studies of adaptive radiation (Osborn, 1902; Simpson, 1937; Simpson, 1944; Hunter, 1997; Alroy, 1999; O'Leary et al., 2013; Halliday and Goswami, 2016), tempo and mode of evolution (Simpson, 1944; Slater, 2013), gradualism versus punctuated equilibrium (Gould and Eldredge, 1977; Gingerich, 1980), key innovations (Hunter and Jernvall, 1995), phylogenetic hypotheses (Murphy et al., 2001; Wible et al., 2007; Meredith et al., 2011; dos Reis et al., 2012; Rougier et al. 2012; O'Leary et al., 2013; Halliday et al., 2015), and responses to mass extinctions and environmental change (Collinson and Hooker, 1991; Janis, 2000; Gingerich, 2006; Meredith et al., 2011; Grossnickle and Polly, 2013; O'Leary et al., 2013; Wilson, 2013; Wilson, 2014; Halliday et al., 2016). Thus, studies of early therians have contributed greatly to modern evolutionary theory.

Despite the strong interest in the evolution of cladotherians, the early history of the clade remains surprisingly enigmatic. This is due in part to a limited fossil record that is comprised primarily of teeth and jaw fragments. Cladotheria likely originated in the Early or Middle

Jurassic (Luo et al., 2011), a period during which mammaliaforms were rapidly diversifying (Luo, 2007; Newham et al., 2015; Close et al., 2015). Non-therian cladotherians, such as dryolestoids, were globally diverse in the Late Jurassic but were largely limited to South America by the Cretaceous (Kielan-Jaworowska et al., 2004; Grossnickle and Polly, 2013) and went extinct in the Cenozoic (Rougier et al., 2012). Ecomorphological and taxonomical diversity levels of therians remained low through the Early Cretaceous, with the fossil record indicating that they were primarily small insectivores during this time (Kielan-Jaworowsk et al., 2004, Grossnickle and Polly, 2013).

However, by the mid-Cretaceous, approximately 100 million years ago (Ma), the clade experienced a taxonomic diversification (Benson et al., 2013; Grossnickle and Polly, 2013), which was subsequently followed by an ecomorphological diversification in the latest Cretaceous (Chapters 3 and 4). The Cretaceous-Paleogene (K-Pg) mass extinction event may have resulted in new ecological opportunity that further catalyzed the therian diversification, which was led by placentals (Osborn, 1902; Simpson, 1937; Alroy, 1999; O'Leary et al., 2013). In Chapters 3 and 4 of this dissertation, I focus on the Cretaceous and Paleogene taxa to better analyze the timing and dynamics of these diversification events.

1.3 EVOLUTIONARY HYPOTHESES

I perform three research initiatives (i.e., Chapters 2-4), each with a specific hypothesis that is tested using paleontological and modern morphological data. Here I summarize the specific hypotheses that are tested in each chapter.

The evolutionary origin of jaw yaw. In Chapter 2, I hypothesize that morphological changes in cladotherian molars and jaws evolved in conjunction with increased yaw rotation (i.e.,

rotation around a dorsoventral-oriented axis), which results in greater transverse molar movements during occlusion. Three major morphological adaptations to the masticatory apparatus evolve at the cladotherian node: i) the appearance of the talonid shelf of molars, ii) the emergence of a posteriorly-positioned angular process of the jaw (Fig. 1.2), and iii) the loss of an ossified Meckel's cartilage that is attached to the jaw. I posit that these changes are all related to increased yaw rotation during mastication, and this hypothesis is tested with three-dimensional jaw models that measure torque for various musculoskeletal configurations.

The evolutionary changes at the cladotherian node may have been especially important because yaw rotation during mastication is still present in most modern mammal groups. Further, yaw may have been a prerequisite for the evolution of tribosphenic molars, which require transverse movement for crushing material in the talonid basin. Thus, this study demonstrates the importance of considering biomechanical properties in light of macroevolutionary changes to morphologies.

Jaw correlates of diet. To further examine the functional and ecological relevance of evolutionary changes to the jaw, I first investigate potential jaw correlates of diet in modern mammals. In Chapter 3, I hypothesize that diet has influenced the evolution of specific jaw metrics such as moment arm lengths for the superficial masseter and temporalis muscles. This hypothesis is supported by results of certain jaw metrics, such as the distance between the angular process and jaw joint (a proxy for the superficial masseter moment arm), which is strongly correlated with diet. Thus, I apply the angular process metrics to the fossil record to examine macroevolutionary patterns of dietary diversity through time. I focus on the timing of the early therian radiation, especially in relation to the Cretaceous-Paleogene (K-Pg) mass

extinction event. Results from modern and fossil jaws both suggest the presence of distinct adaptive peaks for mammalian carnivores and herbivores.

The Suppression Hypothesis. Immediately following the K-Pg boundary, average body mass of mammals increased sharply (Alroy, 1999; Smith et al., 2010), frugivorous/omnivorous archaic ungulates appeared in abundance (Hunter, 1997), and placental mammals radiated (Wible et al., 2009; O'Leary et al., 2013; Halliday et al., 2016). This suggests that mammals were confined ecologically in the Mesozoic, possibly due to the presence of diverse reptilian groups such as dinosaurs, and they then experienced an adaptive radiation in the earliest Paleocene in response to novel ecological opportunity (Osborn, 1902; Simpson, 1937; Collinson and Hooker, 1991; Patzkowsky, 1995; Alroy, 1999; O'Leary et al., 2013; Halliday and Goswami, 2016; Slater, 2013; Halliday et al., 2015). I refer to this as the Suppression Hypothesis (SH), and I note that SH is supported if ecomorphological disparity and taxonomic diversity of mammals were suppressed until the K-Pg boundary at 66 Ma.

However, several molecular and paleontological studies are in conflict with SH, arguing that mammals were diversifying prior to the K-Pg boundary (e.g., Clauset and Redner, 2009; Meredith et al., 2011; Wilson et al., 2012). Further, recent fossil discoveries demonstrate that latest Cretaceous therians may have achieved greater size and dietary diversity than previously recognized (e.g., Fox and Naylor, 2003; Wilson and Riedel, 2010; Wilson et al., 2016). Therefore, our understanding of mammalian evolutionary patterns before and after the K-Pg boundary remains unresolved.

In light of these conflicting lines of evidence, I test SH with a combination of morphometric jaw data (Chapter 3) and molar shape data (Chapter 4). Because molar and jaw

morphologies are influenced by diet, their disparity patterns and morphospace occupation through time should reflect ecological diversity of therians.

Results from both datasets demonstrate a dietary diversification beginning approximately 80 Ma, which is a pattern also seen in multituberculate mammals (Wilson et al., 2012). Thus, results from Chapters 3 and 4 are in conflict with SH, and I argue that mammals began to radiate prior to the K-Pg boundary. The latest Cretaceous includes the ecological diversification of flowering plants, and it is therefore posited that the mammalian radiation is more closely linked to angiosperms (and possibly insects) than it is to the presence or absence of non-avian dinosaurs.

In summary, testing the hypotheses of this dissertation provides significant contributions to our understanding of early cladotherian evolution. I present and test a novel hypothesis on the origin of the modern mammalian masticatory apparatus (Chapter 2), and I challenge a long-held hypothesis (i.e., the Suppression Hypothesis) that mammalian diversification was suppressed by the presence of non-avian dinosaurs in the Mesozoic Era (Chapters 3 and 4). Whereas most previous analyses of early mammal evolutionary patterns are based on morphological changes and phylogenetic relationships, the analyses in this dissertation focus on ecological and biomechanical aspects of fossils. This provides a more complete understanding of early cladotherian history and presents potential adaptive explanations behind observed evolutionary changes.

CHAPTER 2

Increased transverse jaw movement during mastication was a critical evolutionary change in cladotherians

2.1 ABSTRACT

Theria comprises all but three living mammalian genera and is one of the most ecologically pervasive clades on Earth. Yet, the origin and early history of therians and their close relatives (i.e., cladotherians) remains surprisingly enigmatic. A critical biological function that can be compared among early mammal groups is mastication. Morphometrics and modeling analyses of the jaws of Mesozoic mammals indicate that cladotherians evolved musculoskeletal anatomies that increase mechanical advantage during jaw rotation around a dorsoventrally-oriented axis (i.e., yaw) while decreasing the mechanical advantage of jaw rotation around a mediolaterally-oriented axis (i.e., pitch). These changes parallel molar transformations in early cladotherians that indicate their chewing cycles included significant transverse movement, likely produced via yaw rotation that results from asynchronous contractions of muscle groups. Thus, I hypothesize that cladotherian molar morphologies and musculoskeletal jaw anatomies evolved concurrently with increased yaw rotation of the jaw during chewing cycles. The increased transverse movement resulting from yaw rotation may have been a crucial evolutionary prerequisite for the functionally versatile tribosphenic molar morphology, which underlies the molars of all therians and is retained by many extant clades. I further hypothesize that the increased yaw rotation likely

allowed increased grinding during occlusion, allowing a broader range of diets and assisting in the survival and diversification of the therian clade.

2.2 INTRODUCTION

The evolution of mammals from pre-mammalian cynodonts was accompanied by significant changes to dentitions and musculoskeletal anatomies of jaws (Osborn, 1907; Simpson, 1936; Crompton, 1963; Crompton and Jenkins, 1968; Crompton and Parker, 1978; Crompton, 1995; Sidor, 2003; Luo et al., 2004; Lautenschlager et al., 2016; Conith et al., 2016). These include the appearance of diphyodonty (i.e., single dental replacement) and increased occlusal complexity (Luo et al., 2004; Crompton and Jenkins, 1968; Crompton and Parker, 1978; Crompton, 1995; Conith et al., 2016), suggestive of greater masticatory efficiency and precise control of jaw musculature. In addition, evolution of the jaw articulation between the dentary and squamosal resulted in the loss of load-bearing jaw joint functions for middle ear elements, possibly allowing for a greater diversity of jaw morphologies by permitting increased resultant forces at the jaw joint (Crompton and Hylander, 1986; Reed et al., 2016). These evolutionary changes likely played a role in a taxonomic and morphological diversification of mammaliaforms in the Jurassic (Crompton and Parker, 1978; Luo, 2007; Grossnickle and Polly, 2013; Newham et al., 2015; Close et al., 2015) (Fig. 2.1), which included the origin of therians (i.e., eutherians and metatherians) and australosphenidans (including monotremes).

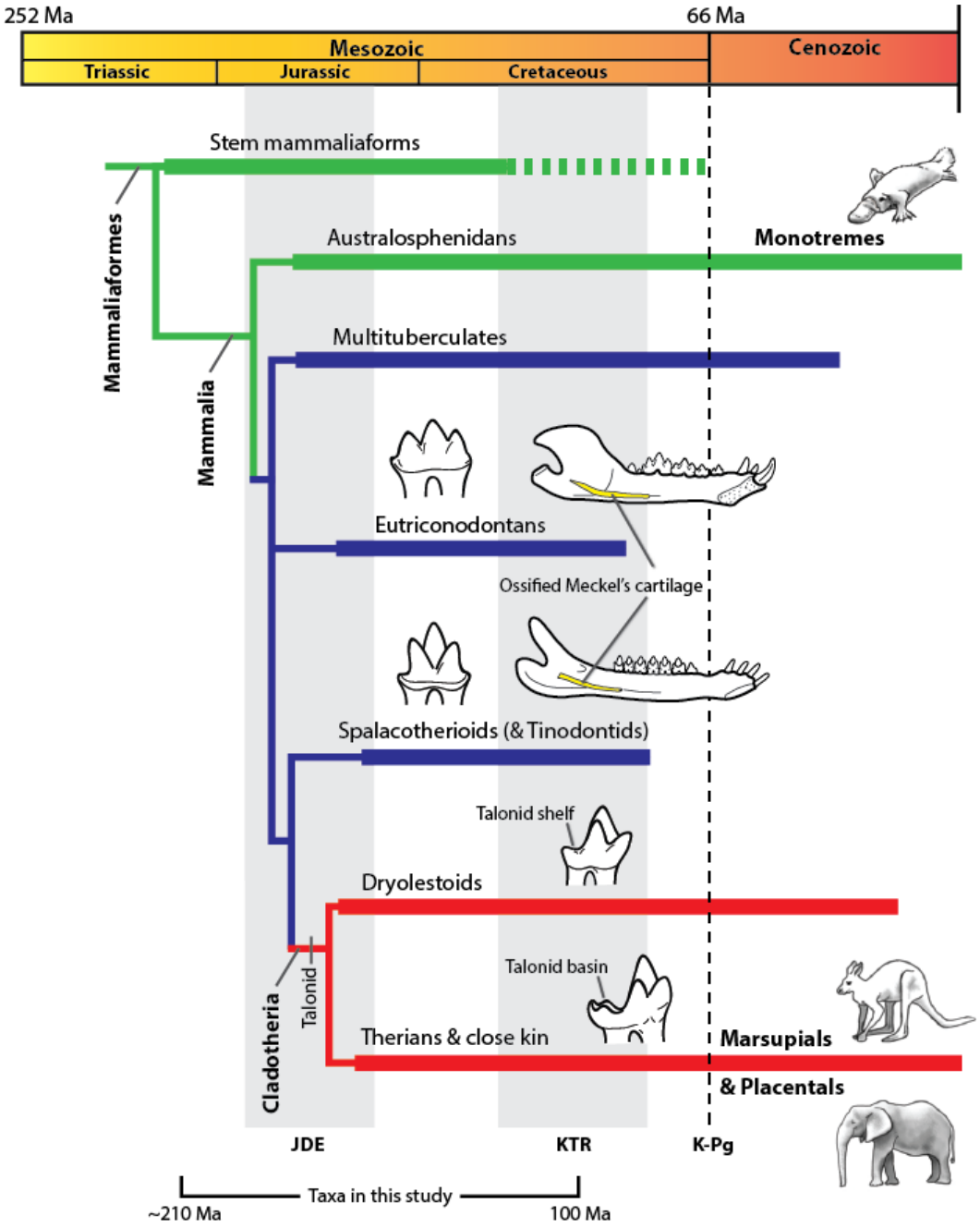

Figure 2.1. Phylogeny of early mammaliaforms (Martin et al., 2015). Marsupials and placentals are crown therians, and monotremes are crown australosphenidans. The branch colors are based on morphological similarities of the mandibles (see below). A Jurassic diversification event (JDE) resulted in the origination of many Mesozoic mammalian lineages (Luo, 2007; Newham et al., 2015; Close et al., 2015), and the Cretaceous Terrestrial Revolution (KTR) included a taxonomic turnover of mammalian faunas (Grossnickle and Polly, 2013; Lloyd et al., 2008; Benson et al., 2013). The eutriconodontan jaw is *Yanoconodon* (Luo et al., 2007A), the spalacotherioid jaw is *Maotherium* (Ji et al., 2009), and mammal images are courtesy of April Neander. Abbreviations: K-Pg, Cretaceous-Paleogene boundary; Ma, million years ago.

Therians and australosphenidans now comprise all modern mammals, and therians in particular have achieved considerable taxonomic, morphological, and ecological diversity. However, their origin and early history remains surprisingly enigmatic, due in large part to limited fossil evidence. Paleontological research on early therians often focuses on morphological transitions, phylogenetic relationships, and the timing of the clade's origination and early diversification (Luo et al., 2011; Patternson, 1956; Crompton, 1971; Kielan-Jaworowska and Dashzeveg, 1989; Cifelli, 1993; Davis, 2011; Luo, 2011; Halliday et al., 2015; Grossnickle and Newham, 2016). However, paleontological examinations of jaw biomechanics are lacking, and a better understanding of this aspect of therian biology may offer considerable insight into the early evolution of the clade.

Therians and australosphenidans evolved tribosphenic molar morphologies, likely through convergent evolution (Luo, 2007; Martin et al., 2015; Rauhut et al., 2002; Davis, 2011; Luo et al., 2002; Rougier et al., 2012; although see Rich et al., 2002, for an opposing view). Evidence suggests that the evolution of the tribosphenic molar morphology was a critical development in mammalian history. For instance, tribosphenic molar occlusion is extremely precise and involves multiple shearing crests (Crompton, 1971; Davis, 2011; Crompton and Kielan-Jaworowska, 1978; Stern et al., 1989; Evans and Sanson, 2003; Polly et al., 2005; Schultz and Martin, 2014), resulting in a system that seems especially effective for rapidly cutting chitinous exoskeletons of insects. The molars are also capable of crushing food matter in the talonid basin (Fig. 2.1; Stern et al., 1989; Schultz and Martin, 2014), a function that is not apparent in earlier molar morphologies and may allow for a broad diversity of diets. The functional significance of the morphology is supported by the continued prevalence of

tribosphenic (or tribosphenic-like) molars in many modern mammal groups (e.g., microchiropterans, didelphids, dasyurids, scandentians, and many eulipotyphlans), despite evolving at least 160 million years ago (Ma) (Rauhut et al., 2002; Luo et al., 2011).

An essential step in the evolution of the tribosphenic molar morphology of therians was the appearance of a talonid shelf in the lower molars of stem cladotherians (i.e., "eupantotherians") (Fig. 2.1; Osborn, 1907; Simpson, 1936; Patternson, 1956; Crompton, 1971). The shelf acts as an extended shearing surface for the paracone of the upper molar. In tribosphenic molars the talonid shelf expands into the talonid basin and has a crushing function (Osborn, 1907; Simpson, 1936; Crompton, 1971; Davis, 2011; Stern et al., 1989; Schultz and Martin, 2014). Non-therian cladotherians (comprised primarily of Dryolestida, Amphitheriida, and "peramurans") were abundant in the Late Jurassic and regionally diverse in South America in the Cretaceous. Together with therians they form Cladotheria. Thus, cladotherians have been globally diverse for over 150 million years, and examining the early history of the clade is critical to understanding the origins of modern mammalian diversity.

The earliest cladotherians evolved notable morphological changes to molars, jaws, and ears. These include:

1. Molars with a talonid shelf, an evolutionary precursor to the talonid basin of tribosphenic molar morphologies (Fig. 2.1).
2. A prominent, posteriorly positioned angular process (APr) of the mandible (Grossnickle and Polly, 2013; Prothero, 1981; Martin, 1999).
3. The potential loss of a bony attachment between the middle ear elements and jaw. Early crown mammals such as eutriconodontans and spalacotherioids often possess a bony connection between the middle ear and jaw via an ossified Meckel's cartilage

(Luo et al., 2007A; Ji et al., 2009; Luo, 2011; Wang et al., 2001; Meng et al., 2003) (Fig. 2.1), but this connection does not appear to be present in cladotherians. (However, mandibles of early cladotherians often possess a Meckel's groove (Kielan-Jaworowska and Dashzeveg, 1989; Davis, 2012; Close et al., 2016; Urban et al., 2017), indicating that an ear-jaw connection may be maintained by cartilage.)

In light of these morphological changes, this study has two goals. The first is to use morphometrics to quantify the morphological changes to the jaw processes in early mammal groups, with a focus on comparing early cladotherians to closely related clades. The second goal is to model the changes to the jaw muscle vectors that are expected to accompany the morphological changes, allowing the functional significance of musculoskeletal changes in cladotherians to be assessed. The superficial masseter (SM) and medial pterygoid (MP) are two of the major masticatory muscles and they insert on the APr (Fig. 2.2), which shows considerable morphological variation among early mammal groups (Grossnickle and Polly, 2013). Thus, changes to the force vectors of these muscles are the focus of the functional analyses, although the temporalis muscle (TM) is also incorporated. Results of these analyses are considered in light of concurrent morphological and functional changes to the molars, with special focus on the evolution of the tribosphenic molar morphology.

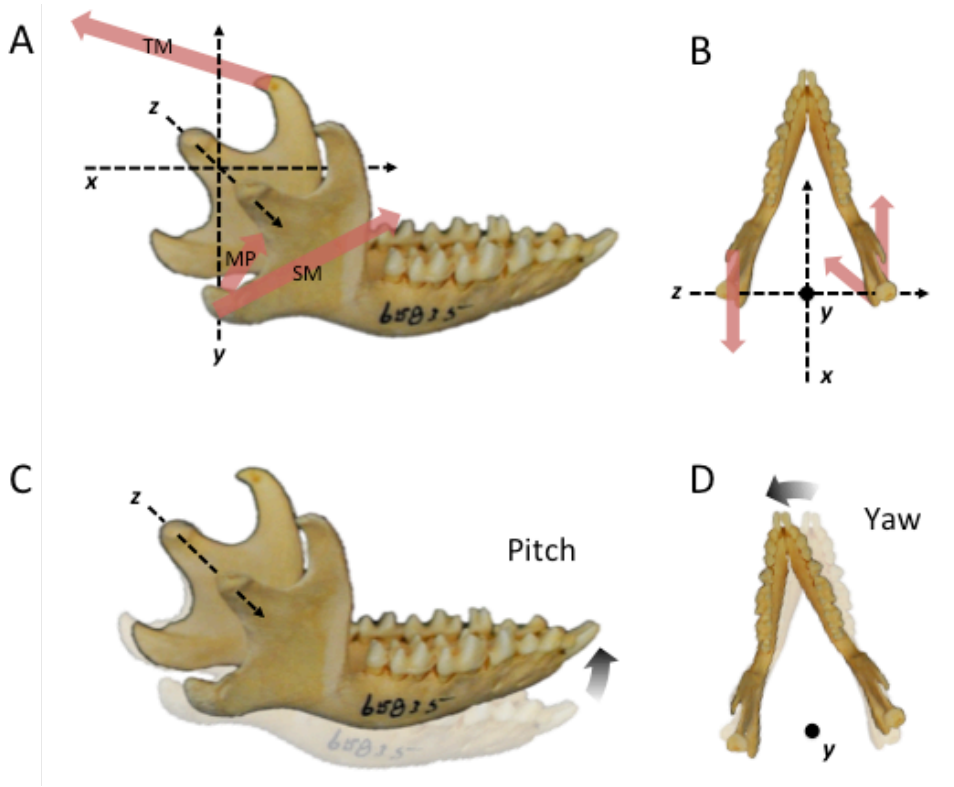

Figure 2.2. *A*-*B*) The *x*, *y*, and *z* coordinate planes used in this study, displayed on a mandible in oblique lateral view (*A*) and dorsal view (*B*). The red arrows represent the approximate force vectors of a Triplet muscle group, which contract concurrently in many modern mammals (Williams et al., 2011). This group includes the medial pterygoid (MP) and superficial masseter (SM) muscles of one hemimandible, and the temporalis muscle (TM) of the opposing hemimandible. *C*) Pitch rotation around a mediolaterally oriented (*z*) axis through the condylar processes. *D*) Yaw rotation around a dorsoventrally oriented (*y*) axis. (The axes of rotation in *C* and *D* are arbitrarily positioned to demonstrate potential jaw movements.) The mandible is of a hedgehog (*Atelerix*) from the Field Museum of Natural History (FMNH65835).

Based on results of the morphometrics and functional analyses, I develop a novel hypothesis for the simultaneous origin of unique jaw, dental, and ear characters in cladotherians. Central to this hypothesis is the observation that a majority of modern and extinct mammals, including early cladotherians, possess chewing cycles with substantial transverse movement of the molars (Schultz and Martin, 2014; Williams et al., 2011; Ryder, 1878; Maynard Smith and Savage, 1959; Mills, 1966; Mills, 1967; Crompton and Hiiemae, 1970; Crompton and Sita-

Lumsden, 1970; Butler, 1972; Butler, 1973; Herring and Scapino, 1973; Kay and Hiiemae, 1974; Weijs, 1994; Hylander, 2006; Crompton et al., 2010; Crompton, 2011; von Koenigswald et al., 2013; Menegaz et al., 2015; Davis, 2014). This includes taxa with tribosphenic molar morphologies (or slight derivatives), which appear to require mediolateral molar movement for extended shearing and crushing functions (Simpson, 1936; Kallen and Gans, 1972; Fish and Mendel, 1982; Schultz and Martin, 2014; Mills, 1966; Mills, 1967; Crompton and Hiiemae, 1970; Crompton and Sita-Lumsden, 1970; Butler, 1972). There are at least three means of producing transverse molar movement: (i) mediolateral translation of the jaw (along the *z* axis of Figure 2.2), (ii) yaw rotation of the jaw around a dorsoventrally oriented axis (Fig. 2.2d), and (iii) roll rotation of a hemimandible around an anteroposteriorly oriented axis. However, considerable evidence indicates that yaw is the primary means of producing transverse molar movement during occlusion in modern and fossil therians, with studies demonstrating yaw in didelphids, diprotodontians, eulipotyphlans, scandentians, *Solenodon*, suids, cervids, and primates (Williams et al., 2011; Ryder, 1878; Maynard Smith and Savage, 1959; Mills, 1966; Mills, 1967; Crompton and Hiiemae, 1970; Crompton and Sita-Lumsden, 1970; Butler, 1972; Butler, 1973; Herring and Scapino, 1973; Kay and Hiiemae, 1974; Weijs, 1994; Hylander, 2006; Crompton et al., 2010; Crompton, 2011; Menegaz et al., 2015). For instance, primates and tree shrews with tribosphenic (or tribosphenic-like) molar morphologies have been described as having two phases of occlusion that both involve yaw rotation (Butler, 1972; Kay and Hiiemae, 1974). In contrast, transverse movement produced from mediolateral translation along the *z* axis during occlusion may be considerably less common in mammals, with jaw movements in carnivorans being a notable exception (Evans and Fortelius, 2008; Evans and Fortelius, 2008). Roll rotatation during occlusion is present in many mammal groups, especially those with

unfused mandibular symphyses that permit independent movement of hemimandibles (Dötsch, 1986; Dötsch, 1994; Scapino, 1981; Oron and Crompton, 1985; Lieberman and Crompton, 2000) However, I do not expect that roll is as significant as yaw in producing transverse molar movement in many modern taxa (Fish and Mendel, 1982; Kallen and Gans, 1972; Kay and Hiiemae, 1974, Crompton, 2011; Menegaz et al., 2015), especially during the power stroke of the chewing cycle (e.g., Crompton, 1995). However, taxa such as tenrecs and some shrews may be an exception (Oron and Crompton, 1985; Dötsch, 1986; Dötsch, 1994), and special consideration is given to these taxa in the results section.

Yaw rotation is produced by asynchronous contractions of jaw muscle groups (Williams et al., 2011; Herring and Scapino, 1973; Weijs, 1994; Hylander, 2006; Crompton et al., 2010; Crompton, 2011; Menegaz et al., 2015). For instance, in many modern taxa, concurrent peak contractions of the balancing-side (i.e., non-chewing side) MP, balancing-side SM, and working-side (i.e., chewing side) temporalis muscle (TM) (during the fast close phase of the chewing cycle) causes the working-side hemimandible to move laterally via yaw. The three muscles involved in this movement (Fig. 2.2) were termed the Triplet I muscle group by Weijs (1994). The fast close is followed by the power stroke (or slow close) phase of the chewing cycle in which molars are in occlusion and the complementary Triplet II muscles (i.e., working-side MP, working-side SM, and balancing-side TM) reach peak contraction, rotating the working-side mandible medially (and dorsally and slightly anteriorly).

Considerable variation in muscle activity exists, even within groups such as primates that are often categorized as using Triplet muscle groups (e.g., Ram and Ross, 2018). In addition, transverse movement of molars via roll rotation is common in many mammalian groups, and this movement is not expected to result from Triplet muscle patterns. Therefore, the Triplet activity

pattern is not the only means of producing yaw rotation and transverse movement. However, the coordinated activity of Triplet muscle groups has been argued to be a primitive trait of therians (Williams et al., 2011; Weijs, 1994; Crompton, 2011) and is therefore used in the jaw models of this study.

The origin of significant yaw rotation in early crown mammals has not previously been investigated using fossil jaw data. Further, previous studies on jaw biomechanics and mammalian origins have largely focused on pre-mammalian lineages rather than early crown mammals (Crompton and Hylander, 1986; Reed et al., 2016; DeMar and Barghusen, 1972). Thus, musculoskeletal changes seen in early cladotherians may offer new insight into the evolutionary origin of the chewing cycles that are observed in modern mammals.

2.3 METHODS

2.3.1 Mammal groups

Prior to morphometric analyses, stem mammaliaform and early crown mammal genera from the latest Triassic through Early Cretaceous (i.e., ~210-100.5 Ma) were assigned to major groups. These groups are based primarily on the strict consensus phylogeny of Martin et al. (2015) (modified for Figure 2.1). The tree topology of the analysis in Martin et al. (2015) is similar to the topologies in Luo et al. (2015A) and Luo et al. (2015B), which use derivatives of a similar phylogenetic character matrix. The phylogenetic relationships of early mammal groups are important for inferences made in this study, and the following section includes discussion of issues related to these groupings.

It is worth noting that a benefit of considering the average jaw shapes of major groups is that it helps minimize the error associated with individual jaws and potential incorrect

phylogenetic assignments of genera. For instance, many jaw images are reconstructions or photographs of incomplete jaws. Thus, the accuracy of specific jaw morphologies may be questionable in some cases. However, by considering the average jaw morphology for each major mammal group, the effect of this error on broad evolutionary trends is minimized.

Stem mammaliaforms. The stem mammaliaform group is paraphyletic and includes *Sinoconodon*, morganucodontids, *Hadrocodium*, docodonts and haramiyids. The phylogenetic position of haramiyids is contentious. For instance, I follow Martin et al. (2015) and Luo et al. (2015A) and treat haramiyids as stem mammaliaforms, but haramiyids have also been hypothesized to be crown mammals that are sister to multituberculates (e.g., Bi et al., 2014). However, it is unlikely that moving haramiyids to this alternative phylogenetic position would have a major effect on results. For instance, stem mammaliaforms (including haramiyids) and multituberculates both occupy similar regions of the angular process (APr) geometric morphometric morphospace (PC1 and PC2) (see 2.4 Results). Thus, moving haramiyids to the multituberculate group (*sensu* Bi et al., 2014) would not affect the broad conclusions concerning the evolution of the APr. Also, neither stem mammaliaforms nor multituberculates are included in the jaw model analyses, so the placement of haramiyids does not affect these analyses.

Australosphenidans (and *Pseudotribos*). Australosphenidans are commonly recovered in cladistic analyses as stem monotremes that branch from the crown mammalian node (Bi et al., 2014; Krause et al., 2014; O'Meara and Thompson, 2014; Martin et al., 2015; Luo et al. 2015A; Luo et al., 2015B). In these analyses, shuotheriids (which include *Pseudotribos* of this study) are generally recovered as the sister group to australosphenidans, forming a monophyletic clade. Thus, I include *Pseudotribos* with the australosphenidans.

It has been hypothesized that australosphenidans are more closely related to (or members of) Theria rather than stem monotremes (Rich et al., 1997; Rich et al., 2002). However, it is unlikely that altering the phylogenetic position of australosphenidans would have a large impact on the broad patterns observed in this study. For instance, some austalosphenidan jaws (e.g., *Henosferus*) are morphologically very similar to therian jaws, meaning that if australosphenidans are placed with the therian group (*sensu* Rich et al., 1997) it is not expected to have a major effect on the morphometric and modeling results for therians.

Multituberculates. Multituberculates included in analyses are limited to plagiaulacidan multituberculates because preserved jaws of cimolodontan multituberculates do not appear in the fossil record until the Late Cretaceous, which is after the time period of interest. Despite being closely related to additional crown mammal groups of this study (Fig. 2.1), multituberculates are excluded from the jaw modeling analyses because of their palinal (rather than orthal and transverse) jaw movement. See Gambaryan and Kielan-Jaworowska (1995) and Wall and Krause (1992) for considerations of multituberculate feeding mechanics.

Eutriconodontans. Phylogenetic analyses often recover Eutriconodonta as a monophyletic clade of early crown mammals that are outside of Cladotheria (Bi et al., 2014; Krause et al., 2014; Martin et al., 2015; Luo et al., 2015A), although some analyses recover the group as stem mammals (Rougier et al., 2011; Rougier et al., 2012; O'Meara and Thompson, 2014). Due to the early-branching position of eutriconodontans and the primitive triconodont dentition, it could be argued that eutriconodontans possess primitive jaw and molar morphologies that are ancestral to spalacotherioids and cladotherians. However, it is worth noting that the eutriconodontan taxa may possess derived morphologies that are not representative of the ancestral condition. For instance, many eutriconodontans (e.g.,

Repenomamus) are relatively large and carnivorous (Hu et al., 2005B), whereas most spalacotherioids and early cladotherians are small and likely insectivorous (Grossnickle and Polly, 2013; Kielan-Jaworowska et al., 2004). Thus, eutriconodontans may have jaw and molar morphologies that are adapted for a derived dietary preference. Even if this is the case, however, eutriconodontan jaws represent a functional morphology that is significantly different than those of cladotherians. Thus, it still provides an opportunity for comparative analyses of different functional morphologies among closely related early mammal groups.

Spalacotherioids (and tinodontids). Spalacotherioids are acute-angled "symmetrodonts" that are members of Trechnotheria (Kielan-Jaworowska et al., 2004; Martin et al., 2015), and they are often recovered as monophyletic. However, the phylogenetic position of tinodontids varies among cladistic analyses (Bi et al., 2014; Krause et al., 2014; O'Meara and Thompson, 2014; Martin et al., 2015; Luo et al., 2015A), and *Tinodon* is recovered in Martin et al. (2015) in a polytomy with eutriconodontans, multituberculates, and trechnotherians (i.e., spalacotherioids and cladotherians). However, tinodontids possess symmetrodont molars and are often grouped with (or recovered in phylogenetic analyses near) symmetrodont taxa such as spalacotherioids (e.g., Kielan-Jaworowska et al., 2004; Luo et al., 2015A; Martin et al., 2015). Thus, I tentatively place the two tinodontids of this study (i.e., *Tinodon* and *Yermakia*) with spalacotherioids. *Yermakia*'s angular process (APr) region is not preserved (Lopatin et al., 2005), and therefore only *Tinodon* is included in the geometric morphometrics (GM) analysis of APr shape. Consistent with both eutriconodontans and spalacotherioids, a distinct APr is not present in *Tinodon*. Thus, if *Tinodon* were moved to the eutriconodontan group, it is expected to have little effect on the morphometric results for either clade.

Dryolestoids. This group is a lineage of early stem cladotherians (i.e., "eupantotherians") that possess a eupantothere molar morphology. The diagnostic feature of this morphology is a talonid shelf on the lower molars (Fig. 2.1). The dryolestoids examined in this study are believed to be monophyletic (e.g., Rougier et al., 2011; Martin et al., 2015). Closely related to dryolestids are meridiolestidans, which are nested within Dryolestoidea in the analysis of Rougier et al. (2011). In the phylogenetic analyses of Rougier et al. (2012) and O'Meara and Thompson (2014), dryolestids and meridiolestidans (and close kin) form a paraphyletic clade. However, no meridiolestidans are included in this study since they do not appear in the fossil record until the Late Cretaceous, which is after the time period of interest. Further, their closest kin (e.g., *Paurodon*) are not represented in the fossil record by jaws with preserved posterior processes.

Therians and close kin (i.e., Zatheria + *Amphitherium*). This group includes late-branching stem cladotherians (i.e., *Amphitherium* and peramurans) and early tribosphenidans (i.e. boreosphenidans), which are comprised primarily of therians. The two peramurans in this study are *Peramus* and *Tendagurutherium*. In cladistic analyses, *Amphitherium* and *Peramus* are recovered as sister taxa that form a branch between dryolestoids and Theria (Rougier et al., 2012; Bi et al., 2014; Krause et al., 2014; O'Meara and Thompson, 2014; Martin et al., 2015; Luo et al., 2015A). Peramurans and tribosphenidans form Zatheria (McKenna, 1975; Kielan-Jaworowska et al., 2004), and therefore the 'therians and close kin' group could also be titled Zatheria + *Amphitherium*.

Amphitherium possesses a lower molar with a talonid that has one cusp, which is likely the hypoconid or hypoconulid (Kielan-Jaworowska et al., 2004; Davis, 2011), and peramurans possess a talonid with an incipient basin with diminutive cusps (Kielan-Jaworowska et al., 2004). Since *Amphitherium* and peramurans have talonids that are considered more derived than the

talonid shelves (or hypoflexids) of dryolestoids, it can be argued that their jaws and molars will function more similarly to early therians (which possess talonid basins) than dryolestoids. Thus, I include these taxa with therians rather than with the additional stem cladotherian taxa of this study, dryolestoids. Further, these group assignments form two monophyletic clades (i.e., dryolestoids and Zatheria + *Amphitherium*), but placing *Amphitherium* and peramurans with dryolestoids would result in a paraphyletic stem cladotherian group.

The tribosphenic molar morphology it considered an apomorphy of Tribosphenida (i.e., Boreosphenida) (Luo et al., 2002, Kielan-Jaworowska et al., 2004). However, no stem tribosphenidans are included (due to a lack of preserved jaw fossils), and taxa are often given the taxonomic assignment of stem tribosphenidan when their affinity to a therian group (i.e., Eutheria or Metatheria) is unknown (Kielan-Jaworowska et al., 2004). Thus, for simplicity, I use 'therians' instead of 'tribosphenidans' in this study when referring to cladotherian taxa with tribosphenic molars.

Many metatherians possess a medially inflected angular process (APr), which is problematic for 2D morphometric analyses. However, *Sinodelphys* is the only preserved metatherian jaw in the time period of interest and its APr is not inflected, at least as it is preserved (Luo et al., 2003).

Fruitafossor* and *Vincelestes. *Fruitafossor* and *Vincelestes* were included in the morphometric analyses (see 2.4 Results) but are not included in a specific mammal group due to uncertain phylogenetic affinities and derived features. *Fruitafossor* is recovered as an early crown mammal, but it is a single-branch lineage that is not nested within any group of this study (Martin et al., 2015; Luo et al., 2015A; Luo et al., 2015B). *Vincelestes* is a stem cladotherian that is also recovered as a single-branch lineage that is not nested within any group of this study. In

some phylogenetic analyses, it is recovered outside of Zatheria (Theria + peramurans) (Krause et al., 2104; Martin et al., 2015; Luo et al., 2015A; Luo et al., 2015B), but in additional analyses it is recovered within Zatheria (Rougier et al., 2012; O'Meara and Thompson, 2014).

An additional issue with *Fruitafossor* and *Vincelestes* is that they appear to have derived dental and jaw features that may be due to adaptations for specialist diets. *Fruitafossor* has tubular molars that are indicative of obligate insectivory (Luo and Wible, 2005). The jaw of *Fruitafossor* is unique in possessing a distinct (yet diminutive) and inflected APr, and a small coronoid process that is at the approximate elevation of the raised jaw joint. This combination of dental and jaw features is not present in any mammal group of this study. In addition, *Vincelestes* demonstrates characters indicative of carnivory, such as very large canines and a short tooth row (Rougier, 1993). Like *Fruitafossor*, it possesses jaw traits that are unique to any other group in this study. The coronoid process is extremely elevated relative to the molar row, which is common for many modern and extinct carnivorous mammals (including eutriconodontans such as *Repenomamus*). However, unlike most carnivores, it also has a relatively elevated jaw joint and, unlike eutriconodontans, it has a distinct APr. The tooth row relative to the length of the jaw is also shorter than crown mammals of this study besides several multituberculates. Thus, if *Fruitafossor* and *Vincelestes* were included with any mammal group of this study they would be outliers in morphometric analyses, and they are unlikely to be ideal representatives of morphologies of any group.

2.3.2 Morphometrics

Specimens. Images of stem mammaliaform and early crown mammal jaws were collected from the primary literature. Sources, geologic ages, and specimen information are

provided in Appendix A. If more than one jaw specimen is known for a genus, the best-preserved (or most complete) specimen was chosen to represent the genus. All specimens are from the latest Triassic through Early Cretaceous (i.e., ~210-100.5 Ma). This time period was chosen because it captures all phylogenetic nodes of interest for this study and includes a substantial sample of taxa. In addition, only two major groups of mammals (i.e., cimolodontan multituberculates and crown therians) remain diverse after the mid-Cretaceous (Grossnickle and Polly, 2013), at least in Laurasian landmasses, and both groups experience an ecomorphological radiation in the Late Cretaceous in which evolutionary changes in jaw shape are likely associated with increased dietary diversity (Wilson et al., 2012; Grossnickle and Polly, 2013; Grossnickle and Newham, 2016). Thus, I believe that truncating the study at the mid-Cretaceous is important for examining the primitive morphologies of therians and multituberculates.

One potential concern with performing morphometrics analyses on jaw images is that the methods only capture two dimensions of the jaw. This concern is highlighted by the fact that marsupials (i.e., metatherians) tend to possess a prominent, medially inflected APr that cannot be well represented by two-dimensional (2D) landmarks. However, 2D analyses of jaw function allow for a much greater sample size and are commonplace in the literature. Therefore, it is expected that broad evolutionary patterns and functional considerations can be obtained from the 2D jaw morphometric analyses performed in this study. Further, only one jaw of a metatherian, *Sinodelphys*, is preserved from the time period of this study, and it does not possess an inflected APr (Luo et al., 2003).

Linear jaw measurements. All linear measurements and geometric morphometrics landmarks (see below) were collected from specimen images using *ImageJ* (Schneider et al., 2012).

To measure jaw joint elevation (or depression), an extended line was first drawn from the alveolar margin (i.e., dorsal edge of the jaw body at the base of the molar row) posteriorly to the condylar process. (I chose to use this line rather than a line from the molar cusps because molars are not always preserved in fossil jaws. Further, molar cusps are often worn or include multiple occlusal surfaces at different elevations, making it especially difficult to determine a horizontal line based on the molars.) From the initial line, a perpendicular line was drawn to the jaw articulation surface of the condylar process (i.e., jaw joint), or posterodorsal-most point of the condylar process. I used the midpoint of the articulation surface for genera with an extensive articulation surface (e.g., multituberculates). The length of this line was measured as the jaw joint elevation (or depression), and dividing this value by jaw length standardized the measurements.

Coronoid process elevation was measured as the maximum elevation of the coronoid process from the base of the molar row (i.e. alveolar margin). I standardized all measurements by dividing by jaw length. Sample sizes vary among the morphometric analyses due to the lack of preservation of some jaw processes in certain fossil specimens.

I measured the length of the tooth row as a means of testing whether the typical out-lever length (i.e., distance from the axis of rotation to the bite point) was likely to vary significantly among mammal groups. My assumption is that similar tooth row lengths relative to jaw length will result in similar bite point locations. Conversely, if one mammal group has significantly longer tooth rows in which molars are more posteriorly positioned, I would expect that the typical bite points during molar occlusion are also relatively posterior in position.

The tooth row length was measured from the base of the anterior-most incisor to the posterior edge of the ultimate molar, and this was then standardized by dividing by the length of

the jaw. For a few genera, the anterior tips of jaws are not preserved, and in these cases the jaw and tooth row lengths were estimated.

Geometric morphometrics (GM). The morphology of the posteroventral region of the dentary, which includes the APr when present, was quantified by collecting two-dimensional (2D) outlines using jaw images of fossil taxa from the literature (Appendix A). The sample includes 64 mammaliaform and crown mammalian genera from the latest Triassic through Early Cretaceous (i.e., ~210-100.5 Ma).

For the GM analysis of the APr region of the jaw, one landmark was placed between the ultimate and penultimate molars. This landmark served to maintain the correct polarity for the outline during the Procrustes analysis (otherwise, the Procrustes analysis might flip outlines vertically to better align morphologies), and capture variance associated with thickness of the jaw body and elevation/depression of the APr.

Using Wolfram's Mathematica and Geometric Morphometrics for Mathematica (Polly, 2016), 20 equally spaced semilandmarks were placed along the outer margin of the jaw. This was accomplished by first outlining the APr region of the jaw using 25 points (with *x* and *y* coordinates of the points collected using *ImageJ*), and then using the BreakOutline function within Geometric Morphometrics for Mathematica to equally space semilandmarks along the outline. The semilandmarks begin along the ventral edge of the jaw, at a spot that is perpendicular to the base of the molar row (i.e., the horizontal line at the alveolar margin that was also used in the linear morphometric measurements). The semilandmarks end at the ventral-most point of the jaw joint articulation surface (or head of the condylar process if the articulation surface is not apparent). See 2.4 Results (Fig. 2.3) for an image of the landmark and

semilandmark locations, and see the discussion below for reasons why semilandmarks were used instead of sliding semilandmarks.

Ideally, landmarks and semilandmarks of GM analyses should represent homologous points of a structure, but this is unlikely to be the case for many landmarks/semilandmarks in this study. For example, the number of molars varies among mammal groups, so the single landmark between the ultimate and penultimate molars is unlikely to be homologous among all taxa. In addition, the presence/absence of the APr varies among mammal groups, meaning that the semilandmarks cannot possibly capture homologous points if some taxa have structures that other taxa lack. However, I consider these landmarks to still fall within the 'Type III' landmark category of Bookstein (1997) because they are outlining the same region of the jaw in all taxa and likely capturing homologous muscle insertion locations for the SM and MP. Also, the goal of the GM analysis of the APr region is simply to quantify the shape of the posteroventral region of the jaw to examine the variation among early mammal groups. Differences among mammalian groups can be demonstrated through qualitative descriptions of the jaws as well, but the GM analysis provides strong support for observations via quantitative evidence.

The coordinates of the 20 semilandmarks and one landmark were subjected to GM procedures (Polly, 2016; Bookstein, 1997; Rohlf, 1993; Rohlf, 1990), which include a Procrustes superimposition (Rohlf, 1990) and ordination using a principal components analysis (PCA). The Procrustes analysis realigns shapes (in this case, sets of *x* and *y* coordinates representing shapes) to eliminate variation associated with size (i.e. scaling), translation, and rotation. This results in shapes (represented by Procrustes values) that only vary in terms of shape differences. The Procrustes values are then ordinated using a PCA. The mean shape for the APrs was calculated

for each mammalian group using all Procrustes values, and thin plate splines of the average shapes for groups were produced.

The Procrustes analysis, PCA, calculation of group means, and production of thin plate splines were performed using Wolfram's Mathematica and Geometric Morphometrics for Mathematica (Polly, 2016). See the User's Guide for Geometric Morphometrics for Mathematica (available at http://mypage.iu.edu/~pdpolly/Software.html) and citations within for additional information.

Semilandmarks versus sliding semilandmarks. It is common for GM studies that use equally spaced semilandmarks to adjust the semilandmarks by 'sliding' them along tangents of the shape outline to minimize 'bending energy' or Procrustes distances (e.g., Gunz et al., 2005, Grossnickle and Newham, 2016), helping to increase the likelihood of capturing homologous points along an outline. However, I did not use sliding semilandmarks in this study for two reasons. First, the PCA results for analyses using sliding semilandmarks and non-sliding semilandmarks are very similar (see Supplementary Information file of Grossnickle, 2017). Second, sliding the semilandmarks disrupts the original shapes by moving the semilandmarks along tangents of the outline. In the analysis of this study, semilandmarks on the posterior tip of prominent angular processes are 'slid' away from the tip to minimize Procrustes distance. (It should be noted that minimizing Procrustes distance is the default method in the geomorph package (Adams and Otárola-Castillo, 2013) for R (R Core Team, 2016), but additional settings may offset this issue.) Gunz et al. (2005) note a similar problem with sliding semilandmarks (Figure 8a in Gunz et al. 2005) and suggest that this error can be corrected by adding an additional landmark at the tip of the extended region. However, this correction is not possible in my analysis because of a lack of clear homologous points due to many taxa (multituberculates,

spalacotherioids, and eutriconodontans) not having an angular process. Thus, the resulting thin plate splines using sliding semilandmarks do not capture the shape of the angular process as well as non-sliding semilandmarks (see Supplementary Information file of Grossnickle, 2017). This issue is especially problematic because the average shapes produced with sliding semilandmark analyses are less informative (and may not be accurate due to the sliding) for inferring the locations of muscle origins for the jaw models.

2.3.3 Jaw biomechanics

I created 3D models of jaws using Wolfram's Mathematica to calculate the moment (i.e., moment of force, or torque) for various musculoskeletal configurations. The modeling analyses build upon concepts and methods in previous biomechanical analyses of synapsid jaw evolution (Crompton and Hylander, 1986; Reed et al., 2016; DeMar and Barghusen, 1972). I focus on four early crown mammal groups: eutricondontans, spalacotherioids, dryolestoids, and therians (and close kin) (Fig. 2.1). Multituberculates are excluded because of their palinal (rather than orthal and transverse) jaw movement during occlusion. Results of the morphometric analyses for each group (Appendix B) and modern taxa (Appendix C) are used as the framework for determining the model dimensions and expected muscle vector locations. The following sections describe how these models were produced and used for calculating moment values.

It is worth noting that mammals typically employ unilateral mastication, meaning they have chewing cycles in which molars of a single hemimandible at a time occlude with upper molars. Thus, only the working-side hemimandible needs to be considered when examining the power stroke of the chewing cycle in which molars are in occlusion. This is especially relevant

for calculations of roll rotation, since only one hemimandible is used for this analysis (see below).

Jaw models – dimensions. In the jaw models, the base of the tooth row (i.e., dorsal edge of the jaw body, or alveolar margin) is set as a horizontal line at $y = 0$ (see Figure 2.2 for coordinate planes). The y axis length from the mandibular symphysis to the jaw joint is set at 10 arbitrary distance units (d.u.), and this is kept constant for all jaw models (i.e., those of eutriconodontans, spalacotherioids, dryolestoids, and early therians and close kin).

To determine the posterior width of the jaw (i.e., the z axis distance between hemimandible jaw joints) for the models, direct measurements of specimens could not be used for early mammal genera for two reasons. First, preserved fossils of intact lower jaws with both hemimandibles are extremely rare. Further, it is unlikely that preserved jaws maintain a reliable angle of attachment at the mandibular symphysis since many fossils are flattened or distorted. Second, even if both hemimandibles are preserved intact, the angle at the symphysis remains unreliable because early mammals are believed to have had unfused symphyses (Crompton, 1995; Lieberman and Crompton, 2000), which allows for 'wishboning' of the jaw and changes to the angle at the symphysis.

Thus, the posterior jaw width for the models was determined using the average dimensions of six fossil mammaliaforms and 25 extant mammal genera (Appendix C). The extant mammals chosen for measurements are primarily small insectivores or omnivores that are appropriate analogs of Mesozoic mammals. In addition, they are taxonomically diverse, representing several orders of eutherians and metatherians. Measurements of extant mammals were taken at the Field Museum of Natural History (FMNH), and measurements of extinct mammals were obtained from images in the published literature (Appendix C). Since many

mammalian species have unfused mandibular symphyses, the angle at the symphysis (and width of the jaw) is not reliable for many specimens. Thus, jaw widths (i.e., distances between jaw joints) were measured as the distance from the centers of the articular surfaces of the glenoid fossae of the skull. These measurements were then divided by the jaw length. Results indicate that the average jaw width at the jaw joint (or glenoid fossae) is approximately 60% of jaw length (Appendix C). Hence, the posterior jaw width for the models was set at 6 d.u. (because the length was arbitrarily set at 10 d.u.), and this was kept constant for all mammal groups.

For each mammal group, the average (median) jaw joint elevation above (or depression below) the base of the molar row (Appendix B) is used to assign the vertical (i.e., *y* axis) jaw joint locations. For instance, the average jaw joint elevation for dryolestoids is 12.6% of the jaw length. Thus, the *y* axis value for the dryolestoid jaw joint in the model is 1.26 d.u. Similarly, the average (median) coronoid process elevations (Appendix B) were used for each group and represent the approximate muscle insertion locations for the TM. (It is recognized that the TM includes an extended attachment along the dorsal edge of the coronoid process, and the *y* axis location for the center of the force vector could vary among groups. However, examining these variables is beyond the scope of this study.)

Jaw models – muscle insertion locations. To determine the *x* and *y* coordinates for the SM and MP muscle insertion locations, thin plate splines from the GM analysis of APr shape (see 2.4 Results, Figure 2.4) were overlaid atop one another with the single landmark (which is between the ultimate and penultimate molars) aligned. The splines were horizontally stretched so that the length between the single landmark and the posterior-most semilandmark is equal for all splines. For the dryolestoid and therian groups, the SM and MP insertion location is assigned to the posterior-most point along the edge of APr. For spalacotherioids and eutriconodontans,

which don't have a distinct APr, the posterior portion of the masseteric fossa was considered when designating the central location of the insertion site.

It is worth noting that although the APr is relatively gracile in many early cladotherians, this does not necessarily indicate that only a small amount of muscle attaches to the APr. For instance, the MP and SM of modern mammals tend to produce a large, muscular sling that wraps around the APr and the posteroventral region of the jaw (Turnbull 1970). Even taxa such as shrews that have an elongate and very thin APr maintain a considerable amount of muscle mass in the APr region.

Jaw models – muscle origin locations. As with the posterior jaw width, determining *x* and *z* coordinates for the SM and MP muscle origins on the skull could not be obtained by direct measurements of specimens, largely because 3D skull fossils of early mammals are extremely rare. Thus, the same 31 specimens of modern and extinct mammals that were used for posterior jaw width calculations were also used to determine approximate locations of the SM and MP origins (Appendix C). The SM origin is the approximate location of the anterior zygoma, and the MP origin is the center of the pterygoid process of the sphenoid bone (Abdala and Damiani, 2004; Hiiemae and Jenkins, 1969; Turnbull, 1970). The distance between the anterior right zygoma and left zygoma was measured and divided by the width of the jaw. On average, the width between anterior zygomae is 96.24% of the jaw width (Appendix C), and therefore the width at the SM origins was set at 5.8 d.u., or 96.7% of the jaw width (6 d.u.). Similarly, the distance from pterygoid process to pterygoid process is 24.0% of the width of the jaw, and therefore the width at the MP origins was set at 1.44 d.u., or 24.0% of the jaw width.

Because of the curvature of the TM around the braincase, the origin of the TM was not estimated from linear measurements of skulls. In the models, the TM vector is directed

posteriorly and slightly dorsally, which is how it is reconstructed in many extant mammals (Turnbull, 1970) and stem mammaliaforms (Crompton, 1963; Crompton and Parker, 1978; Lautenschlager et al., 2016). The TM is treated as a single muscle rather than being split into the anterior temporalis and posterior temporalis. However, merging the anterior and posterior regions of the temporalis as a single muscle vector is common in the literature (e.g. Turnbull, 1970, Davis et al., 2010, Law et al. 2016). Further, the anterior and posterior portions of the TM contract concurrently in *Didelphis* (Crompton and Hylander, 1986), and *Didelphis* is viewed as having the primitive condition of Triplet muscle groups that was likely present in the earliest therians (Weijs, 1994; Crompton et al., 2011; Williams et al., 2011). Thus, separating the TM into different portions for the modeling analyses is unlikely to have a significant effect on results.

2.3.4 Moment calculations

Muscle forces. To determine force contributions of each muscle to a particular type of rotation, the line representing the muscle (i.e., the line drawn between the muscle origin and insertion in 3D) is first separated into *x*, *y*, and *z* components (see Figure 2.2 for coordinate planes). Each component (e.g., *y* in Equation 2.1) is then divided by the muscle length (*d*) and multiplied by the assigned force (*F*) of that muscle, resulting in the force contribution of the muscle in a single direction. For example, the force contribution (F_y) of the *y* axis component (*y*) of one muscle is:

$$F_y = F(y/d) \tag{2.1}$$

Force assignments (*F*) in Equation 2.1 are relative muscle masses (i.e., each value is a percentage of the total mass of the jaw musculature). The relative sizes and forces of jaw

muscles are expected to vary considerably among mammals, and therefore multiple force assignments are used. These values are based on relative muscle masses reported by Turnbull (1970) for *Didelphis virginiana* (TM, 0.57; SM, 0.14; and MP, 0.07), *Echinosorex gymnurus* (TM, 0.61; SM, 0.11; and MP, 0.09), and *Canis familiaris* (TM, 0.67; SM, 0.10; and MP, 0.03). These values represent percentages of the overall mass of the jaw musculature (i.e., a TM value of 0.61 indicates that the TM comprises 61% of the total weight of the jaw musculature). The three species were chosen because they represent distinct mammalian orders and possess unique diets: *D. virginiana*, generalist; *E. gymnurus*, insectivore; and *C. familiaris*, carnivore. Analyses are run with relative muscle masses for the three mammalian species to help capture the range of relative muscle forces that might be found in early mammals.

The deep masseter is excluded from analyses because it is not one of the Triplet muscles (as defined by Weijs, 1994) and therefore is not expected to reach peak contraction concurrently with Triplet muscle groups. Further, the deep masseter does not insert on the jaw processes (i.e., APr and coronoid process) that are a large focus of this study, making it difficult to track the evolutionary changes to the vector of this muscle. However, the expected effects of inclusion of the deep masseter in analyses are discussed in the 2.4 Results section.

Rather than relative muscle masses, physiological cross-sectional area (PCSA) is often used in analyses of jaw mechanics to estimate muscle forces. PCSA is calculated using an equation that includes several variables: muscle mass, muscle density, fiber length, and fiber pennation angle (see Davis et al., 2010, and citations within). Unfortunately, this equation cannot be implemented in this study because information such as fiber lengths (for extinct taxa and most modern analogs) is unknown. However, a muscle density value near zero and a pennation angle of zero degrees are often used in the PCSA equation for all jaw muscles (e.g. Davis et al. 2010,

Law et al. 2016). Thus, these factors should have little effect on calculations of PCSA, and muscle masses are expected to be an appropriate proxy for PCSA in this study. Alternatively, PCSA can be estimated based on the area of the infratemporal fossa. However, Davis et al. (2010) demonstrate that PCSAs based on infratemporal fossa area severely overestimate the contribution of the medial pterygoid and superficial masseter. Thus, estimates from muscle masses seem to be more appropriate estimates of relative muscle forces.

Moments. Moment calculations based on the jaw models of this study extend beyond conventional 2D jaw mechanics analyses (e.g., Crompton and Hylander, 1986) by incorporating the third dimension (i.e., *z* axis of Figure 2.2). Including the additional dimension is considerably beneficial by allowing for analyses of yaw rotation and roll rotation (Fig. 2.2). These analyses would not be possible if only 2D models based on lateral jaw images were used.

Moment arm lengths (L) are the lengths of the perpendicular lines from the x, y, and z vectors to the axis of rotation. For simplicity, these lengths are treated as positive values in calculations unless the force vector works against the direction of rotation. To calculate the moment (M) about an axis of rotation, the moment arm lengths are multiplied by the relevant x, y, and z force components (e.g., results of Equation 2.1 for the y component), and results are summed. Finally, the moments for the working-side SM, working-side MP, and balancing-side TM (i.e., Triplet II muscle group) are summed to produce the total moment for the mandible. As an example, the total moment for pitch rotation around a mediolateral oriented axis (in which F_z would not contribute because it is parallel to the axis of rotation) is calculated with the equations:

$$M_{SM} = F_x * L_y + F_y * L_x \tag{2.2}$$

$$M_{MP} = F_x * L_y + F_y * L_x \tag{2.3}$$

$$M_T = F_x * L_y + F_y * L_x \quad (2.4)$$

$$M_{Total} = M_{SM} + M_{MP} + M_T \quad (2.5)$$

The resulting moments are nearly proportional to the mechanical advantages of the muscle vectors since the distance from the bite point to the axis of rotation (i.e., out-lever) is not treated as a variable and is expected to remain very similar among groups (see discussion on mechanical advantage below). Calculations are repeated for average musculoskeletal configurations of eutricondontans, spalacotherioids, dryolestoids, and therians.

Moments are calculated for a mediolaterally oriented axis (i.e., *z* axis) of rotation through the jaw joints for pitch rotation, an oblique axis through the jaw joint and mandibular symphysis for roll rotation, and two dorsoventrally oriented axes (i.e., *y* axes) of rotation for yaw rotation (Fig. 6). For roll rotation, only a single hemimandible is used in the models because the mandibular symphysis of early mammals was unfused and permits independent rotation of hemimandibles (Crompton and Hiiemae, 1970; Crompton, 1995; Lieberman and Crompton, 2000). For yaw rotation, two dorsoventrally oriented axes are used because the location of this axis is expected to be variable both among mammals and during chewing cycles in individuals (Ryder, 1878; Mills, 1966; Mills, 1967; Butler, 1972; Butler, 1973; Herring and Scapino, 1973; Kay and Hiiemae, 1974). One is placed just medial to the balancing (i.e., non-chewing) side jaw joint. A second axis is placed on the midline (i.e., sagittal plane) of the jaw and at 75% of the jaw length, similar to the position predicted for some primates (Kay and Hiiemae, 1974).

Calculations of moment values can be simplified (i.e., Equations 2.2-2.4 do not include force components for all three directional planes) because not all force vector components contribute to rotation around axes (see Reed et al., 2016, and discussion within). For instance, if

the axis of rotation is mediolaterally-oriented through both jaw joints (for pitch), the axis is parallel to the *z* axis. In this case, the *x* axis and *y* axis force components contribute to the moment while the z axis component does not. Hence, for calculations involving pitch (Equations 2.2-2.4), *z* axis force components can be ignored. Similarly, *y* axis force components do not contribute to yaw. Although the axis of rotation for roll is oblique for each group, the axis is rotated prior to moment calculations so that it falls along the *x* axis (see below). Thus, the *x* axis force component does not contribute to roll after rotation of the axis.

Moment calculations for roll rotation present a unique challenge in that the axes of rotation are oblique. The axis for roll is defined here as the line from the mandibular symphysis to the jaw joint, and this axis varies among mammal groups due to differences in jaw joint elevation (Appendix B). For pitch and yaw, the axes of rotation are parallel to the *z* axis and *y* axis, respectively, and calculations can be simplified by only considering the two relevant force vector components, as described above. However, due to the oblique axis for roll, all three force components (i.e., *x*, *y*, and *z* axis components) must be considered for roll analyses. To avoid the additional computation necessary for this analysis, I simply rotated the hemimandible model (and all associated points such as muscle origins) so that the axis of rotation was parallel to the *x* axis. This included two rotations, which were performed using the RotationTransform function in Wolfram's Mathematica. First, the model was rotated horizontally so that all points on the hemimandible were in a sagittal plane and had a *z* axis value of zero. Second, the model was rotated vertically so that the axis of rotation was parallel to the *x* axis. This second rotation was repeated individually for the models for each mammal group, because each group possessed a different axis of rotation that depends on the elevation of the jaw joint. After the rotations, roll rotation was calculated in the same manner as pitch and yaw.

Sensitivity analysis – muscle origin locations. Muscle origin locations of the jaw models, which are based largely on modern mammals, are kept constant for the primary analyses. However, it is possible that evolutionary changes to these locations could have accompanied musculoskeletal changes to the jaw, and these changes could significantly affect moment values. Thus, I examined variation associated with potential changes to muscle origin locations among mammal groups. This was accomplished using a sensitivity analysis in which moment results were re-calculated using different muscle origin locations, and variance associated with these locations is considered. Additional methodological details of this analysis are provided in the 2.4 Results section.

Mechanical advantage. Mechanical advantage of a system is a commonly calculated performance metric for jaw mechanics (e.g. Nabavizadeh, 2016), and it is calculated as the in-lever (i.e., moment arm) length divided by the out-lever length. Values can then be multiplied by the force vector components and summed for multiple muscles, as done for calculations of moment. For the jaw models in this study, the out-lever length would be the distance from the axis of rotation to the bite point. However, this measurement is disregarded here for several reasons: the molars are missing or worn in many taxa; the elevation of the bite point could vary for molars that have wear facets of different elevations (e.g., tribosphenic molars have elevated trigonid cusps and a depressed talonid basin); and the relative length of the tooth row and position of the ultimate molar from the axes of rotation appear to be fairly consistent among mammal groups (Appendix B), indicating that the out-lever distance would not change significantly among mammal groups (see additional discussion in 2.4 Results). Further, if the bite point is kept constant among mammal groups, the out-lever distance would remain the same for all calculations of yaw because the axes of rotation do not vary among groups. The out-lever

length will change among mammal groups in the calculations for pitch and roll because the axes of rotation are altered, but the effect of this change is expected to be minor. Future studies could explore the effects of this variable to a greater extent, especially for well-preserved taxa in which common bite points can be accurately identified.

2.4 RESULTS

2.4.1 Morphometrics

Angular process (APr) shape. Results of the GM analysis of APr shape are shown in Figure 2.3, which includes three morphospace plots of the first two principal component analysis (PCA) axes. PC1 (54.5% of variance) is the horizontal axis and PC2 (17.4% of variance) is the vertical axis. The three plots are identical but are replicated to highlight results for different mammal groups, which are designated by polygons. The group means (i.e., average APr shapes) are represented by large, black points.

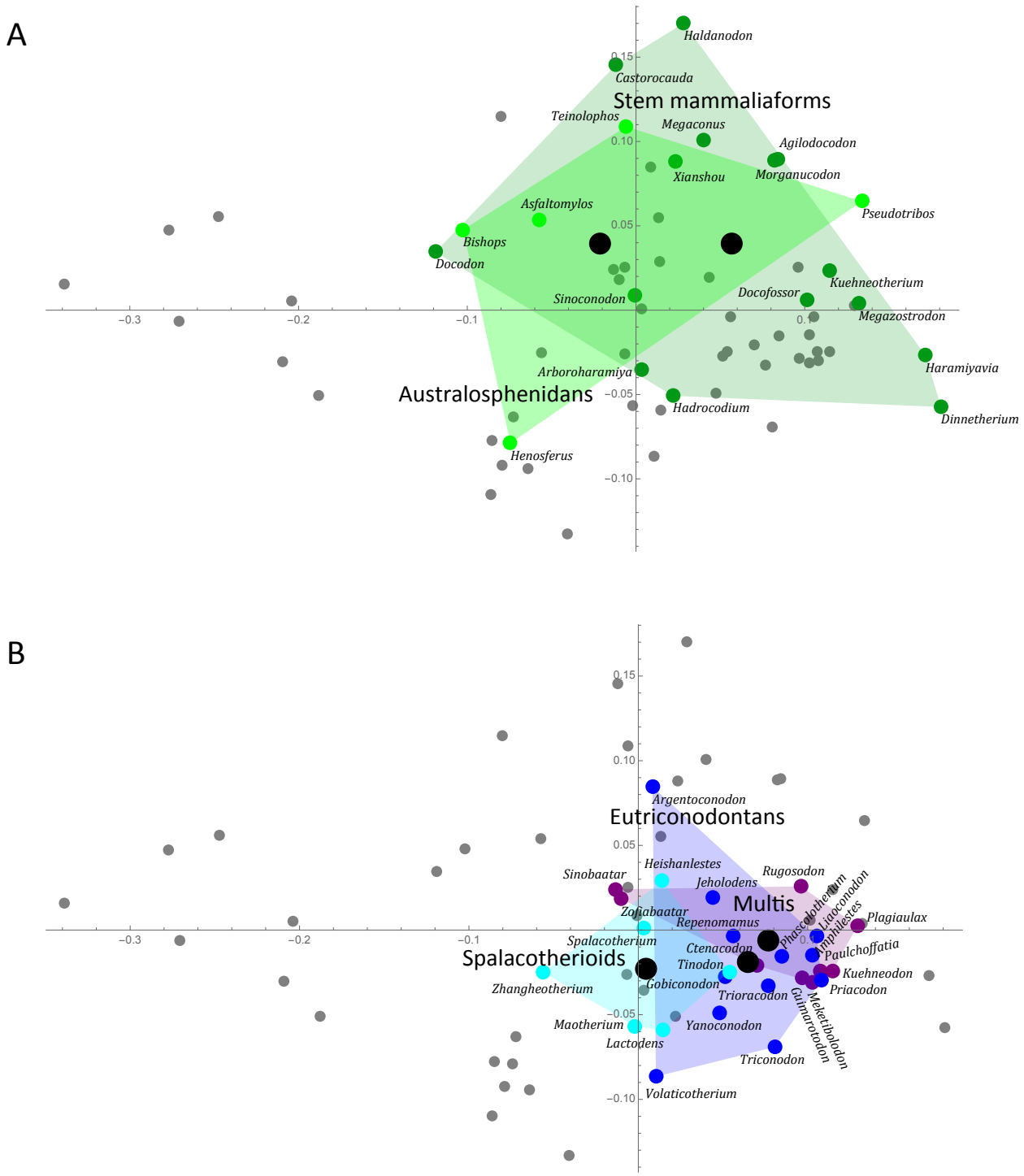

Figure 2.3. Geometric morphometric analysis of angular process shapes for early mammals.

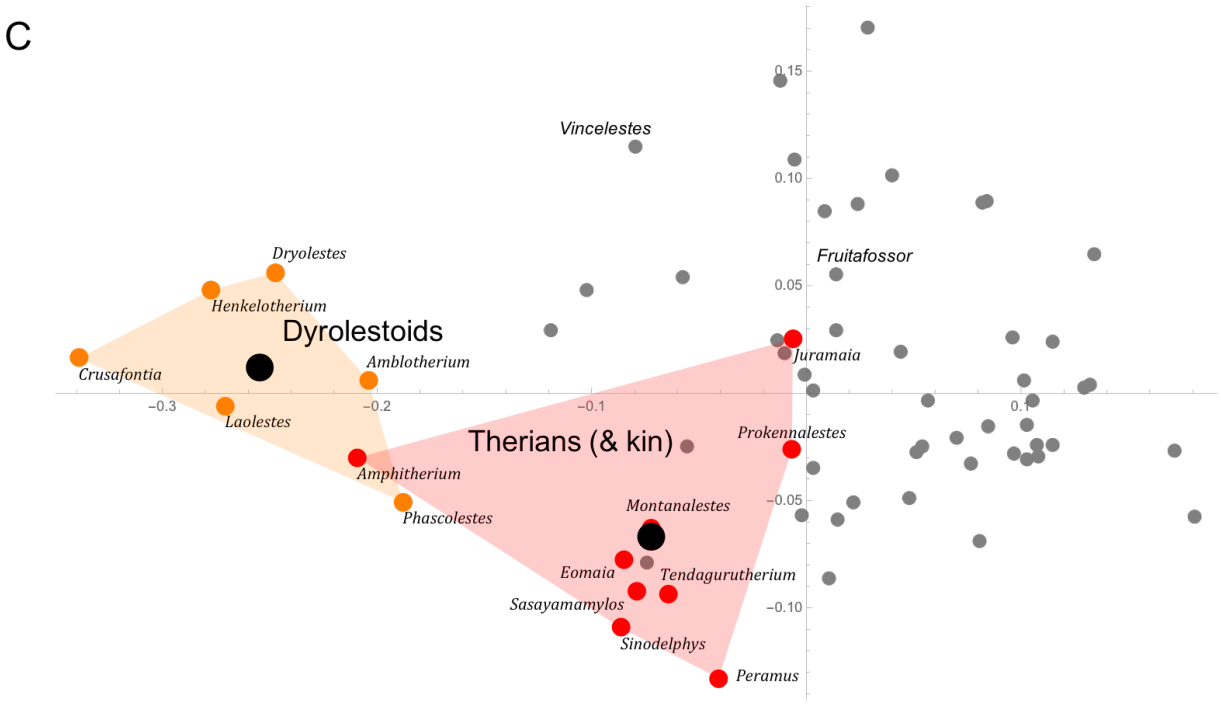

Figure 2.3, continued. Geometric morphometric analysis of angular process (APr) shapes for mammaliaform and mammalian genera from the latest Triassic through Early Cretaceous (i.e., ~210-100.5 Ma). The three PCA morphospace plots (*A*-*C*) are replicates of the same plot, but in each replicate different mammal groups of the phylogeny (Fig. 2.1) are designated by polygons. Landmarks used for the GM analysis are shown in Figure 2.4. Large, black points represent the mean APr shape for each mammal group. The horizontal axis is PC1 (54.5% of variance), and the vertical axis is PC2 (17.4% of variance). *Vincelestes* and *Fruitafossor*, which are not included in a mammal group (see 2.3.1 Mammal groups), are labeled in *C*. See the text and Figure 2.4 for additional details. Abbreviation: multis, multituberculates.

Figure 2.4 includes the same APr shape results as Figure 2.3 (without labels for genera), but it includes a phylogeny, example jaws, and thin plate splines of group means. This allows for an assessment of the macroevolutionary patterns for the APr.

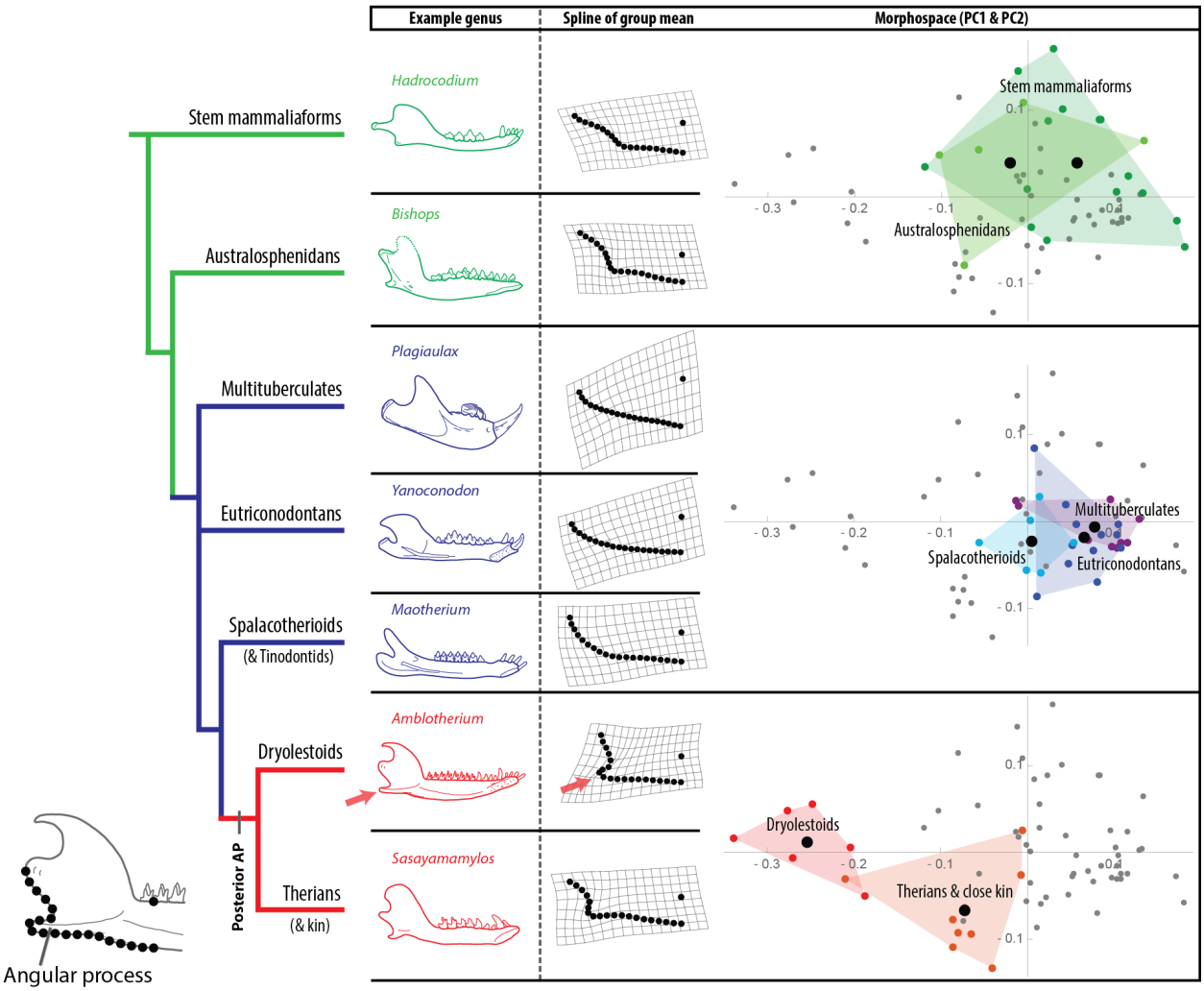

Figure 2.4. Results of the GM analysis of APr shapes (as in Figure 2.3 but without genera labels), with the addition of example jaws and thin plate splines for the group means. 'Green' lineages possess an anteriorly positioned APr. The 'blue' lineages are clades that do not possess a distinctive APr. A posterior, prominent APr appears in cladotherians ('red' lineages) and is highlighted by red arrows. Thin plate splines for each group show the mean shape of the APrs. As with Figure 2.3, the three PCA morphospace plots (right) are replicates of the same plot. Black points in the polygons represent the mean APr shape for each group. The *Amblotherium* jaw is after Simpson (1928), and sources for additional jaw images are provided in Appendix A.

A considerable shift in average jaw morphology occurs early in the crown mammalian tree. Compared to stem mammaliaforms (which have an anteriorly positioned APr), the most notable morphological change is the lack of an APr in three of the early crown mammal groups:

multituberculates, eutriconodontans, and spalacotherioids (Figs. 2.3 and 2.4). These are the 'blue' lineages in Figures 2.1, 2.3, and 2.4. However, it is worth noting that this lack of an APr does not necessarily indicate reduced medial pterygoid and superficial masseter muscles, since these taxa often possess deep fossae allowing for considerable muscle attachment.

At the cladotherian node, a second major shift in average jaw morphology occurs: cladotherians evolve a prominent, posterior APr. Cladotherians include dryolestoids and early therians, which are the 'red' lineages in Figures 2.1, 2.3, and 2.4. In dryolestoids, the distal end of the APr is located directly ventral to the jaw joint, whereas the APrs in stem mammaliaforms are located in a position that is anterior to the jaw joint. Thus, dryolestoids do not overlap in PCA morphospace with earlier lineages that also possess an APr (Figs. 2.3 and 2.4). Early therians also possess prominent APrs, but they are not as posteriorly positioned as the APrs of dryolestoids. The prominent APr of early cladotherians is especially noteworthy because a distinct APr is not present in closely related spalacotherioids, eutriconodontans, and multituberculates (Fig. 2.4).

Results of the GM analysis of APr shape suggest that a posterior, prominent APr is a derived trait of Cladotheria (Fig. 2.4). In light of the phylogenetic positions of the mammal groups, the results of the APr analysis support previous suggestions that the APrs of non-mammalian cynodonts (which have been referred to as "pseudangular" processes) are not homologous to the APrs of therians (Patternson, 1956; Jenkins and Crompton, 1983; Gow, 1986). This is in contrast to recent studies that have argued that the APrs of non-mammalian cynodonts and mammals are homologous, based in part on the observation that the APrs serve as insertion sites for the same jaw muscles in all groups (Abdala and Damiani, 2004, Rougier et al., 2015B). This debate over the homology of the APr seems to focus in part on whether the non-

mammalian cynodont APr is homologous to the APr of the earliest crown mammals, australosphenidans. Here, the results support homology of the APr between these two groups, especially since they partially overlap in the GM morphospace (Fig. 2.4). This is in congruence with conclusions of Rougier et al. (2015B). However, results of this study also conflict with conclusions of Rougier et al. (2015B) by suggesting that the APr of australosphenidans and cladotherians are not homologous. Additional research and considerations may be needed to help resolve this issue.

In addition to the posteriorly positioned APr of jaws, the talonid shelf of lower molars is a character that appears at the cladotherian node (Martin et al., 2015; Rougier et al., 2012) (Fig. 2.1). Thus, the prominent APr of jaws and the talonid shelf of molars seem to have evolved concurrently in the earliest cladotherians.

Jaw joint elevation. The articular surface of the condylar process (i.e., jaw joint surface) is considerably elevated in dryolestoids (Fig. 2.5a; Appendix B). Spalacotherioids and therians (and close kin) also have moderately elevated jaw joints, relative to the depressed jaw joints of eutriconodontans and multituberculates.

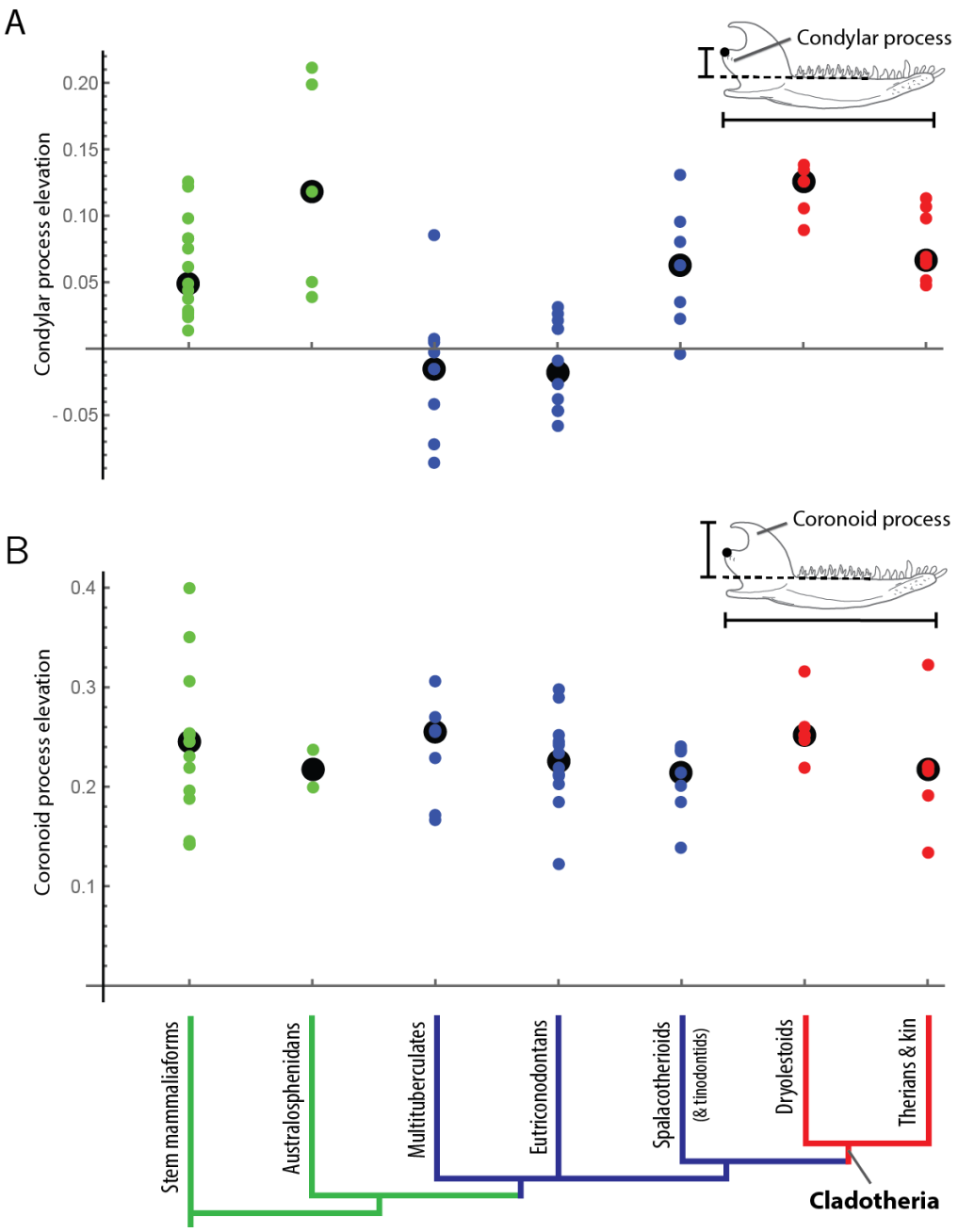

Figure 2.5. Condylar process (i.e., jaw joint) elevation (*A*) and coronoid process elevation (*B*) for mammaliaform genera, measured as the elevation (or depression) from the alveolar margin (dashed line) and standardized by dividing by jaw length. Large, black points represent the median value for each group, and these values are used in the jaw models and moment calculations. See Appendix B for individual results.

Eutriconodontans possess depressed jaw joints (Fig. 2.5a, Appendix B). In addition, they lack an APr and have very little curvature of the posterior-ventral region of the jaw (Fig. 2.4). These traits are comparable to modern mammalian carnivores, which tend to possess a very reduced APr and a depressed condylar process. One eutriconodontan, *Repenomamus*, is a confirmed carnivore (Hu et al., 2005B). These results suggest that the jaw features of eutriconodontans evolved as adaptations for a carnivorous diet. Spalacotherioids tend to be smaller than eutriconodontans and therefore more likely to have been insectivores. Their jaw joints are less depressed than those of eutriconodontans (Fig. 2.5a) and the posteroventral region of the lower jaw often forms a "bulge," although a distinct APr is not present (Fig. 2.4). Thus, they appear to be morphological intermediates between eutriconodontans and cladotherians.

It is possible that the elevated jaw joint in dryolestoids is associated with the posterior position of the APr in this group (Fig. 2.4). Elevating the jaw joint provides space for the APr in the posteroventral region of the lower jaw, and it helps maintain the lengths of moment arms (i.e., in-levers) between the jaw joint (i.e., fulcrum) and force vectors of the SM and MP during pitch rotation.

Coronoid process. In comparison to APr shape (Fig. 2.4) and jaw joint elevation (Fig. 2.5a), the differences in coronoid process elevations among early mammal groups are not as distinct (Fig. 2.5b). The average (median) elevation above the molar row for all groups is between 21.5% and 25.5% of the length of the jaw, with the greatest range of values in stem mammaliaforms. The most notable result is that dryolestoids have coronoid processes with greater elevations than those of additional mammal groups. This could be related to the elevated jaw joint in this group, since a concurrent elevation of the coronoid process (and TM force vector) would help maintain the length of the moment arm for pitch rotation.

In this study, morphological changes to the coronoid process are emphasized to a lesser extent than changes to the APr. This is largely due to the observation that the major morphological change in early cladotherian jaws is the appearance of a prominent, posterior APr (Fig. 2.4) (along with a concurrent elevation in jaw joint, especially in dryolestoids; Fig. 2.5A). Hence, changes to the force vectors of MP and SM, which insert on the APr, are a major focus of this study. Further analyses of the coronoid process shape (such as a GM analysis that is similar to the one performed on APr shape) were not performed for two reasons. First, the coronoid process in early mammal fossils is not as commonly preserved as the condylar or angular processes, meaning the sample size is smaller for this jaw process (e.g., the australosphenidan group only includes coronoid elevation results for two genera) and jaws are reconstructed in publications with less confidence. Second, there is considerable within-group variation in coronoid process shape, meaning shape differences among early mammal groups are less distinct and it is more difficult to discern broad evolutionary trends.

Tooth row length. In the jaw model analyses, the locations of the bite points are not incorporated. The importance of this variable becomes apparent when considering morphological and functional differences between pre-mammalian synapsids and mammaliaforms (e.g., Crompton and Hylander, 1986). Pre-mammalian synapsids such as cynodonts tend to have shorter tooth rows (relative to total jaw length) than mammaliaforms. Thus, the typical bite points along the tooth row for cynodonts are expected to be more anteriorly located than the bite points of mammaliaforms. Variation in the bite point position is likely to alter the mechanical advantages and bite forces of different groups. For instance, calculation of mechanical advantage includes dividing the in-lever (i.e., moment arm) length by the out-lever length. The out-lever in

the jaw models is the distance between the bite point and the axis of rotation, and therefore this value will vary among taxa with different bite point locations.

To help address whether bite point locations are expected to vary considerably among early mammal groups, I measured the relative tooth row lengths for the genera of this study (Appendix B). My assumption is that taxa with similar tooth row lengths will have similar bite point locations, on average, especially for the molars. Results are very similar among the mammal groups for which I produced jaw models (Appendix B). Average (median) tooth row lengths relative to jaw length: eutriconodontans, 63.4%; spalacotherioids, 63.9%; dryolestoids, 63.4%; and therians (and close kin), 60.7% (Supplementary Table S3). Based on these results, the lengths between axes of rotation and the bite points (i.e., out-lever lengths) are not expected to vary considerably among these mammal groups and are not examined in more detail.

2.4.2 Jaw biomechanics

Moment arms. Moment arm (i.e., in-lever) lengths are critical components of moment calculations (2.3 Methods). Moment arms are the perpendicular distances from individual force components to the axis of rotation. Figure 2.6 shows an example of moment arms (black lines, labeled *Lx* and *Ly*) in 2D for the eutriconodontan SM for pitch rotation around an axis through the jaw joints. The *x* and *z* axis components for the SM force vector are also shown (gray arrows, labeled *Fx* and *Fy*), although they are scaled to the length of the muscle and not the size of the force vector. Moment arm lengths were calculated for all directional components of all muscle vectors. These are multiplied by the force components and then summed to calculate moment (i.e., torque) values (see 2.3 Methods).

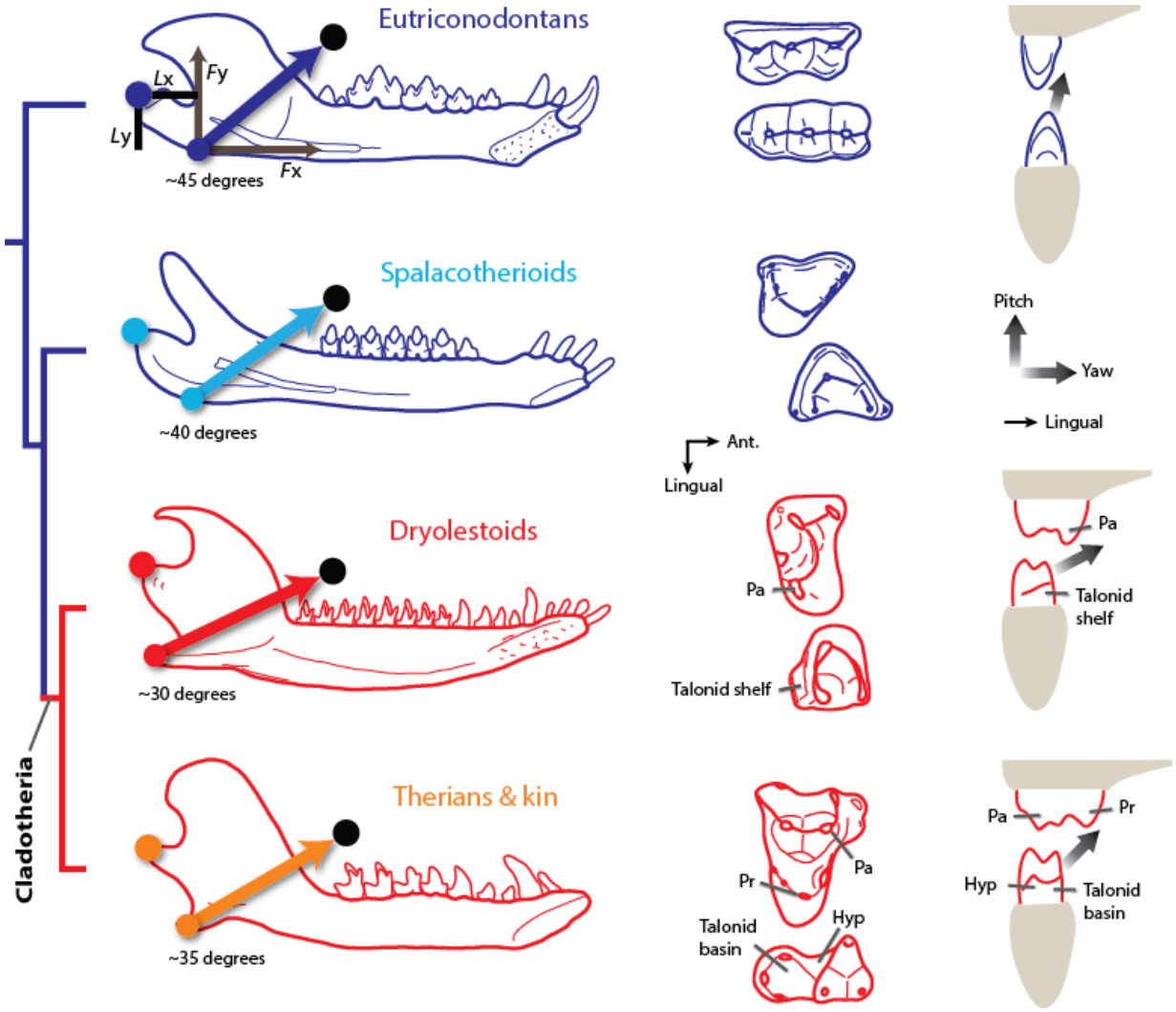

Figure 2.6. Representative jaws and molars of early cladotherians and their close relatives. Arrows signify the superficial masseter (SM) muscle, and black points represent the predicted muscle origin location. The approximate angles of the SM force vector (relative to the molar row) are given, and it is predicted that this angle decreased with the evolution of the posterior APr of cladotherians. As an example to help illustrate moment calculations (see 2.3 Methods), the eutriconodontan jaw image includes the 2D *x* and *y* force components (*F*x and *F*y; scaled to muscle length for simplicity) and corresponding moment arms (*L*y and *L*x, respectively) for the SM. Representative upper and lower molars are shown in occlusal view. On the far right are schematic illustrations of lower molar movement during occlusion in eutriconodontans, dryolestoids, and therians (Butler, 1972). Eutriconodontan occlusion is largely orthal in direction and cladotherian occlusion includes considerable medial movement via yaw as the paracone (Pa) occludes with the talonid shelf or hypoflexid (Hyp). The protocone (Pr) of therian tribosphenic molars occludes with the talonid basin. Sources for jaw images are given in Appendix A. From top to bottom, the molar images are *Priacodon* (Simpson, 1929), *Spalacotherium* (Crompton and Jenkins, 1968), *Dryolestes* (Martin, 1999), and *Prokennalestes* (Kielan-Jaworowska and Dashzeveg, 1989).

Jaw model dimensions. To examine functional changes in therians and their close ancestors, three-dimensional (3D) jaw models were constructed for eutriconodontans, spalacotherioids, dryolestoids, and early therians (and close kin) (Fig. 2.7). These are based largely on the various measurements and considerations discussed previously (see 2.4.1 Morphometrics; Figs. 2.3-2.6; Appendix B). For instance, jaw joint and coronoid process elevations in the models are based on the median values for mammal groups in Figure 2.5 (and Appendix B). Further, the expected muscle insertion sites for the MP and SM are based on mean shapes of the APr region from Figure 2.4 and locations of fossae in the jaws. 3D coordinates were produced for muscle origins, muscle insertions, and jaw joints. Muscle insertion and jaw joint coordinates (*x, y, z*) are provided in Figure 2.7. The coordinate system is based on that shown in Figure 2.2. The mandibular symphysis and muscle origin coordinates are kept constant in all models. The muscle origin coordinates used in the models are not given in Figure 2.7, but are provided here: SM (4.35, 1.1, 2.9), MP (1.75, 0.75, 0.72), and TM (-1.5, 2.9, -2.7). The working-side SM, working-side MP, and balancing-side TM are used in the model because these represent a Triplet muscle group that contracts synchronously during the power stroke of a chewing cycle in many modern taxa (Weijs, 1994; Williams et al., 2011). The TM muscle vector is truncated due to the curvature of the braincase. Thus, the TM origin is not expected to reflect the true location of the muscle origin.

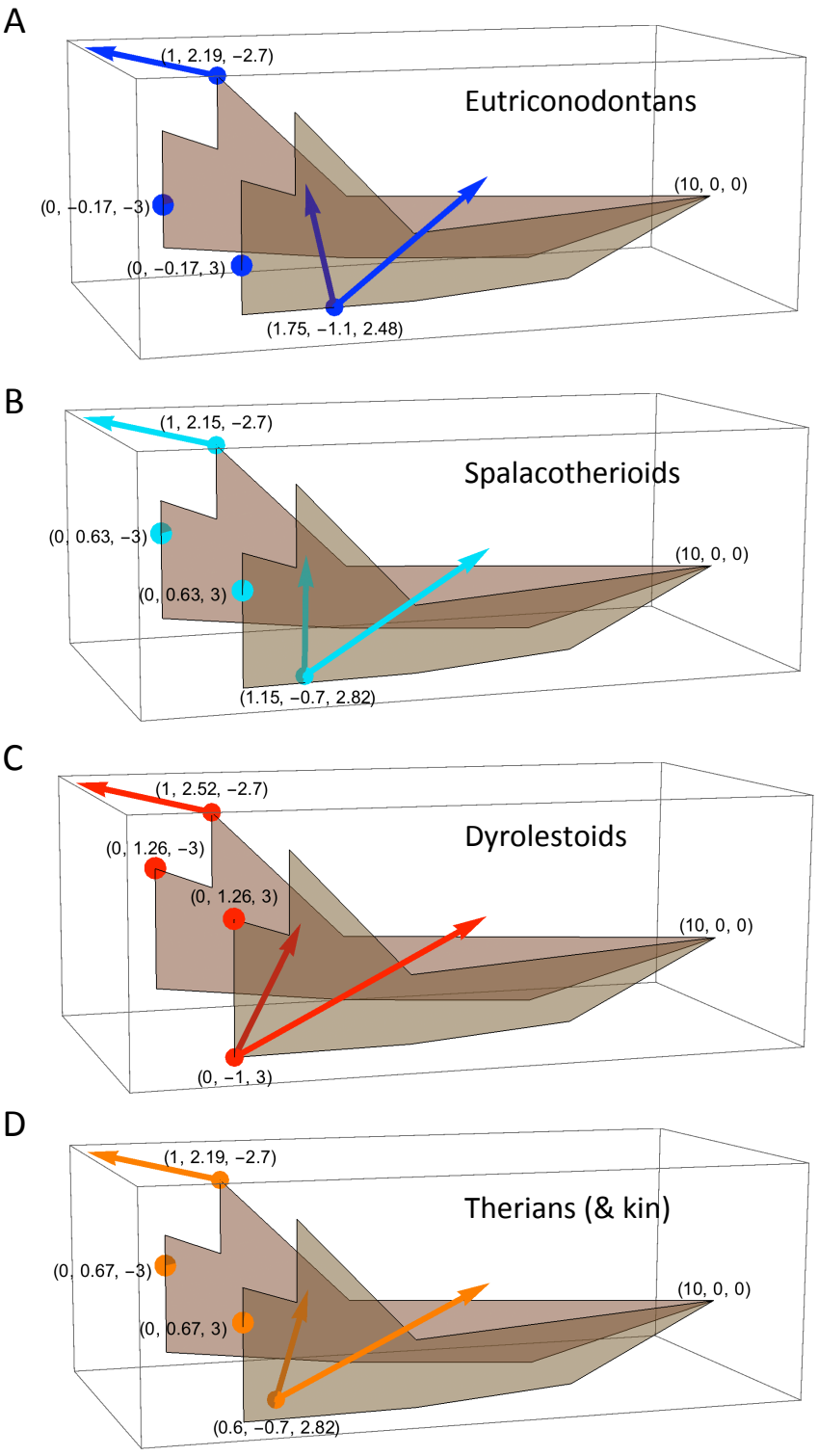

Figure 2.7. 3D jaw models for early mammal groups in oblique lateral view with point coordinates (*x, y, z*) for the jaw joints and muscle insertions. The SM and MP force vectors for all models end at the muscle origins, the coordinates for which are provided in the text. Force vector lengths do not represent the relative force magnitudes of the vectors. The *x, y,* and *z* coordinate system is based on that shown in Figure 2.2.

As discussed in the 2.3 Methods, locations of muscle origins are uncertain and are based primarily on average measurements of modern mammal analogs (Appendix C). Origin locations are kept constant in the models shown in Figure 2.7, but see below (2.4.3 Sensitivity test) for additional analyses that examine variation associated with potential evolutionary changes to these positions.

Moment results. As the posterior processes of the lower jaw underwent evolutionary changes among early mammal groups, performance metrics (e.g., torque and mechanical advantage) for the musculoskeletal jaw configurations would have been altered for various movements. The 3D jaw models of the four mammal groups (Figs. 2.7 and 2.8) help assess differences in moment (i.e., torque or moment of force) for three types of jaw rotation (i.e., pitch, roll, and yaw). Results for the moment analyses are shown in Figure 2.8 and Table 2.1, and the following sections discuss the moment results for pitch, roll, and yaw.

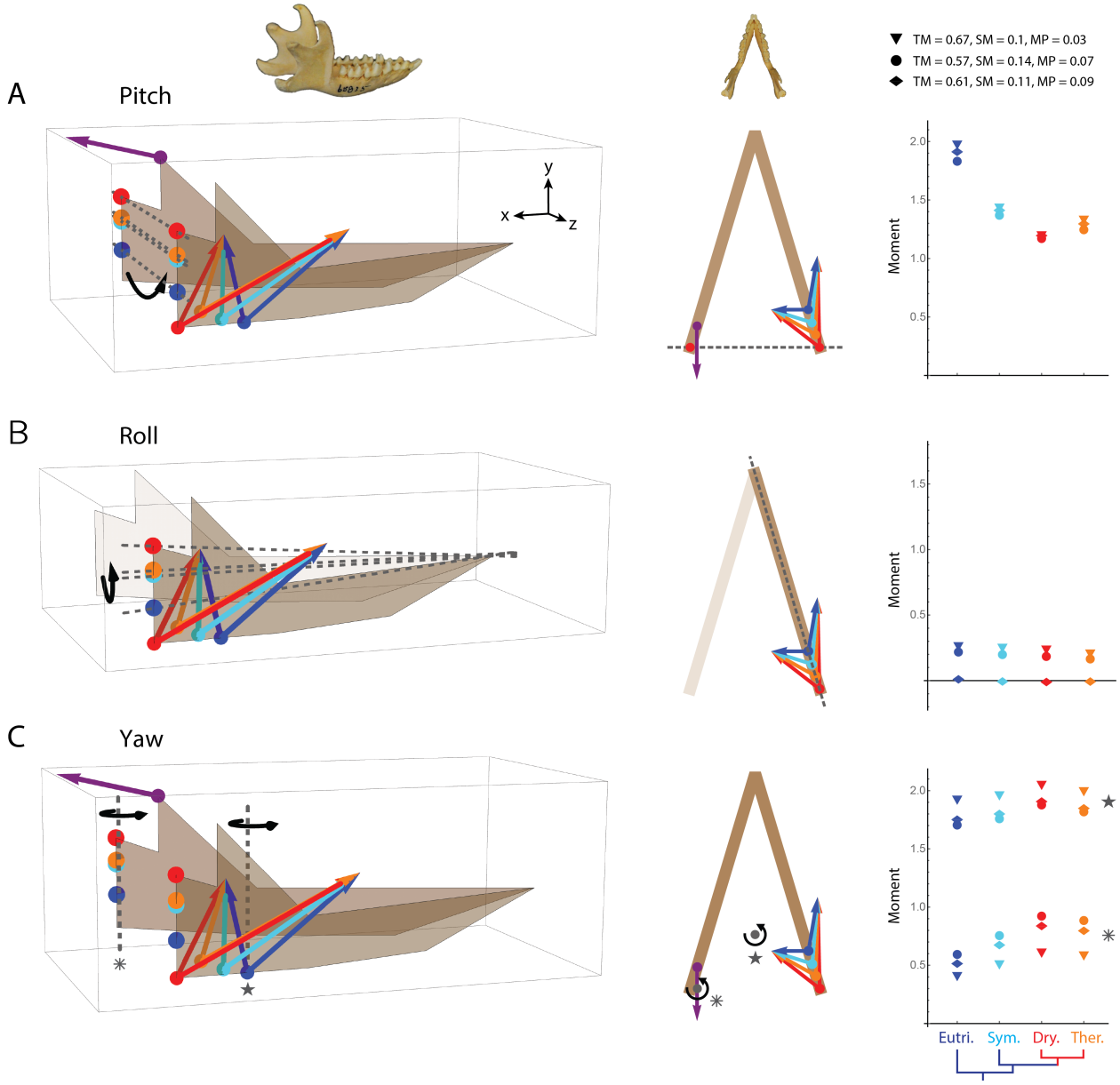

Figure 2.8. 3D jaw models in oblique lateral view (left) and dorsal view (center), and moment (i.e., torque) values for musculoskeletal configurations of the mammal groups (right). Locations of the jaw joint and muscle insertions for each group are inferred from average results of the morphometric analyses (Figs. 2.3-2.5; Appendix B). See Figure 2.2 for muscle labels and Figure 2.7 for point coordinates. Arrows represent the direction of the muscle forces (the lengths do not reflect the magnitude of the force vectors), with SM and MP vectors ending at the expected muscle origins but the TM vector is truncated. For simplicity, the TM vector (purple arrow) and coronoid process elevation are kept constant among groups in this figure, but slight changes in coronoid elevation among groups (Appendix B) are incorporated in calculations of moment values. Color assignments: blue, eutriconodontans (Eutri.); cyan, spalacotherioids (Spalac.); red, dryolestoids (Dry.); and, orange, therians and close kin (Ther.). Dashed lines represent axes of rotation and black

Figure 2.8, continued. arrows denote the direction of rotation. (*A*) Models and moment calculations for pitch rotation around mediolaterally oriented (*z*) axes through both jaw joints. (*B*) Models and moment calculations for roll rotation around axes through the jaw joint and mandibular symphysis. (*C*) Models and moment calculations for yaw rotation around two dorsoventrally oriented (*y*) axes, which are matched with moment results for each axis by corresponding gray stars. All moment calculations were repeated for three different force vector assignments for the jaw muscles (see key and 2.3 Methods), and results are reported in Table 2.1.

Table 2.1. Moment values associated with the jaw model results in Figure 2.8. Results are given for the two yaw axes of rotation shown in Figure 2.8c. Results were calculated using multiple force assignments for the superficial masseter (SM), medial pterygoid (MP) and temporalis (TM) muscles (see text). These are based on the relative muscle weights reported by Turnbull (1970) for *Didelphis virginiana* (*Didelphis v*.) (TM, 0.57; SM, 0.14; and MP, 0.07), *Echinosorex gymnurus* (*Echinosorex g*.) (TM, 0.61; SM, 0.11; and MP, 0.09), and *Canis familiaris* (*Canis f*.) (TM, 0.67; SM, 0.10; and MP, 0.03).

Rotation	Relative muscle masses	Eutricono-dontans	Spalaco-therioids	Dryolestoids	Therians (& kin)
Pitch	*Canis f.*	1.963	1.425	1.186	1.334
	Didelphis v.	1.827	1.368	1.173	1.256
	Echinosorex g.	1.902	1.403	1.192	1.298
Roll	*Canis f.*	0.250	0.239	0.226	0.198
	Didelphis v.	0.217	0.199	0.186	0.163
	Echinosorex g.	0.004	-0.014	-0.017	-0.014
Yaw (central axis)	*Canis f.*	1.914	1.951	2.040	1.989
	Didelphis v.	1.701	1.759	1.875	1.818
	Echinosorex g.	1.744	1.793	1.900	1.842
Yaw (axis through jaw joint)	*Canis f.*	0.399	0.500	0.600	0.576
	Didelphis v.	0.592	0.758	0.924	0.883
	Echinosorex g.	0.507	0.667	0.830	0.789

The jaw models in Figure 2.8 are the same jaw models as in Figure 2.7 except that models for multiple groups are combined in Figure 2.8. Also, because the relative elevation of the coronoid process does not vary considerably among the mammal groups (Fig. 2.5b; Appendix B), the model images are simplified by keeping the TM insertion location (purple

point in Figure 2.8) and vector (purple arrow in Figure 2.8) constant in the jaw model. However, the slight differences in the height of the coronoid are included in calculations of moment values.

It is worth noting that results remain relatively similar when using the different force assignments (see 2.3 Methods, Figure 2.8, and Table 2.1), suggesting that potential variation in muscle forces among mammal groups is unlikely to alter the broad trends seen in this study.

Pitch. For pitch rotation of the jaw, results indicate that moment (i.e., moment of force, or torque) values decrease with the evolution of the prominent, posterior APr of early cladotherians (Fig. 2.8a; Table 2.1). This pattern remains when various force values are assigned to the muscles and when analyses are repeated using different muscle origin locations (see 2.4.3 Sensitivity test). Moment values for therians are slightly greater than for dryolestoids but remain less than the values of eutriconodontans and spalacotherioids. The decrease in moment values of dryolestoids is due in large part to the increased elevation in jaw joint (without a concurrent rise in coronoid process), which shortens the moment arm for the TM.

Roll. For roll rotation of a hemimandible, moment values are small for all mammal groups and do not show a distinct trend (Fig. 2.8b; Table 2.1). The values are likely low because the relatively large balancing-side TM is not involved in the calculations (since only the working-side hemimandible is tested; Fig. 2.8), and because the MP force vector counteracts the SM force vector and works against roll (in the direction tested here). This is consistent with the observation by Crompton (1995) that there is minimal roll of the working-side hemimandible in *Didelphis* during the power stroke of the chewing cycle (although roll is significant during additional phases of the chewing cycle), with the MP helping to stabilize the working-side hemimandible against roll during this phase.

It is worth noting that this result is inconsistent with predictions that could be made from modern analogs of dryolestoids that have zalambdadont dentitions, such as *Tenrec ecaudatus*. Tenrecs (and possibly the convergently evolved *Solenodon*; Wible, 2008) produce considerable roll during occlusion (Oron and Crompton, 1985), and much of the medial movement of the molars may be due to this rotation. In addition to tenrecs, soricid shrews such as *Suncus murinus* and *Crocidura flavescens* also produce considerable roll, although they probably utilize this movement for a unique purpose—they independently rotate hemimandibles to pinch and squeeze food items (e.g., worms) between their incisors (Dötsch, 1986; Dötsch, 1994). *Tenrec ecaudatus*, *Solenodon*, and soricid shrews have all convergently evolved unique derived features that likely assist in roll rotation. This includes a loss of a zygomatic arch (and possibly deep masseter), and laterally flaring coronoid processes. These evolutionary changes are expected to increase the space for a large TM and may produce a larger medial component of the TM vector (Oron and Crompton, 1985). Contractions of the TM are expected to pull or invert the coronoid process medially. Thus, I expect that the TM is largely responsible for the significant roll in these taxa. This is supported by relatively elevated conoroid processes above the jaw joint in *Solenodon* and soricids. Tenrecs generally have a coronoid process that is elevated above the tooth row, although is is not expecially elevated in comparison to the jaw joint. The elevated coronoid processes will increase the moment arm length for the medial component of the TM.

In contast to tenrecs, *Solenodon*, and soricid shrews, early cladotherians do not have a coronoid process that is as elevated above the jaw joint or tooth row (Fig. 2.5; Oron and Crompton, 1985; Dötsch, 1986; Dötsch, 1994; Wible, 2008). Thus, it is not expected that moment values for roll would increase if a medial component of the working-size TM is incorporated into the models (i.e., the TM arm for roll would be shorter for cladotherians than for

spalacotherioids or eutriconodonts). Further, there is no evidence of early cladotherians possessing laterally flaring coronoid processes or losing their zygomatic arch (as in tenrecs, *Solenodon*, and soricids), although there is currently minimal cranial or 3D jaw material in which to make this conclusion. Other morphological clues that could offer support for additional roll, such as evidence for the types of connections at the mandibular symphysis (i.e., Scapino, 1981) and aspects of the jaw joint (e.g., 3D shape of glenoid fossae and condylar processes) are also lacking in the fossil record. Thus, future studies can further test for a potential increase in roll at early mammal phylogenetic nodes by incorporating additional fossil material.

Yaw. Unlike results for pitch and roll, the moment values for yaw were greater for early cladotherians than for eutriconodontans or spalacotherioids (Fig. 2.8; Table 2.1). This is especially apparent when the axis of rotation is near the balancing-side jaw joint, as moments are approximately 50% greater for dryolestoids than eutriconodontans. The results for therians (and close kin) are slightly less in value than those of dryolestoids, but they are greater than those of eutriconodontans and spalacotherioids. These results suggest that the posterior APr evolved in response to selection for increased mechanical advantage during yaw rotation. The greater mechanical advantage may be beneficial during both the fast close and power stroke phases of the chewing cycle, since yaw typically occurs during both phases (Ryder, 1878; Maynard Smith and Savage, 1959; Mills, 1966; Mills, 1967; Crompton and Sita-Lumsden, 1970; Butler, 1972; Butler, 1973; Weijs, 1994; Hylander, 2006; Crompton, 2011).

The results for jaw yaw in dryolestoids are consistent with molar morphologies and wear patterns, which provide evidence for significant mediolateral movement during occlusion (Schultz and Martin, 2014; Crompton and Sita-Lumsden, 1970; Butler, 1972; von Koenigswald et al., 2013; Schultz and Martin, 2011). For instance, microwear scratches are often at a 35°

angle relative to horizontal in dryolestoids (Schultz and Martin, 2011), and the talonid shelf surface that occludes with the paracone of the upper molar is at a similar angle (Fig. 2.6). Thus, lower molars of dryolestoids must include considerable medial movement during occlusion, which is most likely produced by yaw, based on evidence from additional mammal groups (Williams et al., 2011; Ryder, 1878; Maynard Smith and Savage, 1959; Mills, 1966; Mills, 1967; Crompton and Hiiemae, 1970; Crompton and Sita-Lumsden, 1970; Butler, 1972; Butler, 1973; Herring and Scapino, 1973; Kay and Hiiemae, 1974; Weijs, 1994; Hylander, 2006; Crompton et al., 2010; Crompton, 2011; Menegaz et al., 2015). This provides support for the conclusion that cladotherian jaw and molar morphologies evolved in concert with additional yaw rotation.

During occlusion, molar morphologies may influence the specific directional path of molars and jaws (Evans and Fortelius, 2008; Schultz and Martin, 2011; Mellett, 1984; Evans and Sanson, 2006), and this could suggest that coordinated muscle activity may not be necessary for production of yaw rotation. However, even if molar morphologies direct the medial jaw movement during occlusion, this movement necessitates opposing lateral movement via yaw during the fast close phase of the subsequent chewing cycle to re-align the molars for occlusion. Further, muscle activity is likely required to redirect the molars from a dorsolateral movement during the fast close phase of the chewing cycle to a dorsomedial movement at the onset of the power stroke phase (in which the molars have occluded), thus initiating the power stroke but not necessarily controlling precise movement during occlusion. Finally, studies of modern pigs and primates demonstrate yaw rotation during occlusion even though their bunodont molar morphologies are not expected to be passively directing the movement (Hylander, 2006; Menegaz et al., 2015). Thus, these taxa represent examples in which jaw muscles (and not molar morphologies) must be initiating yaw rotation during mastication.

Spalacotherioids may represent morphological and functional intermediates between eutriconodontans and early cladotherians. They have moment values that are between those of eutriconodonts and cladotherians for the three types of rotation (Fig. 2.8). Spalacotherioid molar morphologies suggest that their occlusion includes more mediolateral movement than that of eutriconodontans (Fig. 2.6; Crompton and Sita-Lumsden, 1970), and their jaws possess a posteroventral 'bulge' that may alter muscle vectors in a similar manner as an angular process (Figs. 2.4 and 2.6). However, the lack of a talonid suggests that the transverse movement of lower molars in spalacotherioids is not as extensive as that seen in dryolestids and early therians.

Recent fossil discoveries suggest that eutriconodontans and spalacotherioids possess an ossified Meckel's cartilage that connects the lower jaw and middle ear (Luo et al., 2007A; Ji et al., 2009; Luo, 2011; Wang et al., 2001; Meng et al., 2003). Although a Meckel's groove is present in some early cladotherians (Kielan-Jaworowska and Dashzeveg, 1989; Davis, 2012; Close et al., 2016; Urban et al., 2017), no cladotherian fossils have been discovered with an ossified Meckel's cartilage. Thus, it is likely that an ear-jaw connection in early cladotherians was either not present (at least in adults) or was maintained by cartilaginous tissue rather than bone. If this is the case, it represents an additional morphological change that may have evolved concurrently with greater yaw rotation of the jaw. In jaws with attached middle ears, yaw might create additional stress on attached middle ear elements because, unlike pitch (if the axis of rotation is at the jaw joint), it involves protraction and retraction of hemimandibles at the condyles (Fig. 2.2), likely resulting in tension and compression for attached ear elements. Therefore, the lack of a rigid ear-jaw connection in cladotherians may have allowed greater jaw mobility and decreased the amount of strain on the ear during yaw rotation.

However, this conclusion about middle ear elements is based on two assumptions that should be noted. First, I assume some rigidness at the mandibular symphysis. However, if there is considerable flexibility at the mandibular symphysis or physical restrictions at the glenoid fossae, some retraction and protraction may be replaced by *z* axis translation of hemimandibles (although this movement could also result in stress on middle ear elements). Second, I assume that pitch rotation is around a horizontal axis through the jaw joints. However, if the axis of rotation for pitch is not at the jaw joint (e.g., it is often ventral to the jaw joint in primates; Iriarte-Diaz et al., 2017), then pitch rotation will result in protraction and retraction of the mandible. Thus, future studies could expand on this conclusion about ear elements by testing a broader range of rotational movements.

Therians and close kin. In comparison to dryolestoids, the average jaw morphology of early therians and close kin (i.e., Zatheria + *Amphitherium*) includes an APr that is not as posteriorly positioned and a jaw joint that is not as elevated (Figs. 2.4 and 2.5). Due to these differences, yaw moment values for therians are not as great as those for dryolestoids (Fig. 2.8). Based on the hypothesized correlation between jaw morphology and yaw rotation, this suggests that therian chewing cycles include less mediolateral movement via yaw than the chewing cycles of dryolestoids. This prediction is corroborated by evidence from molar morphologies. In the tribosphenic molars of therians, the talonid shelf expands into a talonid basin (Figs. 2.1 and 2.6). The extended shearing groove of the talonid shelf (i.e., the hypoflexid groove) is reduced in size and its slope is often vertically steeper in tribosphenic molars of early therians (Davis, 2011; Crompton and Kielan-Jaworowska, 1978; Schultz and Martin, 2014; Butler, 1972), indicating that molar movement is more dorsally oriented (and likely involves less transverse movement via yaw) in early therians than in dryolestoids (Fig. 2.6). Further, occlusal contact between the

protocone and hypoconid of the talonid basin in tribosphenic molars may truncate the transverse movement during occlusion (Schultz and Martin, 2014). Thus, molar and jaw morphologies of therians appear to be consistent with the hypothesis that APr position (and possibly jaw joint elevation) is correlated with the amount of mediolateral movement during mastication.

Modern mammalian clades tend to possess derived musculoskeletal jaw anatomies and functions, meaning that analogous comparisons to early mammal groups should be made with caution. However, a couple similarities are worth noting. Tenrecs, *Solenodon*, and several extinct therian lineages possess zalambdodont molars that are morphologically analogous to dryolestoid molars in possessing a talonid shelf instead of a talonid basin (Asher et al., 2002; Lopatin, 2006; Oron and Crompton, 1985; Wible, 2008), and these taxa are believed to produce transverse molar movement via jaw yaw (Mills, 1966; Mills, 1967). Consistent with dryolestoids and the predictions of this study, zalambdodont taxa possess APrs that are positioned strongly posteriorly (Asher et al., 2002; Lopatin, 2006; Oron and Crompton, 1985; Wible, 2008). However, it is worth noting that modern zalambdodont taxa also have chewing cycles with considerable roll rotation (Oron and Crompton, 1985). Although the jaw models of this study do not speak to the question of the degree of roll at the cladotherian node, it is possible that early cladotherians did experience greater roll via passive means (e.g., due to molar morphology) or unique patterns of muscle contractions that are not examined in this study.

In contrast to zalambdodont taxa, the occlusion in most carnivorans is primarily dorsoventrally oriented (i.e., orthal) with little transverse movement (Weijs, 1994; von Koenigswald et al., 2013; Mellett, 1984; Evans and Sanson, 2006), although mediolateral translation along the *z* axis may occur (Menegaz et al., 2015; Evans and Fortelius, 2008). Yaw in many carnivorans is also likely limited by the wrapping of the glenoid fossa around the condyle

of the jaw, creating a hinge-like joint that does not permit the protraction and retraction of condylar processes that occurs during yaw (Fig. 2.2). Consistent with the predictions of this study, carnivorans typically possess a reduced APr and depressed jaw joint (Grossnickle and Polly, 2013; Maynard Smith and Savage, 1959). These traits are analogous to those of eutriconodontans, which include carnivorous taxa such as *Repenomamus* (Hu et al., 2005B), and likely improve mechanical advantage for pitch rather than yaw. The musculoskeletal anatomies of carnivorans and eutriconodontans may also permit greater bite force during wide gape (see discussion on gape below).

Australosphenidans. Evidence suggests that australosphenidans and therians convergently evolved similar morphological changes to the jaws, molars, and ears. This includes the appearance of a tribosphenic molar morphology and loss of a rigid attachment between the middle ear and jaw (Rauhut et al., 2002; Luo, 2011; Luo et al., 2002; Ramírez-Chaves et al., 2016). Australosphenidans possess APr morphologies that are similar to those of therians (Fig. 2.4), and some taxa have elevated jaw joints like those of early cladotherians (Fig. 2.5a). These convergences suggest selective pressures for similar functional morphologies, and they may provide an additional line of evidence for the hypothesized functional link between these changes and increased yaw rotation during mastication. However, the scarcity of australosphenidan fossils and questions concerning their phylogenetic affinity (Luo et al., 2002; Rougier et al., 2012; Rich et al., 2002) prohibit further conclusions regarding this group.

Docodonts. Docodonts are a diverse group of mammaliaforms that are included within the ‘stem mammaliaforms’ group of this study. They are an additional group (besides therians and australosphenidans) with tribosphenic-like molars that suggest mediolateral movement

during occlusion (e.g., Pfretzschner et al., 2005). They often have a distinct APr (e.g., Rougier et al., 2015B), although it is not as posteriorly positioned as that of early therians (Fig. 2.4).

In some respects, the results for docodonts conflict with the conclusions of this study. For instance, the molar morphologies suggest mediolateral movement during occlusion (Pfretzschner et al., 2005) like that seen in early cladotherians, but the jaw joints are not as elevated and the APr is not as posteriorly positioned as those of early cladotherians. Thus, the musculoskeletal configurations in docodonts are not expected to be as ideal for yaw, at least in comparison to early cladotherians. However, there are a couple considerations that may help explain these conflicting results. First, docodont jaws maintain attached middle ear elements, which may inhibit the evolution of potential jaw morphologies. For instance, the middle ear elements may prohibit posterior migration of the angular process, and if taxa need to maintain small resultant forces at the jaw joint region because of attached ear elements then a depressed jaw joint may be necessary (Crompton and Hylander, 1986). Thus, if docodonts are experiencing yaw rotation during occlusion, ideal musculoskeletal jaw configurations (like those in early cladotherians) may simply not be possible due to additional factors. Second, there is a possibility that the transverse molar movements in docodonts are produced by mediolateral translation (along the *z* axis) rather than by yaw. For instance, the molar morphologies of docodonts are complex in shape and may direct molar movement during occlusion, meaning that jaw muscle control of yaw may not be necessary. Prominent X and Y cusps (of the medial portion of the upper molars) appear to truncate medial movement of lower molars during occlusion (Pfretzschner et al., 2005). Also, the medial region of the upper molars (analogous to the trigon of tribosphenic molars) is often directed posteromedially (e.g. Luo and Martin, 2007). This is in contrast to early cladotherians and tribosphenic taxa in which the trigon is often directed medially or

anteromedially. This suggests that a relatively unique type of occlusal movement may be occurring in docodonts, such as posteromedial movement of lower molars (Gingerich, 1973). For instance, yaw rotation may be occurring around a vertical axis of rotation that is at or near the working side jaw joint (rather than the balancing side jaw joint as modeled in Figure 2.8), and yaw around an axis in this position was not tested in this study. Thus, the docodont musculoskeletal jaw configuration may be more ideal for yaw around an axis in this position, although this possibility will need to be explored in future studies.

Deep masseter. The deep masseter muscle is not included in functional analyses primarily because it is not considered a member of the Triplet muscle groups, as defined by Weijs (1994). Also, it does not insert on the jaw processes that are a focus of the morphometric analyses of this study, making it more difficult to examine evolutionary changes to the muscle vector. Further, estimation of deep masseter position in 3D is especially difficult without a distinct process for the muscle insertion (in contrast to the other muscles of this study) and preservation of the zygomatic arches for muscle origins.

Because the deep masseter is not one of the Triplet muscles, it is not expected to reach maximum contraction concurrently with the Triplet muscles. Instead of including the deep masseter with Triplet muscle groups, Weijs (1994) described the working-side deep masseter and balancing-side deep masseter as 'Vertical Closers.' However, Crompton et al. (2011) included the working-side deep masseter in their 'Group 1' muscles and balancing-side deep masseter in their 'Group 2' muscles for *Didelphis*, although they also note that the deep masseter is involved in the fast close and fast open phases of the chewing cycle. They depict Group 1 and Group 2 muscles contracting concurrently, similarly to the Triplet muscles of Weijs (1994). Thus, if the

deep masseter were included in analyses, the balancing-side deep masseter would be included with the Triplet II muscles that are modeled in Figure 2.8.

Unlike the SM and MP, which have a large *x* axis (horizontal) component (Figs. 2.2, 2.6-2.8), the deep masseter is directed dorsolaterally (i.e., it has significant *z* axis and *y* axis components). The dorsally-directed component of the force vector is parallel to the axes of rotation during yaw, meaning that it does not affect yaw rotation. Similarly, the laterally-directed component is parallel to the axis of rotation during pitch, meaning that it does not affect pitch rotation. Thus, incorporation of the deep masseter into moment calculations for yaw and pitch may have a minimal effect on results for these types of rotation. Unlike yaw and pitch, the deep masseter may have a considerable effect on results for roll rotation (Fig. 2.8b). It connects the masseteric fossa of the jaw to the zygomatic arch, and the force vector likely has a relatively large moment arm for the axis of rotation for roll, especially if the zygomatic arch extends laterally from the skull. However, the deep masseter does not insert on the APr and is not expected to experience as great of change in vector as that of the MP and SM among mammal groups. Therefore, including it in analyses is likely to alter results for all mammal groups in a similar manner, which is not expected to change the broad trends seen here.

As noted in the main text, some mammals such as carnivorans may produce transverse molar movements via mediolateral translation (along the *z* axis of this study) rather than via yaw rotation. The deep masseter may be especially involved in this movement since it has a large lateral (i.e., *z* axis) component. This is supported by results in Davis (2014), which show evidence of a late-contracting deep masseter causing significant mediolateral translation in the kinkajou.

Gape. The moment results from modeling analyses (Fig. 2.8) suggest that morphological jaw changes in early cladotherians (i.e., dryolestoids and early therians) may be adaptations associated with greater yaw rotation during mastication. However, it is possible that additional performance metrics played a role in the morphological changes in cladotherian jaws. For instance, musculoskeletal configurations of the jaw can have a considerable impact on gape, both in terms of the amount of gape allowed and the force produced by adductor muscles during varying degrees of gape. In general, the greater a muscle is put in tension (i.e., stretched), the greater the reduction in force output (Herring and Herring, 1974). Therefore, muscles that stretch to a greater degree during jaw opening will produce less force during a wide gape. In the jaw models of this study (Figs. 2.7 and 2.8), the SM and MP are longer in dryolestoids and therians than in eutriconodontans and spalacotherioids due to the posteriorly extended APr. Thus, it is expected that the jaw muscles in early cladotherian would experience relatively less stretch of the muscle during jaw opening. This assumption suggests that increased gape and greater muscle forces during wide gape may be possible in early cladotherians, and that this may have been an additional factor in the evolution of an extended APr.

However, additional considerations indicate that gape is unlikely to have played a role in the evolution of an extended APr in early cladotherians. First, stem cladotherians were likely insectivores, based on their relatively small body sizes (especially compared to eutriconodontans), dentitions that are analogous to zalambdodont dentitions of modern "insectivorans" such as tenrecs, and jaw morphologies (Grossnickle and Polly, 2013). Consuming insects is unlikely to require increased gape or strong forces during wide gape. Second, lengths and directions of muscle fibers affect force-tension curve of muscles and the amount of gape possible, and these variables are unknown for fossil taxa. Thus, additional

analyses are necessary to further examine the effect of potential muscle fiber lengths and directions on gape in early mammals. Third, the APr of dryolestoids (and some insectivorans such as shrews) tends to be long and thin (Fig. 2.4), with the long axis of the APr pointed anteriorly in the direction of the inferred superficial masseter origin (near the anterior zygoma) during jaw closure (e.g., Turnbull, 1970). Thus, the muscle force vectors are assumed to be largely parallel to the long axis of the APr (and mostly horizontal) when the teeth are in occlusion. However, during wide gape the posterior tip of the APr will rotate dorsally behind the jaw joint, bringing the muscle vectors of the SM and MP closer to the jaw joint and significantly reducing their moment arm lengths for pitch rotation (around an axis through the jaw joints). This suggests much weaker bite forces for pitch during wide gape. Also, as the APr rotates during wide gape its long axis is no longer pointed toward the muscle origins (instead it will point ventromedially). If the SM and MP place a strong tensile force on this gracile APr while it is not aligned with (or parallel to) the direction of force, it is likely to put considerable strain on the APr.

Gape is more likely to have been a factor in the evolution of the eutriconodontan jaw morphology rather than the cladotherian jaw. For instance, modern taxa like carnivorans that require a wide gape for large food items tend to have a small APr that is positioned close to the jaw joint, and the jaw joint tends to be depressed (Herring and Herring, 1974; Grossnickle and Polly, 2013). Similarly, eutriconodontans have a depressed jaw joint, and the MP and SM insert close to the jaw joint. Eutriconodontans are some of the largest Mesozoic mammals and at least one genus, *Repenomamus*, has been shown to be carnivorous based on fossilized gut contents (Hu et al., 2005B). This convergent musculoskeletal configuration of carnivorans and eutriconodontans likely results in minimal muscle stretch during wide gape and/or maintains

moment arm lengths for the muscles during pitch rotation (unlike taxa with a posteriorly extended APr), allowing a strong bite force to be maintained even during wide gape.

2.4.3 Sensitivity test – muscle origin locations

The focus of the jaw model analyses is on evolutionary changes to muscle insertion locations and jaw joint elevations (Figs. 2.2-2.8). However, an additional variable that is expected have a considerable effect on muscle vectors and moments is the locations of muscle origins. Muscle origin locations of the jaw models are based primarily on measurements of skulls of modern analogs and well-preserved mammaliaform skulls (see 2.3 Methods and Appendix B), and these locations are kept constant in the jaw models (Figs. 2.7 and 2.8).

It is possible that concurrent evolutionary changes to muscle insertion and muscle origin locations would negate the changes in moment values that are reported here. For instance, the SM muscle vector angles in Figure 2.8 are shown as being closer to horizontal in dryolestoids (in comparison to eutriconodontans and spalacotherioids) due to the posterior extension of the APr. However, if the SM origin evolved posteriorly with the concurrent evolution of a more posterior muscle insertion, this would negate the inferred change in muscle vector angle (Figs. 2.6-2.8). This could alter the moment value trends reported in Figure 2.8 and Table 2.1.

To examine the effect of potential variation in muscle origin locations on moment calculations, a sensitivity test was performed. This involved altering muscle origin locations for the three muscles of this study (i.e., the working-side SM, working-side MP, and balancing-side TM) and repeating moment value calculations. The SM and MP muscle origins were altered along the *x* axis and *y* axis, and the TM was altered along the *y* axis and *z* axis (Fig. 2.9). For the SM and MP, muscle origins were shifted two standard deviations in both directions away from

the original origin location (Figs. 2.7 and 2.8). The standard deviations are those reported in Appendix B and are therefore based on variation seen in modern analogs and fossil skulls. Because the locations were moved two standard deviations, this means that approximately 95% of the variation seen in these taxa is captured in the analyses. For the TM, muscle origin location was not based on measurements of skulls, so the muscle vector was moved approximately the same amount in each direction as was done for the SM (Fig. 2.9). Muscle force assignments in all calculations are based on *Didelphis* muscle masses (see 2.3 Methods). Moment calculations were repeatedly calculated using the same methodology as described previously. However, roll rotation was excluded because results for roll remained low in all previous calculations (Fig. 2.8 and Table 2.1) and is not expected to change significantly with different muscle origin locations, especially since the TM is not included in roll calculations (see 2.3 Methods). Results for the muscle origin sensitivity test are provided in Figure 2.9, with model images for spalacotherioids shown with muscle vectors based on the varying muscle origins (i.e., multiple blue arrows from the same muscle insertion location).

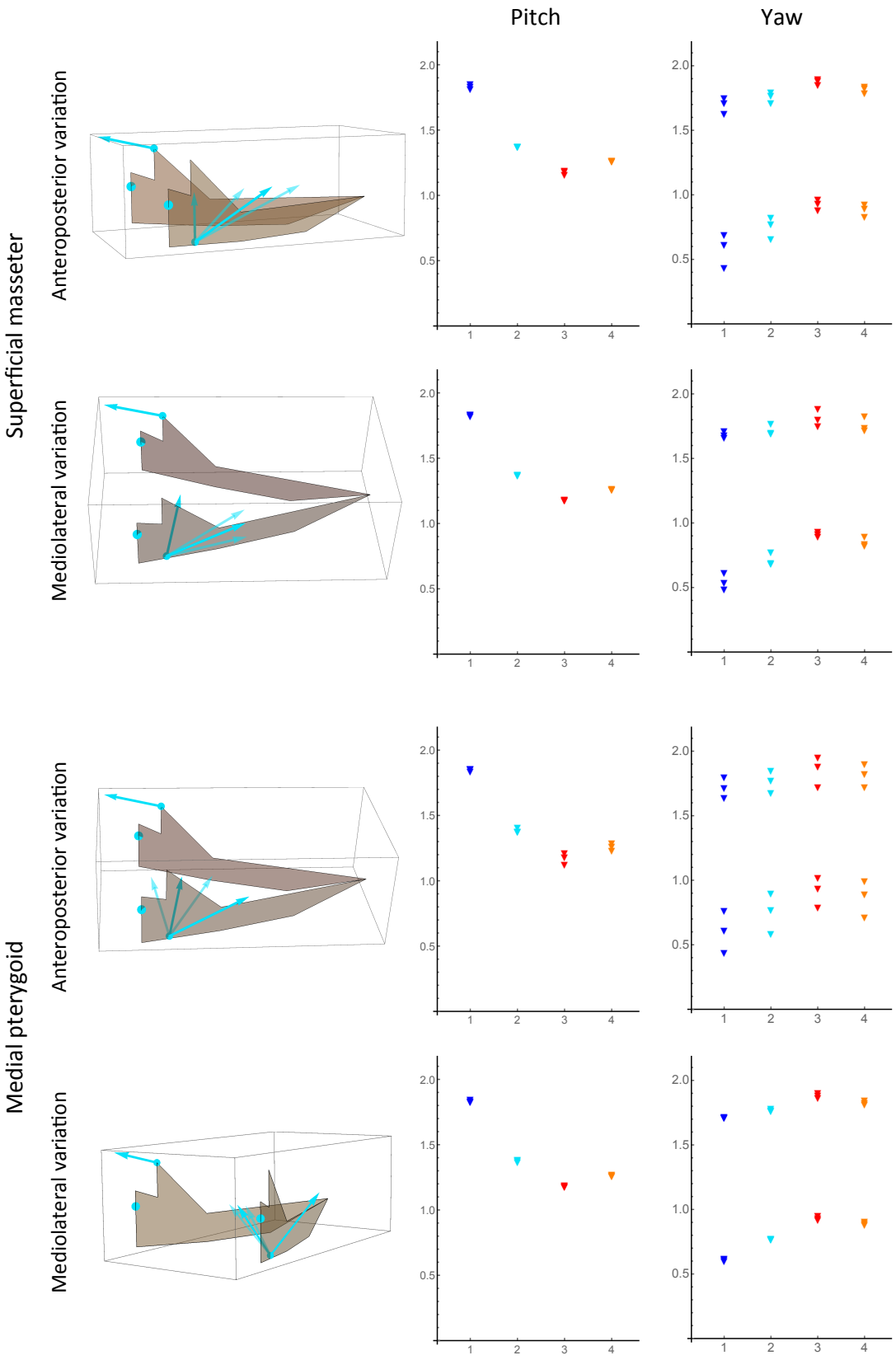

Figure 2.9. Sensitivity test with altered muscle origin locations of the jaw models.

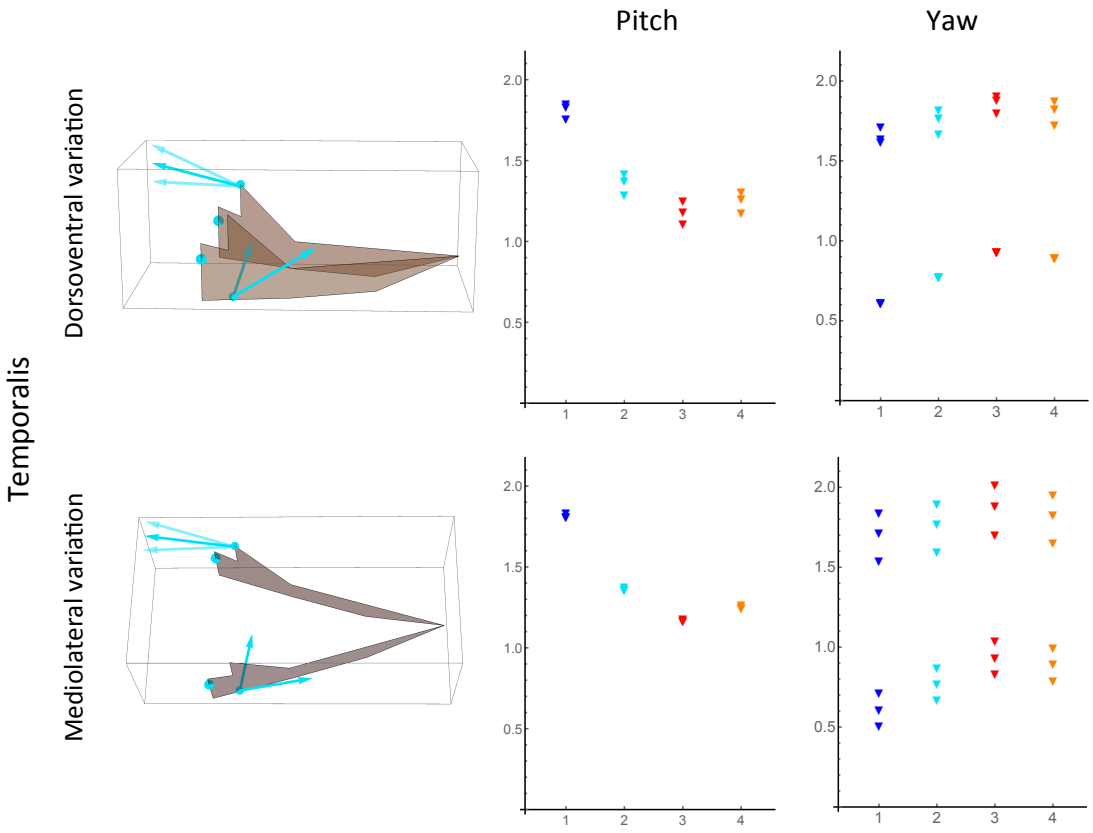

Figure 2.9, continued. Sensitivity test in which muscle origin locations of the jaw models (Fig. 2.7) have been altered to examine variation associated with potential evolutionary changes to these locations. The model images (left) are spalacotherioids, although moment analyses (right) were performed for the four mammal groups: eutriconodontans (blue, 1), spalacotherioids (cyan, 2), dryolestoids (red, 3); and therians and close kin (orange, 4). For the superficial masseter and medial pterygoid, origin locations were moved two standard deviations in both directions from the original muscle origin, and these new vectors are denoted with additional arrows in the model images. (The standard deviations are based on results of measurements in Appendix C). Only pitch and yaw were examined (see text), and the muscle force assignments in all analyses are based on muscle masses of *Didelphis*. As in analyses shown in Figure 2.8, there are two sets of results for yaw that are based on two potential locations for the axis of rotation. The greater values always correspond to the vertical axis that is just medial to the balancing side jaw joint. See Figure 2.8 for locations of these axes and additional information.

In the original moment calculations, early cladotherians (i.e., dryolestoids and therians) show relatively small moments for pitch and relatively large moments for yaw (Fig. 2.8). This pattern remains in all analyses of the sensitivity test in which muscle origin locations are altered

(Fig. 2.9). In addition, for some calculations (e.g., mediolateral variation of the MP) the results for pitch and yaw remain nearly unchanged when the origin location is altered.

Results for pitch rotation are especially consistent for all calculations of the sensitivity test (Fig. 2.9). This suggests that the pattern shown for pitch in the original analysis (Fig. 2.8) is unlikely to have been altered by evolutionary changes to the muscle origin locations among mammal groups. This is likely due to pitch results being based largely on jaw joint elevation and coronoid process elevation, since the distance between these points roughly represents the moment arm length for the large TM during pitch. Thus, changes to the angle of the TM force vector are unlikely to alter pitch results significantly unless the TM vector changes considerably more than the amount that is tested here. This provides additional evidence for the conclusion that musculoskeletal jaw configurations of early cladotherians were less ideal for pitch rotation than those of eutriconodontans and spalacotherioids.

Compared to pitch, results for yaw show greater variation when muscle origin locations are altered (Fig. 2.9). However, this variation is still minimal for many of the calculations. The greatest variation is for anteroposterior changes to the MP origin and mediolateral changes to the TM origin. Thus, moment results for yaw in Figure 2.8 should be considered with some caution, although it is worth reiterating that the general trends for the four mammal groups are not altered when the muscle origins are varied. Considerable evolutionary change in muscle origin would have had to occur among early mammal groups to disrupt the original results pattern from Figure 2.8.

The sensitivity analysis tests the variation in muscle origin locations of modern taxa, but it cannot be ruled out that early mammal groups had muscle origin locations that are outside of the range of variation seen in modern analogs (and fossil mammals) that were measured for this

study (Appendix C). However, there is little or no evidence to suggest that this is the case for these taxa, especially since the skull material of early mammals in this study (e.g., *Yanoconodon, Maotherium, Juramaia*, *Vincelestes*, *Eomaia*, *Sinodelphys*) do not indicate significant morphological divergence beyond the variation seen in modern analogs.

2.5 DISCUSSION

2.5.1 Mammalian evolution

Middle ear evolution. The evolutionary transition that resulted in the origin of the definitive mammalian middle ear (i.e., a single dentary squamosal jaw joint and middle ear elements that are detached from the jaw) is somewhat paradoxical. That is, bones expected to receive considerable compression and tension at the jaw joint during mastication (i.e., the quadrate and articular bones) transitioned to delicate sound transmitting ossicles (i.e., the incus and malleus, respectively) in the middle ear. It has been suggested that in taxa with bones serving dual roles as jaw and ear components, musculoskeletal configurations must have minimized forces at the jaw joint while preserving strong bite forces (e.g., Crompton and Hylander, 1986). Although a diversity of jaw morphologies satisfies these requirements (Reed et al., 2016), it is expected that some morphologies and functions would not be plausible. For example, an elevated jaw articulation relative to the molar row can result in greater reaction forces at the jaw joint (especially when muscle forces are anteriorly directed), meaning that a substantially elevated jaw joint is unlikely in taxa with dual functioning ear and jaw components (Reed et al., 2016). Thus, it has been hypothesized that constraints on musculoskeletal configurations of the jaw diminished when ear components were relieved of jaw joint functions (i.e., the dentary-squamosal joint became the sole jaw joint), resulting in a diversification of morphologies in early

mammal groups (Crompton and Parker, 1978). This hypothesis is supported by the observed morphological and taxonomic diversifications in Jurassic mammaliaforms (Fig. 2.1; Luo, 2007; Grossnickle and Polly, 2013; Close et al., 2015), in addition to the variety of jaw morphologies documented in this study (Figs. 2.4 and 2.5).

Although pre-mammaliaform cynodonts are not included in this study, it is worth considering their jaw and ear morphologies when examining macroevolutionary patterns of stem mammaliaforms and early crown mammals. The cynodont APr tends to be anteriorly positioned relative to that of crown mammals (Crompton and Hylander, 1986). This is similar to stem mammaliaforms, which also have an anteriorly positioned APr (Fig. 2.4). However, unlike stem mammaliaforms, the APr is ventrally deeper (due to a ventrally extended APr and/or a deeper mandibular body) on average. An issue with an anteriorly positioned APr is that the attached adductor muscles may impede gape, since muscle stretch will be greater (if all other variables are kept constant) when the muscles are further from the axis of rotation. By extending the angular process ventrally, cynodonts lengthen the jaw adductor muscles and likely lessen the forces lost to stretched muscles during gape. In addition, cynodonts appear to have a shortened tooth row relative to the length of the jaw (e.g., Crompton and Hylander, 1986), which means the typical bite point (of molars) is expected to be more anteriorly positioned relative to that of mammaliaforms. The combination of the anterior APr and anterior bite point may have helped lessen the reactionary forces at the jaw joint during pitch rotation (Crompton and Hylander, 1986; Reed et al., 2016).

In stem mammaliaforms in which the ear elements no longer perform a load-bearing function at the jaw joint, evolutionary constraints on the musculoskeletal configurations of the jaw may have been reduced. As noted above, this may have allowed for jaw joints that were

significantly elevated. Further, it may have permitted jaw configurations with greater reactionary forces on the jaw joint because the delicate ear elements were no longer attached. Thus, the bite point and APr could move posteriorly, likely raising reactionary forces but benefitting the taxa in additional ways (e.g., allowing for a longer tooth row). See Crompton and Hylander (1986) and Reed et al. (2016) for additional considerations.

Early crown mammals such as eutriconodontans and spalacotherioids possess a bony connection between the middle ear and jaw via an ossified Meckel's cartilage (Fig. 2.1; Wang et al., 2001; Meng et al., 2003; Luo et al., 2007A; Ji et al., 2009; Luo 2011), but this connection does not appear to be present in early cladotherians. It is worth noting that mandibles of early cladotherians often possess a Meckel's groove (e.g., Davis, 2012; Close et al., 2016), indicating that a cartilaginous ear-jaw connection may be maintained in adults. However, the lack of fossil evidence for a strong ear-jaw attachment suggests that any connection that remained was not rigid. Thus, the possible loss of a strong attachment between the jaw and middle ear in cladotherians may have permitted further diversification of jaw morphologies and functions, although this is speculative due to the limited fossil evidence.

Triplet muscle groups. In the jaw models, the Triplet II muscles (Fig. 2.2) were chosen for moment calculations since they contract concurrently during the power stroke of the chewing cycle (i.e., during occlusion) in many modern mammal groups (Williams et al., 2011; Weijs, 1994; Crompton, 2011). Using these muscles for calculations assumes that the early mammal clades have asynchronously contracting Triplet muscle groups in which the balancing-side TM (rather than the working-side TM) is contracting with the working-side SM and MP. However, this assumption is unlikely to affect results for pitch and roll. For instance, using the working-side TM instead of the balancing-side TM for calculations would result in the same values for

pitch because the moment arm length would be identical. In addition, if the working-side TM was included in the calculations for roll, it would likely have little effect because the vector is largely parallel to the axis of rotation (resulting in small force contributions to this type of rotation). In addition, if the working-side TM includes a significant medial component (e.g., as seen in tenrecs, Oron and Crompton, 1995), the TM moment arm for cladotherians is expected to be shorter than that of spalacotherioids and eutriconodonts, indicating that cladotherians would have lower moment values for roll (see further discussion in 2.4 Results). Thus, if the asynchronous contractions of Triplet muscles were not present in early mammal groups, it is unlikely that revised calculations would alter the broad patterns seen here for pitch and roll, including the decreased moment values for pitch at the cladotherian node.

In contrast to the results for pitch and roll, the results for yaw are largely dependent on the asynchronous contractions of the Triplet muscle groups. For instance, if the working-side TM (rather than balancing-side TM) contracted with the working-side SM and MP, then the posteriorly directed force vector would counteract the SM and MP vectors, and yaw rotation in the medial direction would be unlikely to even occur. Thus, I recognize that the choice to use a Triplet muscle group in the models may be influencing the conclusion that yaw increases at the cladotherian node. However, it is worth noting that even if the Triplet contraction pattern was not present in the earliest cladotherians, it is still likely that they had asynchronous contractions of jaw muscles, as these are present in most modern mammals even if there is not a specific Triplet pattern (e.g., Williams et al., 2011; Ram and Ross, 2018; Vinyard et al., 2005). If it is assumed that the muscle contraction patterns in early mammals are unknown, then I could have instead modeled each muscle individually. In this case, I expect that at the cladotherian node the moment values for yaw would increase for the SM and MP (due to the vectors having a greater x-axis

component than spalacotherioids and eutriconodonts), and it is expected that pitch moment values would significantly decrease for TM (with little effect on yaw) and stay relatively consistent for SM and MP. Thus, if muscles were modeled individually, the conclusion that jaw changes at the cladotherian node increase moment values for yaw would remain supported.

Tribosphenic molar evolution. Medial movement of the working-side hemimandible was a likely prerequisite for the evolution of tribosphenic molars. It allows for extended contact between the protocone and the talonid basin, as well as the hypoflexid and paracone, during the power stroke phase of a chewing cycle (Fig. 2.6; Schultz and Martin, 2014). Considerable evidence suggests that this medial movement of the working-side hemimandible is produced via yaw rotation (rather than *z* axis translation) in early therians (Williams et al., 2011; Ryder, 1878; Maynard Smith and Savage, 1959; Mills, 1966; Mills, 1967; Crompton and Hiiemae, 1970; Butler, 1972; Butler, 1973; Herring and Scapino, 1973; Kay and Hiiemae, 1974; Weijs, 1994; Hylander, 2006; Crompton et al., 2010; Crompton, 2011; Menegaz et al., 2015), especially since yaw rotation occurs in modern and fossil taxa with tribosphenic (or tribosphenic-like) molars (Mills, 1966; Mills, 1967; Crompton and Hiiemae, 1970; Crompton and Sita-Lumsden, 1970; Butler, 1972; Butler, 1973; Kay and Hiiemae, 1974; Crompton, 2011). Thus, yaw appears to be a particularly important component of tribosphenic molar occlusion, and increased yaw may have been a critical early step in the evolution of tribosphenic molars.

The additional mediolateral movement via yaw in early cladotherians could have aided taxa by increasing the amount of shearing per chewing cycle. Not only are the primitive trigonid shearing crests (i.e., those of spalacotherioid molars) maintained in early cladotherians, but the novel talonid also permits extended shearing (Fig. 2.6; Schultz and Martin, 2014). Crompton (1971) and Davis (2011) document an increased number of wear facets on molars in

cladotherians relative to mammaliaforms, suggesting increased occlusal complexity and precision.

Mammaliaforms experienced an evolutionary radiation in the Jurassic that was marked by the appearance and diversification of numerous clades (Fig. 2.1; Luo, 2007; Grossnickle and Polly, 2013; Close et al., 2015). Most of these groups persisted for tens of millions of years and achieved considerable ecomorphological diversity (e.g., Luo, 2007; Grossnickle and Polly, 2013; Meng et al., 2015; Chen and Wilson, 2015). However, many mammaliaform and early crown mammalian clades went extinct or were greatly diminished during the Cretaceous Terrestrial Revolution (KTR) at ~125-80 million years ago (Ma) and K-Pg mass extinction event at 66 Ma, periods of considerable environmental perturbation and ecological change (e.g., Alvarez et al., 1980; Labandeira et al., 2002; Lloyd et al., 2008; Bond and Scott, 2010; Tobin et al., 2012; Grossnickle and Polly, 2013). Cladotherians survived the KTR and K-Pg extinction event and, led by therians, diversified after both events (Alroy, 1996; Benson et al., 2013; Grossnickle and Polly, 2013; Wilson, 2014; Grossnickle and Newham, 2016). The differential survival and subsequent diversification of therians hints at a potential functional advantage for lineages with tribosphenic molars. For instance, by allowing crushing of food items such as plant matter and soft insect parts, the tribosphenic molar morphology probably assisted in broadening the dietary diversity of early therians. In turn, the dietary versatility and efficiency of therian molars may have been critical for the survival of the clade during its early history. This conclusion is supported by evidence suggesting that early mammals with generalist diets were less prone to extinction than dietary specialists (Simpson, 1944; Smits, 2015; Grossnickle and Newham, 2016). However, since diet is not directly tested in this study, further examination is needed to test this hypothesis.

It is worth noting that the only additional extant mammalian group to survive the KTR and K-Pg extinction events is Australosphenida (including monotremes), which convergently evolved a tribosphenic molar morphology early in their history. This provides additional support for the hypothesis that the tribosphenic molar may have assisted in mammalian survival during these events.

2.5.2 Conclusions

An improved understanding of the early evolution and biology of Theria will help elucidate the origins of modern mammalian diversity. Here, I examine concurrent evolutionary changes to functional anatomies of jaws, molars, and ears in early cladotherian mammals, and I posit that these changes are associated with increased transverse movement via yaw rotation during chewing cycles. The appearance of the talonid shelf of molars in stem cladotherians (e.g., dryolestoids) likely assisted in medial movement during occlusion and acted as an extended shearing surface (Figs. 2.1 and 2.6). Further, a posteriorly positioned APr may have evolved due to selection for muscle force vectors that produce greater mechanical advantages during yaw (Fig. 2.8). Finally, the potential loss of a rigid connection between the jaw and middle ear in early cladotherians might have resulted in fewer restrictions on mediolateral movement of the mandible, although further studies are needed to fully examine this hypothesis. The jaws, molars and ears of australosphenidans (which include monotremes) are morphologically similar to those of therians, suggesting convergent evolution of similar functional traits in this group.

I hypothesize that these morphological and functional changes were a critical step in the evolutionary origin of the therian feeding system. For instance, increased mediolateral jaw movement may have been a prerequisite for the evolution of the functionally diverse and

efficient tribosphenic molar morphology in therians (and possibly australosphenidans), and this movement was likely produced via yaw rotation. The continued presence of tribosphenic molars in many modern mammalian lineages provides strong evidence of its evolutionary importance. Thus, the concurrent evolutionary changes to jaws, molars, ears, and chewing cycles in early cladotherians may have been an especially significant event in mammalian evolution.

The masticatory changes in early cladotherians may have resulted in greater occlusal precision, more efficient food processing, and greater dietary diversity. For instance, the appearance of a crushing function in the tribosphenic molars of therians may have allowed for improved mastication of plant matter. Thus, this consideration offers a possible explanation for the differential survival of cladotherians during periods of ecological perturbations and elevated extinction rates, such as the KTR and K-Pg extinction event.

CHAPTER 3

Jaw correlates of diet provide insight on the adaptive radiation of early therian mammals

3.1 ABSTRACT

Mandibular shape can offer considerable insight into the dietary preferences and evolutionary histories of mammals, including fossil lineages. However, studies that broadly examine the relationship of jaw morphology and diet across Mammalia are rare. Jaw shape is expected to correlate with diet due to common functional demands on the masticatory apparatus of taxa with similar diets. I test this prediction by applying phylogenetic comparative methods to linear jaw measurements and dietary information for a taxonomically diverse mammalian sample. Results indicate that the distance between the jaw joint and angular process is an especially powerful predictor of diet, increasing with greater herbivory. This metric (and a similar angular measurement) reflects insertion area sizes and moment arm lengths for two masticatory muscles, the superficial masseter and medial pterygoid, which are particularly important for jaw movements used by herbivores. To further test the influence of diet on jaw evolution, I compare the fit of evolutionary models to the morphological data. I find strong support for the hypothesis that there are unique selective regimes associated with herbivory and faunivory, and results suggest that mandibular morphologies of herbivores evolve more rapidly than those of faunivores. Having established the strong evolutionary link between diet and the angular process-to-jaw joint length, I next apply this jaw metric to the mammalian fossil record to

examine the functional diversity of therian mammals through time. Results support the conclusion that there are unique adaptive peaks for herbivores and faunivores, as the two dietary groups show strong divergence in morphologies and a bimodal distribution pattern by the Eocene. In addition, I find evidence for multiple bursts of diversification during early therian history, with the most notable increase in dietary diversity occurring in the latest Cretaceous. This challenges the popular hypothesis that therian mammals were ecologically suppressed until the extinction of non-avian dinosaurs. Thus, this study demonstrates the strong correlation between jaw morphology and diet, and it offers new insight on the early radiation of therian mammals.

3.2 INTRODUCTION

The correlation between form and function is a central theme in biology, and identifying ecologically relevant correlates has been especially informative for examining evolutionary adaptations to various ecological niches (Bock and von Wahlert, 1965; Janis, 1995; Kirk et al., 2008; Polly et al., 2011; Angielczyk and Schmitz, 2014; Winchester et al., 2014; Chen and Wilson, 2015; Figueirido et al., 2015; Mitchell and Makovicky, 2014; Panciroli et al., 2017; Meng et al., 2017). It is particularly common for researchers to investigate relationships between morphology and dietary preference, as diet represents a direct and critical interaction with the environment. Identifying dietary correlates can provide insight into the functional morphology of modern species and allow for dietary inferences of taxa with unknown diets, such as extinct species (Damuth and Janis, 2011; Wilson et al., 2012; Grossnickle and Polly, 2013; Grossnickle and Newham, 2016; Slater, 2015; Olsen, 2017).

Biomechanical hypotheses underlie many studies that test for a link between diet and morphology. Different foods possess unique physical properties that require various means of mechanical digestion (Evans and Sanson, 1998; Janis, 1995; Evans et al., 2007; Lucas et al., 2008; Yamashita, 2008; Lucas et al., 2009; Ross et al., 2012; Ungar and Sponheimer, 2011; von Koenigswald et al., 2013). Because jaw morphology has a direct role in mandibular function (e.g., jaw shape helps determine in-lever lengths of attached muscles), it is expected that evolutionary changes in jaw shape will accompany evolutionary shifts in diet. Natural selection probably acts on functional trade-offs for various performance metrics (i.e., bite force, gape, mechanical advantage, occlusal precision, etc.), presumably resulting in convergent evolution of jaw morphologies in taxa with similar diets.

Considerable effort and progress has been made toward understanding associations between dental morphology and diet in mammals. Studies have examined dental correlates within mammalian subclades (e.g., taxonomic orders or families) (Kay, 1975; Hylander, 1975; Janis, 1988; Janis, 1990; Boyer, 2008; Lucas et al., 2008; Winchester et al., 2014; Santana and Cheung, 2016; Van Valkenburg, 1988; Purnell et al., 2013) and broadly across Mammalia (Evans et al., 2007; Christensen, 2014; Pineda-Munoz et al., 2017). Besides dentition, researchers have assessed additional morphological traits that may correlate with diet, such as body size, cranial morphology and jaw shape (Greaves, 1974; Radinsky, 1981; Herring and Herring, 1974; Antón, 1996; Mendoza et al., 2002; Figueirido et al., 2009; Nogueira et al., 2009; Monteiro and Nogueira, 2011; Meloro, 2011; Samuels, 2009; Price and Hopkins, 2015; Maestri et al., 2016; Pineda-Munoz et al., 2016; Lazagabaster et al., 2016; Arregoitia et al., 2017; Zelditch et al., 2017). The cranial and mandibular studies primarily focus on mammalian

subclades, increasing the likelihood of comparing homologous morphological features and providing an improved understanding of the evolution and ecology of specific clades.

However, broad comparisons of jaw morphologies and dietary preferences across Mammalia are rare, and studies that have considered general trends related to diet are often qualitative (e.g., Maynard Smith and Savage, 1959) or lack statistical correction for phylogenetic non-independence (e.g., Herring and Herring, 1974; Grossnickle and Polly, 2013). Examining morphological patterns at a broad taxonomic scale (i.e., across Theria or Mammalia) offers several benefits. For instance, it may be more likely to identify common, convergent evolutionary changes that are consistently selected for due to functional demands related to consumption of similar food items. Further, at this scale the anatomical variation associated with diet is expected to outweigh variation resulting from numerous additional factors that may affect jaw morphology, such as functional demands due to additional uses of the jaw beyond feeding (Ross et al., 2012; Davis and Pineda-Munoz, 2016). Finally, broad scale analyses will include taxa that occupy a considerable area of morphospace, which is therefore more likely to encapsulate the morphologies of diverse fossil taxa, making results more applicable to paleontological studies.

In this study, I investigate potential correlations between jaw morphology and diet in extant mammals using linear morphometrics and phylogenetic comparative methods. I examine a taxonomically and morphologically diverse sample of 203 therian (i.e., marsupial and placental) species representing 20 mammalian orders. I perform correlation analyses using both continuous dietary data and discrete dietary categories. The results identify several jaw (and dental) dimensions that are strongly correlated with diet. The most notable correlate is the distance between the jaw joint and angular process, which may be especially important because it

approximates muscle insertion areas and moment arm (i.e., in-lever) lengths of two masticatory muscles, the superficial masseter and medial pterygoid.

To further examine the influence of diet on the evolution of jaw morphologies, I use a suite of evolutionary models to test the hypothesis that there are unique selective regimes associated with herbivory and faunivory. Price and Hopkins (2015) demonstrate that mammalian body mass evolution is impacted by dietary preference, and I further test this pattern using jaw morphologies of modern mammals. Results demonstrate that correlations between diets and mandibular morphologies likely arose due to convergent evolution and distinct selective regimes. This is further supported by evidence from fossil mammals, which show a strong divergence between morphologies of herbivores and faunivores by the Eocene Epoch.

3.3 METHODS

3.3.1 Data Collection

Diets. Dietary information for 203 mammalian species was collected from the primary literature and recorded as the proportion of plant (and fungal) material in the diet (Appendix D). This builds upon the dataset compiled by Pineda-Munoz and Alroy (2014). A majority of dietary data are based on quantitative analyses of stomach contents (*sensu* Pineda-Munoz and Alroy, 2014), although diets of some taxa are based on other types of data (e.g., fecal content studies). Additional species were added to the dataset based on dietary information from the University of Michigan Museum of Zoology Animal Diversity Web (ADW) (Myers et al., 2017), but these only include entirely herbivorous (i.e., 100% plant material in diet) or faunivorous (i.e., 0% plant material in diet).

Prior to regression analyses, these data were arcsine-transformed, which is recommended for proportional data (Sokal and Rohlf, 1995). Warton and Hui (2011) argue that logit transformation is preferred to arcsine transformation. However, this requires arbitrary adjustment of 1's (i.e., 100% plant diet) and 0's (i.e., 0% plant diet) in the dataset to avoid transformed values of infinity or negative infinity, respectively. This is especially problematic for my dataset because approximately half of the species have diets of 100% plants or 0% plants, meaning that the choice of arbitrary adjustment values has a large influence on regression results. In addition, I ran analyses using logit transformation of plant data (after reassigning 1's to 0.99 and 0's to 0.01), and results were very similar to those in which data were arcsine transformed. Therefore, I chose to report results that use arcsine transformed diet data.

I recognize that the percentage of plant/animal material consumed is an oversimplification of diet, especially because material and nutritional properties of plant and animal products can vary substantially. However, using continuous dietary data offers benefits, such as allowing for application of phylogenetic generalized least squares (PGLS) analyses. In addition, compiling continuous data permits strict definitions of dietary categories, which is beneficial because a majority of taxa are some degree of omnivore (Pineda-Munoz and Alroy, 2014) and dietary classification can be particularly subjective. For one-way analyses of variance (ANOVAs) in which dietary classification in necessary, I define faunivores (i.e., insectivores and carnivores) as taxa with diets consisting of 0-5% plant material, omnivores as 5-95% plant material, and herbivores as 95-100% plant material. Although this is a broad definition of omnivore, it results in less than half of the sample (i.e., 87 of 203 species) being assigned to the omnivore group (Appendix D).

All mammals in the sample are terrestrial except for the crabeater seal (*Lobodon carcinophaga*) and two semiaquatic species, the capybara (*Hydrochoerus hydrochaeris*) and otter shrew (*Potamogale velox*). Incorporation of additional aquatic mammals into jaw shape analyses is challenging because of derived morphologies that often include the loss or severe reduction of jaw processes.

Morphometric data. Lateral jaw images were collected by photographing specimens at the Field Museum of Natural History (Appendix D). Jaws were oriented so that the jaw body was horizontal and perpendicular to the camera. Additional images were obtained from alternative sources, such as primary literature articles and the ADW (Appendix D). Morphometric jaw and molar data were collected in ImageJ (Schneider et al., 2012) for 12 linear measurements (scaled using a scale bar) and one angle (Fig. 3.1, Table 3.1, Appendix E). Jaw length (measurement 1) was always collected first, and the line for this measurement was drawn on the jaw image. This provided a guide for subsequent measurements that are parallel or perpendicular to the jaw length line (Fig. 3.1, Table 3.1).

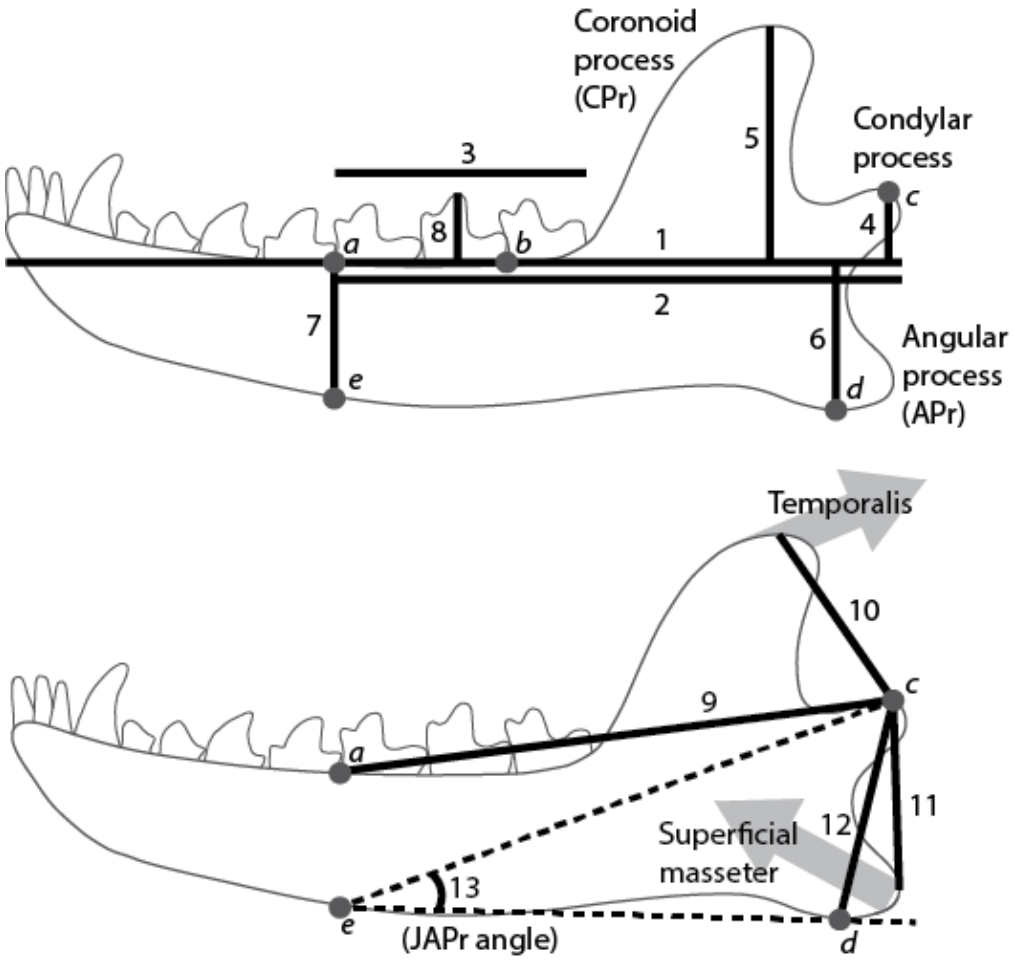

Figure 3.1. Mandibular measurements tested for correlation with diet. The top image displays measurements that are perpendicular or parallel to the jaw length line (i.e., measurement 1), which is drawn through point *a* (between the ultimate premolar and first molar at the alveolar margin) and point *b* (between the penultimate and ultimate molars at the alveolar margin). The bottom image displays measurements involving the articulation surface of the condylar process (i.e., jaw joint, point *c*). This includes measurements associated with functional aspects of rotation around an axis through the jaw joints, including measurements that approximate the out-lever when bites are at the first lower molar (measurement 9), in-lever lengths for the temporalis muscle (measurement 10), and in-levers for the superficial masseter and medial pterygoid muscles (measurement 12). Measurement 8 is the maximum erupted height of any molar above the jaw length line. Measurement 13 is an angle that is similar to measurement 12 in that it captures the distance between the jaw joint and the ventral edge of the angular process (point *d*). Descriptions of all measurements are provided in Table 3.1.

Table 3.1. Descriptions of jaws measurements that were collected in this study (Appendix E) and are shown in Figure 3.1. Numbers in parentheses after measurements correspond to the numbers in Figure 3.1. Lateral jaw images were used for all measurements, although if the coronoid process was blocking the view of posterior molars (which is often the case in rodents; Fig. 3.2) then medial and dorsal views were used to assist with the molar row measurement (3) and placement of point *b*.

Measurement	Description
Jaw length (1)	Distance from the anterior-most point of the mandible (excluding incisors) to the posterior-most margin of the condylar process (CPr). The measurement is made as a line that passes along the alveolar margin (i.e., base) of the molar row (Fig. 3.1). Curvature of jaw bodies and molar rows in some species (Figs. 3.1 and 3.2) can make the placement of this measurement line difficult or subjective, and therefore I define the base of the molar row as a line between points *a* and *b*. Point *a* is between the base of the ultimate lower premolar and first lower molar (m1), and point *b* is between the base of the penultimate and ultimate molars. All additional measurements shown in the upper jaw image of Figure 3.1 (i.e. measurements 2-8) are either parallel or perpendicular to this line.
m1 to posterior jaw (2)	Distance from point *a* to the posterior-most margin of the condylar process, parallel to the jaw length line (i.e., parallel to the base of the molar row as defined above).
Molar row (3)	Maximum length of the molar row, with the measurement taken parallel to the jaw length line. The number of molars can vary between taxa (e.g., marsupials tend to have four and placentals tend to have three), but all molars of a species were included in this measurement.
Joint elevation (4)	Elevation of the jaw joint (point *c*) above the jaw length line, measured orthogonal to the jaw length line. The jaw joint is defined as the medial point of the condylar process articulation surface, and if an articulation surface is not visible or apparent then the posteroventral-most point of condylar process is used.
CPr elevation (5)	Maximum elevation of the coronoid process (CPr) above the jaw length line, measured orthogonal to the jaw length line and ending at the dorsal-most point of the CPr margin.
APr depth (6)	Maximum depression of the angular process (APr) below the jaw length line, measured orthogonal to the jaw length line and ending at the ventral-most point of the angular process margin (point *d*). If the angular process is not well defined (e.g., it is often a rounded region in primates and ungulates, or inflected in marsupials), then the dorsal-most point of the mandibular ramus region is used. See Figure 3.2 and the accompanying text for additional discussion on the placement of point *d*.
Corpus depth (7)	Depth of the mandibular corpus, measured from point *a* (i.e., point between the base of the ultimate premolar and first molar) to the ventral margin of the jaw (point *e*). The measurement is orthogonal to the jaw length line.
Molar depth (8)	Maximum elevation of any molar above the jaw length line (i.e., alveolar margin), measured orthogonal to the jaw length line. The most elevated point of any molar is used for each specimen, meaning that any molars (and any cusps) along the molar row can be used. However, the ultimate molar is excluded from this measurement if it is significantly upturned with the coronoid process.
Joint to m1 (9)	The distance between point *a* and point *c* (jaw joint). See above for definitions of these points.

Table 3.1, continued.

JCPr (10)	The jaw joint-to-coronoid process (JCPr) distance, measured between point *c* (jaw joint) and the dorsal-most point along the margin of the CPr (see measurement 5).
JAPr posterior (11)	The jaw joint-to-angular process (JAPr) distance, measured between point c (jaw joint) and the posterior-most point along the margin of the APr.
JAPr ventral (12)	The jaw joint-to-angular process (JAPr) distance, measured between point c (jaw joint) and the ventral-most point along the margin of the angular process (point *d*). See the description of measurement 6 for a definition of point *d*, and see Figure 3.2 and accompanying text for additional discussion of this point.
JAPr angle (13)	The jaw joint-angular process (JAPr) angle, created by point c (jaw joint), point *e*, and point *d*. See descriptions above for definitions of these points, and see Figure 3.2 and accompanying text for additional discussion of this measurement.

These jaw measurements are expected to capture functionally relevant aspects of the jaw morphology. For instance, the distance from the jaw joint to the dorsal margin of the coronoid process (measurement 10 in Figure 3.1) roughly represents the in-lever (or moment arm) for the temporalis muscle (Turnbull, 1970) when the axis of rotation is mediolaterally-directed and through the jaw joint. The single angle metric (measurement 13, JAPr angle) was inspired by a similar measurement in Arregoitia et al. (2017), which they found to be correlated with diet in rodents. See the Table 3.1 for descriptions and discussion of these measurements. Jaw measurement data are available in Appendix E.

Although a majority of jaw measurements are collected from jaw images without issue, some taxa include derived jaw (or molar) morphologies that make particular measurements challenging or subjective. Thus, I provide additional notes on my methods and measurement decisions here. Because I use the jaw joint-to-angular process (JAPr) angle for evolutionary modeling analyses, I primarily focus on issues related to the angular process (APr) and the points (from Figure 3.1) that are necessary for the JAPr measurement (Figure 3.2).

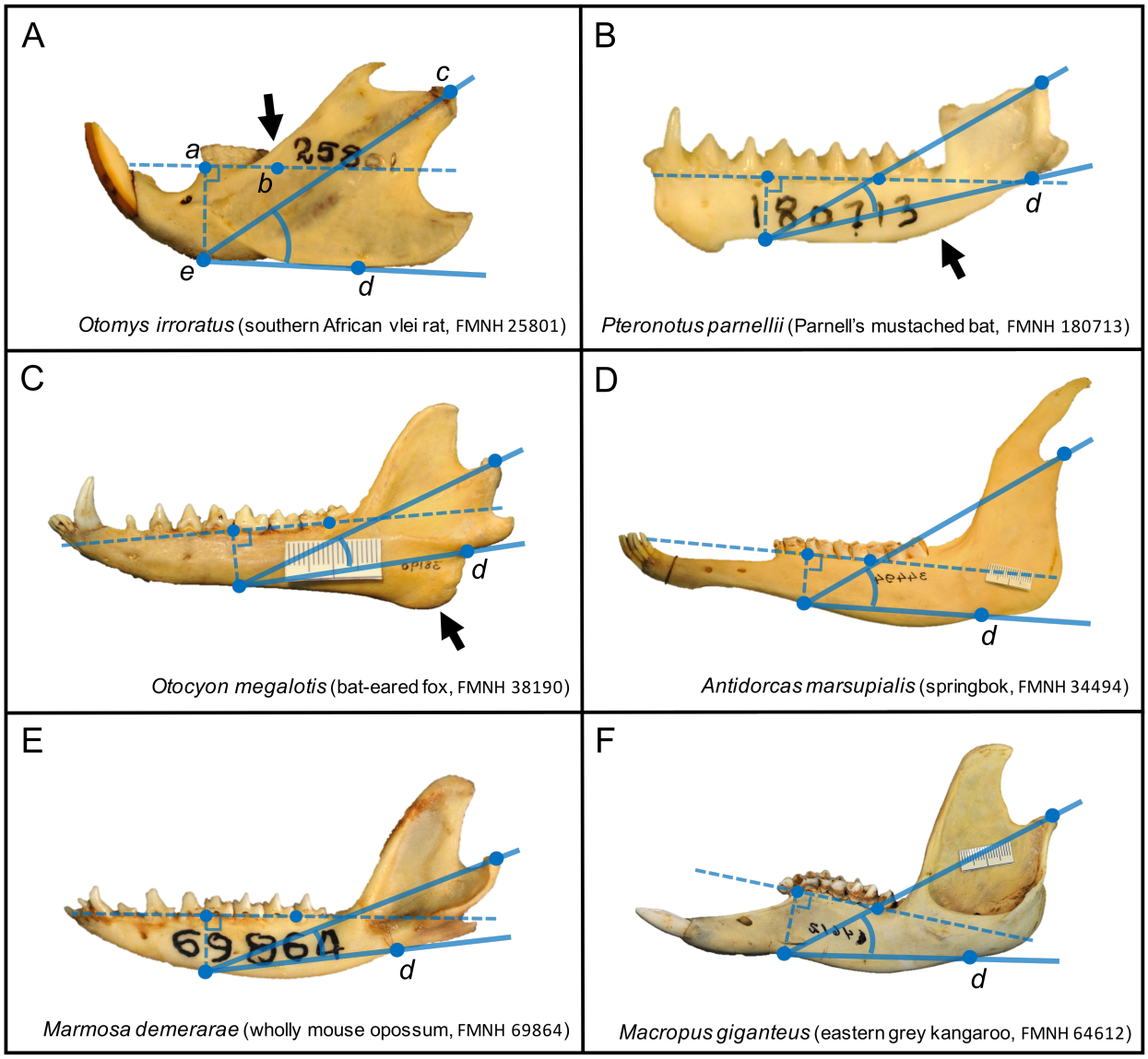

Figure 3.2. Examples of jaws that present unique challenges for measurement collection. The horizontal dashed line represents the jaw length (measurement 1 in figure 1), the vertical dashed line is the corpus depth (measurement 7) that is also used to determine point *e*, and the solid blue lines denote the jaw joint-angular process angle (JAPr angle, measurement 13). The *Otomys* jaw (*A*) includes labels of points from figure 1, and it highlights the anterior extension of the coronoid process (arrow) which can obstruct the view of point *b*. Bat mandibles (*B*) can have especially curved jaw bodies (arrow) and small rami, with point *d* at the approximate level of the jaw length line. *Otocyon* (C) and *Urocyon* have a subangular lobe (arrow), which is ignored for APr measurements. Some taxa have angular processes that are difficult to define due to broad expansion (e.g., ungulates, *D*) or somewhat hidden due to medially inflection (e.g., marsupials, *E* and *F*). For these taxa, point *d* was placed at the merger between the mandibular body and the anterior margin of the APr. See text for additional explanations.

Many primates, ungulates, and herbivorous marsupials do not possess distinct APrs and instead have broad, rounded processes (Fig. 3.2). In addition, taxa such as rodents may have expanded APrs that extend anteriorly (Fig. 3.2). These expanded processes can make APr-related measurements challenging because the ventral-most and posterior-most APr points, which are used as guides in measurements (Fig. 3.1), are not as apparent as in additional taxa. For ungulates and marsupials, the anterior-most point of the APr (i.e., where it merges with the mandibular body) is often also the most ventral point, and therefore I commonly placed point *d* at this location. See point *d* for jaws in Figure 3.2 for examples.

It is worth noting that APr-related measurement issues are less likely to affect the JAPr angles than the JAPr distances. For instance, altering the location of point *d* for *Otomys* (Fig. 3.2A) by shifting it anteriorly or posteriorly along the APr margin will result in a considerable change to the JAPr distance (measurement 12), which is measured from the jaw joint to point *d*. However, the same change in position of point *d* is not expected to significantly alter the JAPr angle because the vector through point *e* and point *d* should remain almost identical. Similarly, if inflected APrs (which are present in some marsupials and rodents) were less inflected (i.e., they were rotated ventrally and laterally), it may result in point *d* being shifted posteriorly, shortening the JAPr distance. But the posterior shift of point *d* is less likely to significantly alter the JAPr angle, because a posterior shift in point *d* does not necessarily mean that the vector through points *e* and *d* will change. This consideration is one of the reasons why the JAPr angle was chosen for evolutionary modeling analyses instead of the JAPr distance, and it provides evidence that the subjective nature of some APr measurements do not affect the broad results of this study.

A unique issue for APr measurements of *Otocyon* and *Urocyon* is that the taxa possess a subangular lobe that is anteroventral to the angular process (Fig. 3.2C). This lobe is not homologous to the APr, and it is unlikely to be functionally analogous because it is an insertion site for the digastric muscle, not the superficial masseter or medial pterygoid (Ewer 1973). Thus, APr measurements were taken of the true APr, not the subangular lobe (Fig. 3.2C).

Molar-related measurements can present unique concerns, such as determining locations of points *a* and *b* (figs. 1 and A1). For instance, the number of molars can vary between taxa. Most placentals possess three molars, but some carnivores have fewer than three and *Otocyon* has four (Fig. 3.2C). In addition, marsupials tend to have four molars (Fig. 3.2E and F). Despite the differences in number of molars, the molar row (measurement 3) was always measured as the anteroposterior length of all molars of that species. Also, I define point *a* based on m1 (which is present in all mammals of this study), and point *b* is defined as being between the penultimate and ultimate molars. *Crocuta crocuta* and *Lynx rufus* possess only one molar (a large carnassial), and therefore point *b* was placed at the posterior margin of m1 in these taxa.

Rodents often possess posterior molars that are partially hidden by the anterior extension of the coronoid process (Fig. 3.2A). This makes it challenging to collect measurements that include molars (i.e. measurements 3 and 8) or determine point *b* for drawing the jaw length line (Fig. 3.1, Table 3.1). To help measure the molar row length for these species, I took dorsal photographs of the dentitions. These photographs also assisted in locating the anterior-posterior position of point *b* because they provide a view of the junction of the penultimate and ultimate molar (see black arrow in Figure 3.2A).

Some modern mammals were excluded from analyses because their jaw morphologies are too derived. These primarily include taxa with long, slender jaws that are often missing

distinct jaw processes or dentitions (e.g., pangolins, cetaceans, honey possums, monotremes). However, many of these taxa are insectivorous or carnivorous, and if JAPr measurements were collected it is expected that these would be relatively small values (due to the long, slender shape of the jaws), matching the expectations of this study. Thus, exclusion of these taxa is not expected to influence the overall conclusions of this study.

Body mass. Body mass estimates were primarily obtained via the PanTHERIA database (Jones et al. 2009), and body masses for additional species that are not in the PanTHERIA database were supplied by the ADW or primary literature. These data are provided in Appendix D. Linear measurements and body mass data were $\log_{10}$-transformed prior to correlation analyses.

3.3.2 Phylogeny

I produced an informal supertree by grafting together pruned versions of previously published phylogenies. Merging multiple trees instead of pruning the species-level supertree of Bininda-Emonds et al. (2007) (or a derivative) was preferred because branch lengths and topology of the Bininda-Emonds et al. (2007) tree are often inconsistent with phylogenies of mammalian subgroups (Slater et al., 2012). All source trees are molecular phylogenies, and time scaled branch lengths of the tree are molecular clock estimates reported in the source publications. No polytomies are present in the tree topology. Separate analyses are performed for glirans and non-gliran datasets, and therefore the supertree was altered for these datasets.

The following is a complete list of sources for the phylogenetic data, with the primary source after the major clade and supplementary sources noted separately:

Basal nodes: dos Reis et al. (2012)

Metatherians: Mitchell et al. (2014)

- Dasyuromorphia, including the approximate divergence age for the extinct thylacine (*Thylacinus cynocephalus*): Westerman et al. (2015)
- Topology of *Marmosa* species: Voss et al. (2014)

Afrotheria: Meredith et al. (2011)

- Afrosoricia: Tabuce et al. (2008)

Bovidae: Bibi (2013)

Carnivora: Eizirik et al. (2010)

- Canidae: Slater et al. (2012)
- Mustelidae: Koepfli et al. (2008)

Chiroptera: Agnarsson et al. (2011)

- Phyllostomidae: Baker et al. (2010)
- *Myotis*: Ruedi et al. (2013)
- *Nycticeius*: Lack et al. (2010)
- Pteropodidae: Almeida et al. (2014)

Eulipotyphla: Sato et al. (2016)

- *Myosorex*: Dubey et al. (2007)
- Talpidae: He et al. (2016)

Primates: Springer et al. (2012)

Macroscelididae: Smit et al. (2011)

Rodentia: Fabre et al. (2012)

- Murinae: Kimura et al. (2015)
- Gerbillinae: Alhajeri et al. (2015)

- Cricetidae: Maestri et al. (2017) and Steppan et al. (2004)
- Caviomorpha: Patterson & Upham (2014)
- *Peromyscus*: Platt et al. (2015)
- *Tamias* and *Neotamias*: Sullivan et al. (2014)

Xenarthra: Gibb et al. (2015)

Additional taxa/nodes: Meredith et al. (2011) and Bininda-Emonds et al. (2007)

The informal supertree allows for the phylogenetic relatedness of taxa to be incorporated into analyses. However, there are several concerns with using an informal supertree. First, there are inconsistencies in topology and branch lengths between overlapping portions of the source phylogenies, and I arbitrarily resolved some of these issues. Second, the topologies of source trees may be altered if the original phylogenetic analyses were performed with a different sample of taxa, such as the species in my dataset. Third, the supertree cannot account for uncertainty associated with tree topology and branch lengths.

Due to these concerns with the supertree, future work should replace this phylogeny with a molecular phylogeny either produced by downloading gene sequences from GenBank and running an independent analysis, or by using a species-level tree to be published in the near future (Nathan Upham, personal communication 2017).

3.3.3 Correlation and modeling analyses

Size correction. There is considerable variation in body size among mammals, but the primary goal of this study is to examine the correlation between jaw shape and diet. Thus, differences in jaw sizes were accounted for by regressing $\log_{10}$-transformed linear measurements against $\log_{10}$-transformed jaw length using PGLS. This and all subsequent analyses were

implemented using R software (R Core Team, 2016). PGLS was performed using the *gls* function in the *nlme* package (Pinheiro et al., 2016), and the regression model was fit while simultaneously estimating Pagel's lambda via maximum likelihood (Revell, 2010). Residuals from this regression were used for subsequent correlation analyses with dietary data. This method of size correction is beneficial in that it also removes variation associated with allometry. Values for the single angle measurement were left untransformed.

Glires versus non-Glires. A primary goal of this study is to identify mandibular correlates of diet. Thus, several types of statistical analyses were used to explore the ability of morphological traits to predict diet, and these are described below. In addition to running these analyses for all mammals of this study, analyses were performed independently for non-glirans and glirans (i.e., rodents and lagomorphs). The Glires group includes two lagomorphs and 71 rodents (Appendix D). The decision to separate glirans from the overall sample is due to their derived features, such as ever-growing incisors, evolution of unique jaw musculature (e.g., Cox and Baverstock, 2016), and the propensity to use proal (i.e., forward) jaw movement and occlusion during mastication (rather than orthal or transverse occlusion as in most other mammals).

Regressions and pANOVAs. I analyzed the relationship between the dietary data (i.e., arcsine-transformed proportion of dietary plant material) and the residuals from the size-correcting regressions for jaw metrics. First, I used bivariate PGLS regressions to predict the proportion of plant material in the diet using the residuals for 11 jaw measurements (fig. 3.1). Log-transformed body mass and jaw joint-to-angular process angle (i.e., JAPr angle; measurement 13) were also independently modeled against diet. Further, I tested for statistical differences among dietary groups (faunivores, omnivores, and herbivores) using phylogenetic

one-way analysis of variance (pANOVA), performed with the *phylANOVA* function in the *phytools* package (Revell 2012).

In addition to bivariate regressions, multiple regressions were performed to simultaneously model 11 linear metrics against diet data via PGLS. Body mass and JAPr angle were excluded from these analyses. To help determine which combinations of variables are the best predictors of diet, the *dredge* function of the *MuMIn* package (Barton 2016) was used to evaluate model performance based on sample-size-corrected Akaike information criterion (AICc) values (Akaike, 1974; Hurvich and Tsai, 1989). AICc calculations are based on maximum likelihood values and penalize models with greater numbers of parameters. All models with ΔAICc values below 2.0 are reported here and used to calculate Akaike weights (Burnham and Anderson, 2003), which allows for easier interpretation of the relative performances of models.

Mode of evolution. To further test the hypothesis that dietary preference has influenced the evolution of mammalian jaw morphologies, I first categorized extant species and ancestral nodes of the phylogeny into two regimes: 1) plant-dominated diet (i.e., greater than 50% of diet is plant material; 'herbivore') and 2) animal-dominated diet (i.e., less than 50% of diet is plant material; 'faunivore'). Diets at ancestral nodes were inferred with the *ace* function of the *ape* package (Paradis et al. 2004), using the default settings of residual maximum likelihood and a Brownian motion (BM) model of evolution. Ancestral states were reconstructed using continuous data (i.e., percentage of plant material in diet), and from these results the nodes were assigned to the herbivore regime (>50% plant material) or faunivore regime (<50% plant material). I do not test for an omnivore selective regime because omnivores include a considerable diversity of diets (Pineda-Munoz and Alroy, 2014; taxa with between 5% and 95%

plant material in their diet as defined in this study) and a majority of ancestral nodes would classify as omnivores.

Four evolutionary models were fit to the data for the JAPr angle (measurement 13 in Figure 3.1) to test the influence of diet on the evolution of jaw morphology. The JAPr angle was chosen for modeling because it (and the similar JAPr distance) shows the strongest association with diet. (Rationale for using the JAPr angle instead of the JAPr distance is provided in 3.4 Results.) The early burst (EB) model was fit using the *fitContinuous* function in the package *geiger version 2.0* (Pennell et al., 2014), and all other models were fitted using functions in the *OUwie* package (Beaulieu and O'Meara, 2016). Model performance was evaluated using AICc weights.

A BM model (i.e., "BM1") with a single phylogenetic mean (θ) serves as the null hypothesis, and it models evolutionary rate (σ^2) under the assumption of stochastic evolutionary change from a central tendency. For my dataset, support for this model would indicate that dietary category is not having a strong influence on the evolution of the jaw morphology. The second model is a single optimum Ornstein-Uhlenbeck (OU) model (Hansen, 1997; Butler and King, 2004). OU models include an additional parameter, α, which represents the strength of attraction toward a trait optimum (θ) and is commonly described as the "rubber band parameter." If results support this model, it would indicate that jaw morphologies are attracted to an optimum morphology, but, like the BM model, it would not provide support for the hypothesis that diet is influencing the evolution of jaw morphologies. Third, I tested an EB model (Harmon et al., 2010), which assumes that evolutionary rates of morphological change decrease exponentially over time, and this change is modeled using a rate change parameter (*a*). Support for this model (and a positive *a* value) would sugest that mammals radiated rapidly early in their history and

then evolutionary rates slowed down over time, possibly as niches or adaptive zones were filled. Finally, a BMS model was fit to the data. This is a variation of a BM model in which taxa of the two selective regimes (i.e., faunivores and herbivores) are permitted unique phylogenetic means (θ) and evolutionary rates (σ^2). In contrast to multiple optima OU models (see below), BMS does not model a mechanism for the shift from one selective regime to another. Rather, changes in diet are modeled as instantaneous shifts. It is worth noting, however, that fluctuating phylogenetic means could help explain how this change occurs and why both diets show considerable variation in morphologies. Unlike the previous models, support for BMS will provide evidence for the hypothesis that diet is having a large influence on the evolution of jaw morphologies.

In addition to the single optimum OU model, multiple optima OU models were initially fit to the data. However, I chose to exclude these models from the results because multiple lines of evidence contradict an OU process for the evolution of JAPr angles (and body mass). First, the reported phylogenetic signal for JAPr angles is very high (Pagel's $\lambda = 0.973$), indicating a BM mode of evolution that discounts an OU process. Second, α parameter estimates for multi-peak OU models were very low (e.g., $\alpha = 0.006$ for the best-fitting OU model). The phylogenetic half-life for $\alpha = 0.006$ is approximately 115 million years, which is considerably longer than the age of all but one node of my phylogeny. This suggests that if an OU process is occurring, it is extremely weak (Cooper et al., 2016). Third, I am interested in comparing evolutionary rates of herbivores and faunivores, and values of these rates can only be interpreted in a model-dependent context (Hunt, 2012). The additional α parameter of an OU model makes interpretation of evolutionary rate estimates more complex in an OU framework. Finally, the

AIC values for the multiple optima OU models were very similar to the AIC value of the BMS model, indicating that these models were not significantly better than BMS at modeling the data.

I predict that diet has a considerable influence on the evolution of jaw morphologies, with herbivores and faunivores evolving toward unique adaptive peaks. This hypothesis is supported if the BMS model outperforms additional models, because this model allows for unique phylogenetic means for the two dietary groups.

3.3.4 Fossil analysis

A goal of this study is to identify one or more jaw correlates of diet that can be readily applied to fossil taxa to examine the evolutionary patterns of mammals The JAPr angle (measurement 13) is strongly correlated with diet and does not require size correction, and it is the focus of the evolutionary modelling analyses. Thus, I chose to apply this metric to early therian fossils, with the objective of examing the early evolutionary patterns of this clade.

Fossil jaw images were collected for 142 genera from the Cretaceous through Eocene (i.e., 145-33.9 million years ago (Ma)), and the JAPr angle was measured for these jaws (Appendix F). Cretaceous fossil jaw images include those used in Grossnickle and Polly (2013) (see citations within), as well as recently published images of *Didelphodon vorax* (Wilson et al., 2016) and *Procerberus* (Clemens, 2017). Paleocene and Eocene fossil jaw images are primarily from Rose (2006) (and citations within), Osborn (1929), Matthew (1937), Lopatin (2006), Scott and Jepsen (1936), and Scott (1940). Data was collected at the genus level, and therefore one jaw was chosen (generally based on preservation quality) to represent a genus if multiple images or species were available. However, one exception was made. JAPr angle results for *Didelphodon vorax* and *D. coyi* were considerably different, and therefore both were included in the analysis.

Temporal age ranges of genera are based on first and last appearances in the fossil record, which were obtained from vetted Paleobiology Database (www.paleobiodb.org) occurrrene data (Appendix F). For calculating the standard deviation and ranges of JAPr angles, taxa were assigned to time bins. For the Cretaceous and early Paleocene, these bins are consistent with Grossnickle and Newham (2016) and Chapter 4. A full list of time bins (with dates from Gradstein et al., 2012) is given here: *1*, Barremian-Aptian (130.8-113 Ma); *2*, Albian (113-100.5 Ma); *3*, Cenomanian-Turonian (100.5-89.6 Ma); *4*, Coniacian-Santonian (K4; 89.6-83.6 Ma); *5*, Early Campanian (83.6-78 Ma); *6*, Middle-Late Campanian (78-72.1 Ma); *7*, Maastrichtian (72.1-66 Ma); *8*, Early Danian (66-64.6 Ma); *9*, Late Danian (D2; 64.6-61.3 Ma); *10*, Selandian (61.6-59.2 Ma); *11*, (59.2-56 Ma); *12*, early Ypresian (56-51 Ma); *13*, late Ypresian (51-47.8 Ma); *14*, Lutetian (47.8-41 Ma); *15*, Bartonian (41-38 Ma); and *16*, Priabonian (38-33.9 Ma). I treat the early Danian (8) bin as equivalent to the Puercan North American Land Mammal Age (NALMA) and the late Danian (9) bin as equivalent to the Torrejonian NALMA.

As a metric for JAPr disparity through time, standard deviation of JAPr angles were calculated independently for each time bin. In addition, the overall range of angles per time bin were recorded. The range is expected to be heavily influenced by sample sizes in the time bins, and therefore I subjected samples from each bin to subsampling via rarefaction. This allows for a more accurate comparison between bins of various sample sizes (Foote, 1992). Five taxa were subsampled (without replacement) and the range was calculated, and this procedure was reported 1000 times and median values were recorded.

3.4 RESULTS

3.4.1 Mandibular correlates of diet

Results of PGLS regressions and pANOVAs identify several jaw and molar metrics that are significantly associated with diet even after accounting for the phylogenetic non-independence of data (Tables 3.2-3.4, Fig. 3.3). The best performing jaw and molar correlates are displayed in Figure 3.3A for non-glirans and Figure 3.3C for glirans (rodents and lagomorphs). These metrics show significant correlations with diet in bivariate regressions, multiple regressions, and/or pANOVAs (Tables 3.2-3.4). Note, however, that glirans and non-glirans do not display the same trends for all variables. For instance, the maximum erupted molar depth (measurement 8) is significantly correlated with diet in glirans and in non-glirans, but the correlations are in the opposing directions: gliran herbivores have taller erupted molars than faunivores, and non-gliran herbivores have shorter erupted molars than faunivores (Tables 3.2 and 3.3, Fig. 3.3). As a result, the total sample of mammals does not show a significant correlation between erupted molar depth and diet.

Table 3.2. Summary statistics for phylogenetic one-way analyses of variance (pANOVAs). Numbers in parentheses after variable names correspond to the measurement number in Figure 3.1, and measurements are described in Table 3.1. Results in bold are the jaw-diet correlations that are depicted in Figures 3.3A and 3.3C, and results in italics are those that are displayed in Figures 3.3B and 3.3D. Prior to analyses, jaw measurements (except JAPr angle) were $\log_{10}$ transformed and regressed (via PGLS) against jaw length to minimize the influence of body mass as a variable (see Methods), and the proportion of plant material in the diet was arcsine transformed. Abbreviations: APr, angular process; CPr, coronoid process; *F*-stat., *F*-statistic; JAPr, joint-to-angular process; JCPr, joint-to-coronoid process; m1, first lower molar; post., posterior.

	Variable	***F*-stat.**	***p*-value**
Mammalia	Body mass	10.590	0.050
(n = 203)	JAPr angle (13)	38252	<0.001*
	m1 to post. jaw (2)	1.702	0.628
	Molar row (3)	1.638	0.609
	Joint elevation (4)	7.478	0.109
	CPr elevation (5)	2.244	0.498
	APr depth (6)	27.638	<0.001
	Corpus depth (7)	29.632	<0.001
	Molar depth (8)	15.186	0.010
	Joint to m1 (9)	0.180	0.948
	JCPr (10)	2.734	0.433
	JAPr post. (11)	31.542	<0.001
	JAPr ventral (12)	43.622	<0.001*
Non-Glires	Body mass	11.706	0.015
(n = 130)	JAPr angle (13)	23.816	0.001
	m1 to post. jaw (2)	1.685	0.455
	Molar row (3)	0.657	0.738
	Joint elevation (4)	**2.405**	**0.327**
	CPr elevation (5)	**3.379**	**0.231**
	APr depth (6)	**11.706**	**0.007**
	Corpus depth (7)	6.177	0.062
	Molar depth (8)	**5.967**	**0.072**
	Joint to m1 (9)	0.982	0.591
	JCPr (10)	*6.078*	*0.071*
	JAPr post. (11)	14.163	0.003
	JAPr ventral (12)	***19.501***	***0.002***
Glires	Body mass	6.698	0.016
(n = 73)	JAPr angle (13)	4.089	0.051
	m1 to post. jaw (2)	**1.723**	**0.306**
	Molar row (3)	**11.163**	**0.003**
	Joint elevation (4)	3.207	0.106
	CPr elevation (5)	5.182	0.035
	APr depth (6)	2.211	0.208
	Corpus depth (7)	**19.01**	**0.001**
	Molar depth (8)	**7.371**	**0.004**
	Joint to m1 (9)	0.581	0.716
	JCPr (10)	*0.265*	*0.864*
	JAPr post. (11)	7.384	0.004
	JAPr ventral (12)	***17.50***	***0.001****

*Pairwise comparisons of dietary groups are all significantly different ($p < 0.01$) via the Holm-Bonferroni post hoc test.

Table 3.3. Summary statistics for bivariate regression PGLS. Numbers in parentheses after variable names correspond to the measurement number in Figure 3.1, and measurements are described in Table 3.1. Results in bold are the jaw-diet correlations that are depicted in Figures 3.3A and 3.3C. Prior to analyses, jaw measurements (except JAPr angle) were $\log_{10}$ transformed and regressed (via PGLS) against jaw length to minimize the influence of body mass as a variable (see Methods), and the proportion of plant material in the diet was arcsine transformed. Abbreviations: λ, Pagel's lambda; APr, angular process; CPr, coronoid process; Est., estimate; JAPr, joint-to-angular process; JCPr, joint-to-coronoid process; m1, first lower molar; post., posterior; SE, standard error, *t*-stat; *t*-statistic.

	Variable	**Est.**	**SE**	***t*-stat.**	***p*-value**	λ
Mammalia	Body mass	0.162	0.047	3.415	0.001	0.989
(n = 203)	JAPr angle (13)	0.019	0.004	4.999	<0.001	0.973
	m1 to post. jaw (2)	2.445	0.971	2.519	0.013	0.996
	Molar row (3)	0.749	0.310	2.416	0.017	0.993
	Joint elevation (4)	0.478	0.140	3.411	0.001	0.989
	CPr elevation (5)	1.098	0.273	4.028	<0.001	0.985
	APr depth (6)	0.250	0.094	2.675	0.008	0.988
	Corpus depth (7)	1.574	0.288	5.457	<0.001	0.983
	Molar depth (8)	0.063	0.248	0.253	0.801	0.993
	Joint to m1 (9)	2.488	0.870	2.856	0.005	0.994
	JCPr (10)	0.409	0.283	1.445	0.150	0.992
	JAPr post. (11)	1.473	0.331	4.438	<0.001	0.980
	JAPr ventral (12)	2.215	0.295	7.486	<0.001	0.983
Non-Glires	Body mass	0.206	0.057	3.624	<0.001	0.994
(n = 130)	JAPr angle (13)	0.018	0.004	4.012	<0.001	0.973
	m1 to post. jaw (2)	0.975	1.118	0.872	0.385	0.995
	Molar row (3)	-0.711	0.465	-1.530	0.129	0.997
	Joint elevation (4)	**0.451**	0.161	**2.810**	**0.006**	0.994
	CPr elevation (5)	**1.499**	0.456	**3.29**	**0.001**	0.995
	APr depth (6)	**0.211**	0.100	**2.109**	**0.037**	0.990
	Corpus depth (7)	0.955	0.449	2.126	0.035	0.988
	Molar depth (8)	**-0.965**	0.325	**-2.966**	**0.004**	0.990
	Joint to m1 (9)	1.094	1.082	1.011	0.314	0.994
	JCPr (10)	0.415	0.467	0.887	0.377	0.994
	JAPr post. (11)	1.263	0.420	3.246	0.002	0.980
	JAPr ventral (12)	**1.891**	**0.379**	**4.983**	**<0.001**	**0.975**
Glires	Body mass	0.103	0.084	1.234	0.222	0.954
(n = 73)	JAPr angle (13)	0.022	0.008	2.648	0.010	0.921
	m1 to post. jaw (2)	**6.971**	1.887	**3.694**	**<0.001**	0.980
	Molar row (3)	**2.031**	0.342	**5.936**	**<0.001**	0.951
	Joint elevation (4)	0.593	0.287	2.069	0.042	0.929
	CPr elevation (5)	1.068	0.315	3.391	0.001	0.871
	APr depth (6)	0.323	0.289	1.119	0.267	0.953
	Corpus depth (7)	**2.033**	**0.362**	**5.612**	**<0.001**	**0.877**
	Molar depth (8)	**1.542**	**0.242**	**6.365**	**<0.001**	**1.023**
	Joint to m1 (9)	5.145	1.422	3.619	0.001	0.961
	JCPr (10)	0.322	0.357	0.903	0.370	0.970
	JAPr post. (11)	1.626	0.583	2.792	0.007	0.946
	JAPr ventral (12)	**2.956**	**0.497**	**5.946**	**<0.001**	**0.781**

Table 3.4. Summary statistics for multiple regression PGLS. Numbers in parentheses after variable names correspond to the measurement number in Figure 3.1, and measurements are described in Table 3.1. Results in bold are the jaw-diet correlations that are depicted in Figures 3.3A and 3.3C. Prior to analyses, jaw measurements (except JAPr angle) were $\log_{10}$ transformed and regressed (via PGLS) against jaw length to minimize the influence of body mass as a variable (see Methods), and the proportion of plant material in the diet was arcsine transformed. See Table 3.3 caption for abbreviations.

	Variable	**Est.**	***t*-stat.**	***p*-value**
Mammalia	m1 to post. jaw (2)	0.165	0.154	0.878
(n = 203)	Molar row (3)	0.637	1.558	0.121
	Joint elevation (4)	0.268	1.550	0.123
	CPr elevation (5)	0.150	0.473	0.637
	APr depth (6)	0.195	1.868	0.063
	Corpus depth (7)	0.572	1.541	0.125
	Molar depth (8)	-0.549	-1.917	0.057
	Joint to m1 (9)	-0.005	-1.523	0.129
	JCPr (10)	0.007	0.797	0.426
	JAPr post. (11)	-0.712	-1.511	0.132
	JAPr ventral (12)	1.758	3.191	0.002
Non-Glires	m1 to post. jaw (2)	1.442	1.145	0.255
(n = 130)	Molar row (3)	-0.513	-0.858	0.393
	Joint elevation (4)	**0.357**	**1.889**	**0.061**
	CPr elevation (5)	**0.601**	**1.114**	**0.268**
	APr depth (6)	**0.191**	**1.670**	**0.098**
	Corpus depth (7)	-0.067	-0.129	0.898
	Molar depth (8)	-0.943	**-2.527**	**0.013**
	Joint to m1 (9)	-0.005	-1.192	0.236
	JCPr (10)	0.005	0.476	0.635
	JAPr post. (11)	-0.246	-0.409	0.683
	JAPr ventral (12)	**1.358**	**2.061**	**0.042**
Glires	**m1 to post. jaw (2)**	**-0.765**	**-0.352**	**0.726**
(n = 73)	**Molar row (3)**	**1.141**	**1.809**	**0.075**
	Joint elevation (4)	-0.516	-1.163	0.249
	CPr elevation (5)	0.252	0.530	0.598
	APr depth (6)	-0.298	-0.842	0.403
	Corpus depth (7)	**1.239**	**2.290**	**0.026**
	Molar depth (8)	**0.321**	**0.751**	**0.455**
	Joint to m1 (9)	0.026	1.026	0.309
	JCPr (10)	-0.052	-1.388	0.170
	JAPr post. (11)	-0.366	-0.528	0.599
	JAPr ventral (12)	**1.605**	**1.533**	**0.130**

Table 3.5: Best performing models (i.e., those with ΔAICc values less than 2) of phylogenetic generalized least squares (PGLS) multiple regression using various combinations of jaw measurements. Numbers in parentheses correspond to measurements in Figure 3.1. The PGLS analyses were run using residuals of the PGLS regressions against jaw length (measurement 1), and therefore measurement 1 was not included in these analyses. Because JAPr angle (measurement 13) was not regressed against jaw length (see Methods), it was also excluded from these analyses. Note the prevalence of the JAPr distance (measurement 12) in the models, including it being the sole measurement for the second best performing model for the Mammmalia sample. Abbreviations: AICc, corrected Akaike information criterion; df, degrees of freedom; log-lik., logarithmic-likelihood; weight, Akaike weight.

Group	Model	Jaw measurements							df	log-lik.	ΔAICc	Weight
Mammalia	1				(7)			(12)	5	-71.435	0	0.121
	2							(12)	4	-72.490	0.01	0.120
	3	(2)						(12)	5	-71.620	0.37	0.100
	4	(2)			(7)			(12)	6	-70.612	0.48	0.095
	5				(7)		(11)	(12)	6	-70.846	0.95	0.075
	6						(11)	(12)	5	-72.005	1.14	0.068
	7	(2)			(7)		(11)	(12)	7	-69.997	1.39	0.060
	8	(2)					(11)	(12)	6	-71.095	1.44	0.059
	9			(5)				(12)	5	-72.164	1.46	0.058
	10		(3)			(8)		(12)	6	-71.218	1.69	0.052
	11			(5)	(7)			(12)	6	-71.246	1.75	0.050
	12		(3)		(7)	(8)		(12)	7	-70.212	1.82	0.049
	13	(2)		(5)				(12)	6	-71.328	1.91	0.047
	14	(2)	(3)			(8)		(12)	7	-70.293	1.98	0.045
Non-Glires	1			(5)		(8)		(12)	6	-57.79	0	0.181
	2	(2)		(5)		(8)		(12)	7	-56.75	0.16	0.167
	3	(2)				(8)		(12)	6	-58.19	0.79	0.122
	4					(8)		(12)	5	-59.29	0.80	0.121
	5	(2)	(3)	(5)		(8)		(12)	8	-56.20	1.33	0.093
	6			(5)		(8)	(11)	(12)	7	-57.40	1.45	0.087
	7		(3)	(5)		(8)		(12)	7	-57.49	1.63	0.080
	8	(2)		(5)		(8)	(11)	(12)	8	-56.36	1.65	0.079
	9			(5)	(7)	(8)		(12)	7	-57.61	1.88	0.071
Glires	1	(2)	(3)		(7)			(12)	7	5.68	0	0.120
	2	(2)	(3)		(7)				6	4.43	0.05	0.117
	3	(2)	(3)		(7)		(11)	(12)	8	6.87	0.14	0.112
	4	(2)	(3)		(7)	(8)			7	5.38	0.59	0.090
	5	(2)	(3)		(7)	(8)		(12)	8	6.52	0.83	0.079
	6		(3)		(7)				5	2.78	0.97	0.074
	7		(3)		(7)		(11)	(12)	7	5.18	1.00	0.073
	8		(3)		(7)			(12)	6	3.86	1.19	0.066
	9		(3)		(7)	(8)			6	3.77	1.37	0.060
	10	(2)	(3)		(7)	(8)	(11)	(12)	9	7.52	1.45	0.058
	11	(2)	(3)		(7)		(11)		7	4.95	1.46	0.058
	12		(3)		(7)	(8)		(12)	7	4.77	1.82	0.048
	13	(2)	(3)	(5)	(7)				7	4.70	1.96	0.045

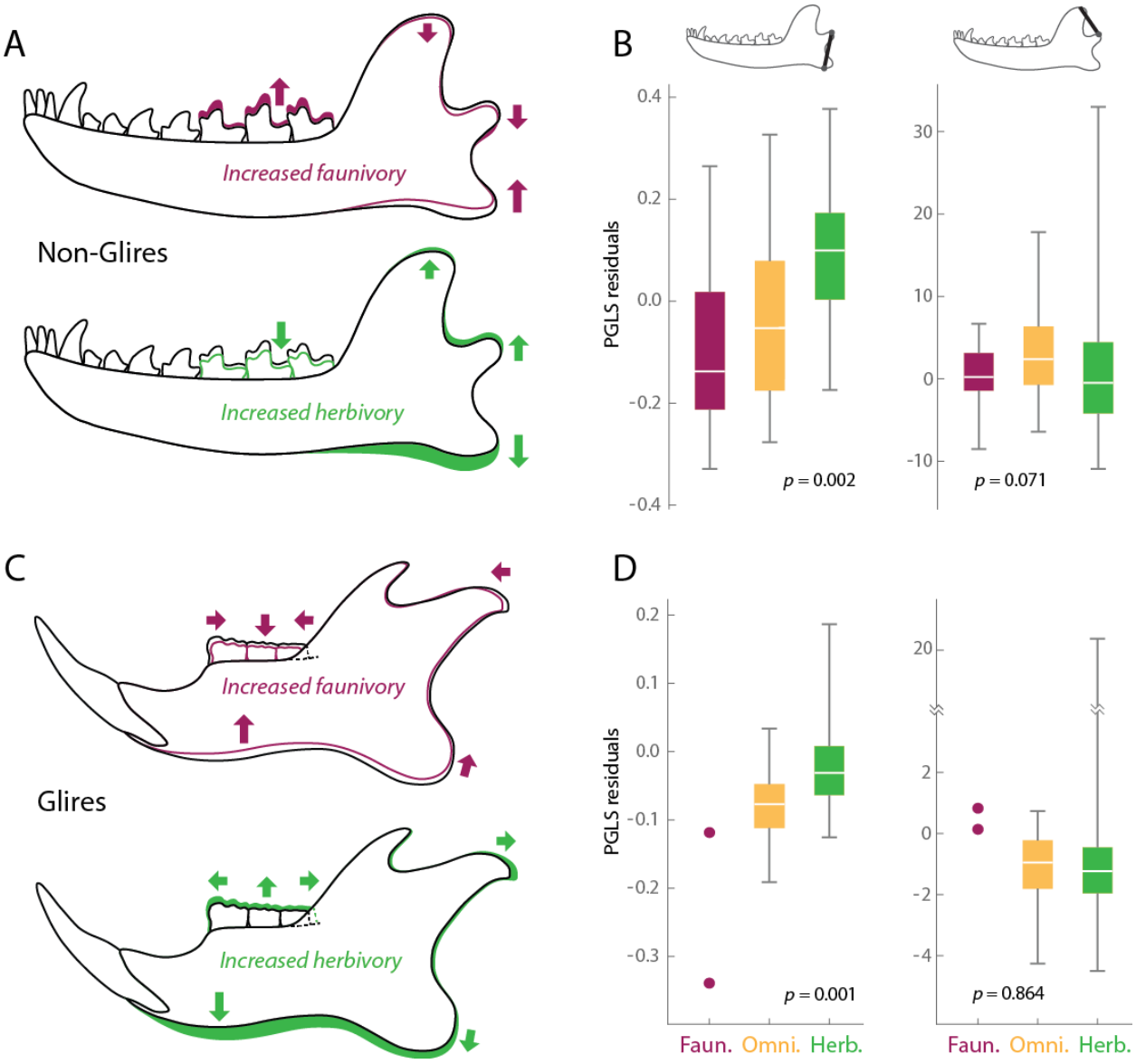

Figure 3.3. Morphological traits of jaws that have strong predictive power for diet (Tables 3.2 and 3.3) are displayed using schematic jaw images (*A* and *C*). *B* and *D* display pANOVA results for the angular process depth (*B*; measurement 12), which is strongly associated with diet, and coronoid elevation (*D*; measurement 10), which is not significantly correlated with diet. Prior to performing pANOVAs, jaw metrics were regressed against jaw length (via PGLS) to help account for differences in body mass, and residuals from these regressions were then used for the pANOVAs. Due to the unique patterns for non-glirans (*A* and *B*) and glirans (*C* and *D*), results are shown separately for these two groups. The arrow lengths and relative sizes of jaw changes in *A* and *C* roughly reflect the strength of correlations between jaw metrics and diet. Box and whisker plots display medians (white lines), 25% to 75% quantiles (boxes), and ranges (whiskers). Abbreviations: faun., faunivores; herb., herbivores; omni., omnivores; PGLS, phylogenetic generalized least squares.

The distance between the jaw joint and the angular process (i.e., JAPr distance) is found to be an especially powerful predictor of diet (Tables 3.2 and 3.3, Fig. 3.3). Measuring the angular process (APr) to the ventral-most point along its margin (measurement 12) outperformed a similar measurement to the posterior-most point of the APr (measurement 11), and it outperformed APr depth from the tooth row (measurement 6). In addition, when multiple regression models were tested using various combinations of measurements, the JAPr distance (ventral) is included in a greater number of reported models (i.e., those with ΔAICc values less than two) than any other jaw measurement (Table 3.5). The angle created by the jaw joint and APr (i.e., JAPr angle; measurement 13) is similar to the JAPr distance in terms of capturing the distance between the jaw joint and APr, and, as expected, it shows similarly strong correlations with diet (Tables 3.2 and 3.3). The *gls* function does not return an r^2 (or pseudo-r^2) value for PGLS (due to alteration of the variance-covariance matrix by the error term), but an ordinary least squares regression of diet data versus JAPr angle reports an adjusted r^2 value of 0.351 ($p < 0.001$). This suggests that a considerable amount of variance in jaw morphology across Mammalia can be explained by this single metric.

Some notable metrics did not show a strong correlation with diet. This includes the distance between the jaw joint and the dorsal-most point of the coronoid process (i.e., JCPr distance; measurement 10) and the elevation of the jaw joint about the tooth row (measurement 4). Results for the JCPr distance are shown in Figure 3.3 for comparison to the stronger performing JAPr distance. CPr elevation above the tooth row (measurement 5) generally outperforms JCPr distance, but it only results in a statistically significant correlation to diet in some analyses (Tables 3.2 and 3.3).

3.4.2 Evolutionary models

Jaw joint-angular process (JAPr) angle. To test the mode of evolution in mammalian jaw morphology, I chose to use the JAPr angle (measurement 13, Table 3.1). This metric is significantly correlated with diet in the mammalian, non-gliran, and gliran datasets (Tables 3.2 and 3.3). Although the JAPr angle did not perform as well as the distance from the jaw joint to the ventral-most point of the APr (measurement 12) in most analyses, I chose to use the JAPr angle because it offers several benefits: size correction is unnecessary, it can be measured for a greater sample of fossil jaws because the entire length of the jaw does not need to be preserved (in contrast to metrics that include size correction using jaw length), it may be less affected by subjective measurements of indistinct or inflected APrs (see 3.3 Methods), and Arregoitia et al. (2017) independently observed a strong correlation between this angle and diet in a large sample of rodents.

Although size correction is not necessary for JAPr angles (in contrast to linear measurements), it is possible that evolution of the JAPr angle is not independent of body size. Thus, I performed a phylogenetic ANCOVA with body mass (ln grams) incorporated as a covariate, and results indicate that JAPr angles of herbivores and carnivores remain significantly different ($F = 2.176$, $p = 0.025$).

Mode of evolution. The influence of diet on the evolution of the JAPr angle in mammals was examined using a suite of evolutionary models. The phylogeny in Figure 3.4B displays the selective regimes (i.e., faunivory and herbivory) associated with extant species, and Figures 3.4A and C provide frequency data for the mammalian sample. The JAPr angle data create a bimodal distribution, with faunivores and herbivores producing distinct distribution peaks (Fig. 3.4C). The large herbivore peak includes a considerable number of rodents, which comprise about one

third of the sample and mostly possess plant-dominated diets. However, rodents alone cannot account for the distinct JAPr angle patterns for faunivores and herbivores, as there remains a strong correlation between the JAPr angle and diet in non-glirans (Tables 3.2 and 3.3).

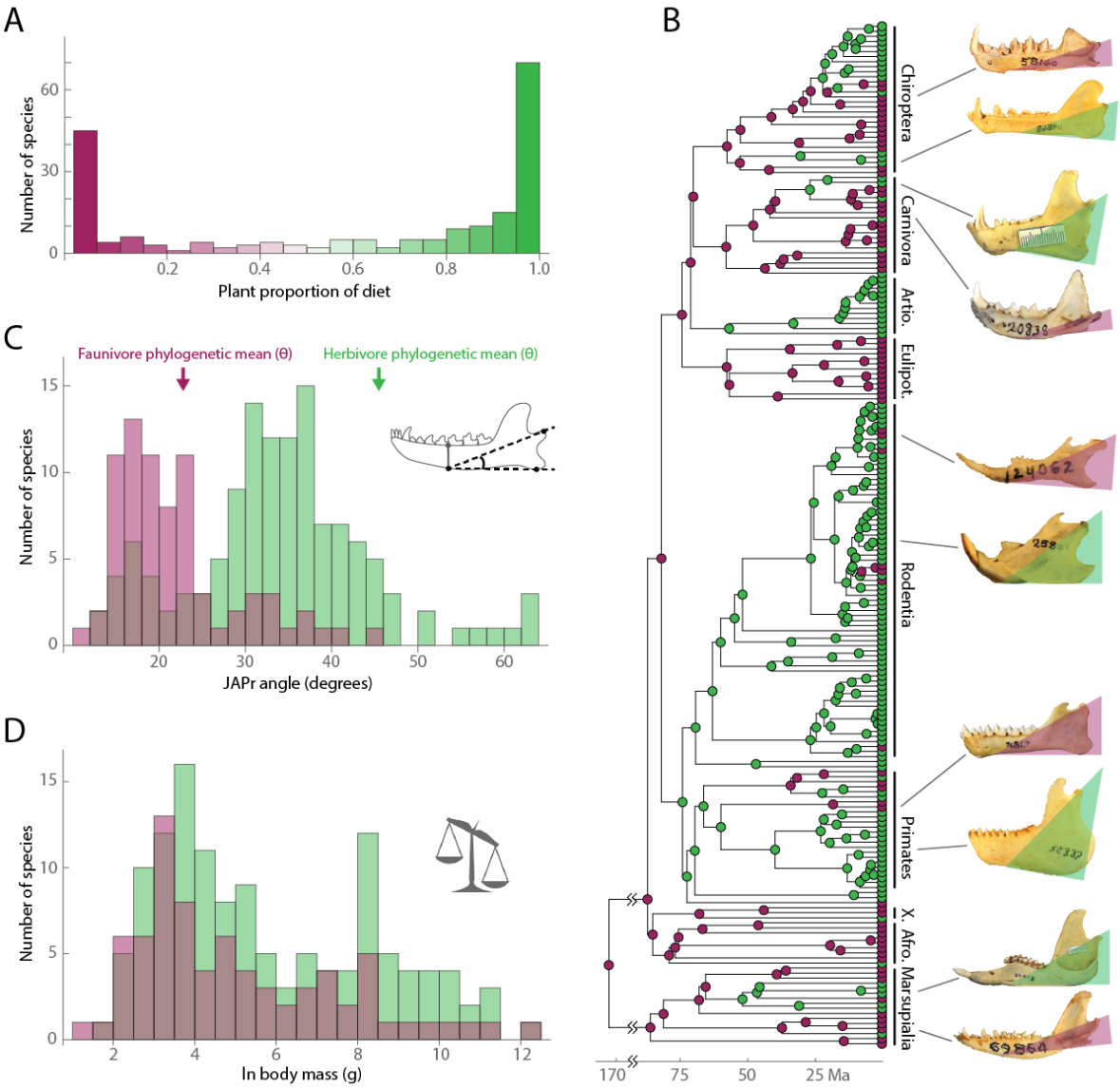

Figure 3.4. Selective regimes for animal-dominated diets ('faunivore'; maroon) and plant-dominated diets ('herbivore'; green) in mammals, based on proportion of plant material consumed (*A*; Appendix D). *B*, Mammalian phylogeny with ancestral state reconstructions at nodes. Exemplar jaws are shown for five mammalian orders, each represented by one faunivore jaw and one herbivore jaw. Triangles on jaws depict JAPr angles, highlighting the tendency for the JAPr angle to be greater in herbivores. *C*, Frequency of faunivores and herbivores based on JAPr angles, with arrows marking their approximate phylogenetic means from the best performing evolutionary model (Table 3.6). *D*, Frequency of faunivores and herbivores based on natural log-transformed body masses. Brown bars in histograms represent overlap of the two dietary groups. Jaw specimens in *B* represent the following species (top to bottom): *Vampyrum spectrum*, *Pteropus alecto*, *Potos flavus*, *Mustela nivalis*, *Geoxus valdivianus*, *Otomys irroratus*, *Tarsius bancanus*, *Callicebus personatus*, *Macropus giganteus*, and *Marmosa demerarae* (Appendix D). Abbreviations: Afro., Afrotheria; APr, angular process of jaw; Artio., Artiodactyla; Eulipot., Eulipotyphla; JAPr, joint to angular process; Ma, millions of years ago; X., Xenarthra.

The small peak of herbivores that possess relatively small JAPr angles (i.e., those overlapping with faunivores in Figure 3.4C) include many fruit bats, suggesting that Chiroptera may not adhere to the trend of greater JAPr values with increased herbivory. Thus, independent PGLS regression analyses were performed for bat APr measurements. Results are consistent with the overall mammalian sample: diet is significantly correlated with JAPr distance ($t = 2.37$, $p = 0.025$) and JAPr angle ($t = 2.26$, $p = 0.026$). Thus, despite the relatively small JAPr angles for bats, there remains a tendency toward greater JAPr angles and distances with increased herbivory (see the example chiropteran jaws in Figure 3.4B).

Results from the evolutionary modeling analyses provide strong evidence that the jaws of faunivores and herbivores evolve toward different adaptive peaks and at different rates (Table 3.6). The model that best explains the JAPr angle data (determined by Akaike weights) is BMS, which allows the phylogenetic means of the JAPr angles to vary between the two dietary regimes. This model performs substantially better than all other models (Table 3.6), and it shows a considerable difference in phylogenetic means for faunivores (22.6 degrees) and herbivores (45.5 degrees). These values are marked in figure 3C. Further, BMS shows evolutionary change rates for herbivores that are considerably greater than those of faunivores.

Table 3.6. Fits of trait evolution models to JAPr angle and body mass data in mammals. Strongly performing models with ΔAICc values below two are in bold. The ΔAICc values are the differences between the AICc value of the best performing model (BMS) and those of additional models. If two values are given for a parameter in the table, the first value always corresponds to faunivores and the second value always corresponds to herbivores. Parameters include the evolutionary rate of trait evolution (σ^2), trait attractors (θ), strength of attraction (α), and, for EB models only, rate change (*a*). See Methods for descriptions of the specific evolutionary models and parameters. Abbreviations: AICc, corrected Akaike information criterion; BM, Brownian motion; log-lik., logarithmic-likelihood; EB, early burst; NA, not applicable; OU, Ornstein-Uhlenbeck; SE, standard error; weight, Akaike weight.

	Model	Log-lik.	ΔAICc	Weight	σ^2	α	θ	SE
JAPr angle	BM1	-678.90	56.314	<0.001	1.890	NA	27.26	9.57
	BMS	-648.67	0	1.000	0.434, 2.634	NA	22.66, 45.53	4.65, 8.34
	EB	-678.90	58.375	<0.001	1.890	>-0.001*	27.26	
	OU	-676.37	53.303	<0.001	2.26	0.007	27.42	4.83
Body Mass	BM1	-337.48	0.260	0.296	0.065	NA	6.051	1.78
	BMS	-335.38	0.0	0.337	0.081, 0.055	NA	5.92, 7.42	1.99, 2.31
	EB	-336.57	0.500	0.262	0.235	-0.008*	6.012	
	OU	-337.48	2.321	0.106	0.065	<0.001	6.051	1.78

*This value represents the *a* parameter of EB models.

In addition to JAPr angle, body mass data are also best explained by the BMS model (Table 3.6). Evolutionary rates for body mass are greater in faunivores than herbivores, consistent with results in Price and Hopkins (2015). However, unlike JAPr angle, the BMS model of body mass performs only slightly better than BM1 and EB. In addition, the phylogenetic means for faunivores and herbivores are very similar (5.92 and 7.42 ln grams, respectively). This suggests that diet is not influencing the evolution of body mass to nearly the extent that it is influencing jaw shape.

3.4.3 Fossil patterns

To examine the dietary diversity and macroevolutionary patterns of early therians, JAPr angles of fossil genera were measured and plotted through time in Figure 3.5. Dietary assignments of genera are based on classification by the Paleobiology Database.

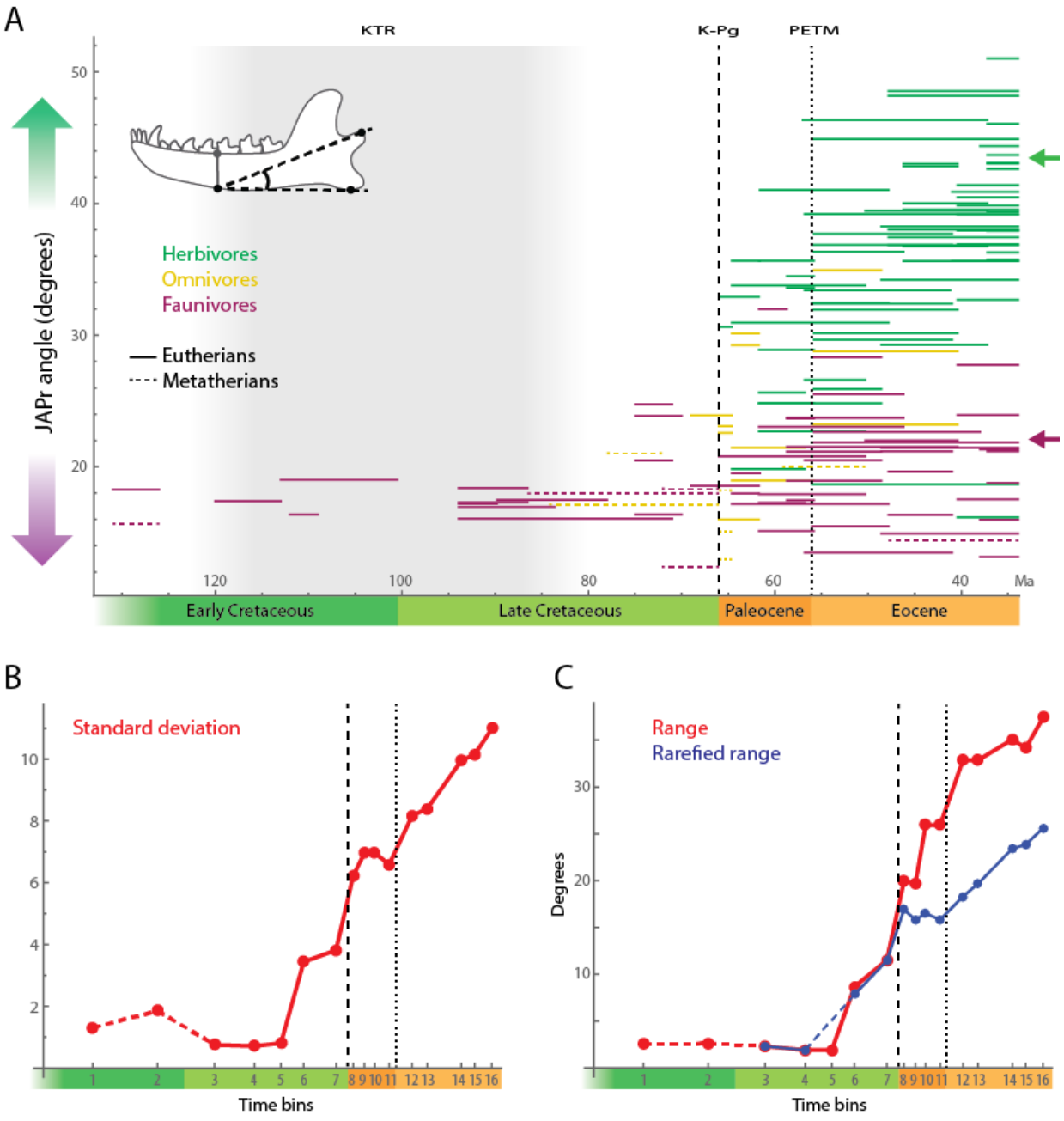

Figure 3.5. *A,* JAPr angles for fossil therians from the Cretaceous through Eocene. The arrows mark the approximate phylogenetic means for faunivores (maroon) and herbivores (green) in the best performing evolutionary model (BMS) for modern species (Table 3.6, Fig. 3.4), and they match the arrows in Figure 3.4B. Dietary assignments are those given in the Paleobiology Database. *B* and *C*, Disparity metrics for the JAPr angles. Results in time bins 1 and 2 are based on less than four taxa. Time bin ages and rarefaction information are provided in 3.3 Methods. Abbreviations: JAPr, jaw joint-to-angular process; K-Pg, Cretaceous-Paleogene boundary; KTR, Cretaceous Terrestrial Revolution; Ma, million years ago; PETM, Paleocene-Eocene Thermal Maximum.

Results of the fossil analysis demonstrate a rapid increase in therian dietary diversity beginning in the late Campanian (~78 million years ago; time bin 6 in Fig. 3.5) and continuing through the Eocene. This conclusion is supported by disparity metrics, as standard deviation (Fig. 3.5B), range, and rarefied range (Fig. 3.5C) all show strong increases starting in the Campanian. One of the most rapid increases between time bins is that from the Maastrichtian (bin 7) to the early Danian (bin 8), suggesting a dietary diversification immediately following the Cretaceous-Paleogene (K-Pg) mass extinction event. Based on standard deviation and rarefied range, there is little increase in dietary diversity during the remainder of the Paleocene, and it is not until immediately after the Paleocene-Eocene Thermal Maximum (PETM) that dietary diversity begins to increase again.

JAPr results for dietary groups of the Eocene appear to have a very similar distribution to those of modern mammals, with herbivores and faunivores centered around the approximate attractor values for those dietary regimes in the best performing evolutionary models (Fig. 3.4, Table 3.6). This is highlighted in Figure 3.5 by the green and maroon arrows, which match those of Figure 3.4B.

3.5 DISCUSSION

3.5.1 Jaw joint to angular process (JAPr) distance

Of the jaw measurements tested in this study, the strongest correlate of diet in mammals is the distance between the jaw joint and ventral-most point of the angular process (i.e., JAPr distance). The metric performs well for datasets consisting of chiropterans (see Results text), glirans (rodents and lagomorphs), non-glirans, and all mammals (Tables 3.2 and 3.3). This result is consistent with qualitative observations (e.g., Maynard Smith and Savage 1959) and a

geometric morphometric analysis of jaw shape in Grossnickle and Polly (2013), which found the JAPr distance to account for much of the variation between small mammalian faunivores and herbivores. In addition, previous studies found the JAPr distance (or a comparable metric) to be correlated with diet in carnivorans (Radinsky 1981, Figueirido et al. 2010), ungulates (Mendoza et al. 2002), and rodents (Arregoitia et al. 2017). However, this correlation was not especially strong in carnivorans (Radinsky 1981) or ungulates (Mendoza et al. 2002), at least relative to additional metrics tested within the studies. This suggests that the strongly significant results of this study rely on sampling a taxonomically diverse group of mammals, which allows for convergent trends across mammalian orders to be recognized.

The JAPr distance can increase in two ways. First, it can increase due to elevation of the jaw joint, which appears to be the case for ungulates that possess very elevated jaw joints. Second, the JAPr distance increases when the APr is enlarged and/or depressed, as in some rodents with APs that extend strongly posteroventrally and jaw joints that are not especially elevated. In either case, the increased distance between the APr and jaw joint provides greater attachment areas for the superficial masseter and medial pterygoid muscles, which insert on the APr (Fig. 3.1). These muscles tend to be proportionally larger (relative to the overall mass of masticatory muscles) in herbivorous mammals (Turnbull 1970), suggesting that the increase in the JAPr distance evolves with herbivory to increase the attachment areas for these muscles in the APr region of the jaw. This supports the conclusion that these muscles are especially important for herbivory (Maynard Smith and Savage 1959, Turnbull 1970, Herring and Herring 1974, Crompton et al. 2010).

Besides simply increasing the insertion areas for muscles, there are several potential biomechanical hypotheses for why the JAPr distance increases with herbivory. First, the greater

distance is expected to increase the moment arm lengths for the medial pterygoid and superficial masseter during some rotational jaw movements (Maynard Smith and Savage 1959). For jaw rotation around a horizontal axis through the jaw joints (i.e., pitch), which results in orthal molar occlusion, the JAPr distance reflects the moment arms (or in-levers) for the superficial masseter and medial pterygoid muscles. Increased JAPr distances should therefore result in greater mechanical advantages for these muscles during pitch. In taxa with proal movement during occlusion (e.g., some rodents), the lengthening of the APr may benefit taxa by lengthening these muscles (especially in congruence with increasingly anterior muscle origin locations on the skull, as seen in rodents), which may increase overall muscle mass and help the jaws maintain forceful occlusal contact during extended proal movement. Further, the chewing cycles of most mammals include significant transverse movement produced via rotation around a vertical axis (i.e., yaw) (see Grossnickle 2017 and citations within), and this transverse movement is especially prevalent in herbivores (e.g., Crompton et al. 2010). A prominent APr can result in superficial masseter and medial pterygoid muscle vectors that are closer to horizontal during occlusion, and this can increase the mechanical advantage of these muscles for yaw rotation (Maynard Smith and Savage 1959, Grossnickle 2017).

A second biomechanical hypothesis for the increased JAPr length in herbivores relates to gape. Increasing the JAPr distance results in superficial masseter and medial pterygoid muscles that are further from (i.e., more ventral to) the jaw joint, which increases the stretch of these muscles during jaw opening (Herring and Herring 1974). This limits maximum gape and decreases bite force during wide gape. However, unlike carnivores, herbivores are unlikely to require a large gape for ingestion and mastication of plant materials. Therefore, natural selection may favor the greater muscle sizes of the superficial masseter and medial pterygoid (and greater

JAPr distance) in herbivores because the resulting gape limitations are not detrimental. In contrast, carnivores often require a large gape (and strong force potential at maximum gape) because of relatively large prey. Shorter moment arms of the jaw elevator muscles may also allow for faster jaw closure, which could be especially beneficial to insectivores. Further, because carnivores are more likely to rely on orthal occlusion (for shearing) created by pitch rotation of the jaw (e.g., Evans and Sanson 2006), there may be less selective pressure for maximizing mechanical advantage for the superficial masseter and medial pterygoid muscles, which tend to be more associated with proal and transverse jaw movements (Maynard Smith and Savage 1959, Crompton et al. 2010, Grossnickle 2017).

Interestingly, the JAPr distance considerably outperforms additional metrics that could be expected to correlate with diet, such as the distance between the jaw joint and dorsal-most point of the coronoid process (i.e., JCPr distance). The vastly different results for the JAPr and JCPr distances are highlighted in Figures 3.3B and 3.3D. The JCPr distance represents the approximate moment arm length of the temporalis muscle, which is the largest jaw elevator muscle in most mammals (Turnbull 1970). Thus, it could be expected that this distance would increase with faunivory because the temporalis tends to be relatively larger in carnivores (Maynard Smith and Savage 1959, Turnbull 1970), possibly helping to maximize bite force and shearing ability during pitch rotation of the jaw (Grossnickle 2017). However, results did not show a strong correlation between this metric and diet (Tables 3.2 and 3.3). The CPr elevation above the tooth row (measurement 11) actually decreases with faunivory in non-glirans, although this is offset by a greater decrease in jaw joint elevation (Fig. 3.3A).

3.5.2 Non-Glires versus Glires

Non-glirans and glirans show distinct morphological trends related to diet (Tables 3.2 and 3.3, and Fig. 3.3). For instance, the pattern for the maximum erupted molar depth is opposite in the two groups, with this metric increasing with herbivory in glirans and decreasing with herbivory in non-glirans. This could be due in part to many carnivorans possessing prominent carnassial molars. In contrast, carnivorous rodents are primarily insectivorous and may have reduced molars (e.g., Helgen and Helgen 2009). An additional distinction between glirans and non-glirans is that the jaw corpus depth (measurement 7) is much more strongly correlated with diet in glirans than in non-glirans (Tables 3.2 and 3.3, and Fig. 3.3). This correlation is congruent with the rodent results in Arregoitia et al. (2017). A deeper jaw could reflect stronger mechanical loads resulting from larger jaw elevator muscles, and it could also reflect increased incisor size for gnawing (Radinsky 1968), because the incisor alveoli extend posteriorly through much of the length of the jaw corpus.

Despite the distinct trends for many jaw metrics, glirans and non-glirans both show a significant correlation between JAPr distance and diet (Tables 3.2-3.4). This distance is very similar to the JAPr angle. Arregoitia et al. (2017) measure a similar angle in a large sample of rodents and also find a strong correlation with diet, supporting the conclusion that the JAPr distance (or angle) is an especially strong predictor of diet.

3.5.3 Mode of evolution

Results of model fitting strongly support the initial hypothesis of this study that faunivores and herbivores have experienced unique selective regimes (Table 3.6 and Fig. 3.4C), as the multi-peak BMS model outperforms all additional models. This provides evidence for the

existence of distinct adaptive peaks for the two dietary groups. The JAPr angles show a distinct bimodal distribution for herbivores and faunivores (Fig. 3.4C), and this apparent trend is supported by correlation analyses that account for the phylogenetic non-independence of data (Tables 3.2 and 3.3). Further, the evolutionary pattern is supported by fossil evidence, which also demonstrates herbivorous clades evolving greater JAPr angles in the early Cenozoic Era (Fig. 3.5).

The best performing model, BMS, predicts the phylogenetic means for the JAPr angles to be considerably different for the two selective regimes: approximately 23 degrees for faunivores and 46 degrees for herbivores. As discussed above, this is probably due to biomechanical differences between the two dietary groups, as the superficial masseter and medial pterygoid muscles insert on the APr and appear to have a more prominent role in herbivorous taxa (Maynard Smith and Savage 1959, Turnbull 1970, Crompton et al. 2010). Interestingly, fossil evidence from early therians also shows evidence of mean JAPr angles near 23 degrees for faunivores and 46 degrees for herbivores, as Eocene fossils show distributions that are centered near these values for the two dietary categories. This suggests that diet has influenced jaw evolution in a similar manner for much of therian history, and that many mammalian groups evolved rapidly toward these mean JAPr angles early in their evolutionary history.

In addition, it appears that selection has acted on the two dietary groups in unique ways. For instance, the BMS model includes σ^2 values are considerably different for faunivores and herbivores (i.e., 0.434 and 2.634, respectively), indicating that rates of evolutionary change are much more rapid in herbivores. The data are also congruent with the fossil JAPr data, which show a rapid diversification into herbivorous morphospace in the Paleocene and early Eocene (Fig. 3.5). Because these early herbivores are represented by multiple clades (including

ungulates, rodents, and proboscideans), it suggests that multiple lineages evolved toward an herbivorous morphology during the early Cenozoic. However, it is worth noting that the evolutionary rates may be biased toward greater rates in herbivores because herbivores possess larger JAPr angles (Adams, 2012). Prior to publication of these results, efforts will be made to address this potential bias. For example, the model analyses can be re-run after log transformation of the JAPr angles to examine whether this manipulation has an effect on the evolutionary rate results.

The lack of AICc support for the early burst (EB) model (and the *a* parameter value near zero) indicates that there is no evidence for an overall change in evolutionary rate over time (Table 3.6). This contradicts the hypothesis that therian or placental mammals adaptively radiated early in their history, possibly following the Cretaceous-Paleogene mass extinction event. However, the power to detect adaptive radiations in deep time is greatly enhanced by the incorporation of fossil evidence (Tarver and Donoghue, 2011; Slater et al., 2012; Mitchell, 2015; Grossnickle and Newham, 2016; Halliday and Goswami, 2016), and this may be especially applicable to therian mammals from the Cretaceous and Paleogene because a majority of groups are now extinct.

Because of the distinct evolutionary patterns for faunivores and herbivores, it is expected that extinct mammals experienced similar selective regimes. Thus, the JAPr angle is a metric that can be readily applied to fossil mammals (Fig. 3.5), especially because mammalian jaws are common in the fossil record. The JAPr angle may be preferred to additional metrics of this study (e.g., JAPr distance) when examining fossils because it does not require size correction, and angle results can be easily interpreted and compared to those of modern taxa.

3.5.4 Body mass and ecological diversity

In addition to jaw morphology, I assess the correlation between body mass and diet in mammals, which has also been the focus of recent studies (Price and Hopkins, 2015; Pineda-Munoz et al., 2016). Analyses show significant correlation between diet and body mass for the mammalian and non-gliran datasets (but not the gliran dataset), with body mass increasing with greater plant consumption (Tables 3.2 and 3.3). Like JAPr angle, the best performing model of body mass evolution is a Brownian motion model (BMS), and its rate parameter values suggest that faunivore body masses evolve more rapidly than those of herbivores (Table 3.6; Price and Hopkins, 2015). However, Price and Hopkins (2015) differ from this study in finding that herbivores evolve toward a much larger trait optimum (or phylogenetic mean) than predicted by this study. This discrepancy is possibly due to Price and Hopkin's incorporation of a separate omnivore category, in addition to inclusion of some especially large herbivorous groups in their dataset (e.g., elephants, perissodactyls) that are not represented in this study. Further, Pineda-Munoz et al. (2016) document complex relationships between body mass and diet when more specific dietary categories are examined. Thus, there is strong evidence that diet influences the evolution of body mass in mammals, but this influence may be less significant (or more complex) than that of diet on jaw morphology.

Body mass is often used as a proxy for mammalian ecomorphological diversity in broad macroevolutionary studies (Alroy, 1999; Baker et al., 2015; Cooper and Purvis, 2010; Smith et al., 2010; Venditti et al., 2011; Saarinen et al., 2014; Smits, 2015). This is not surprising because the data are easily accessible for modern taxa (e.g., Jones et al., 2009), and masses of extinct taxa can be readily estimated using regression equations for various fossil elements (e.g., Slater, 2013; Tomiya, 2013; Smits, 2015). In addition, body mass has been shown to be correlated with

a variety of ecological and physiological factors (Smith and Lyons, 2011; Tomiya, 2013; Price and Hopkins, 2015; Pineda-Munoz et al., 2016). However, because many factors are associated with body mass, it may be difficult to decipher which ecological factors are specifically influencing body mass evolution and diversity. In addition, inferring evolutionary patterns in deep time using body mass data of extant taxa may be especially problematic because incorporation of fossils can significantly alter results (Slater et al., 2012; Slater, 2015).

Thus, it is important to identify predictive variables of specific ecological traits that can be applied widely to a diverse sample. Measuring additional functional traits beyond body mass may be especially informative when examining ecomorphological patterns on a macroevolutionary scale (Smits, 2015; Grossnickle and Newham, 2016; Slater, 2015). The jaw correlates of diet presented in this study, especially JAPr distance and JAPr angle, may offer new functional traits that can be easily applied to broad studies of modern and fossil mammals.

3.5.5 Radiation of early therians

Radiation hypotheses. A commonly promoted hypothesis is that mammalian diversity and disparity were suppressed during the Mesozoic Era due to the presence of non-avian dinosaurs (and additional diverse reptilian groups), and this was followed by an adaptive radiation immediately after the K-Pg mass extinction event (Osborn, 1902; Alroy, 1999; O'Leary et al., 2013, Halliday and Goswami, 2016). I refer to this as the Suppression Hypothesis (SH) and note that it is supported if ecological disparity of therians remains depressed in the Cretaceous (see Chapters 1 and 4 for additional discussion). The perceived diversification in the earliest Paleocene (as predicted by SH) is considered adaptive because mammals evolved a considerable number of ecomorphologies in a relatively short time span.

However, recent research has challenged SH. Several studies suggest that mammals began to radiate prior to the K-Pg boundary (Clauset and Redner, 2009; dos Reis et al., 2012; Wilson et al., 2012; Clemens, 2002; Meredith et al., 2011; Wilson et al., 2016), led by Late Cretaceous metatherians and multituberculates. Additional research, however, indicates that modern placental orders initiated a more significant diversification after the PETM (Hunter and Jernvall, 1995; Gingerich, 2006; Bininda-Emonds et al., 2007; Tapaltsyan et al., 2015; Wu et al., 2017).

Thus, three different points in time are argued to have been the start of the mammalian adaptive radiation. Further, the three diversification hypotheses have each been linked to a period of considerable environmental perturbation: i) a pre-K-Pg diversification coincides with the end of the Cretaceous Terrestrial Revolution (KTR; Lloyd et al., 2008), ii) an early Paleocene diversification follows the K-Pg mass extinction event, and iii) an Eocene diversification occurs immediately following the PETM. These three environmental events are noted in Figure 3.5.

JAPr angles of fossils. The fossil analysis (Fig. 3.5) makes a significant contribution to the debate over the timing of the early mammal radiation, which in turn helps identify which environmental factors may have been most influential on mammalian evolution. The results of this analysis are especially valuable for two reasons. First, they are based on fossil data, and not molecular or morphological data from modern taxa. This is important because ecomorphological patterns in deep time cannot adequately be assessed by modern-only datasets (Tarver and Donoghue, 2011; Slater et al., 2012; Mitchell, 2015). Second, the fossil metric (i.e., JAPr angles) is shown to be highly correlated with one ecological trait, diet (Tables 3.2 and 3.3). This allows for a more specific interpretation of the data (and evolutionary patterns) than analyses of body masses (Alroy, 1999; Clauset and Redner, 2009), discrete morphological characters (Halliday

and Goswami, 2016), or taxonomic diversification (Patzkowsky, 1995; Halliday et al., 2016; Grossnickle & Newham 2016), which can all be influenced by many factors (e.g., see discussion in 3.5.4 Body mass and ecological diversity).

The fossil JAPr angle results indicate that the dietary diversity of early therians began to increase rapidly prior to the K-Pg boundary (Fig. 3.5), which is in conflict with SH. This diversification initiates in the mid-Campanian (~78 Ma), which coincides with the end of the KTR, and it appears to have been led by metatherians (Chapter 4; Wilson et al., 2016). The pattern is also supported by body mass data (Chapter 4; Clauset and Redner, 2009). Further, diverse archaic ungulates from the earliest Paleocene of North America have been interpreted as immigrants (Wilson, 2013; Clemens, 2002), suggesting that these taxa diversified elsewhere, prior to the K-Pg boundary. The latest Cretaceous is also a period of diversification for multituberculate mammals (Wilson et al., 2012), and it corresponds to the ecological diversification of flowering plants. These results suggest that all mammals may have benefitted from the novel food sources provides by the rise of angiosperms in the Late Cretaceous. The dietary diversity does not increase considerably in the Maastrichtian (72.1-66 Ma), but it is worth noting that the Eurasian fossil record is especially poor for this geologic stage. Thus, the lack of a strong global sample in the Maastrichtian may dampen the signal of any ecomorphological diversification that occurred during this time.

Despite the dietary diversification prior to the K-Pg boundary, jaw morphologies do not indicate the presence of herbivores. Instead, it appears that the earliest therians, which were mostly small insectivores, evolved into omnivorous and carnivorous niches after the KTR in the Campanian (Fig. 3.5). Although non-therian herbivorous mammals may have been present in the latest Cretaceous (Wilson et al., 2012; Krause et al., 2014), these were rodent-like allotherians

that never achieved the relatively large body masses that are seen in Cenozoic herbivorous groups (e.g., ungulates and proboscideans). It could be argued that if body mass and JAPr angles are correlated, then the relatively small body sizes of Cretaceous mammals is leading to a misclassification of any herbivores that are present. However, results from the phylogenetic ANCOVA show that there is a significant difference between JAPr angles of modern herbivores and faunivores even when body mass is included as a covariate (see section 3.4.2 Evolutionary models). This is supported by the presence of small, modern mammals with herbivorous diets, such as fruit bats and many rodents. Thus, it is unlikely that the small body sizes of early therians are responsible for the JAPr angle results that suggest they are faunivores.

The first herbivorous therians appear in the earliest Paleocene (Fig. 3.5), and they are primarily archaic ungulates and taeniodonts (Chapter 4). These two clades were present in the latest Cretaceous (Clemens, 2002; Fox and Naylor, 2003; Archibald et al., 2011; Kelly, 2014), but the earliest lineages of archaic ungulates are often inferred to have been omnivorous (Hunter, 1997; Wilson, 2013). Thus, evidence suggests that mammals experienced a dietary diversification in response to the K-Pg mass extinction. However, the question remains as to whether this diversification was a continuation of that which started in the Late Cretaceous or was novel diversification event.

The results for standard deviation and rarefied range show that therian dietary diversity did not increase significantly in the Paleoecene after the initial burst in the early Danian (Fig. 3.5). Instead, dietary diversity appears to remain relatively level until the PETM, at which point it begins to increase again. The early Eocene is the period in which modern placental orders become abundant and taxonomically diverse in the fossil record (Hunter and Jernvall, 1995; Janis, 2000; Gingerich, 2006; Tapaltsyan et al., 2015), suggesting that the Eocene diversification

represents a replacement of the Paleocene fauna by members of crown placental orders (Figueirido et al., 2012). Dietary diversity continues to increase throughout the Eocene (Fig. 3.5).

In summary, JAPr angles of fossil mammals indicate that a dietary diversification begins in the Late Cretaceous, and the K-Pg mass extinction and PETM may have triggered an even greater radiation by creating new ecological opportunities for surviving clades. For instance, the evolution of large mammalian herbivores may have been accelerated by the loss of herbivorous dinosaurs at the K-Pg. This suggests the possibility that all three hypotheses concerning the initiation of the therian adaptive radiation (see above) may be partially supported. That is, it is possible that the adaptive radiation was a multi-step process that initiated in the Cretaceous and was later catalyzed by both the K-Pg extinction event and PETM.

3.5.6 Conclusions

By examining mandibular morphologies of mammals at a broad taxonomic scale, I identify several traits that are significantly associated with diet (Tables 3.2 and 3.3). The strongest correlate of diet is the distance between the jaw joint and the angular process (JAPr distance), probably reflecting an increasing role for the superficial masseter and medial pterygoid muscles with evolutionary shifts to herbivory. In contrast, the distance between the jaw joint and dorsal-most point of the coronoid process (a proxy for the moment arm of the temporalis muscle) is not significantly correlated with diet (Tables 3.2 and 3.3, Figs. 3.3B and 3.3D). Glirans and non-glirans display unique trends (Fig. 3.3), but both groups appear to evolve greater JAPr distances with increased herbivory. To further examine the evolutionary influence of diet on jaw morphology,

a variation of the JAPr distance (i.e., the JAPr angle) was applied to evolutionary models using all mammals of this study. Results indicate that diet has strongly influenced the evolution of mammalian jaw morphologies, with herbivores and faunivores evolving toward distinct adaptive peaks (Table 3.6, Fig. 3.4), and this conclusion is reinforced by evidence from fossil mammals (Fig. 3.5). In addition, evolutionary rates of change appear to be much more rapid in herbivores.

A major goal in examining correlations between diet and jaw morphology is to identify correlates that can be readily applied to fossil mammals. Due to the ease at which the JAPr angle can be measured and the prevalence of jaws (and jaw fragments) in the mammalian fossil record, the JAPr angle is especially applicable to paleontological studies. It offers an additional ecomorphological or dietary indicator beyond those commonly found in the literature (e.g., body size and dental metrics) that can be readily applied to fossil mammals. Thus, I utilize this metric as a means of examining the diversification patterns of early therian mammals. Results support the hypothesis that the radiation of therian mammals began prior to the K-Pg boundary, although there is also evidence that the K-Pg mass extinction and PETM created additional ecological opportunity that further catalyzed this diversification.

CHAPTER 4

Therians experience an ecomorphological radiation during the Late Cretaceous and selective extinction at the K-Pg boundary

4.1 ABSTRACT

It is often postulated that mammalian diversity was suppressed during the Mesozoic Era and increased rapidly after the Cretaceous-Paleogene (K-Pg) extinction event. I test this hypothesis by examining macroevolutionary patterns in early therian mammals, the group that gave rise to modern placentals and marsupials. I assess morphological disparity and dietary trends using morphometric analyses of lower molars, and I evaluate generic-level taxonomic diversity patterns using techniques that account for sampling biases. In contrast to the suppression hypothesis, results suggest that an ecomorphological diversification of therians began 10-20 million years prior to the K-Pg extinction event, led by disparate metatherians and Eurasian faunas. This diversification is concurrent with ecomorphological radiations of multituberculate mammals and flowering plants, suggesting that mammals as a whole benefitted from the ecological rise of angiosperms. In further contrast to the suppression hypothesis, therian disparity decreased immediately after the K-Pg boundary, likely due to selective extinction against ecological specialists and metatherians. However, taxonomic diversity trends appear to have been decoupled from disparity patterns, remaining low in the Cretaceous and substantially increasing immediately after the K-Pg extinction event. The conflicting diversity and disparity patterns suggest that earliest Paleocene extinction survivors, especially eutherian dietary

generalists, underwent rapid taxonomic diversification without considerable morphological diversification.

4.2 INTRODUCTION

Therian mammals (i.e., eutherians and metatherians) underwent a major evolutionary radiation that included vast increases in taxonomic, morphological, and ecological diversities. It is often postulated that this radiation accelerated rapidly after the Cretaceous-Paleogene (K-Pg) extinction event 66.0 million years ago (Ma) (Osborn, 1902; Patzkowsky, 1995; Alroy, 1999; Smith et al., 2010; O'Leary et al., 2013; Halliday and Goswami, 2016), following a period during which diversity and disparity levels were suppressed by competition with non-avian dinosaurs. I title this the Suppression Hypothesis (SH) and conceptualize it in Figure 4.1A. SH is supported by paleontological evidence suggesting that Cretaceous mammals were taxonomically depauperate, limited to small body sizes, predominantly insectivorous, and likely included few crown eutherian (i.e., placental) lineages (Osborn, 1902; Patzkowsky, 1995; Alroy, 1999; Smith et al., 2010; O'Leary et al., 2013; Halliday and Goswami, 2016; Simpson, 1937; Collinson and Hooker, 1991; Wible et al., 2009; Slater, 2013; Halliday et al., 2015; Grossnickle and Polly, 2013). While previous studies have identified taxonomic and ecomorphological diversification events of Mesozoic mammals, these events were largely confined to the Jurassic, or involved non-therian lineages (Grossnickle and Polly, 2013; Luo, 2007; Wilson et al., 2012; Newham et al., 2014; Close et al., 2015). After the K-Pg extinction event, which eliminated non-avian dinosaurs, fossil evidence indicates immediate increases in therian body sizes, body size disparity, taxonomic diversity, and dietary diversity (Osborn, 1902; Patzkowsky, 1995; Alroy, 1999; Smith et al., 2010; Halliday and Goswami, 2016; Simpson, 1937; Collinson and Hooker,

1991; Slater, 2013; Hunter, 1997), implying that therian mammals adaptively radiated during the earliest Paleocene (Osborn, 1902). Further, O'Leary et al. (2013) conclude that placental mammals radiated extremely rapidly in the first 200,000-400,000 years after the K-Pg extinction event. Although this conclusion has been challenged (e.g., dos Reis et al., 2014), recent phylogenetic studies suggest increased intraordinal diversification of therians, especially placentals, after the K-Pg boundary (Wible et al., 2009, Halliday et al., 2015; dos Reis et al., 2014; Meredith, 2008; Meredith et al, 2011).

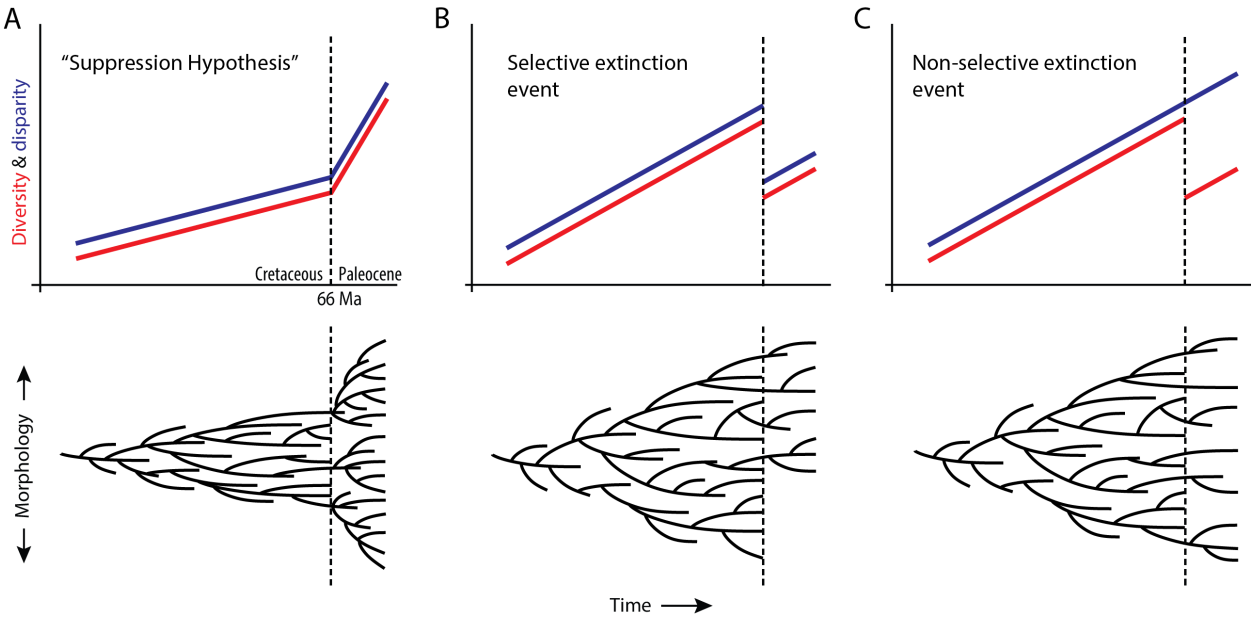

Figure 4.1. Taxonomic diversity (red) and morphological disparity (blue) patterns for idealized clade histories. The Suppression Hypothesis (SH) refers to the theory that mammalian diversity and disparity were suppressed until the K-Pg boundary at 66 million years ago (Ma), likely due to the presence of dinosaurs (A). A selective extinction event that claims taxa with specific morphologies is expected to cause a decrease in disparity (B). A non-selective (i.e., random) extinction event is expected to cause a decrease in diversity but not disparity (C). Dashed vertical lines represent a mass extinction event. B and C are after Foote (1993).

However, some lines of evidence are inconsistent with SH. For instance, recent studies demonstrate that end-Cretaceous therians achieved greater ecomorphological diversity than previously realized (Fox and Naylor, 2003; Fox et al., 2007; Archibald et al., 2011; Prasad, et al., 2007; Wilson, 2013; Wilson et al. 2016), and the Cretaceous therian (or tribosphenidan) fauna as a whole may have experienced greater morphological diversity than commonly appreciated (Rougier et al., 1998; Cifelli, 1999; Davis et al., 2016). Further, mammals began a trend of increasing average body size 10-20 million years before the K-Pg boundary (Grossnickle and Polly, 2013; Wilson et al., 2012; Clauset and Redner, 2009). Multituberculates, a diverse clade of extinct non-therian mammals, experienced a Late Cretaceous radiation that included increases in dietary, morphological, and taxonomic diversities (Grossnickle and Polly, 2013; Wilson et al., 2012). Further, Wilson (2013) reports a decrease in mammalian disparity immediately across the K-Pg boundary in Montana, suggesting a selective extinction event followed by a recovery period (Fig. 4.1B; Foote, 1993) rather than a rapid morphological radiation. Finally, diverse archaic ungulates from the earliest Paleocene of North America have been interpreted as immigrants (Wilson, 2013; Clemens, 2002), suggesting that these taxa diversified elsewhere, prior to the K-Pg boundary.

These conflicting lines of evidence suggest that our understanding of the timing and dynamics of the start of the therian radiation is incomplete. SH predicts that mammals adaptively radiated in the earliest Paleocene, and Schluter (2000) defines an adaptive radiation as including increases in taxonomic, morphological, and ecological diversities. However, previous studies on the early therian radiation have been limited in their ability to examine all three types of diversity. For instance, body mass patterns have been used to test for a mammalian radiation in the earliest Paleocene (Alroy, 1999; Smith et al., 2010; Slater, 2013), but body sizes alone may

be a poor metric for ecomorphological diversity (Slater, 2015). Further, the timing of the early therian radiation has been assessed in a phylogenetic context by examining the timing of originations of crown mammalian clades (O'Leary et al., 2013; Meredith et al, 2011). However, for taxa in deep time, taxonomic and ecomorphological diversities cannot adequately be assessed with phylogenetic data of modern taxa (Tarver and Donoghue, 2011; Mitchell, 2015), especially since many radiating clades may not have living representatives. Halliday and Goswami (2015) use paleontological data to test for an adaptive radiation of early Paleocene eutherians, but their analyses are limited to eutherian disparity patterns.

I assess SH using fossil data from the mid-Early Cretaceous to the mid-Paleocene (i.e., 130.8-61.6 Ma). With assistance from a colleague (Elis Newham), taxonomic diversity was calculated using two techniques that account for sampling biases: shareholder quorum subsampling (Alroy, 2010) and modeling-based residual analyses (Lloyd, 2012). I examine morphological disparity using morphometric analyses of molar shape. The tribosphenic molar morphology of early therians provides a structure with homologous landmarks among diverse taxa separated by considerable temporal spans. Further, molar morphology reflects diet, meaning that the diversity of morphologies can be indicative of ecological diversity (e.g., Wilson et al., 2012). Thus, the methods of this study allow for a more complete examination of the tempo of the early therian radiation by examining taxonomic, morphological, and ecological diversities.

4.3 METHODS

4.3.1 Study taxa

Following the Cretaceous Terrestrial Revolution of the mid-Cretaceous (Lloyd et al., 2008), the North American mammalian fauna was dominated by therians and multituberculates

(Grossnickle and Polly, 2013; Benson et al., 2013). Both clades also survive the K-Pg mass extinction event. However, therians (or tribosphenidans) are the focus of this study because they comprise a majority of the modern mammalian fauna (whereas multituberculates are extinct), their molars have easily distinguished (and homologous) cusps that can by used for landmark-based geometric morphometrics (GM), recent research has documented the diversity and disparity patterns of multituberculates across the K-Pg boundary (Wilson et al., 2012), and the post-K-Pg radiation of mammals is believed to have been driven by therians, especially eutherians (Osborn, 1902; Simpson, 1936; O'Leary et al., 2013, Halliday and Goswami, 2016).

I analyzed members of Tribosphenida (i.e., Boreosphenida), a monophyletic clade of crown mammals that possess a true tribosphenic molar morphology (Luo et al., 2002). Lower tribosphenic molars possess a developed talonid basin, distinguishing them from molars of closely related "eupantotherians" (i.e., non-therian stem cladotherians). Tribosphenida is slightly more encompassing than Theria (i.e., Metatheria and Eutheria) because it includes stem tribosphenidans, which are any taxa with true tribosphenic molars that could not be classified into Metatheria or Eutheria (Luo et al., 2002). Stem tribosphenidans have also been referred to as "therians of metatherian-eutherian grade" (e.g., Kielan-Jaworowska et al., 1979), tribotherians (e.g., Montellano-Ballesteros and Fox, 2015), and stem boreosphenidans (e.g., Kielan-Jaworowska et al., 2004). For simplicity, I generally refer to the sample of taxa as therians rather than tribosphenidans.

The oldest tribosphenidan is known from the Jurassic (Luo et al., 2011). However, the clade does not become abundant or taxonomically diverse until the Early Cretaceous. Thus, the temporal span of my analyses begins at the start of the Barremian, 130.8 million years ago (Ma). Time bins extend through the Danian (66-61.6 Ma). Ideally, I would examine the Paleocene

patterns past the Danian to better evaluate the therian response to the K-Pg extinction event. However, extending GM analyses beyond the early Paleocene becomes problematic due to the increased loss of distinct cusps in worn molars of herbivores and blade-like carnassial molars of carnivores. This prohibits identifying homologous cusp landmarks among the increasingly disparate taxa.

Although the GM analyses were performed at the generic level, an exception was made for *Paranyctoides*. It is the only Cretaceous therian known from both North America and Asia, but the taxonomic affinities of the specimens from the two continents have been debated (Averianov and Archibald, 2013A; Montellano-Ballesteros et al., 2013; Averianov and Archibald, 2013B). Thus, I chose to include a representative taxon from North America, *P. sternbergi*, and a representative taxon from Eurasia, *P. quadrans.* The age ranges for the two taxa were independently based on the occurrences for the genus on each continent (Appendix G).

One recently described genus from the Late Cretaceous, *Tsagandelta* (Rougier et al., 2015A), was included in the GM analysis. However, I excluded Tsagandelta from the time-sliced morphometric analyses because its age is too uncertain (Rougier et al., 2015A). *Tsagandelta* is a deltatheroidan metatherian with a molar morphology that is similar to other deltatheroidans. Many deltatheroidans are likely carnivorous and are outliers in my GM analyses (see 4.4 Results). As a morphological outlier, *Tsagandelta* is likely to increase the disparity results in whichever time bin it is eventually designated.

I chose to include molars belonging to genera of questionable taxonomic assignment (i.e., those labeled “cf.” or “?” in the literature). My reasoning is that for a molar to be considered a member of a specific genus, it must possess a morphology that is very similar to other members of that genus. Thus, even if it is later determined that the molar was incorrectly assigned, the

molar shape that is measured by the morphometric methods should be similar to that of the genus it is representing for this study. This concept is similar to concerns of over-splitting or under-splitting of taxa. As discussed below, inconsistencies in taxonomic assignments are unlikely to have a large effect on disparity results.

4.3.2 Ages of time bins and rock formations

Time bins and fossil occurrence data. For morphometric analyses, genera were assigned to time bins based on their temporal ranges, which were determined by first and last appearances of fossils for each genus. For taxonomic diversity analyses, all fossil occurrences were assigned to time bins. (The slight discrepancy between morphometric analyses and taxonomic diversity analyses is due to the different goals of the two analyses. The morphometric analyses attempt to capture disparity of genera within time bins, and details about specific occurrences are unnecessary. Diversity analyses try to capture 'true' diversity values by subsampling or modeling the occurrence data for collections or rock formations, and therefore all occurrences are included in data sets.) Cretaceous time bins (K1-K7) are approximately 5-10 million-year intervals. Early Paleocene (i.e., Danian, D1-D2) time bins are shorter to account for the considerable number of observed fossil occurrences after the K-Pg boundary, and to interpret diversity patterns at a higher resolution. Time bins (with dates from Gradstein et al., 2012) include the Barremian-Aptian (K1; 130.8-113 Ma), Albian (K2; 113-100.5 Ma), Cenomanian-Turonian (K3; 100.5-89.6 Ma), Coniacian-Santonian (K4; 89.6-83.6 Ma), Early Campanian (K5; 83.6-78 Ma), Middle-Late Campanian (K6; 78-72.1 Ma), Maastrichtian (K7; 72.1-66 Ma), Early Danian (D1; 66-64.6 Ma), and Late Danian (D2; 64.6-61.3 Ma). I treat the early Danian (D1) bin as equivalent to the Puercan North American Land Mammal Age (NALMA) and the late Danian

(D2) bin as equivalent to the Torrejonian NALMA. Appendix G provides time bin assignments for taxa used in the morphological analyses.

If lower molars for known genera have not been discovered, then the genera could not be included in the morphometric analyses. However, almost all known tribosphenidan genera from the time period of this study were included in the taxonomic diversity analyses. For occurrence information for taxa used in the taxonomic diversity analyses, see the fossil occurrence dataset that is available via Dryad (doi:10.5061/dryad.qk643). This dataset was originally downloaded from the *Paleobiology Database* (www.paleobiodb.org), and then was vetted based on information in the primary literature. In addition to changes described below, corrections to the original dataset include removing ichnofossils, combining synonymous taxa, assigning rock formations to some occurrences listed as "unknown" formation, updating the absolute ages of some occurrences, and eliminating collections described as "reworked" (e.g., "Bug Creek Anthills (reworked)") since these are often of dubious ages.

Rock formation ages. Absolute ages for taxa and rock formations of this study are often poorly resolved. By assigning genera to time bins rather than assigning absolute ages, the issue becomes less pronounced. However, uncertainties remain. Dating issues are further complicated by genera that span multiple time bins and are found on multiple continents, and formations that were deposited over millions of years. Time bin assignments are based predominantly on information provided by the *Paleobiology Database*, *Fossilworks* (www.fossilworks.org), Kielan-Jaworowska et al. (2004), and Woodburne et al. (2004). In addition, the primary literature was used to confirm many age and taxonomic assignments. The following paragraphs provide discussion concerning some of the age assignment decisions that were made.

Mammals from the Antlers Formation of the Trinity Group are described as Aptian-Albian in age (e.g., Davis and Cifelli, 2011), a period that extends ~25 million years. I cautiously follow the *Paleobiology Database* in assigning taxa from the middle members of the Antlers formation to the Aptian (K1) bin and taxa from the upper members of the formation to the Albian (K2) bin. The Cloverly Formation is also often listed as Aptian-Albian in age (e.g., Kielan-Jaworowska et al., 2004), but Cifelli and Davis (2015) cite preliminary reports of radiometric dating analyses that suggest fossil mammal localities are Albian in age. Therefore, I include all taxa from the Cloverly Formation in the Albian (K2) time bin. Deposition of the Cedar Mountain Formation spans the Barremian (or earlier) through the early Cenomanian. However, all Cedar Mountain genera in this study are from the upper portion of the Mussentuchit Member, which is the youngest member of the formation and Cenomanian in age. Thus, all Cedar Mountain taxa are assigned to the Cenomanian-Turonian (K3) bin.

The *Paleobiology Database* labels some Bissekty Formation taxa as Turonian in age and some as early Coniacian in age. However, recent studies describe the Bissekty as Turonian (e.g., Redman and Leighton, 2009). Thus, I placed all taxa from the Bissekty in the Cenomanian-Turonian (K3) bin. Similarly, the *Paleobiology Database* often labels taxa from the Aitym Formation as Turonian or Coniacian. However, the Aitym Formation overlies the Bissekty Formation and therefore is most likely younger. Thus, I cautiously assign all Aitym taxa to the Coniacian-Santonian (K4) time bin, although I recognize that one or both of these formations may span the K3-K4 boundary.

The Milk River Formation is often described as late Santonian (K4) or early Campanian (K5) in age. I assign Milk River taxa to the Coniacian-Santonian (K4) time bin due to

information provided by Eaton and Cifelli (2013) and Davis et al. (2016). Further, I assign the contiguous Eagle Formation to K4 based on Davis et al. (2016).

Mammal-producing rock formations from the Campanian and Maastrichtian of Mongolia include the Djadokhta, Baruungoyot (i.e., Barun Goyot), and Nemegt formations. The Djadokhta is oldest, and Dashzeveg et al. (2005) conclude that the formation was deposited between 75 and 71 Ma, indicating a late Campanian or earliest Maastrichtian age. I assign Djadokhta taxa to the middle-late Campanian (K6) bin. The Nemegt Formation is considered the youngest of the three formations and is likely Maastrichtian in age. However, the Nemegt Formation has not produced therian fossils. Although traditionally inferred to be Campanian in age (and currently described as Campanian in the *Paleobiology Database*), the Baruungoyot has recently been described as late Campanian-early Maastrichtian (e.g., Fanti et al., 2012). Here, I cautiously assign Baruungoyot mammals to the Maastrichtian (K7) bin for two reasons. First, a recent study demonstrated interfingering of the Nemegt and Baruungoyot formations and concluded that many of the Nemegt and Baruungoyot faunas co-existed (Eberth et al., 2009). This suggests an early Maastrichtian age for Baruungoyot. Second, the *Geologic Time Scale 2012* by Gradstein et al. (2012) pushes back the Campanian-Maastrichtian boundary (i.e., K6-K7 boundary) from 70.6 Ma to 72.1 Ma. The previous boundary was at or near the transition from chron 32 to chron 31. However, the new Campanian-Maastrichtian boundary indicates that the Maastrichtian encompasses much of chron 32. A preliminary magnetostratigraphic analysis of the Nemegt and Baruungoyot formations suggests that they were deposited through chron 32 and into the lower half of chron 31 (Hicks et al., 2001), suggesting that an early Maastrichtian age is likely.

The Straight Cliffs Formation includes two members that have produced mammal fossils: the Smoky Hollow Member and the John Henry Member. The Smoky Hollow Member is

considered Turonian in age, and the John Henry Member is considered Coniacian-Santonian in age (Gradstein et al., 2012). Therefore, I assign Smoky Hollow taxa to the K3 time bin and John Henry taxa to the K4 bin. However, only the John Henry Member has produced enough taxa for inclusion in the disparity analysis of rock formation faunas. The mammals that I include in the disparity analysis of the Straight Cliffs John Henry Member are based on those listed by Eaton and Cifelli (2013), which is an extended list compared to that of the *Paleobiology Database*.

To improve the temporal resolution of patterns for the well-sampled Campanian stage, I split the Campanian into two time bins. The boundary between the early Campanian (K5) time bin and the middle-late Campanian (K6) bin is designated by the Aquilan NALMA-Judithian NALMA boundary, which is approximately 78 Ma (Woodburne, 2004). The Edmontonian NALMA spans the Campanian-Maastrichtian boundary, but I tentatively follow the Paleobiology Database in assigning most Edmontonian mammals to the Maastrichtian bin (K7).

The *Paleobiology Database* assigns taxa from the St. Mary River Formation to the Maastrichtian (K7). However, data within Wilson et al. (2010) suggest that taxa from the Scabby Butte localities, which comprise a majority of the St. Mary River taxa, are likely to be late Campanian (K6) in age. Thus, the St. Mary River Formation taxa are assigned to the K6 time bin.

I treat the early Danian (D1) and late Danian (D2) bins as roughly equivalent to the Puercan NALMA and Torrejonian NALMA, respectively. Renne et al. (2013) dated the K-Pg boundary at 66.0 Ma, and Gradstein et al. (2012) consider the Danian geological stage to extend from 66.0 to 61.6 Ma. The *Paleobiology Database* designates the Puercan as 66.0-63.3 Ma and the Torrejonian as 63.3-61.6 Ma. However, recent studies consider the Puercan to be much shorter in duration, likely extending only 0.9-1.5 million years into the Paleocene (e.g., Sprain et

al., 2015; Williamson et al., 2015). Thus, I cautiously follow Williamson et al. (2015) and designate the early Danian (i.e., Puercan, D1) bin as 66.0-64.6 Ma and late Danian (i.e., Torrejonian, D2) as 64.6-61.6 Ma. However, it should be noted that changes to these dates would not significantly alter results, since most Danian taxa are from North America and are often assigned to NALMAs based on faunal comparisons, not absolute ages. The relatively short duration of the Puercan is a concern, especially because time averaging of data from bins of various temporal lengths could have an affect on disparity patterns through time. Thus, I also calculate disparity for the entire Danian (i.e., D1 and D2 bins merged) to ensure my conclusions about post-K-Pg results are not driven by differences in time bin durations.

Most non-North American taxa in the early Danian (D1) bin are from the Santa Lucía Formation of the Tiupampan South American Land Mammal Age (SALMA), which is considered contemporaneous with Puercan faunas (Gelfo et al., 2009). For the late Danian (D2) bin, most non-North American taxa are from the Shanghu and Wanghudun formations of Asia (Ting et al., 2011). It is possible that some early Shanghu taxa are from the early Danian (D1) bin, but the lack of precise age estimates for the Shanghu formation localities makes it difficult to partition Shanghu taxa into the two bins.

Several rock formations from North America include fossil localities from both the early Danian (D1) and late Danian (D2). For example, the Nacimiento Formation of the San Juan basin in New Mexico includes the Puerco and Torrejon zones, which are the basis for the Puercan and Torrejonian NALMAs. Thus, for the disparity analysis of rock formation faunas, I calculated disparity independently for the Puercan (i.e., D1) Nacimiento taxa and the Torrejonian (i.e., D2) Nacimiento taxa.

4.3.3 Molar images

Penultimate lower molars. For morphometric analyses, I chose to analyze lower molars instead of upper molars primarily because the sample size is greater. Further, the numbers of cusps on upper molars vary between metatherians and eutherians, making it problematic to combine the two clades into a single GM analysis with homologous cusp landmarks. I follow Wilson (2013) in utilizing the lower penultimate molar for metatherians (m3) and eutherians (generally m2), which are likely homologous (O'Leary et al., 2013) and functionally analogous (see discussion and sources within Wilson, 2013). If fossil molars are found in isolation then their dental assignment may be unknown. This occurs most often for m1 and m2 of eutherians, and m2 and m3 of metatherians, which tend to be morphologically very similar, especially in early lineages of these groups. Thus, in an effort to increase the available sample sizes, especially in Cretaceous time bins in which fossils are sparser, molars of uncertain dental assignment (often designated as "m?" in the literature) were used if these were the only available molars. These molars are identified in Appendix H.

Early carnivoramorphans of this study provide a unique concern in that they do not possess an m3, which is the ultimate molar of primitive eutherians. Thus, the carnivoramorphan penultimate molar is m1, unlike all other eutherians in this study. Although I recognize that the m1 of carnivoramorphans is not anatomically homologous to the penultimate molars of other taxa of this study, it is probably functionally analogous and occupies a similar position along the jaw. The carnivoramorphan m1, which is the carnassial molar in modern carnivorans, has a pronounced trigonid with carnassial notches between cusps. This molar is relatively large and likely adapted for shearing of flesh, meaning that it is functionally critical for the carnivoran diet. Conversely, the diminutive ultimate molar of carnivoramorphans (m2) has reduced trigonid

cusps that result in a topographically flatter molar. This molar, along with the talonid basin of the m1, is likely used for grinding rather than shearing (Van Valkenburgh, 1988). Thus, I consider m1 to be the more functionally indicative molar in carnivoramorphans, aiding in my decision to use this molar.

Images. An effort was made to collect lower molar images for as many Cretaceous and Danian tribosphenidan genera as possible. Occlusal surfaces of penultimate lower molars were photographed at the Field Museum of Natural History, New Mexico Museum of Natural History and Science, Sam Noble Oklahoma Museum of Natural History, University of California Museum of Paleontology (UCMP), and Burke Museum of Natural History and Culture. This collection was supplemented with images from the primary literature and Kielan-Jaworowska et al. (2004). Sources for the images are given in Appendix H.

In many cases, multiple molar images were collected for a genus, species, and/or specimen. Thus, images of approximately 400 species and 500 total specimens were collected. The analyses were performed at the generic level, so only one image was chosen per genus. Thus, from the pool of images, 203 occlusal images were chosen for the GM analyses and 202 lateral images were used to calculate cusp heights-to-molar length ratios (see below). Note that some genera used for one analysis may not have been used in the other analysis, depending on the availability of images and preservation of different aspects of the molars (Appendices F and G). Also, note that two *Paranyctoides* species are used (see above), meaning that 202 unique genera were used for the GM analyses and 201 unique genera were used for the cusp heights-to-molar length ratios.

If multiple images of unique molars (either unique specimens and/or unique species) were available for a genus, the molar chosen to represent the genus was based on which one had

ideal positioning (see below), the highest quality image, and/or the least wear or damage. In addition, photographed images (rather than published images) and specimens without questionable taxonomic assignment were preferred. The representative species for each genus is given in Appendix H. Of the published images utilized, high-resolution images of actual specimens were preferred, but reconstructions and drawings were used if no other images were available. Several genera (e.g., *Schowalteria*) with known lower molars were excluded from the analyses because their molars were too worn or damaged. Minor issues concerning preservation or quality of molars used are noted in Appendix I.

The occlusal surface of a molar is not flat, and therefore positioning a molar to photograph the occlusal surface can be subjective. Achieving consistency across diverse taxa with unique molar morphologies can be especially difficult. In addition, published images often include stereopairs of the occlusal surface that are taken at slightly different angles. Thus, a choice had to be made as to which stereopair (or published image among multiple publications) to use for the GM analyses. I chose occlusal images that appear to best center the cusps of the molars into the middle of the molar (i.e. furthest away from the outer edge of the molar). Similarly, when photographing the occlusal surface, the molars were positioned so that the cusps were centered. If the jaw was present/visible, molars were also often positioned so that the jaw was horizontal. Even with these attempts to standardize the imaging, the subjective positioning of molars is a potential source of error, and the effect of this variable was tested (see below).

4.3.4 Morphometric analyses

Geometric morphometrics (GM). A GM analysis of jaw shape (Rohlf and Marcus, 1993) was performed using two-dimensional landmarks, which were collected from images

using *ImageJ* (Schneider et al., 2012). The landmarks include seven landmarks that designate cusps, two landmarks at the junctions between the trigonid and talonid, nine equally spaced semilandmarks around the trigonid, and nine equally spaced semilandmarks around the talonid (Fig. 4.2). However, to obtain the equally spaced semilandmark coordinates for the talonid and trigonid, an outline of these two regions was first acquired by placing 20 points around the outer edge of each region. This amounted to 47 total points collected: 7 'internal' landmarks (Fig. 4.2), 20 points around the talonid, and 20 points around the trigonid. Coordinates for these points are available through Dryad (doi:10.5061/dryad.qk643). Following Wilson (2013), the precingulid and postcingulid were not treated as edges of the molars, in part because adjacent molars often obstruct views of these structures. The junctions of the talonid and trigonid were treated as the points in which the protoconid and metaconid cusps meet or fuse with the outer edge of the molar. The locations of these points are subjective for some molars, and the variance associated with the subjective positioning of these points is included in the error test (see below).

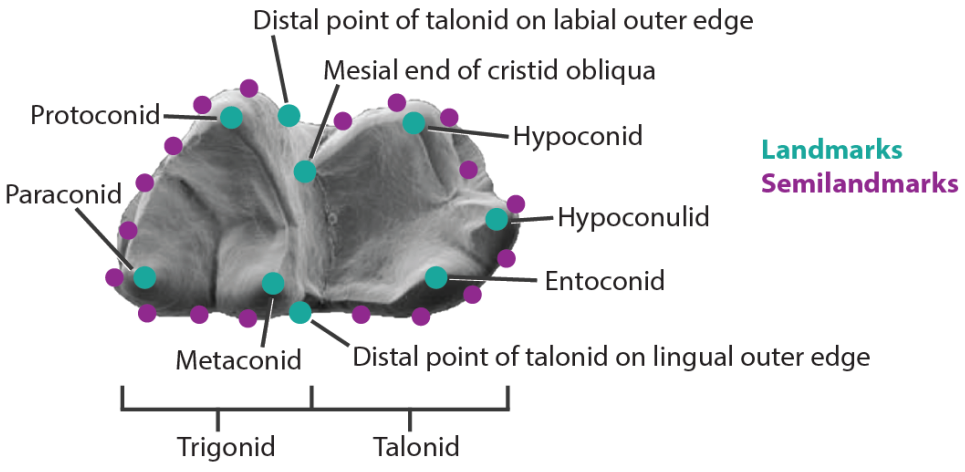

Figure 4.2. Occlusal surface of a lower tribosphenic molar (Davis, 2007) with landmarks (labeled) and semilandmarks. Equally-spaced semilandmarks were produced independently for the talonid outline and the trigonid outline. Anterior is to the left.

Point coordinates were collected for all 203 occlusal molar images of this study. The BreakOutline function within Geometric Morphometrics for Mathematica (Polly, 2016) was used to convert the outline points into equally spaced semilandmarks. The first point of the talonid outline also acts as the last point of the trigonid outline, and the last point of the talonid outline also acts as the first point of the trigonid outline. Since these first and last points are not altered by the BreakOutline function, they are labeled as landmarks rather than semilandmarks in Figure 4.2. Between these first and last landmarks, nine equally spaced landmarks were placed along the outline of the trigonid and nine equally spaced landmarks were placed along the outline of the talonid (Fig. 4.2). This results in 27 total landmarks and semilandmarks: seven "internal" landmarks, two landmarks designating the divides between the trigonid and talonid, nine equally spaced landmarks around the trigonid, and nine equally spaced landmarks around the talonid.

The landmark and semilandmark coordinates were subjected to a Procrustes analysis, which superimposes the landmark shapes to eliminate differences in orientation and size, and minimize differences in shape (Rohlf and Slice, 1990). Using the *geomorph* package (Adams and Otarola-Castillo, 2013) for *R* version 3.2.4 (R Core Team, 2016), I specifically used a Procrustes analysis that treats the equally spaced semilandmarks as sliding semilandmarks that move along their tangent directions to minimize Procrustes distances. Using Geometric Morphometrics for Mathematica (Polly 2016), Procrustes values were ordinated with a principal components analysis and thin plate splines for outlier taxa along axes were produced.

Subcategories. For the GM analyses, genera were subdivided by clade, continent, and formation (Appendix G) for independent calculations of morphological disparity, helping to test potential sampling biases and phylogenetic signals. Independent analyses were run for Eutheria and Metatheria, which are the two major clades within Theria. For simplicity, the eight stem

tribosphenidans of this study were included with the metatherians. These taxa are designated in Appendix G. For the PCA morphospace plots (see 4.4 Results), taxa were designated to more specific taxonomic subgroups to help demonstrate which mammal groups were responsible for occupation of specific morphospace regions. Two paraphyletic groups were included: "early eutherians" and "metatherians and stem tribosphenidans." "Early eutherians" include stem eutherians as well as crown eutherians that are not considered carnivoramorphans, plesiadapiforms, or archaic ungulates. Many of the "early eutherians" in the Paleocene are members of Cimolesta and Leptictida, and have previously been considered members of "Insectivora."

To explore evolutionary trends on a regional scale, genera from North America and Eurasia were separated and disparity trends were considered independently for the two continents. European and Asian taxa are designated separately in Appendix G, but these taxa were merged into a Eurasian subcategory for the continental analyses. In addition, genera were separated based on the rock formations in which they have been found in order to help examine regional disparities. Morphological disparity was calculated for any formation for which at least three genera with adequate occlusal images are known. These formations are indicated in Appendix G.

Several taxa are known from more than one continent and more than one time bin, complicating calculations of morphological disparity per continent. For example, *Pediomys* is known from the Campanian and Maastrichtian (K5-K7) of North America, but it is also known from Europe in the Maastrichtian (K7). Thus, for global and North American analyses, *Pediomys* was included for K5-K7 bins, but for the Eurasian analysis it was only included in the K7 bin.

Cretaceous archaic ungulates and *Deccanolestes*. I include four archaic ungulates (i.e., "condylarths") in the Maastrichtian (K7) time bin: *Protungulatum*, *Kharmerungulatum,* *Paleoungulatum,* and *Baioconodon*. *Baioconodon* and *Paleoungulatum* fossils were recently described from a latest Cretaceous (K7) locality in the Hell Creek Formation (Kelly, 2014). *Baioconodon* is common in the Puercan (D1) but had not previously been found in the Cretaceous. Although it is possible that this locality includes reworked material from Paleocene channel deposits, Kelly (2014) argues against this by noting the lack of deep Paleocene channels at the locality.

The only known *Protungulatum* specimen from the Maastrichtian is a single premolar (Archibald et al., 2011), wheras all other occurrences are from the Paleocene. The phylogenetic analysis of Wible et al. (2009) recovered *Protungulatum* outside of crown placentals, suggesting that it convergently evolved with archaic ungulates within Placentalia. However, O'Leary et al. (2013) recently recovered the genus within Placentalia using an extensive phylogenetic character matrix. The molar of *Kharmerungulatum* from the Maastrichtian of India is heavily worn and its taxonomic assignment as an archaic ungulate is tenuous (Prasad et al., 2007). Thus, I cautiously assign *Protungulatum* and *Kharmerungulatum* to the archaic ungulates group, but I recognize the possibility that they should be included with the stem eutherian group.

Deccanolestes is a eutherian from the Maastrichtian of India. Postcranial material led Boyer et al. (2010) to suggest taxonomic affinities to early euarchontans such as plesiadapiforms. Thus, I cautiously include *Deccanolestes* within the plesiadapiform group.

The uncertain taxonomic assignments of *Protungulatum*, *Kharmerungulatum*, and *Deccanolestes* have little effect on the results of this study. (The only analysis to subdivide taxa by clade was a disparity analysis for eutherians and metatherians, and all three of these genera

fall within Eutheria.) However, if the taxa are considered crown members of Placentalia, this adds support to my conclusion that therians were more diverse prior to the K-Pg boundary than often recognized. It implies that divergent placental groups were already present prior to the extinction event, but they simply may have lived in regions that are not preserved by the rock record.

Calculating morphological disparity using GM results. Variance from the mean is a commonly used disparity metric and the preferred metric of this study. The major benefit of variance is that it is largely immune to differences in sample size between time bins. In addition, variance is likely to be less sensitive to outliers than some alternative metrics. I calculate variance independently for each time bin (or rock formation) as the sum of the squared Procrustes distances from the Procrustes mean, divided by the sample size of that time bin. The Procrustes mean is the mean for each time bin or formation, not the overall mean. Error bars are $\pm$1 standard deviation generated from 1000 bootstrap replicates.

A negative aspect of variance as a measure of disparity is that inconsistencies in taxonomic assignments (i.e., over-splitting or under-splitting of taxa) can notably alter results, especially for time bins (or subcategories) with small sample sizes. For instance, if members of an outlying genus in morphospace were reclassified as multiple genera, this would result in additional outliers and greater overall variance. Similarly, splitting of taxa that are close to the mean shape for the sample would lead to a decrease in variance. Thus, the sum of ranges disparity metric, which is largely immune to inconsistencies in taxonomic assignments, was also calculated for the global dataset. This metric is a measure of the overall area occupied in morphospace. If over-splitting of a genus occurred, the result would be clusters of similar genera in morphospace. Inclusion of more or less taxa that are similar to other taxa would not have a

large effect on the area occupied by the sample in morphospace. I calculated the sum of ranges independently for each time bin by finding the range for each Procrustes value, and then summing the ranges. The sum of ranges metric, however, is biased by differences in sample sizes (i.e., a greater sample size is likely to result in a greater sum of ranges). Thus, I subjected samples from each time bin to rarefaction, which subsamples without replacement and allows for a more accurate comparison between bins of various sample sizes (Foote, 1992). The subsampling value was set at eight because this is the smallest sample size of the bins. The procedure was repeated 1000 times and the median value of the replicates was recorded. Error bars were calculated as the 95% quantile of the 1000 rarefaction replicates.

Error test. An error test was performed to assess the magnitude of variance associated with the photography of occlusal molar surfaces and inconsistent selection of landmark locations. This test is necessary because determining the occlusal plane for photography of a tribosphenic molar and maintaining consistency in method across diverse taxa can be difficult, especially if the molars are not well preserved. In addition, the error test helps determine the effect of performing GM analyses at the generic level rather than species level. For the error test, I photographed molars of 13 species of various ages, preservation qualities, sizes, and taxonomic groups. The 13 molars were photographed six times each, with each set of photographs taken on separate days. Landmark data was collected on each molar and the coordinates were subjected to the same GM procedures as the main dataset. However, the molars were projected onto results of the main dataset (thereby not altering the original PCA morphospace) so that measures of disparity and assessment of morphospace occupation could be accurately compared with the original results. Disparity was calculated as variance of the six replicates for each species.

Molar lengths and cusp heights-to-molar length ratios. To account for morphological features not captured by two-dimensional (2D) GM, additional analyses were performed. Specifically, linear molar measurements were collected, and supplemental measures of disparity were obtained from molar lengths and cusp heights-to-molar length ratios.

As a proxy for body size, I used the length of the penultimate molar because this data was easily accessible from publications and photographs. To remain consistent with the GM analyses, I only used measurements of one species to represent a genus. If multiple measurements were available, I used the measurement for the molar used in the GM analysis. Some measurements obtained from the published literature are averages of multiple specimens (see Appendix I). The molar lengths were natural log transformed. Molar length (ln mm) disparity was calculated independently for each time bin as the standard deviation from the mean of each time bin.

There is a concern that the 2D GM does not adequately capture variance among genera associated with cusp elevation. Thus, I used lateral images of molars to collect cusp heights-to-molar length ratios. To acquire cusp heights-to-molar length ratios, a line was drawn parallel to the occlusal molar surface (or edge of the dorsal jaw surface) through the ventral-most point along the occlusal edge of the molar (red line of Figure 4.3). The line extended the length of the molar. From that line, perpendicular lines were drawn to the tallest points of the trigonid and talonid (Fig. 4.3). For several chipped or worn molars, neighboring molars along the tooth row were used to help estimate cusp heights (see Appendix I). Ratios were calculated by dividing the summed trigonid and talonid elevations by the length of the molar. In addition, I report the ratio of the trigonid height to the molar length (Appendix I). Disparity in cusp heights-to-molar length ratios was calculated independently for each time bin as the standard deviation from the mean of each time bin.

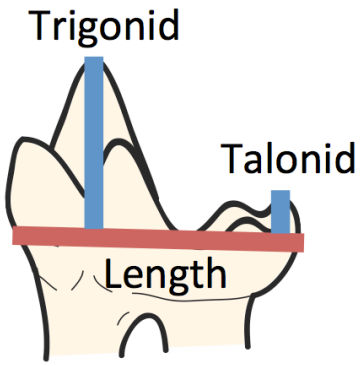

Figure 4.3. Measurements for cusp heights-to-molar lengths. The red line represents the length of the molar and the blue lines represent the elevations of the trigonid and talonid above the talonid basin sufrace. The trigonid and talonid heights were summed and divided by the molar length. Anterior is to the left.

4.3.5 Taxonomic diversity analyses

It is important to assess both morphological disparity and taxonomic diversity when examining macreovolutionary diversity patterns (Fig. 4.1; Foote, 1993; Benton, 2015). I performed all disparity analyses of this study, and I vetted the fossil occurrence dataset used in the taxonomic diversity analyses. However, my colleague, Elis Newham, implemented the taxonomic diversity analyses that are presented here (and published in Grossnickle and Newham, 2016). The following section includes a brief overview of our methods, but for a more thorough description of methodology see Grossnickle and Newham (2016) and Newham et al. (2014).

Counts of unique occurrences of genera were generated for each time bin as a taxonomic diversity estimate (TDE), calculated using fossil occurrence data of Tribosphenida downloaded from the *Paleobiology Database* on November 19, 2015. Ichnofossils were removed from the dataset, occurrence information was vetted, and all unique fossil occurrences were assigned to time bins. The resulting dataset contains 1180 unique occurrences of 280 genera.

Several sources of bias have been shown to apparently mask genuine patterns in biodiversity through time and space (Peter and Foote, 2001). Thus, to confidently analyze taxonomic diversity, the dataset was assessed for potential biases that have been shown to distort observed diversity patterns in the fossil record (Smith and McGowan, 2007; Crampton et al., 2003). Modeling-based residual analyses were performed to attempt to correct for the effects of several aspects of fossil sampling that may affect the proportions of observed occurrences. Residual analyses model theoretic diversity patterns that would be expected to occur if completely controlled by a specific bias, often modeled using a proxy (e.g., (Crampton et al., 2003; Newham et al., 2014). Here, counts of unique therian-bearing formations (TBFs; n = 95) for each time bin were used as a proxy for taphonomic bias. (Grossnickle and Newham (2016) also used counts of unique fossil collections containing therians (n = 378) as a proxy for anthropogenic sampling bias. Results were similar to those for TBFs and are not presented here.) All TDE counts were $\log_{10}$ transformed and ranked. A modeled diversity estimate (MDE) for each interval was then generated for each sampling proxy by applying linear ordinary least squares regression between ranked proxy and TDE data (Crampton et al., 2003). Subtracting the MDE from the TDE of each interval left a residual diversity estimate unexplained by variation in the proxy under scrutiny (i.e., high residual values for a bin indicate 'genuine' diversification). Modeling followed refinements of Lloyd (2012), allowing us to determine via Akaike information criterion scores that a linear model best fits the relationship between global TDE and the proxies in question.

In addition, shareholder quorum subsampling (SQS) was employed to help correct for unevenness in the proportion of fossil observations sampled between intervals, by generating a standardized subsample of observations within each interval (Alroy, 2010). Unlike other

subsampling techniques such as rarefaction, SQS allows the intensity of sampling to change between intervals based on the frequency of observations of particular taxa within the interval in question. Taxa observed within an interval are treated as 'shareholders' whose frequencies of observations form their 'share.' Good's *u* coverage estimate (Good, 1953) is used to estimate the relative proportions of 'true' diversity represented in each interval. Fossil occurrences within an interval are then randomly drawn until taxa that have been sampled at least once have summed a total number of frequencies ('shares') to meet a pre-determined quorum. A range of increasingly stringent quorums from 0.2 to 0.8 was used.

Resources that assisted in the implementation of these taxonomic diversity analyses include *R* version 3.2.4 (R Core Team, 2016), PAST statistical analysis program (Hammer et al., 2008), *R* script available from Dr. Lloyd's website (http://www.graemetlloyd.com), and *R* script available on John Alroy's website (http://bio.mq.edu.au/~jalroy/SQS/html) (Grossnickle and Newham, 2016).

4.4 RESULTS

4.4.1 Morphospace occupation and diet

Dietary inference. The GM analysis of early therian molars results in a dietary spectrum along the first principal component (PC1) axis (Fig. 4.4): frugivorous/omnivorous taxa (e.g., most archaic ungulates, plesiadapiforms, and taeniodonts) are on the left, and carnivorous/insectivorous taxa (e.g., cimolestids, carnivoramorphans, mesonychids, and deltatheroidans) are largely on the right. (I use "frugivore" broadly (*sensu* Collinson and Hooker, 1991) and consider it to include strict frugivores, granivores, and non-high-fiber herbivores/omnivores.) This dietary interpretation is supported by the thin plate splines in Figure

4.4, which demonstrate broader molars to the left and thinner, more blade-like molars to the right.

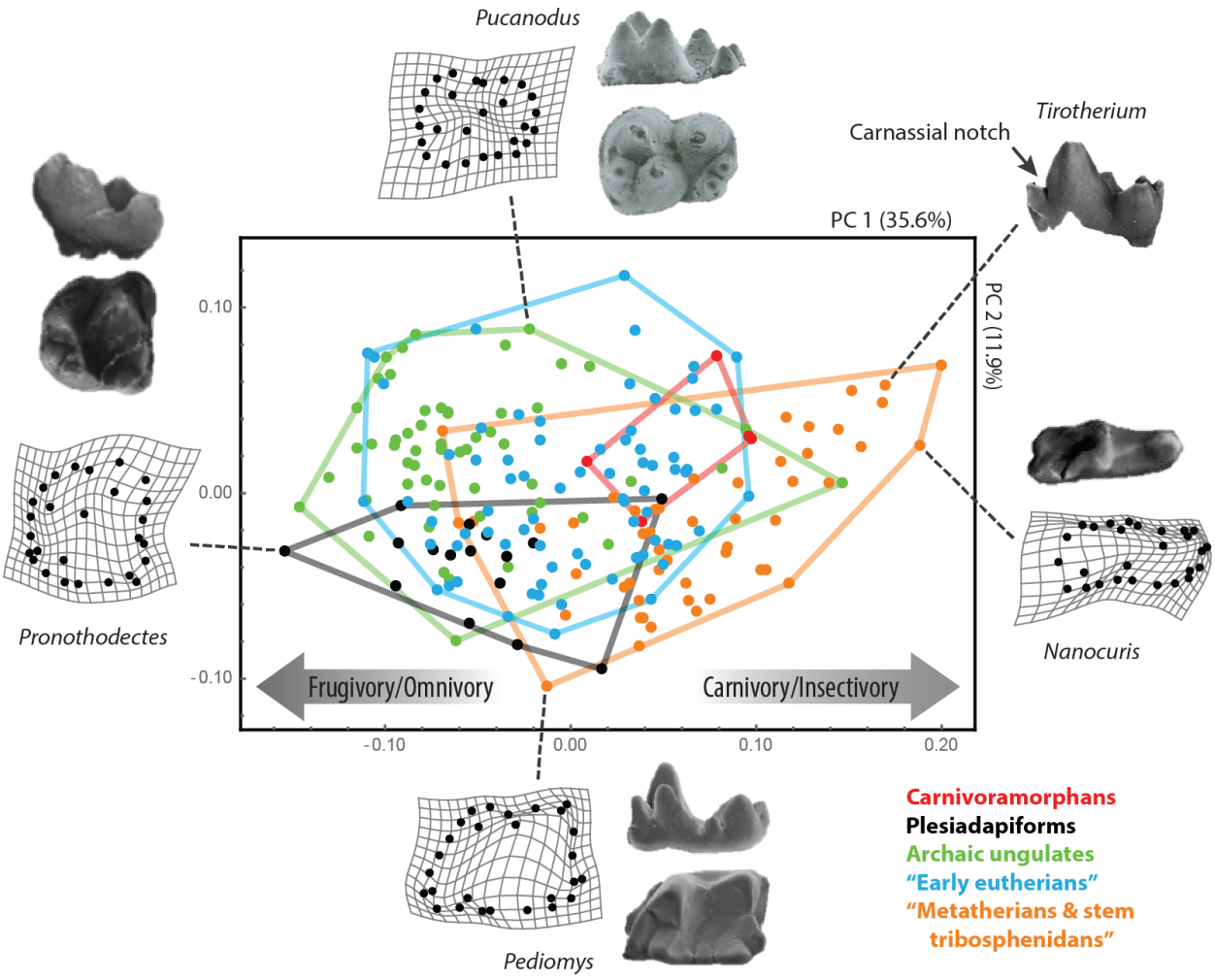

Figure 4.4. The PC1 and PC2 morphospace plot of the geometric morphometric analysis. Landmarks and semilandmarks used in the analysis are shown in Figure 4.2, and changes to their relative positions along PC axes are highlighted by splines (and molar images) of outlying genera. The dietary spectrum along PC1 is supported by the flat, broad molars (indicative of plant-based diets) to the left and thin, bladelike molars (indicative of carnivory) to the right (see text). Carnassial notches are present in molars of many modern carnivores, and the carnassial notch of *Tirotherium* is highlighted to support the conclusion that molars to the right represent carnivorous taxa. See Appendix H for sources of the molar images.

The two major groups to occupy the left (i.e., omnivorous/frugivorous) side of morphospace are archaic ungulates and plesiadapiforms. Hunter (1997) described many archaic ungulates as dietary generalists based on quantitative comparisons to modern taxa. (I use dietary "generalists" to refer to inferred omnivores.) Although plesiadapiforms likely include taxa with a diversity of diets, most are believed to have been frugivorous or omnivorous (see discussion and citations within Eriksson, 2014). Additional groups that occupy the left side of morphospace are polydolopimorphian metatherians, which often possess bunodont molar morphologies indicative of frugivory or omnivory (Goin et al., 2016), and some taeniodonts, which often possess worn molars and relatively large body sizes that are suggestive of herbivorous diets. It is worth noting that high-fiber herbivorous therians do not appear in the fossil record during the temporal range of this study (Collinson and Hooker, 1991; Janis, 2000).

The right side of the PC1 axis in Figure 4.4 includes several therian groups with inferred carnivorous or insectivorous diets. This includes carnivoramorphans, cimolestids, mesonychids, and deltatheroidans. (Mesonychids are archaic ungulates, but unlike most archaic ungulates they are interpreted to be carnivorous.) Some of the molars of these taxa include carnassial notches (e.g., see *Tirotherium* in Figure 4.4), and the deltatheroidan *Nanocuris* appears to have a carnassial-like molar with a much reduced talonid basin. Carnassial molar morphologies are indicative of carnivorous diets in modern mammals. Thus, the similarities to modern carnivoran molars support my interpretation that the right side of morphospace is occupied by carnivorous (or insectivorous) taxa.

In addition to PC1, the PC2 axis in Figure 4.4 appears to capture morphological variance associated with diet. The molars with negative PC2 scores (i.e., lower taxa in Figure 4.4) tend to have taller cusps that are cone-shaped, whereas molars with positive PC2 scores appear to have

bulbous cusps with rounded surfaces. Molars with taller cusps are more likely to possess larger relief indices, and a high relief index is associated with folivory and insectivory in euarchontans (Boyer, 2008). Bunodont molars with bulbous cusps, on the other hand, may be associated with crushing of food items such as nuts and seeds, suggesting a more frugivorous or omnivorous diet. Thus, PC2 may be informative in terms of differentiating taxa by dietary preference. It is also worth noting that both PC1 and PC2 capture variance associated with positions of 'internal' cusps relative to the molar outline, which are traits not easily assessed by traditional molar measurements.

PCA axes. For the principal components analysis (PCA) of the GM analysis of molar morphologies (Fig. 4.4), the PC1 axis captures 35.6% of the total variance and PC2 captures 11.9% of total variance. Thus, a majority of the shape variance is not being displayed in Figure 4.4. Although this is not ideal for visualization of results, it is largely inconsequential for the results and conclusions of this study. For instance, disparity was calculated using all Procrustes values, meaning no shape variance was excluded. Also, the first two PC axes appear to capture morphological variance that is associated with differences in dietary preference (see above). Thus, PC1 and PC2 appear to be the most functionally important axes. Morphospace plots for PC3 (8.3% of variance) and PC4 (7.0% of variance) were produced and examined, but the morphological variance along the axes did not appear to be strongly correlated with diet.

4.4.2 Functional diversity through time

Ecomorphospace occupation. PCA morphospace plots were produced for each of the time bins of this study (Figs. 4.5 and 4.6). They are derived from the original PCA (Fig. 4.4), but each plot only displays those genera which are present in the fossil record at that time (or are

assumed to be present based on ghost lineages). This allows for tracking of morphospace occupation through time. As established in Figure 4.4, there is also an ecological aspect of the morphospace region because morphological changes along PC axes 1 and 2 are associated with diet. Thus, Figures 4.5 and 4.6 display the ecomorphospace occupation of therian mammals through time. This is important in that it allows for inferring adaptive changes to ecological opportunities, providing an especially informative means of examining diversity patterns through time. Because I am considering ecologically relevant traits, the ecomorphological disparity results can also be viewed as functional diversity (Petchey and Gaston, 2006).

D2 – Late Danian, Torrejonian NALMA (64.6-61.6 Ma)

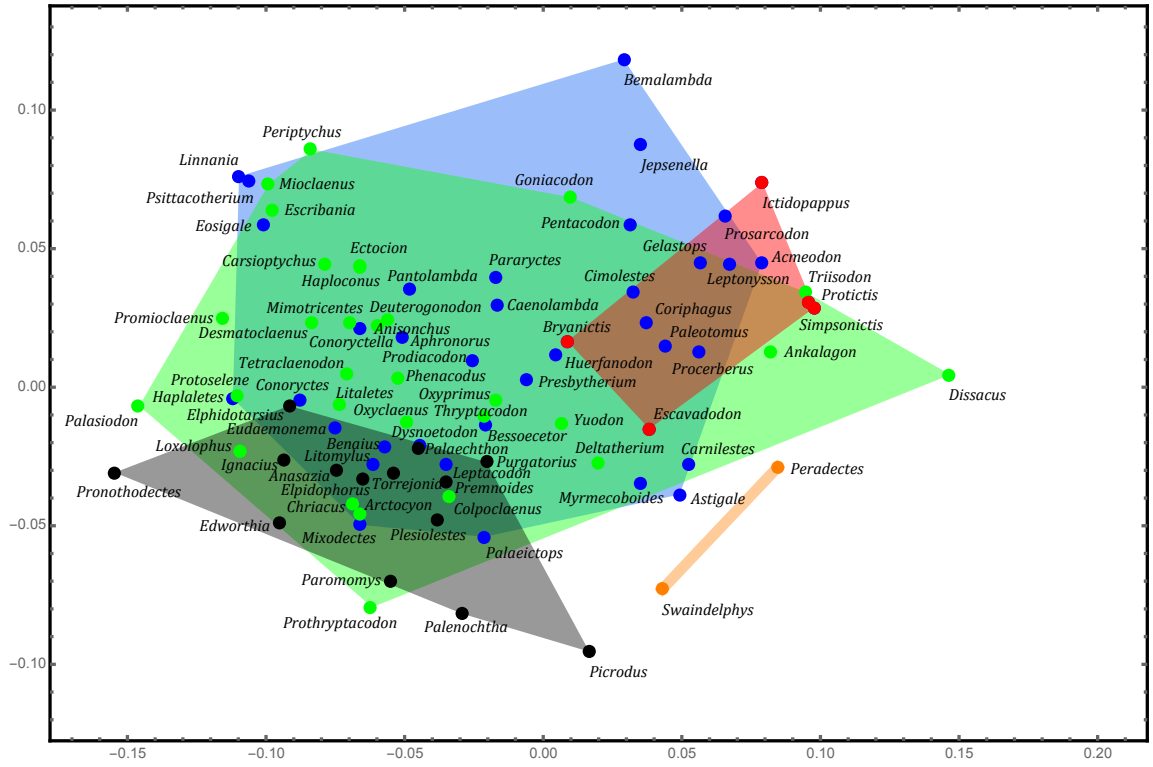

D1 – Early Danian, Puercan NALMA (66.0-64.6 Ma)

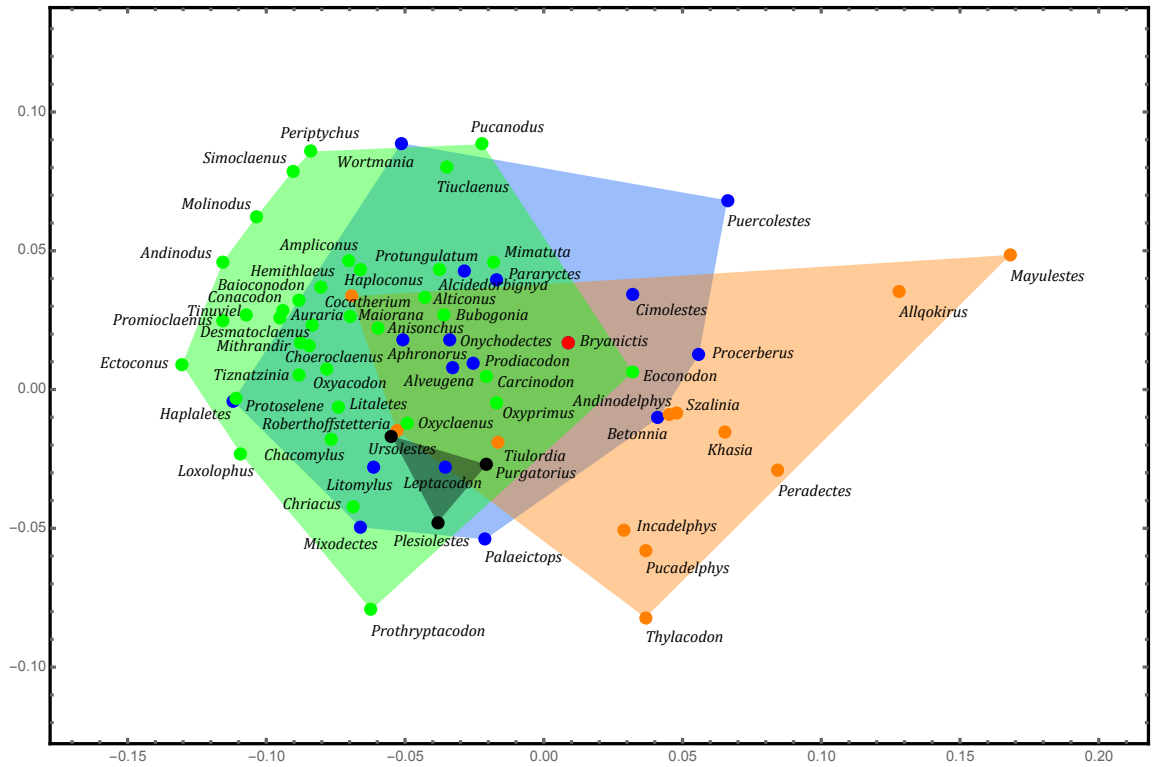

Figure 4.5. Time-sliced morphospace plots of the geometric morphometric analysis.

K7 – Maastrichtian (72.1-66.0 Ma)

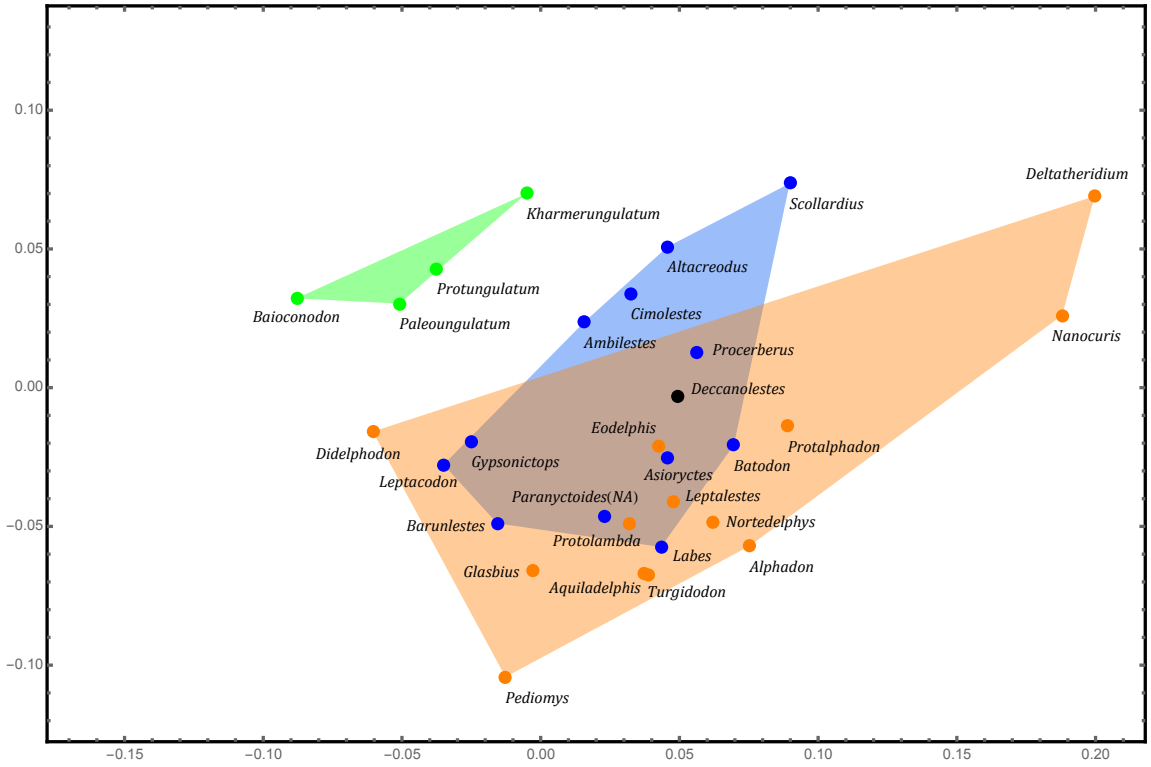

K6 – Middle and Late Campanian (~78-72.1 Ma)

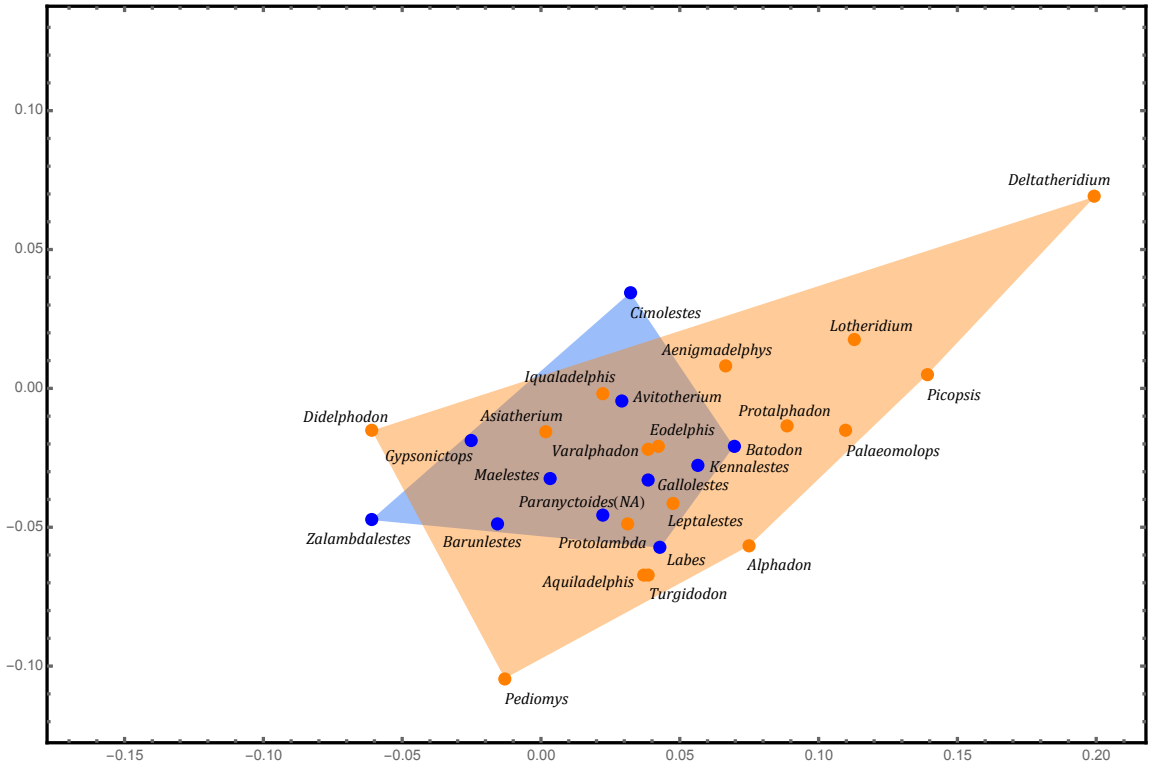

Figure 4.5, continued.

K5 – Early Campanian (83.6-78 Ma)

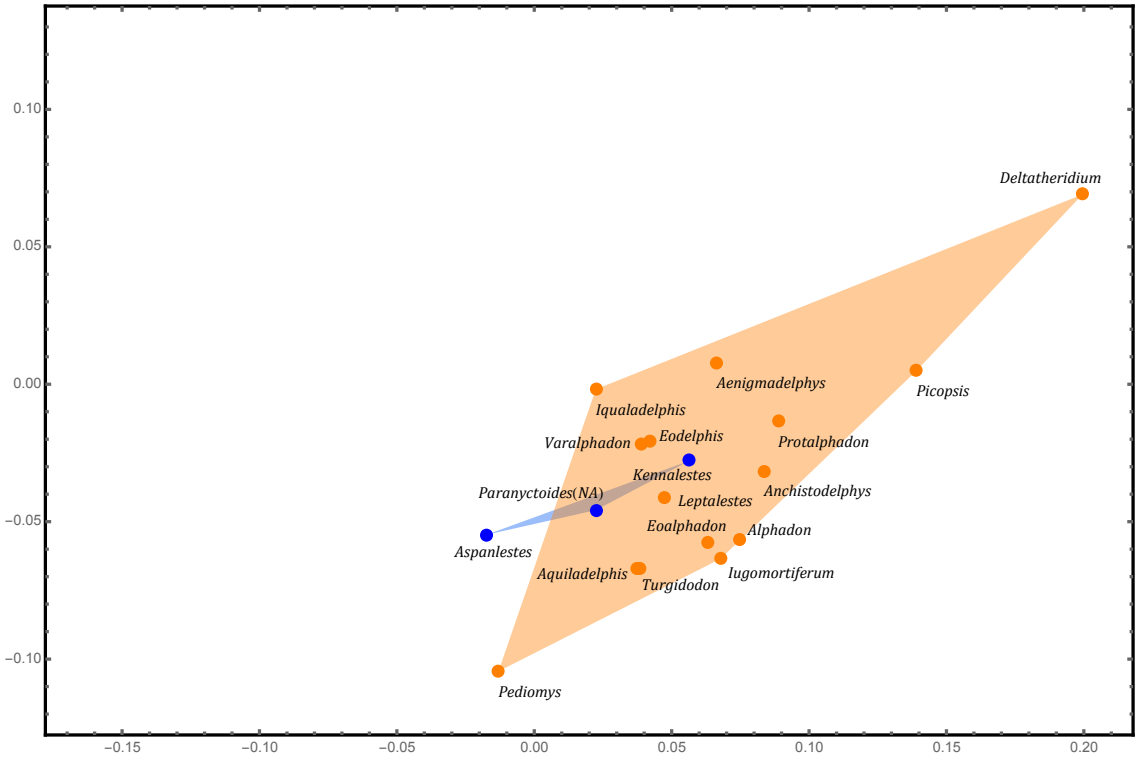

K4 – Coniacian-Santonian (89.6-83.6 Ma)

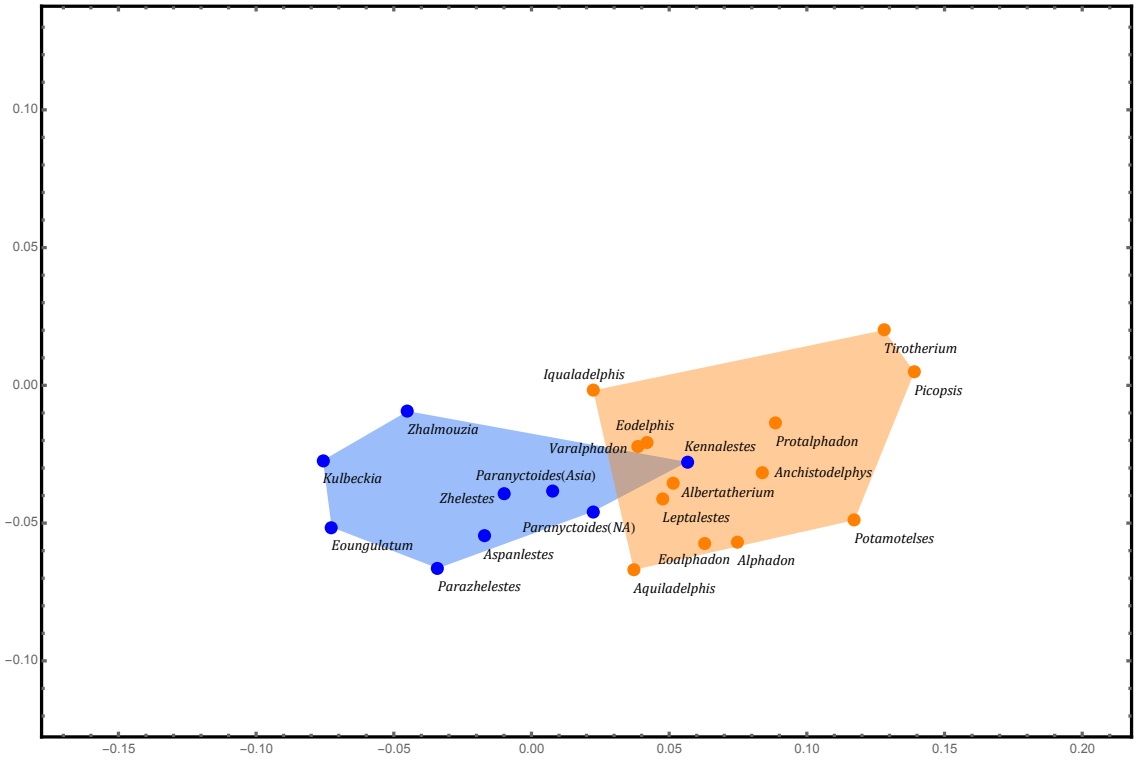

Figure 4.5, continued.

K3 – Cenomanian-Turonian (100.5-89.6 Ma)

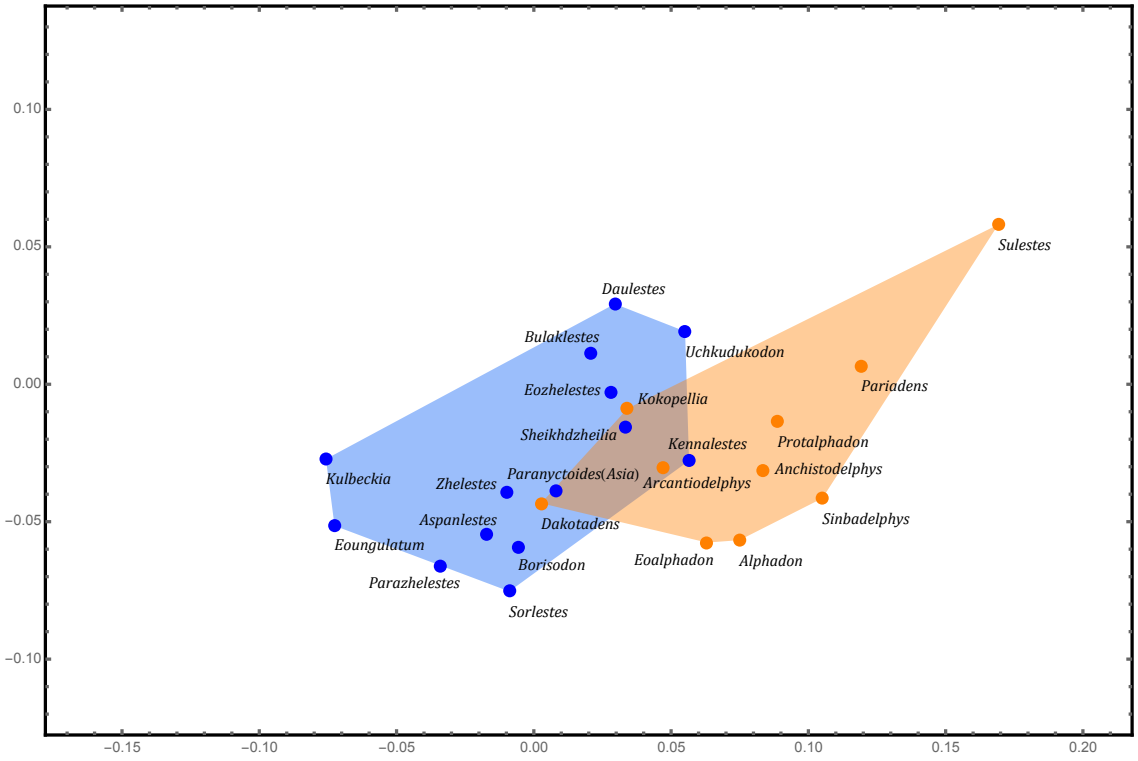

K2 – Albian (113-100.5 Ma)

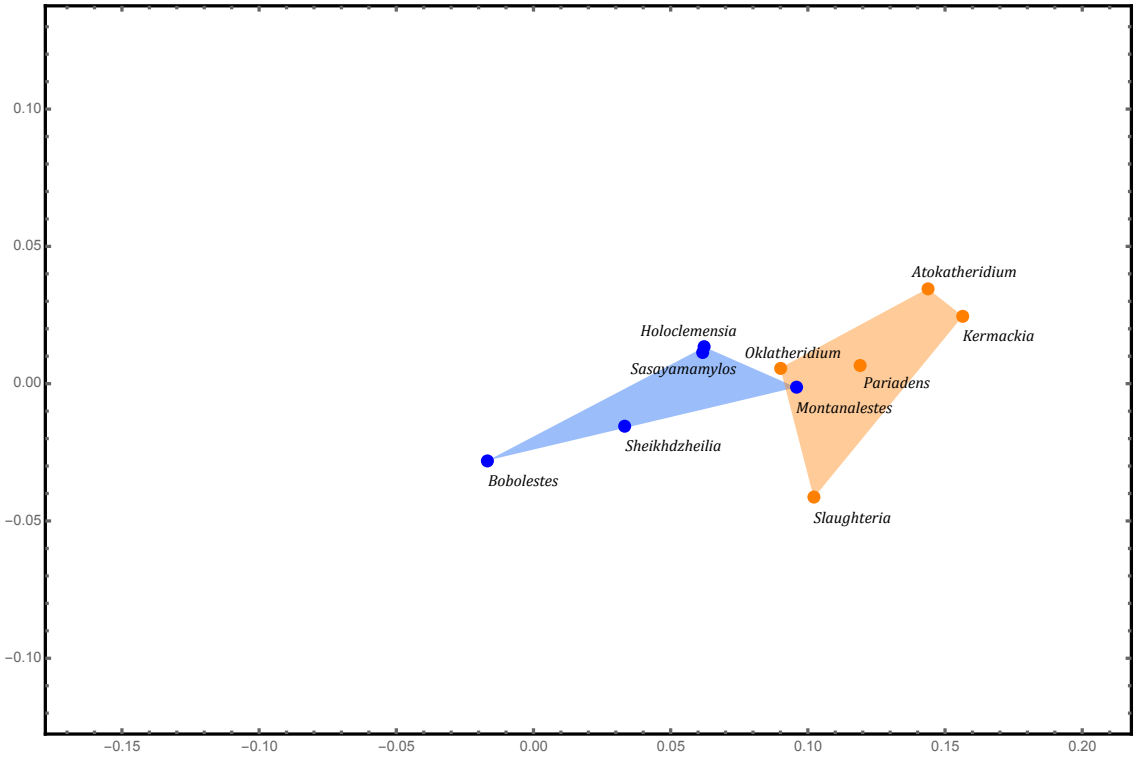

Figure 4.5, continued.

K1 – Barremian-Aptian (130.8-113 Ma)

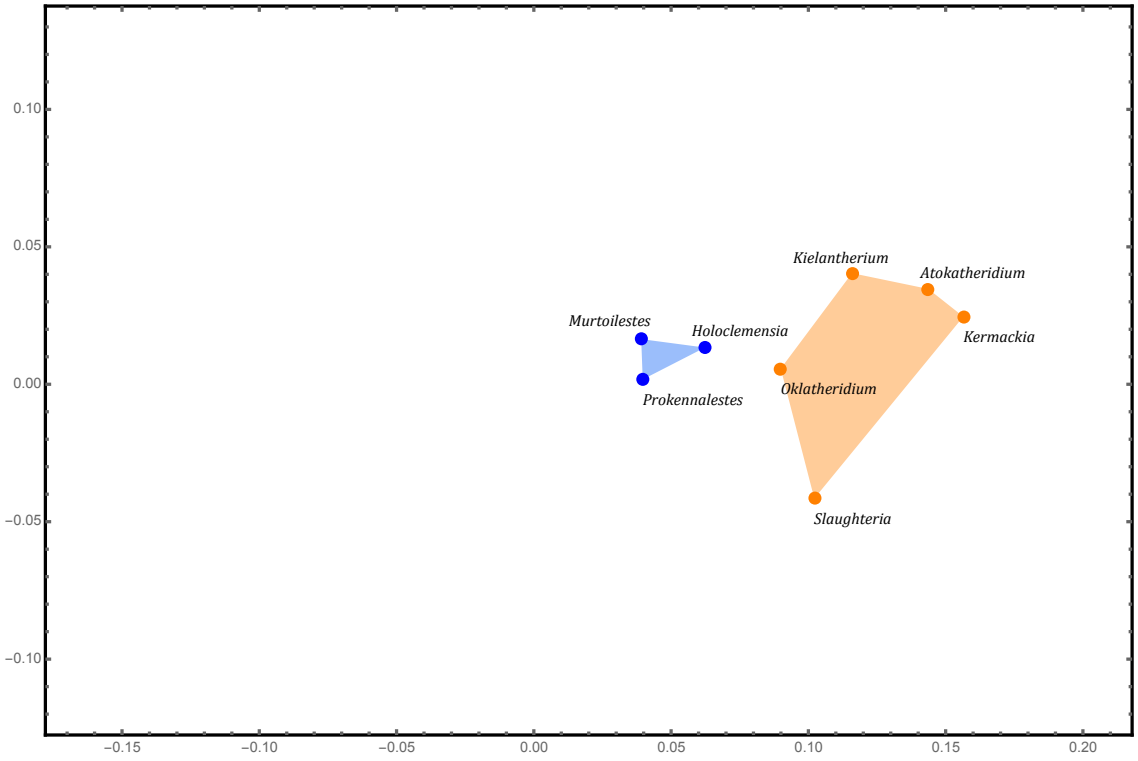

Figure 4.5, contiued. Time-sliced morphospace plots for PC1 (35.6% of variance) and PC2 (11.9% of variance) of the geometric morphometric analysis. The temporal spans of the time bins are noted above the plots. The results are the same as in Figure 4.4 but genera are separated by the time bins in which they are known in the fossil record. Polygon colors are consistent with Figures 4.4 and 4.6: orange, "metatherians and stem tribosphenidans;" blue, "early eutherians;" green, archaic ungulates; black, plesiadapiforms; red, carnivoramorphans. *Paranyctoides (NA)* is *P. sternbergi*, and *Paranyctoides (Asia)* is *P. quadrans* (see text). See Appendices E, F, and G for additional information on the genera and fossil specimens used in the GM analysis. Abbreviations: Ma, million years ago; NALMA, North American Land Mammal Age.

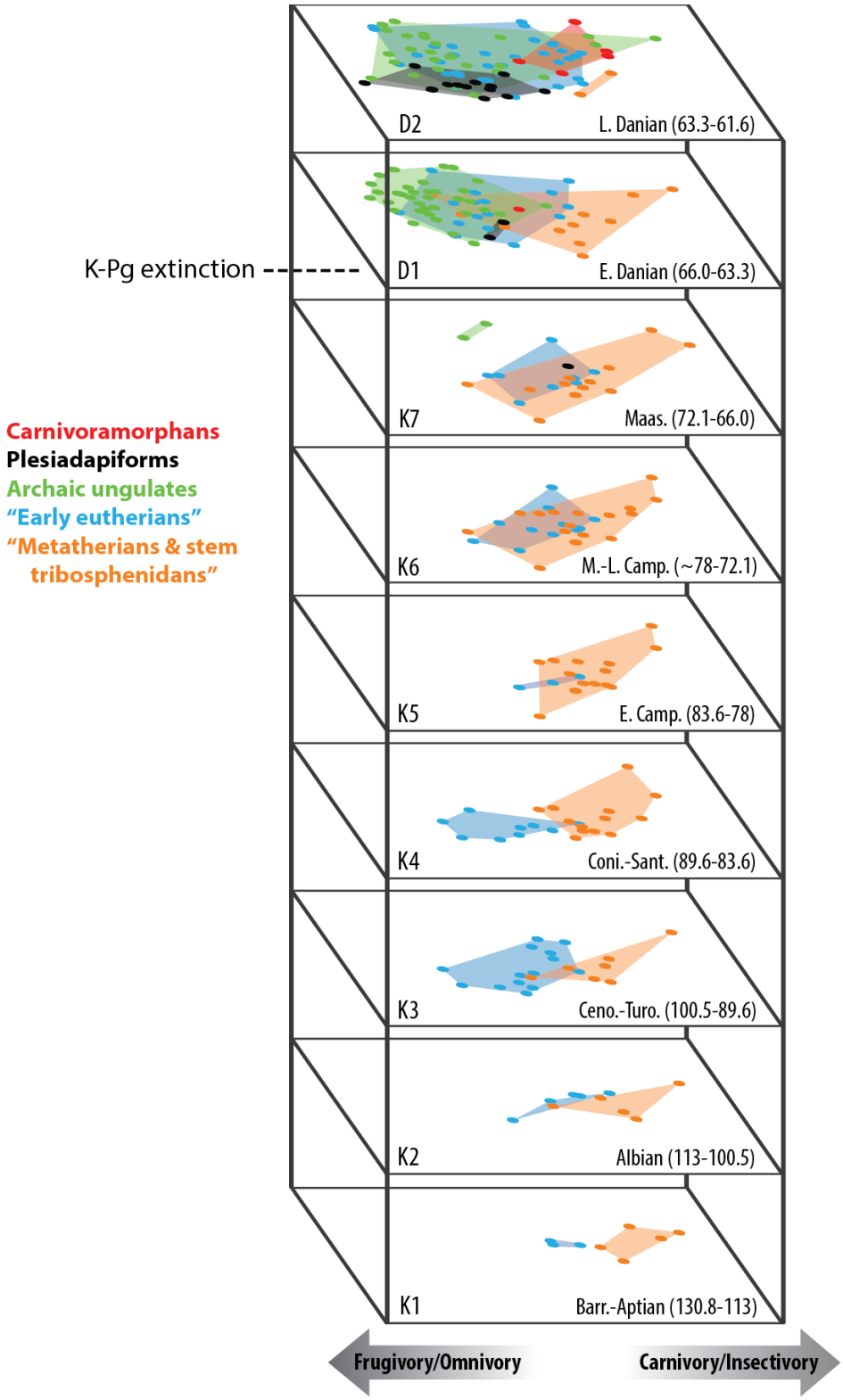

Figure 4.6. Stacked PC1 and PC2 morphospace plots from Figure 4.5. Note that the PC1 axis appears to be strongly correlated with diet (Fig. 4.4), with herbivorous genera to the left and carnivorous taxa to the right. See Figure 4.5 for labels of points.

Figures 4.5 and 4.6 display the same time-sliced morphospace plots, but Figure 4.5 includes labels while Figure 4.6 allows for easier visualization of ecomorphospace occupation through time. See Appendices E, F and G for additional information about the molars and genera that were chosen for this analysis.

Disparity metrics. To further examine the ecomorphological patterns of early therians, I calculated morphological disparity of molar shape for each time bin, using both the global sample (n = 203) and subamples (i.e., continental faunas, major clades, and rock formation faunas). A majority of the results are based on variance of Procrustes values from the mean of each time bin, although sum of ranges was also calculated for the global sample. Results of these analyses are provided in Figure 4.7, Figure 4.8, and Table 4.1.

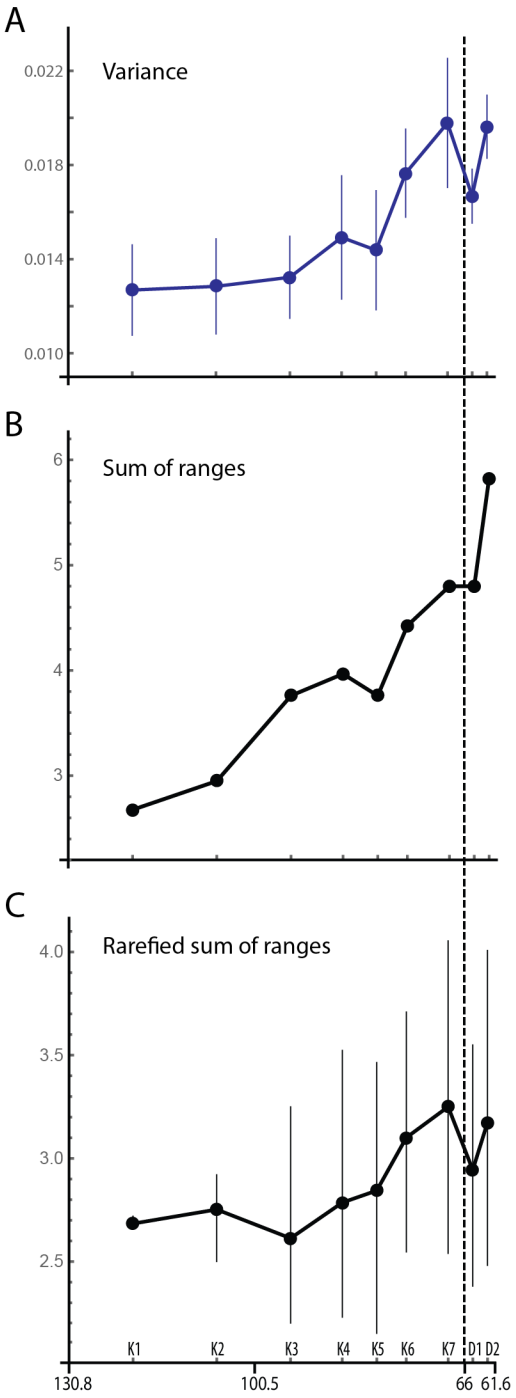

Figure 4.7. Morphological disparity of molar shape through time based on the global sample. Disparity is calculated independently for each time bin as variance (*A*), unrarefied sum of ranges (*B*), and rarefied sum of ranges (*C*), using all Procrustes values for each metric. Error bars for variance (*A*) are ±1 standard deviation generated from 1000 bootstrap replicates. Error bars for rarefied sum of ranges (*C*) are the 95% quantile of the 1000 rarefaction replicates. Ages of time bins are given in the text and Figure 4.5. The dashed vertical line represents the K-Pg boundary.

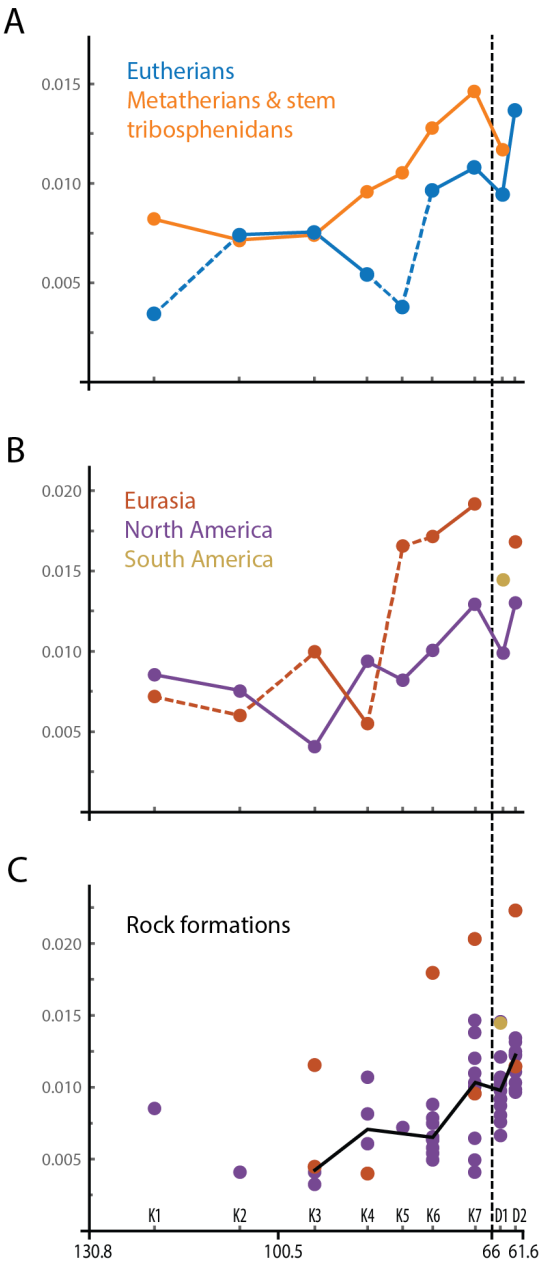

Figure 4.8. Morphological disparity of molar shape through time for major clades (*A*), continents (*B*) and rock formation faunas (*C*). Disparity is calculated independently for each time bin (or rock formation fauna) as variance from the Procrustes mean. It was not calculated for metatherians in D2 or Eurasian taxa in D1 because sample sizes were less than three genera. Dashed lines connect time bins for Eurasian faunas (K1, K2, and K5) and eutherian faunas (K1 and K5) in which variance is based on three or four genera. All other bins include at least five genera. For rock formation faunas (*C*), point colors correspond to the continents from which they are located (see *B* for color key), and the black trend line represents the median formation values for bins with four or more formations. Several formations are represented in multiple bins if they contain significant faunas from more than one bin (Table 4.1, Appendix G). Ages of time bins are given in the text and Figure 4.5.

Table 4.1. Morphological disparity results for individual time bins and rock formations. These results are displayed in Figure 4.7 and 4.8. All disparity values besides the sum of ranges metrics are calculated as variance of Procrustes values from a Procrustes mean. The Procrustes mean is calculated independently for each time bin or rock formation. The values for the rarefied sum of ranges metric are the median value of 1000 replicates. Results based on only three taxa are displayed in italics. Ages of time bins are given in the text and Figure 4.5.

	Time Bins								
	K1	**K2**	**K3**	**K4**	**K5**	**K6**	**K7**	**D1**	**D2**
Global									
Variance	0.0091	0.0091	0.0094	0.0106	0.0103	0.0126	0.0145	0.0116	0.0138
Unrarefied sum or ranges	1.8834	2.0463	2.5895	2.7630	2.6797	3.1608	3.4652	3.4106	4.1842
Rarefied sum of ranges	1.8834	1.8983	1.7649	1.9057	2.0110	2.1599	2.2645	1.9951	2.2139
Continents									
North America	0.0086	0.0076	0.0041	0.0094	0.0082	0.0101	0.0130	0.0099	0.0130
Eurasia	0.0072	0.0060	0.0099	0.0055	0.0165	0.0171	0.0192		0.0168
South America								0.0144	
Major clades									
Eutheria	0.0034	0.0074	0.0076	0.0054	0.0038	0.0096	0.0108	0.0094	0.0137
Metatheria & Stem Tribosphenida	0.0082	0.0072	0.0074	0.0096	0.0105	0.0128	0.0146	0.0117	0.0025
Molar dimensions									
Molar length standard deviation	0.1567	0.1597	0.2827	0.2757	0.2997	0.4279	0.5099	0.5178	0.6864
Cusp heights-to-molar length ratio standard deviation	0.1999	0.1669	0.1472	0.1490	0.1744	0.1846	0.2112	0.1789	0.2017
Rock formations									
Antlers (K1 and K2 faunas)	0.00855								
Cloverly		*0.0041*							
Cedar Mountain (Mussentuchit Member)			*0.0032*						
Dakota			0.0041						
Khodzhakul (K3 & K4 faunas)		*0.0044*							
Bissekty			0.0115						
Aitym				0.0040					
Milk River				0.0107					
Eagle				0.0060					
Straight Cliffs (John Henry Member)				0.0081					
Wahweap					0.0073				
Kaiparowits						0.0088			
Mesaverde						0.0050			
Judith River						0.0063			
Djadokhta						0.0180			
Dinosaur Park						0.0075			
Oldman						0.0064			
Fruitland/Kirtland						0.0065			
Aguja						*0.0058*			
Foremost						0.0054			
St. Mary River						0.0079			
Argilas de Aveiro							*0.0095*		
Baruungoyot							*0.0203*		
Lance							0.0138		
Frenchman (K7 fauna)							0.0146		
Scollard							0.0110		
Hell Creek (K7 fauna)							0.0120		
Fox Hills (K7 fauna)							0.0100		
Ferris (K7 fauna)							*0.0049*		

Table 4.1, continued.

Laramie							0.0065		
North Horn (K7 fauna)							*0.0041*		
Ravenscrag (K7 fauna)							0.0103		
Santa Lucia								0.0145	
Nacimiento								0.0107	
Tullock (D1 fauna)								0.0105	
Polecat Bench (D1 fauna)								0.0098	
Tornillo (D1 fauna)								0.0122	
Hell Creek (D1 fauna)								0.0091	
Bear								0.0076	
Ferris (D1 fauna)								0.0102	
Ravenscrag (D1 fauna)								0.0081	
Fort Union (D1 fauna)								0.0087	
Denver								0.0092	
North Horn (D1 fauna)								0.0067	
Nacimiento (D2 fauna)									0.0123
Fort Union (D2 fauna)									0.0134
Polecat Bench (D2 fauna)									0.0111
Tornillo (D2 fauna)									*0.0122*
North Horn (D2 fauna)									0.0097
Paskapoo									0.0125
Porcupine Hills									0.0103
Black									0.0099
Coalspur									0.0132
Shanghu									0.0223
Wanghudun									*0.0114*

The general trend for ecomorphological disparity (or functional diversity) through time is a steady increase during the Cretaceous (K1-K7), a decrease after the K-Pg boundary in the early Danian (D1), and a rebound in the late Danian (D2). This pattern holds for the global sample (Fig. 4.7, Table 4.1) and for subsampled data (Fig. 4.8, Table 4.1), although results are more variable for subsampled analyses.

The early Danian time bin (D1) is the shortest bin, and it could be posited that the decrease in disparity after the K-Pg boundary for most metrics (Figs. 4.7 and 4.8) is due to this shortened time span. Thus, I tested the effect of the short time duration of D1 by combining it with D2 and calculating disparity. The resulting variance for the Danian (i.e., D1+D2) bin is

0.01340. This value is lower than that for the K7 bin (i.e., 0.01446), supporting the conclusion that disparity decreased across the K-Pg boundary.

Deposition of the Antlers Formation is believed to have spanned the Aptian-Albian boundary (i.e., K1-K2 boundary), and the Khodzhakul Formation spans the Albian-Cenomanian boundary (i.e., K2-K3 boundary). These two formations include therians from both bins that they span (Appendix G). For simplicity, however, the Antlers Formation is assigned to the K1 bin and Khodzhakul Formation is assigned to the K3 bin in Figure 4.8C. A majority of genera for the formations are found in those time bins. Additional formations that span more than one time bin include enough taxa per time bin that they could be analyzed independently (Table 4.1, Appendix G). See 4.3 Methods for additional discussion of time bin assignments for rock formations.

The sum of ranges metric is relatively immune to inconsistencies in taxonomic assignments (i.e., over-splitting or 'lumping' of taxa). Disparity results for the rarefied sum of ranges metric (Fig. 4.7C) show the same disparity pattern as the variance metric (Fig. 4.7A). The congruency of these results suggest that taxonomic inconsistencies are unlikely to have a large effect on the overall disparity trends. Due to the tendency for the raw (i.e., unrarefied) sum of ranges metric to be biased by sample size, it could be expected that D1, which has a much greater sample size than K7, would result in a much greater disparity value than K7. However, this is not the case. The unrarefied sum of ranges results for K7 is slightly greater than that of D1 (Fig. 4.7B). This provides further support for the conclusion that disparity decreased across the K-Pg boundary.

Error test. An error test was performed to examine the amount of variance associated with photography of specimens, landmarking specimens, and intrageneric variation. The median

variance (i.e., disparity) for the 13 taxa was 0.00106 (Table 4.2), which is approximately one order of magnitude lower than the average global variance for the time bins and formations of this study (Table 4.1). Although this level of variance is a concern and undoubtedly has some effect on results, I believe it is not significant enough to account for the broad trends of the study. When disparity was calculated for genera with multiple species (i.e., *Chriacus* and *Litomylus*), results are slightly greater than the disparity averages for individual species (Table 4.2), but they remain considerably lower than average variances for individual time bins and formations.

Table 4.2. Error test results. A penultimate molar for each of the listed species was repeatedly photographed six times, and landmark data for the replicates were subjected to GM procedures. Disparity is calculated as variance in Procrustes values from the Procrustes mean for each species. 'Genus-level analyses' are based on merged data from multiple species of the same genus.

Taxon	Disparity
Species-level analyses	
Chriacus baldwini (NMMNH P-53364)	0.00082
Chriacus calenaneus (NMMNH P-5393, UMVP 1472)	0.00112
Chriacus katrinae (NMMNH P-5353, PU 13949)	0.00074
Altacreodus magnus (UCMP 107747)	0.00114
Scollardius propalaeoryctes (UCMP 107744)	0.00279
Puercolestes simpsoni (NMMNH P-47312)	0.00177
Conacodon entoconus (AMNH 3476)	0.00106
Ectoconus ditrigonus (AMNH 16491)	0.00189
Gypsonictops illuminatus (UCMP 107745)	0.00199
Kennalestes gobiensis (ZPAL Mg M-1/5)	0.00095
Litomylus dissentaneous (AMNH 87543)	0.00094
Litomylus osceoli (NMMNH P-12303)	0.00084
Palaeictops bridgeri (AMNH 56032)	0.00096
Mean for species	**0.00130**
Median for species	**0.00106**
Genus-level analyses	
Chriacus (C. calenaneus, C. katrinae, and C. baldwini)	0.00209
Litomylus (L. dissentaneous and L. osceoli)	0.00149

For three example species that occupy unique regions of morphospace, the results for the six replicates were projected onto the original PC1 and PC2 morphospace (Fig. 4.9). This displays the approximate range of morphospace occupation that can be associated to error in photography and landmarking of molars. The morphospace regions occupied by the replicates of each molar appear to be considerably smaller than the areas occupied by the global samples for each time bin (Figs. 4.5 and 4.9), supporting my conclusion that the error is not substantial enough to affect broad trends of this study.

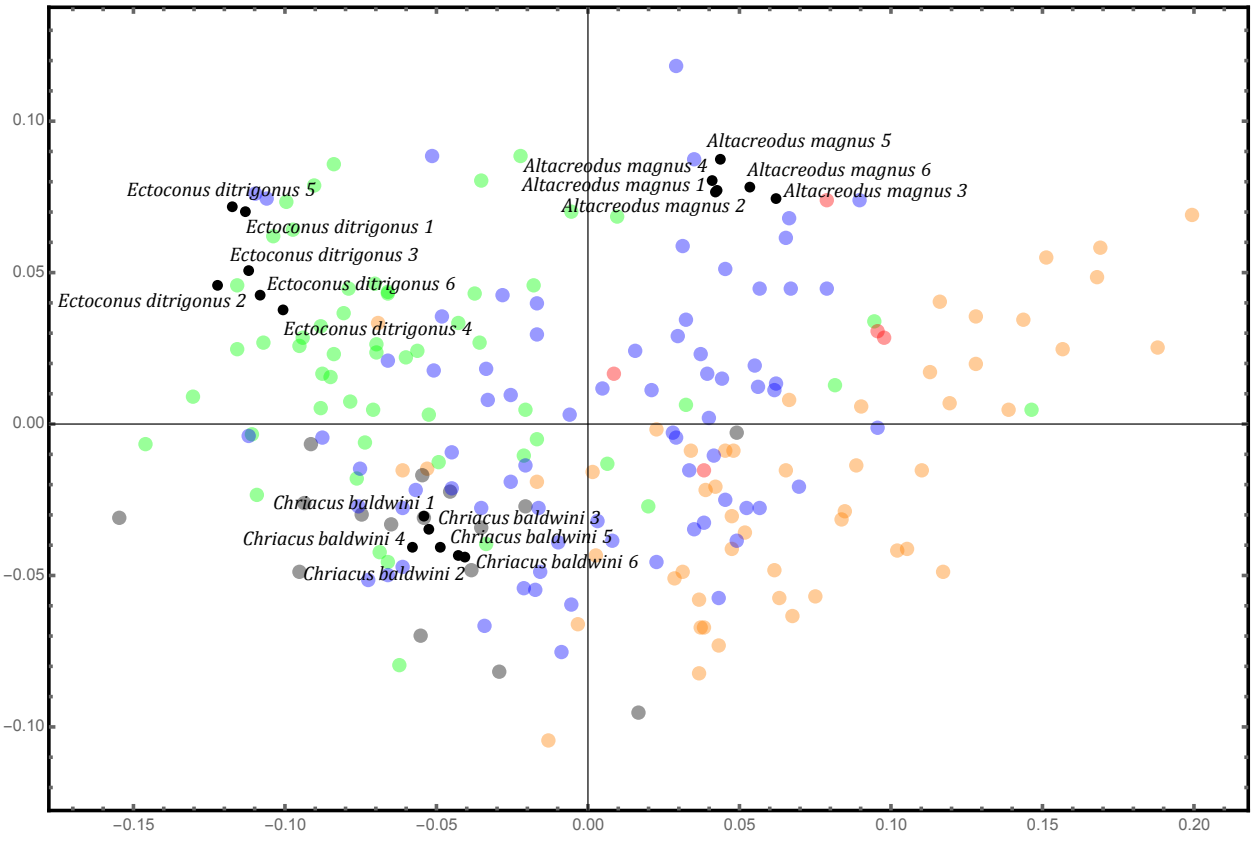

Figure 4.9. Error test results for three therian species. A penultimate molar for each of the species was repeatedly photographed six times and subjected to GM procedures, and then projected onto the original PC1 and PC2 morphospace plot of this study (Fig. 4.4). Each black dot represents one replicate for a given molar. Disparity values (i.e. variance) for these species are given in Table 4.2.

Molar lengths and ratios. Molar lengths of penultimate molars and cusp heights-to-molar length ratios are given in Appendix I. Natural log transformed molar lengths and disparity (i.e., standard deviation) are presented in Figure 4.10, along with cusp heights-to-molar length ratios and their standard deviation. See Appendices E and F for additional information about the genera and molars.

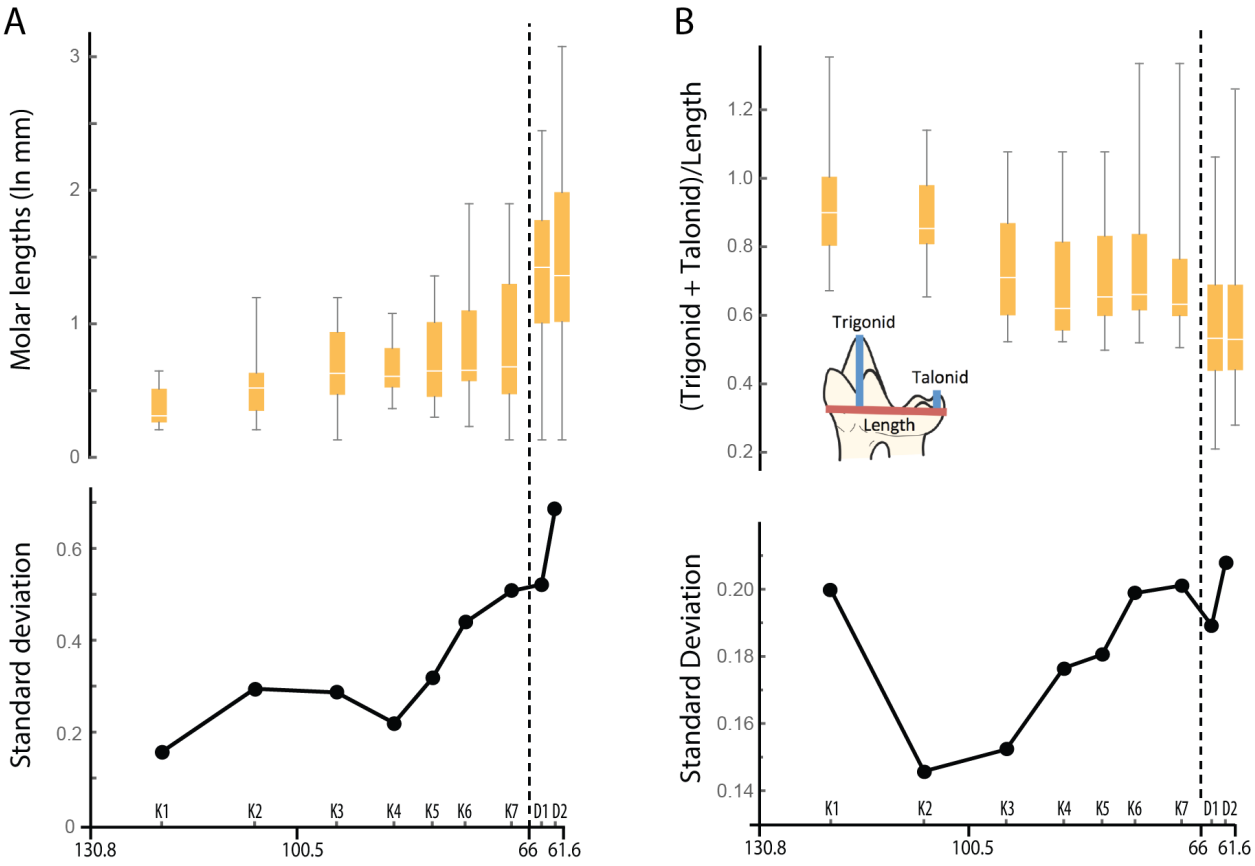

Figure 4.10. Therian molar lengths (natural log mm) (*A*), and cusp heights-to-molar length ratios (i.e., trigonid elevation plus talonid elevation, divided by molar length) (*B*). The molar image in B (from Figure 4.3) is included to help clarify which measurements were used for the analyses. See Appendix I for results for individual molars. As a metric of morphological disparity, the standard deviation of molar lengths and cusp heights-to-molar length ratios from the mean of each time bin are given below each plot. Ages of time bins are given in the text and Figure 4.5.

The range and standard deviation of molar lengths increases steadily over time (Fig. 4.10A). This suggests greater variation in body sizes in therians with time. The largest increase in mean molar length occurs immediately after the K-Pg boundary, consistent with Alroy (1999) and Clauset and Redner (2009), although Alroy (1999) does not note an increasing trend prior to the K-Pg boundary. Despite the increase in mean molar length, the standard deviation of molar lengths does not show a significant increase after the K-Pg boundary. Thus, it appears that there as a shift toward larger body masses without a concurrent increase in body size disparity.

For cusp heights-to-molar length ratios (Fig. 4.10B), the overall trend in disparity (i.e., standard deviation) is similar to additional disparity results of this study and includes the decrease in disparity across the K-Pg boundary that is seen in GM results (Figs. 4.7 and 4.8). However, there is one notable discrepancy: the elevated disparity in K1 of Figure 4.10B is not present in other disparity results (Figs. 4.7, 4.8, and 4.10A). This elevated value is likely due to the inclusion of two taxa with abnormally high ratios: *Eomaia* (Ji et al., 2002) and *Sinodelphys* (Luo et al., 2003). These genera are not included in the GM analysis because occlusal images of the molars are not available. However, they are included in the molar length results (Fig. 4.10A), and disparity (i.e., standard deviation) of molar lengths is low in this time bin. Thus, the elevated K1 disparity value for cusp heights-to-molar length ratios (Fig. 4.10B) may be an anomaly associated with low sample size and outliers (i.e., *Eomaia* and *Sinodelphys*). Interestingly, the decrease in disparity from K1 to K3 in Figure 4.10B is consistent with the conclusion of Grossnickle and Polly (2013) that disparity of mammals decreased in the mid-Cretaceous.

The cusp heights-to-molar length ratios serve as an additional means (besides the GM analysis) of discerning broad dietary patterns. For instance, carnivorous and insectivorous mammals are likely to possess taller, sharper cusps, which would be represented by greater cusp

heights-to-molar length ratios. Very low ratios are indicative of bunodont molars, which have short, bulbous cusps and are common in modern omnivores with plant-dominated diets.

There are two notable decreases in average cusp heights-to-molar length ratios (Fig. 4.10B). First, the ratios decrease in the K3 and K4 bins, likely due to the appearance of zhelestids in the fossil record. Zhelestids have relatively low cusps and share notable similarities to archaic ungulates (Archibald and Averianov, 2012). The second decrease in ratio average occurs after the K-Pg boundary in D1. This coincides with the sudden appearance of archaic ungulates. Both the zhelestids and archaic ungulates overlap in morphospace, occupying the omnivory/frugivory (i.e., left) region in Figure 4.4. Thus, cusp heights-to-molar length ratios help corroborate the GM results that suggest invasions into the omnivory/frugivory morphospace in K3 and D1 (Figs. 4.5 and 4.6).

4.5 DISCUSSION

4.5.1 Ecomorphological diversification during the Late Cretaceous

Morphological disparity results contradict the Suppression Hypothesis (SH; Fig. 4.1A) and demonstrate a steady rise of functional diversity (or ecomorphological disparity) through the Late Cretaceous (Figs. 4.7, 4.8, and 4.10). The increase is maintained when genera are separated by major clade (Fig. 4.8A) and continent (Fig. 4.8B). Increases during the early Late Cretaceous (i.e., time bins K3 and K4) were likely triggered by the appearance of zhelestid eutherians, which inhabit the frugivore/omnivore region of morphospace. Disparity continues to increase during the late Late Cretaceous (K6 and K7) with the appearance of taxa with molars indicating plant-dominated diets (e.g., Fox and Naylor, 2003) and carnivory (e.g., Fox et al., 2007). This increase is most notable in metatherians (Fig. 4.8A) and Eurasian faunas (Fig. 4.8B). Results support

previous studies that have noted elevated levels of ecological and taxonomic diversity of Late Cretaceous metatherians (Wilson, 2014; Wilson et al., 2016). Congruent with the pattern seen in therians, latest Cretaceous multituberculates also experience an increase in disparity (Grossnickle and Polly, 2013; Wilson et al., 2012), suggesting that mammals as a whole were diversifying ecomorphologically during this period.

Disparity was calculated for therian faunas of individual rock formations to help account for sampling biases that may result from differences in the number of fossil-bearing formations between time bins (Fig. 4.8C). Results support the conclusion that therian disparity was increasing prior to the K-Pg boundary. Disparity levels for rock formations in the middle-late Campanian (K6) remain relatively low (Fig. 4.8C) even as global disparity increases (Fig. 4.7). This suggests that middle-late Campanian faunas possessed greater β-diversity/disparity (i.e., proportionally more endemic taxa) whereas Maastrichtian (K7) faunas experienced greater α-diversity/disparity (i.e., increased local diversity and proportionally more cosmopolitan taxa). This is congruent with results for dinosaurs (Vavrek and Larsson, 2010) and local ecosystems (Mitchell et al., 2012).

The ecological diversification of flowering plants in the late Late Cretaceous (Wing and Tiffney, 1987; Lupia et al., 1999, Feild et al., 2011; Coiffard et al., 2012; Boyce et al., 2009) has been suggested as a plausible trigger for the ecomorphological radiation of multituberculates (Grossnickle and Polly, 2013; Wilson et al., 2012), and this may also apply to therians. Angiosperms experienced a rapid taxonomic diversification in the mid-Cretaceous (~100 Ma) (Lidgard and Crane, 1988). However, their ecomorphological diversification was offset from their taxonomic diversification, occurring later in the Cretaceous. This is supported by multiple lines of evidence, including palynological and leaf vein density studies (Lupia et al., 1999;

Coiffard et al., 2012; Feild et al., 2011). In addition, Late Cretaceous angiosperms invaded an increasing number of environments with time (Coiffard et al., 2012) and may have triggered greater overall biodiversity in ecosystems (Boyce et al., 2009). This Late Cretaceous ecological diversification of angiosperms corresponds to the increase in functional diversity of therians (Figs. 4.7 and 4.8) and multituberculates (Wilson et al., 2012). Besides directly benefitting therian omnivores/frugivores by providing novel dietary options, angiosperms could have indirectly aided therian insectivores by prompting co-evolutionary diversifications in insects (e.g., McKenna et al., 2009), although a close association between insect and angiosperm diversities is not supported by fossil evidence (Labandeira and Sepkoski, 1993).

Considerations beyond the morphological disparity results provide additional support for the observed increase in functional diversity during the Late Cretaceous. For instance, individual genera provide direct evidence for greater ecological diversification. *Nanocuris* and *Didelphodon*, relatively large metatherians from the Maastrichtian (K7), appear to have dental adaptations for specialized diets (Wilson and Riedel, 2010; Wilson, 2013; Wilson et al., 2016). *Nanocuris* and additional deltatheroidans may have been especially adapted for carnivory and occupy the far right (i.e., carnivore/insectivore region) of the PC1 and PC2 morphospace plot (Figs. 4.4 and 4.5). Four archaic ungulate genera are also in the K7 time bin and inhabit the omnivore/frugivore region of morphospace. Thus, evidence suggests increasingly specialized diets in the time bins just prior to the K-Pg boundary.

Further evidence for a Late Cretaceous rise in functional diversity is provided by taxa that were not included in the time-sliced GM analyses. The only known Cretaceous taeniodont, *Schowalteria* (Fox and Naylor, 2003), is not included in the GM study because the molars are too worn for accurate landmarking of cusps. If included it would likely occupy the

frugivore/omnivore region of morphospace, acting as an outlier and expanding the K7 disparity level above that of D1 to an even greater degree. Similarly, *Mistralestes* is a zhelestid from the Late Campanian (K6) of Europe with archaic ungulate-like molars (Tabuce et al., 2013), and it is expected to be an outlier in the frugivore/omnivore region of the K6 morphospace if included in analyses. Unfortunately, the molars are too worn and damaged for inclusion in the GM analyses. An additional Cretaceous fossil that was left out of time-sliced disparity results is *Tsagandelta*, a deltatheroidian of uncertain age but is believed to fall within the K3-K6 time bins. The genus is a morphological outlier with molars indicating that it was possibly carnivorous, and it is likely to raise the disparity level in the bin to which it is eventually assigned.

Based on jaw shape data for Mesozoic mammaliaforms (including therians), Grossnickle and Polly (2013) conclude that morphological disparity in mammaliaforms decreased in the mid-Cretaceous (~115-90 Ma). During the Early Cretaceous, many mammal groups went extinct or experienced significant decreases in diversity. This includes docodontans, eutriconodontans, symmetrodontans, placiaulacidan multituberculates, and eupantotherians. Therians and cimolodontan multituberculates are the primary clades in the northern hemisphere to survive past this period. Benson et al. (2013) also highlight this taxonomic turnover. Thus, the increase in disparity seen in therians (Figs. 4.7 and 4.8) and multituberculates (Wilson et al., 2012; Grossnickle and Polly, 2013) during the Late Cretaceous may be a rebound or radiation in response to the bottleneck/turnover event during the mid-Cretaceous. Therians and cimolodontan multituberculates may have expanded into ecological niches vacated by the loss of additional mammalian groups.

4.5.2 Selective extinction

K-Pg boundary. The observed number of unique molar morphologies increased during the earliest Paleocene (D1) time bin (Fig. 2*c*). However, contrary to the prediction of SH (Fig. 4.1A) and the non-selective extinction model (Fig. 4.1C), molar disparity (i.e., variance of morphologies) appears to have decreased in response to the K-Pg extinction event. On smaller temporal and geographic scales, Wilson (2013) also shows a decrease in molar disparity across the K-Pg boundary. The decrease seen here is maintained when disparity is calculated as variance at global (Fig. 4.7A), subclade (Fig. 4.8A), continental (Fig. 4.8B), and formation/regional (Fig. 4.8C) levels, and when global disparity is calculated as rarefied sum of ranges (i.e., area occupied in morphospace) (Fig. 4.7C). To ensure that the relatively short duration time of the D1 bin (i.e., early Danian) is not distorting results, disparity was calculated for a combined D1 and D2 bin and results (0.01340) remain lower than the K7 value (0.01446). Cusp heights-to-molar length ratios were measured to help assess shape variance not fully captured by two-dimensional GM, and the standard deviation of these ratios also decreases after the K-Pg boundary (Fig. 4.10B). Standard deviation of molar lengths is the only disparity metric that does not show a decrease across the K-Pg boundary (Fig. 4.10A), although it also does not show a significant increase.

The decrease in disparity across the K-Pg boundary supports previous conclusions that the accompanying extinction event was selective among mammals, likely targeting ecological specialists (Simpson, 1937; Wilson, 2013; Wilson, 2014). A selective mass extinction is more likely to cause a decrease in disparity than a non-selective (i.e., random) mass extinction because it will have enhanced effects on a particular clade or ecological niche (Fig. 4.1; Foote, 1993). As discussed by Wilson (2013), much of the decrease in disparity may be due to the loss of

metatherian specialists, such as carnivorous deltatheroidans (e.g., *Nanocuris*). Molar images of two metatherian outliers from the Late Cretaceous, *Pediomys* and *Nanocuris*, are shown in Figure 4.4. In contrast, eutherian generalists such as archaic ungulates appear to have preferentially survived and taxonomically diversified after the extinction event. The targeting of specialists is consistent with the broad hypothesis that specialists have a higher risk of extinction than generalists (Simpson, 1944; Smits, 2015), especially during periods of significant variability in resources. In D2, the appearance of eutherian morphological outliers and specialists, such as some plesiadapiforms (e.g., *Picrodus*) and mesonychids (e.g. *Ankalagon*), helped instigate a rebound in disparity.

Assessing the decrease in D1 disparity. Results suggest a decrease in morphological disparity immediately after the K-Pg boundary (Figs. 4.7, 4.8, and 4.10B). However, sampling biases could be cited to help explain this decrease. For instance, it could be argued that the lack of known Eurasian faunas in D1 (i.e., early Danian) artificially deflates the disparity results. However, North American taxa are represented by a continuous fossil record across the boundary and show a decrease in disparity in the early Danian (Fig. 4.8B). In addition, the Santa Lucía Formation from the earliest Paleocene of South American is within the range of disparity values for North American formations (Fig. 4.8C, Table 4.1), providing evidence that North American formations in the early Danian did not experience aberrantly low disparity. The D2 Eurasian fauna is also less disparate than the K7 fauna, suggesting that Eurasian mammals also experienced a decrease in disparity across the K-Pg boundary. Thus, I believe the lack of a D1 Eurasian fauna cannot fully account for the decrease in D1 disparity.

An additional concern is that the GM analyses of individual molars may not adequately capture disparity of D1 taxa, resulting in artificially low values. For instance, Paleocene

carnivorans and insectivorans occupy the same region of PC1 and PC2 morphospace (Fig. 4.4) despite considerable differences (e.g., dissimilarities in body size and number of molars). In addition, many archaic ungulates and taeniodonts have molars indicative of generalists that could have been well adapted for a variety of diets. Thus, these clades may have maintained similar molar morphologies (and low within-group disparity) but diversified ecologically through evolution in body sizes and changes in non-molar dentition. However, disparity was considered for molar length (Fig. 4.10A) and cusp heights-to-molar length ratios (Fig. 4.10B) to help account for differences not captured by the GM methods, and results are largely congruent with the GM results. (Although molar length disparity does not decrease across the boundary like other metrics, it does not show the rapid increase displayed by the taxonomic diversity results.)

As described above, individual fossil specimens provide evidence for the ecomorphological diversification of Late Cretaceous therians. Similarly, the early Danian (D1) therians provide evidence for a decrease in ecomorphological diversity. They lack molar morphologies indicative of high fiber diets, and there is limited evidence for carnassial (or carnassiform) molars, indicative of carnivory, although this molar type was present in Late Cretaceous mammals (Montellano-Ballesteros and Fox, 2015; Wilson and Riedel, 2010). Thus, the scarcity of particular molar morphologies in D1, especially those that are indicative of diets that could be expected at this time, provides qualitative support for the conclusion that disparity was depressed in the earliest Paleocene. There is also strong evidence that metatherians experienced greater extinction rates and loss of morphological disparity than eutherians at the K-Pg boundary (Wilson, 2013; Clemens, 2002), supporting the conclusion that the extinction event was selective.

Archaic ungulates are believed to have immigrated into the western interior of North America in the earliest Paleocene (Wilson, 2013; Clemens, 2002), which suggests that they were diversifying prior to the K-Pg extinction event. The presence of at least one taeniodont, *Schowalteria* (Fox and Naylor, 2003), from the Maastrichtian of North America indicates that this group was also present before the K-Pg boundary. These considerations suggest that prominent clades of therians from the latest Cretaceous are likely being under-sampled (e.g., archaic ungulates) or not sampled (e.g., taeniodonts). This is concerning because my sample of late Late Cretaceous therians may not be accurately representing the global fauna. However, the potential under-sampling of these clades in the Maastrichtian time bin likely works against two major conclusions of this study: (i) disparity increases in the latest Cretaceous and (ii) disparity decreases across the K-Pg boundary. If taeniodonts (e.g., *Schowalteria*) and additional archaic ungulates (beyond *Protungulatum*, *Kharmerungulatum, Paleoungulatum,* and *Baioconodon*) were included in the Maastrichtian (K7) sample they would likely appear in the largely vacant frugivore region of morphospace, thus expanding morphospace occupation for this time bin and raising disparity levels to a greater degree. Consequently, this would also result in a more distinct decrease in disparity across the K-Pg boundary. Thus, I do not believe that this sampling issue can account for the unexpected decrease in disparity across the K-Pg boundary.

4.5.3 Evolutionary dynamics across the K-Pg boundary

Taxonomic diversity. Unlike disparity, taxonomic diversity patterns support SH, showing a rapid generic-level diversification immediately following the K-Pg boundary (Fig. 4.11; Grossnickle and Newham, 2016). This is likely driven by eutherians that include early placentals (Alroy, 1999; O'Leary et al., 2013; Wible et al., 2009; Halliday et al., 2015; Wilson, 2014). The pattern remains after data are corrected for sampling biases using shareholder quorum

subsampling (Fig. 4.11B) and residual analyses for therian-bearing rock formations (TBFs) (Fig. 4.11C). This pattern is also shown in residual analyses for therian-bearing fossil collections, although it is less pronounced (Grossnickle and Newham, 2016). The rapid taxonomic diversification in the earliest Paleocene is especially striking considering the substantial loss of mammalian genera during the extinction event (Wilson, 2014). Alroy (1999) documents elevated extinction and origination rates in the earliest Paleocene of North America, suggesting rapid taxonomic turnover as ecosystems were reestablished. The Danian (DI and D2) bins are dominated (>90%) by North American occurrences, suggesting a potential geographic sampling bias for global patterns. Further, immigration of mammals into North America in D1 may be artificially inflating taxonomic diversity levels (Simpson, 1937; Wilson, 2013; Clemens, 2002; Wilson, 2014). However, both bias correction methods indicate that taxonomic diversity during D1 was considerably greater than during K7, which represents a more geographically diverse assemblage. Thus, I posit that a single geographic region showing substantially higher diversity than a more 'global' preceding stage indicates a significant increase in global taxonomic diversity during D1. This inference is supported by occurrences in a third Paleocene (Selandian) time bin, which contains a more cosmopolitan geographic range in occurrences and a similarly high taxonomic diversity (Grossnickle and Newham, 2016).

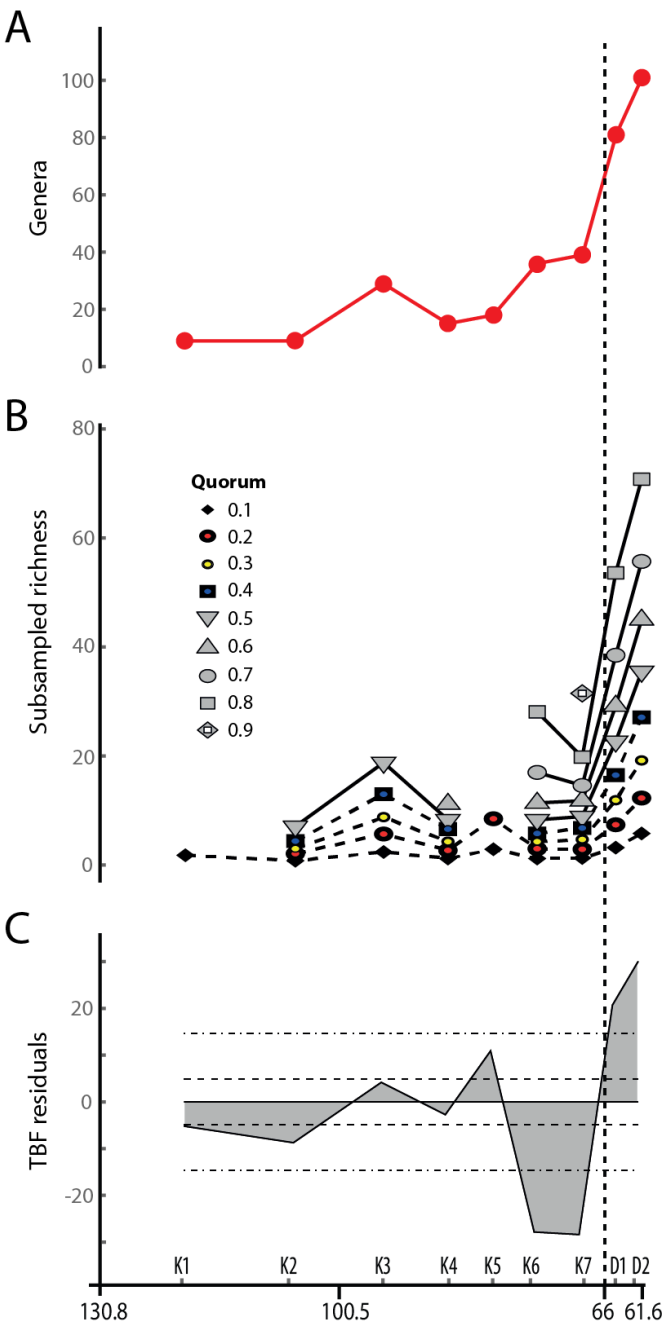

Figure 4.11. Global therian taxonomic diversity through time, after Grossnickle and Newham (2016). Taxonomic diversity is examined as raw counts of unique genera per time bin (A), generic-level richness after employing shareholder quorum subsampling (B), and residual diversity patterns based on therian-bearing rock formations (TBF) (C). Shaded regions in C represent divergence from diversity levels that would be predicted by the TBFs alone. Dashed lines mark standard error 95% confidence intervals. Dash-dot lines mark standard deviation 95% confidence intervals. Note that all three metrics show an increase in diversity after the K-Pg boundary. Ages of time bins are given in the text and Figure 4.5.

Dietary shift. The predominant therian diet shifts from insectivory to frugivory at the K-Pg boundary (Fig. 4.5; Collinson and Hooker, 1991). This is due to an influx of taxa with inferred frugivorous or omnivorous diets, including archaic ungulates (55% of unique Paleocene occurrences), taeniodonts, and polydolopimorphian metatherians. The abrupt increase in taxonomic diversity of relatively large archaic ungulates and taeniodonts instigated the sudden increase in average body size (Fig. 4.10A). In D2, plesiadapiforms and pantodonts further fill the frugivore/omnivore morphospace region. In addition to therians, many multituberculates demonstrate frugivorous/omnivorous diets (Wilson et al., 2012), and multituberculates reach their peak dietary and body size diversities in the earliest Paleocene (Wilson et al., 2012; Williamson et al., 2015). Therian and multituberculates with plant-dominated diets may have profited from increases in average angiosperm seed size and a greater role as seed dispersers (Eriksson, 2014). Further, it has been hypothesized that the loss of large, herbivorous dinosaurs permitted the expansion of dense, closed canopy forests in the Paleocene (Wing and Tiffney, 1987). This may help explain the diversification of frugivorous/omnivorous mammals and lack of larger, high-fiber herbivores that may require open habitats (Janis, 2000; Wing and Tiffney, 1987).

Reconciling conflicting results. Results indicate that the therian response to the K-Pg extinction event was a decrease in morphological disparity and a rapid increase in taxonomic diversity. To help reconcile these conflicting patterns, I posit that extinction survivors, especially generalists, radiated taxonomically without considerable morphological diversification, filling morphospace regions with similar taxa. This resulted in proportionally fewer morphological outliers and disparity levels that remained low even as the number of taxa increased rapidly. This hypothesis is conceptualized in Figure 4.12, and it is consistent with previous conclusions that

generalists such as archaic ungulates dominated the early Paleocene radiation (Halliday and Goswami, 2016; Simpson, 1937; Hunter, 1997; Archibald, 2011).

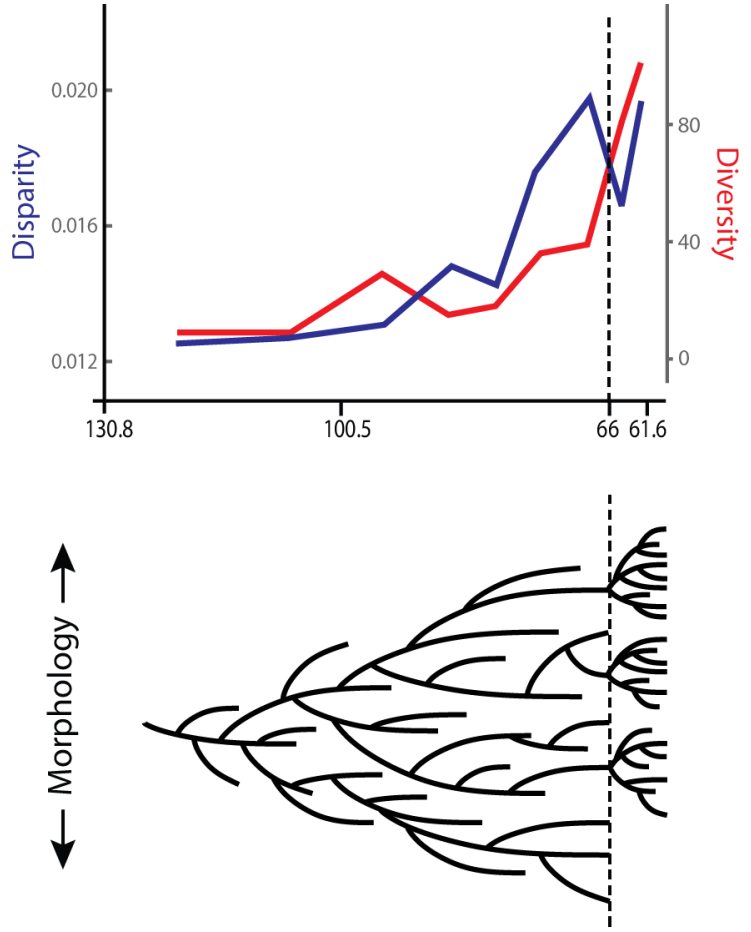

Figure 4.12. Observed generic-level diversity (red; Figure 4.11A) and morphological disparity (blue; Figure 4.7A), highlighting the reversal of diversity and disparity patterns at the K-Pg boundary. The lower figure is an idealized clade history of early therians that displays the increase in Cretaceous disparity, selective extinction event, and taxonomic diversification after the K-Pg boundary.

Interestingly, the therian response to the K-Pg extinction event is inconsistent with the observation that morphological diversification in clades tends to outpace taxonomic

diversification after a mass extinction event (e.g., Benton, 2015). Thus, I posit that the response of a clade to a mass extinction event is largely dependent on ecological factors, and the 'disparity-first' model might only be favored in situations in which ecological opportunities favor specialists over generalists.

Eutherians and metatherians. Based on the observation that metatherians were more adversely affected by the K-Pg extinction event (e.g., Wilson, 2013), it could be assumed that eutherians and metatherians would have very distinct disparity patterns. However, metatherians occupy a considerable region of morphospace in the earliest Danian (Figs. 4.5 and 4.6) and their D1 disparity level remains greater than eutherians (Fig. 4.8A). This is due largely to the Tiupampa local fauna of Bolivia, which includes polydolopimorphian metatherians with molars that are very similar to eutherian archaic ungulates. This suggests that in regions where metatherians were more abundant after the boundary (e.g., South America), they may have experienced a similar initial response to the extinction event as eutherians did elsewhere. In addition, despite Late Cretaceous eutherians often being considered less ecologically diverse than Late Cretaceous metatherians, the presence of Maastrichtian eutherians with plant-dominated diets (e.g., *Schowalteria, Kharmerungulatum*) and carnivorous diets (e.g., *Altacreodus magnus*) suggests that eutherians were also diversifying ecologically during this time. Thus, the eutherian and metatherian disparity patterns may be more similar than could be assumed.

4.5.4 Conclusions

My data refute the hypothesis that the ecomorphological diversity of therian mammals was suppressed during the Cretaceous and dramatically increased following the K-Pg extinction

event. Instead, I suggest that therian disparity and dietary diversity were increasing through the Late Cretaceous, similarly to the pattern observed in multituberculates (Wilson et al., 2012). This suggests that mammals as a whole began to diversify ecomorphologically 10-20 million years prior to the K-Pg extinction event, during a period marked by the ecological radiation of angiosperms. Further, a decrease in morphological disparity immediately after the K-Pg boundary suggests that an adaptive radiation of therians did not begin in the earliest Paleocene, although the extinction event may have been a catalyst for a taxonomic diversification of frugivores/omnivores (e.g., archaic ungulates). The K-Pg extinction event was likely selective against ecological specialists and metatherians, and the ecomorphological diversification of mammals, especially placentals, likely resumed in the mid-Paleocene after the filling of generalist niches.

CHAPTER 5
Conclusions – dietary adaptations and the mammalian radiation

5.1 ORIGINS OF MODERN BIODIVERSITY

A frequent aim in evolutionary biology and paleontology is to assess why specific clades have diversified and achieved long-term survival while related clades have diminished or gone extinct (e.g., Darwin, 1859; Simpson, 1944; Van Valen, 1973; Raup and Gould, 1974; Jablonski, 1986; Hunter and Jernvall, 1995; Alfaro et al., 2009; Benton, 2009; Moczek et al., 2011; Smits, 2015; Rabosky, 2014; Brocklehurst et al., 2015). There is special interest in evolutionarily 'successful' clades such as mammals, teleosts, birds, and flowering plants that have persisted to the modern day and now account for much of modern biodiversity. Their substantial diversity is often attributed to exceptional evolutionary radiations at broad taxonomic scales (e.g., Simpson, 1944; Schluter, 2000; Alfaro et al., 2009). The radiation events frequently involve considerable increases in ecological diversity, in addition to increases in morphological disparity and taxonomic diversity (Simpson, 1944; Schluter, 2000; Stroud and Losos, 2016). However, it remains challenging to assess ecological and biomechanical influences of these radiations, especially if they occur in deep time and require incorporation of fossil data for adequate assessment (Tarver and Donoghue, 2011; Slater et al., 2012; Slater, 2015; Mitchell, 2015).

Theria is an exemplary example of a clade that has persisted and diversified while closely related clades have gone extinct. It was one of many mammalian lineages to arise during an evolutionary radiation in the Jurassic (Luo, 2007; Close et al., 2015). During the Cretaceous

Terrestrial Revolution (KTR) 125-80 Ma, most non-therian lineages perished, with therians (or, more broadly, cladotherians) and cimolodontan multituberculates being the two major mammalian clades to survive and maintain significant taxonomic diversity (Fig. 2.1; Benson et al., 2013; Grossnickle and Polly, 2013). Since the evolutionary bottleneck at the KTR, therians (i.e., metatherians and eutherians) have experienced an exceptional evolutionary radiation. This clade now comprises all but three modern genera of mammals and has achieved incredible taxonomic, morphological, and ecological diversity, with extant taxa occupying an immense array of ecological niches. However, the timing and tempo of this diversification remains contested, especially in relation to the Cretaceous-Paleogene (K-Pg) mass extinction event (Chapter 4 and citations within). In addition, the effect of ecological factors on the evolution of therians and their closest relatives (i.e., cladotherians) has not been fully explored. In the following section, I discuss functional and dietary adaptations in early cladotherians that are expected to have been especially critical to the evolution and long-term survival of therians.

5.2 DIETARY ADAPTATIONS IN EARLY CLADOTHERIANS

Cladotherian fossils. A majority of early cladotherian fossils are teeth and jaws. Although the scarcity of postcranial material may hinder our ability to fully assess their ecomorphological diversity, teeth and jaws are extremely informative and can provide numerous clues about how a taxon lived, functioned, and evolved. The mouth is a critical interface between organism and environment, and ecological changes are expected to be strongly manifested in jaw and molar morphologies. This is supported by the especially strong link between mammalian diet and dental/jaw morphologies (e.g., Evans et al., 2007; Chapter 3). Further, an organism's bauplan is often reflective of its diet and foraging methods. Drastic morphological and physiological

changes accompany evolutionary shifts in diet, and this is due to very different mechanical properties and nutritional contents of plant products versus animal food. Thus, an increase in the dietary (or ecological) diversity within a clade is expected to be reflected in the fossil record by significant adaptive changes to morphologies. Several critical adaptations in early cladotherians are discussed below.

Jaw evolution and yaw rotation. The mandibular angular process appears to have undergone considerable evolutionary changes in early mammalian lineages. Pre-mammalian mammaliaforms (e.g., docodonts and morganucodonts) and cladotherians generally possess a distinct angular process, but some of the earliest crown mammals (e.g., multituberculates, eutriconodontans, and spalacotherioids) lack a definitive angular process (Fig. 2.4). This raises questions about the biomechanical importance of this process, especially because major masticatory muscles (i.e., the superficial masseter and medial pterygoid) attach to the angular region of the jaw (Fig. 1.2).

To examine how the evolution of the angular process affected jaw biomechanics, three-dimensional jaw models of musculoskeletal configurations in early mammal groups were used to calculate torque values for various rotational movements (Chapter 2). Results indicate that the evolution of a posteriorly-positioned angular process in cladotherians increases torque values for rotation around a dorsoventrally-oriented axis (i.e., yaw) and decreases torque values for rotation around a mediolateral-oriented axis (i.e., pitch) (Fig. 2.8). The functional importance of this jaw process is further supported by evidence that the size of the angular process is strongly correlated with diet in therians (Chapter 3). This correlation is likely due in part to increases in size and functional importance of muscles that insert on the angular process (i.e., the superficial masseter and medial pterygoid) in herbivores (Turnbull, 1970). Together, these analyses demonstrate the

functional relevance of this process and its attached musculature, which may have been underappreciated by previous research on mammalian jaw evolution.

Yaw rotation of the mandible results in transverse movement of molars (whereas pitch creates orthal movement), and the cladotherian node is also marked by the evolutionary appearance of molar morphologies that involve transverse movement during occlusion (see below). Besides the angular process and talonid, the cladotherian node includes the loss of a bony attachment between the middle ear elements and the jaw. This may have reduced the functional constraints on jaw movements, permitting greater transverse movement. Thus, the evolutionary changes to jaw, molar, and ear morphologies may all be related to the evolutionary increase of yaw rotation of jaws during occlusion. The increased transverse movement have also been a critical prerequisite for the evolution of the tribosphenic molar morphology.

Tribosphenic molars. The tribosphenic molar morphology is an important evolutionary innovation in early mammals. It evolved at (or just basal to) the therian node of the mammalian phylogeny, and it is believed to have arisen convergently in monotreme ancestors (Luo et al., 2002). An essential step in the evolution of the tribosphenic molar morphology was the appearance of a talonid shelf in the lower molars of non-therian cladotherians (Fig. 1.2), providing a surface for extended shearing. In tribosphenic molars the talonid shelf expands into the talonid basin and has a crushing ability (Osborn, 1907; Simpson, 1936; Stern et al., 1989; Schultz and Martin, 2014), which is a function that is not apparent in earlier molar morphologies (Fig. 1.2) and may allow for a broad diversity of diets. In addition to the crushing ability, tribosphenic molar occlusion is extremely precise and involves multiple shearing crests (Davis, 2011; Schultz and Martin, 2014), resulting in a system that seems especially effective for rapidly cutting chitinous exoskeletons of insects. The functional significance of the morphology is

supported by the continued prevalence of tribosphenic (or tribosphenic-like) molars in many modern mammal groups (e.g., microchiropterans, didelphids, dasyurids, scandentians, and many eulipotyphlans), despite evolving at least 160 Ma (Rauhut et al., 2002; Luo et al., 2011).

One aspect of mastication is especially crucial for understanding the evolution of the tribosphenic molar. In early crown lineages such as eutriconodonts and spalacotherioids, molar occlusion is primarily orthal. However, during the power stroke of occlusion in early cladotherians, molar movement involves considerable transverse movement, which is created by yaw rotation of the jaw (Chapter 2). Transverse movement via yaw rotation is important to the dietary diversity of therians because this motion permits grinding or crushing (e.g., Schultz and Martin, 2014), which is especially critical for omnivorous and herbivorous diets. For instance, the primary means of grinding plant materials in modern therian herbivores (besides rodents) is significant yaw rotation of the jaw, maximizing the amount of contact between enamel ridges of upper and lower molars (e.g., Crompton et al., 2010). Although it is likely that the earliest therians (and cladotherians) were insectivorous (Chapters 3 and 4), they experimented with more diverse diets in the Late Cretaceous. Zhelestids of the early Late Cretaceous have molar morphologies indicative of omnivorous diets, and archaic ungulates of the latest Cretaceous and Paleocene show an even greater shift toward herbivory (Chapter 4; Hunter, 1997). These early invasions of omnivorous/herbivorous niches are reflected by invasions of the herbivorous regions of molar morphospace (Fig. 4.5) and jaw morphospace (Fig. 3.5).

In addition to morphological adaptations for herbivory, tribosphenic molar morphologies are readily adapted for carnivorous diets, often through expansion of trigonid shearing crests of lower molars. Therians of the Late Cretaceous include taxa that shift toward specialized carnivorous diets (Chapter 4), as demonstrated by the evolutionary appearance of carnassial

molars (specialized for shearing) of deltatheroidans (Wilson and Riedel, 2010; Rougier et al., 2015A) and shell-crushing dentitions of *Didelphodon* (Wilson et al., 2016).

Thus, by the end of the Cretaceous, therians had achieved dietary diversity unmatched by additional major clades of Mesozoic mammals, and it can be hypothesized that this dietary diversity is linked to the various masticatory functions permitted by yaw rotation and tribosphenic molars. The clade included insectivores, omnivores, specialized carnivores, and, probably, the earliest therian herbivores (Chapters 3 and 4; Fox and Naylor, 2003). The only other Mesozoic mammal clade to achieve similar dietary diversity was cimolodontan multituberculates, and they were diversifying concurrently with the Late Cretaceous therians (Wilson et al., 2012).

Angiosperms and mammals. The simultaneous ecological diversifications of the two major mammalian groups (i.e., therians and multituberculates) in the latest Cretaceous suggest that ecological or environmental factors were instigating these radiations. The most commonly hypothesized catalyst is the ecological diversification of flowering plants in the latest Cretaceous (Chapters 3 and 4; Wing and Tiffney, 1987; Wilson et al., 2012; Grossnickle and Polly, 2013; Eriksson, 2014), which is expected to have provided novel food opportunities (e.g. larger seeds, fruits) for mammals. In addition, therians and multituberculates may have co-evolved with early angiosperms as seed dispersers (Eriksson, 2014).

Angiosperms diversified taxonomically in the mid-Cretaceous (Lidgard and Crane, 1988), but this was decoupled from the ecological diversification that occurred later in the Cretaceous (Lupia et al., 1999; Feild et al., 2011, Coiffard et al., 2012). Late Cretaceous angiosperms invaded an increasing number of environments with time (Coiffard et al., 2012) and may have triggered greater overall biodiversity in ecosystems (Boyce et al., 2009). Besides

directly benefitting therian omnivores/frugivores by providing novel dietary options, angiosperms could have indirectly aided therian insectivores by prompting co-evolutionary diversifications in insects (e.g., McKenna et al., 2009).

After the K-Pg mass extinction, angiosperm taxonomic diversity remained depressed for much of the Paleocene (Wilf et al., 2006), and it has been shown that angiosperms and insects likely experienced an evolutionary bottleneck that disrupted their ecological interactions (Labandeira et al., 2002; Wilf et al., 2006). However, it has also been demonstrated that fleshy fruits first appeared in the Paleocene (Dilcher, 2001), and average seed size continued to increase after the K-Pg boundary (Eriksson, 2014). Thus, despite the decrease in diversity, angiosperms are expected to have continued to supply increasingly valuable food sources for early mammals. This pattern of plant evolution is consistent with the evolutionary patterns of therian mammals. There is evidence for a decrease in mammalian dietary diversity at the K-Pg boundary due to a selective extinction event (Chapter 4; Wilson, 2013), and this could be expected if plants and insects are also less diverse in the early Paleocene. Further, many mammal lineages shift toward a more herbivorous diet after the K-Pg boundary (Chapters 3 and 4; Collinson and Hooker, 1991; Wilson et al., 2012), and this could also be expected if angiosperm fruits and seeds continue to offer increasingly valuable nutritional sources. The recovery and continued diversification of angiosperms in the Eocene (Dilcher, 2001) may have helped spur the diversification of therian herbivores during this time (Chapter 3). Thus, it is expected that the complex interplay between mammals, plants, and insects helped shape the macroevolutionary patterns of mammals before and after the K-Pg boundary.

5.3 SURVIVAL AND DIVERSIFICATION OF THERIA

Early cladotherian adaptations include the evolutionary appearance of the angular process of jaws, talonid of molars (and tribosphenic molar morphology in therians), complete separation of the middle ear elements from the jaw, and yaw rotation during mastication (Chapter 2). It may be tempting to attribute the adaptive radiation of therian mammals to these evolutionary changes. However, I urge caution in making this assumption. For instance, it could be argued that the tribosphenic molar morphology is a key evolutionary innovation that triggered the diversification of therians. Yet, tribosphenic molars first appear in the Middle Jurassic fossil record 165-160 Ma (Luo et al., 2011; Rauhut et al., 2002), but tribosphenic taxa (which are primarily therians) were taxonomically depauperate until the mid-Cretaceous at ~100 Ma (Grossnickle and Polly, 2013) and were primarily small insectivores until after the end of the Cretaceous Terrestrial Revolution (KTR) at ~80 Ma (Chapters 3 and 4). This suggests that the evolution of this molar morphology did not result in an immediate taxonomic or ecomorphological diversification, which would be expected if it is a key innovation (Rabosky, 2014). Instead, the fossil record indicates that tribosphenic taxa such as therians remained ecologically 'dormant' (i.e., limited to small-bodied insectivores) for the first ~80 million years of their history.

Rather than triggering diversification, I posit that cladotherian adaptations of jaws, teeth, and ears were more critical to long-term survival during periods of significant ecological and environmental perturbation, such as the KTR at ~125-80 Ma and the K-Pg mass extinction event 66 Ma. It was only after the clade's survival of these events, as well as the demise of contemporary mammal groups, that therians experienced considerable ecological diversifications. Both the KTR and K-Pg mass extinction event resulted in evolutionary bottlenecks for mammals (Grossnickle and Polly, 2013; Chapter 4), and cladotherians (led by

therians) appear to have fared much better during these events than most non-cladotherian mammals. The hypothesis that their dietary adaptations were more critical to clade survival than diversification is congruent with evidence from non-mammalian clades that suggest extinction events often serve as catalysts for subsequent diversifications (Brocklehurst et al., 2015), possibly due to the ecological opportunities that emerge for surviving clades (Stroud and Losos, 2016).

One possibility for why therians persisted through the KTR and K-Pg mass extinction event is that their adaptations, such as tribosphenic molars, jaw yaw, and separation of the middle ear elements, permitted more versatile chewing mechanics and greater dietary diversity. Although early therians probably consumed mostly insects, the tribosphenic molars of these taxa also permit crushing and grinding of plant material in the talonid basin. This means that they can possess a more generalized diet than many non-therian groups such as eutriconodontans and spalacotherioids, which are probably limited to insectivory or carnivory due to dentitions that only permit shearing. Previous research has indicated that generalists are less prone to extinction than specialists (Simpson, 1944; Liow, 2004; Smits, 2015), and the potential for a generalist diet in therians may have been extremely valuable during periods in which food items were more limited.

Because of the strong link between molar/jaw morphologies and diet in modern analogs, the functional diversity of fossil mammals can be quantified through morphometric analyses of jaws and teeth. By capturing aspects of ecological diversity, these analyses allow for more robust examinations of the early therian adaptive radiation than examinations of morphology or phylogeny alone.

Morphological disparity patterns offer further evidence that periods of severe environmental and ecological perturbation were critical triggers for the diversification of mammals. Disparity results from analyses of molar and jaw shape suggest that therians diversified ecologically after the KTR, K-Pg mass extinction event, and Paleocene-Eocene Thermal Maximum (PETM; 56 Ma) (Figs. 3.5 and 4.5). Notably, this indicates that the evolutionary radiation of therians had its origins in the Late Cretaceous, and the radiation was not suppressed until the extinction of non-avian dinosaurs at the end of the Cretaceous (Chapter 4). Mammals may have experienced a selective extinction event at the K-Pg boundary that eliminated many specialists (Chapter 4; Wilson, 2013), but this was followed by shift toward herbivory and rapid recovery of therians after the boundary (Chapters 3 and 4; Wilson, 2014). The ecomorphological diversification after the KTR, K-Pg boundary, and PETM suggest that these events resulted in novel ecological opportunity for surviving clades. The events likely eliminated competitors and triggered dispersal, which is expected to cause diversification in clades. In addition, the events may have been especially beneficial to surviving angiosperms and social insects, which subsequently diversified and provided additional food items for therians (see above). Thus, the adaptive radiation of therians may be a product of long-term survival during periods of significant ecological perturbation and subsequent co-evolutionary interactions with angiosperms and insects.

REFERENCES

Abdala, F. & Damiani, R. (2004). Early development of the mammalian superficial masseter muscle in cynodonts. *Palaeontologia Africana, 40*, 23–29.

Adam, P. J. (2005). *Lobodon carcinophaga*. *Mammalian Species*, *772*, 1–14.

Adams, D. C. (2012). Comparing evolutionary rates for different phenotypic traits on a phylogeny using likelihood. *Systematic Biology*, *62*, 181–192.

Adams, D. C., & Otárola-Castillo, E. (2013). geomorph: an R package for the collection and analysis of geometric morphometric shape data. *Methods in Ecology and Evolution*, *4*, 393–399.

Agnarsson, I., Zambrana-Torrelio, C. M., Flores-Saldana, N. P., & May-Collado, L. J. (2011). A time-calibrated species-level phylogeny of bats (Chiroptera, Mammalia). *PLoS Currents*, *3,* RRN1212.

Akaike, H. (1974). A new look at the statistical model identification. *IEEE Transactions on Automatic Control*, *19*, 716–723.

Alfaro, M. E., et al. (2009). Nine exceptional radiations plus high turnover explain species diversity in jawed vertebrates. *Proceedings of the National Academy of Sciences*, *106*, 13410-13414.

Alhajeri, B. H., Hunt, O. J., & Steppan, S. J. (2015). Molecular systematics of gerbils and deomyines (Rodentia: Gerbillinae, Deomyinae) and a test of desert adaptation in the tympanic bulla. *Journal of Zoological Systematics and Evolutionary Research*, *53*, 312–330.

Almeida, F. C., Giannini, N. P., Simmons, N. B., & Helgen, K. M. (2014). Each flying fox on its own branch: a phylogenetic tree for *Pteropus* and related genera (Chiroptera: Pteropodidae). *Molecular Phylogenetics and Evolution*, *77*, 83–95.

Alroy, J. (1996). Constant extinction, constrained diversification, and uncoordinated stasis in North American mammals. *Palaeogeography, Palaeoclimatology, Palaeoecology*, *127*, 285–311.

Alroy, J. (1999). The fossil record of North American mammals: evidence for a Paleocene evolutionary radiation. *Systematic Biology, 48*, 107–118.

Alroy, J. (2010). Fair sampling of taxonomic richness and unbiased estimation of origination and extinction rates. *In* J. Alroy, J. & Hunt, G., editors, *Quantitative methods in Paleobiology. Paleontological Society Papers, 16*, 55–80.

Alvarez, L. W., Alvarez, W., Asaro, F., & Michel, H. V. (1980). Extraterrestrial cause for the Cretaceous-Tertiary extinction. *Science*, *208*, 1095–1108.

Angielczyk, K. D., & Schmitz, L. (2014). Nocturnality in synapsids predates the origin of mammals by over 100 million years. *Proceedings of the Royal Society B, 281*, 20141642.

Anthony, R. M., Barten, N. L., & Seiser, P. E. (2000). Foods of Arctic foxes *Alopex lagopus* during winter and spring in western Alaska. *Journal of Mammalogy, 81*, 820–828.

Antón, S. C. (1996). Cranial adaptation to a high attrition diet in Japanese macaques. *International Journal of Primatology*, *17*, 401–427.

Archibald J. D. (2011). *Extinction and radiation: how the fall of dinosaurs led to the rise of mammals*. The Johns Hopkins University Press, Baltimore.

Archibald, J. D., & Averianov, A. (2012). Phylogenetic analysis, taxonomic revision, and dental ontogeny of the Cretaceous Zhelestidae (Mammalia: Eutheria). *Zoological Journal of the Linnean Society*, *164*, 361–426.

Archibald, J. D., & Averianov, A. O. (2003). The Late Cretaceous placental mammal Kulbeckia. *Journal of Vertebrate Paleontology*, *23*, 404–419.

Archibald, J. D., & Averianov, A. O. (2006). Late Cretaceous asioryctitherian eutherian mammals from Uzbekistan and phylogenetic analysis of Asioryctitheria. *Acta Palaeontologica Polonica*, *51*, 351-376.

Archibald, J. D., Zhang, Y., Harper, T., & Cifelli, R. L. (2011). *Protungulatum*, confirmed Cretaceous occurrence of an otherwise Paleocene eutherian (placental?) mammal. *Journal of Mammalian Evolution*, *18*, 153–161.

Arregoitia, L. D. V., Fisher, D. O., & Schweizer, M. (2017). Morphology captures diet and locomotor types in rodents. *Open Science*, *4*, 160957.

Asher, R. J., McKenna, M. C., Emry, R. J., Tabrum, A. R. & Kron, D. G. (2002). Morphology and relationships of Apternodus and other extinct, zalambdodont, placental mammals. *Bulletin of the American Museum of Natural History*, *273*, 1–117.

Averianov, A., & Archibald, J. D. (2005). Mammals from the mid-Cretaceous Khodzhakul Formation, Kyzylkum Desert, Uzbekistan. *Cretaceous Research*, *26*, 593–608.

Averianov, A., & Archibald, J. D. (2013A). Variation and taxonomy of Asiamerican eutherian mammal *Paranyctoides*. *Canadian Journal of Earth Sciences*, *50*, 895–903.

Averianov, A. O., & Archibald, J. D. (2013B). New material and reinterpretation of the Late Cretaceous eutherian mammal *Paranyctoides* from Uzbekistan. *Acta Palaeontologica Polonica*, *58*, 17-23.

Averianov, A., Archibald, J. D., & Dyke, G. J. (2012). A new eutherian mammal from the Late Cretaceous of Kazakhstan. *Acta Palaeontologica Polonica*, *59*, 537–542.

Averianov, A. O., Archibald, J. D., & Ekdale, E. G. (2010). New material of the Late Cretaceous deltatheroidan mammal Sulestes from Uzbekistan and phylogenetic reassessment of the metatherian-eutherian dichotomy. *Journal of Systematic Palaeontology*, *8*, 301–330.

Averianov, A. O., & Skutschas, P. P. (2001). A new genus of eutherian mammal from the Early Cretaceous of Transbaikalia, Russia. *Acta Palaeontologica Polonica*, *46*, 431–436.

Ayres, J. M. (1989). Comparative feeding ecology of the uakari and bearded saki, *Cacajao* and *Chiropotes*. *Journal of Human Evolution, 18*, 697–716.

Baker, J., Meade, A., Pagel, M., & Venditti, C. (2015). Adaptive evolution toward larger size in mammals. *Proceedings of the National Academy of Sciences*, *112*, 5093–5098.

Baker, R. J., Bininda-Emonds, O. R., Mantilla-Meluk, H., Porter, C. A., & Van Den Bussche, R. A. (2012). Molecular timescale of diversification of feeding strategy and morphology in New World leaf-nosed bats (Phyllostomidae): a phylogenetic perspective. *In* Gunnell, G. F., & Simmons, N. B., editors, *Evolutionary history of bats: fossils, molecules and morphology,* pages 385–409. Cambridge University Press, Cambridge.

Baker, R. H., Newman, C. C., & Wilke, F. (1945). Food habits of the raccoon in eastern Texas. *Journal of Wildlife Management, 9*, 45–48.

Bakker, R. T., & Carpenter, K. (1990). A new latest Jurassic vertebrate fauna, from the highest levels of the Morrison Formation at Como Bluff, Wyoming. Part III. The mammals: a new multituberculate and a new paurodont. *Hunteria*, *2*, 4–8.

Balete, D. S., Rickart, E. A., Rosell-Ambal, R. G. B., Jansa, S., & Heaney, L. R. (2007). Descriptions of two new species of *Rhynchomys* Thomas (Rodentia: Muridae: Murinae) from Luzon Island, Philippines. *Journal of Mammalogy*, *88*, 287–301.

Barkley, L. J., & Whitaker, J. O., Jr. (1984). Confirmation of *Caenolestes* in Peru with information on diet. *Journal of Mammalogy, 65*, 328–330.

Bartoń, K. 2016. MuMIn: multi-model inference. R package, version 1.15.6. http://cran.r-project.org/web/packages/MuMIn/index.html.

Beaulieu, J. M., Jhwueng, D. C., Boettiger, C., & O'Meara, B. C. (2012). Modeling stabilizing selection: expanding the Ornstein–Uhlenbeck model of adaptive evolution. *Evolution*, *66*, 2369–2383.

Beaulieu, J. M., & O'Meara, B. C. (2016). OUwie: analysis of evolutionary rates in an OU framework. R package, version 1.49. https://cran.r-project.org/web/packages/OUwie/index.html.

Beneski, J. T., Jr., & Stinson, D. W. (1987). *Sorex palustris*. *Mammalian Species*, *296*, 1–6.

Benson, R. B., Mannion, P. D., Butler, R. J., Upchurch, P., Goswami, A., & Evans, S. E. (2013). Cretaceous tetrapod fossil record sampling and faunal turnover: implications for biogeography and the rise of modern clades. *Palaeogeography, Palaeoclimatology, Palaeoecology*, *372*, 88–107.

Benton, M. J. (2009). The Red Queen and the Court Jester: species diversity and the role of biotic and abiotic factors through time. *Science*, *323*, 728-732.

Benton, M. J. (2015). Exploring macroevolution using modern and fossil data. *Proceedings of the Royal Society B, 282,* 20150569.

Best, T. L., Clawson, R. G., & Clawson, J. A. (1994). *Tamias speciosus*. *Mammalian Species*, *478*, 1–9.

Bibi, F. (2013). A multi-calibrated mitochondrial phylogeny of extant Bovidae (Artiodactyla, Ruminantia) and the importance of the fossil record to systematics. *BMC Evolutionary Biology, 13*, 166.

Bi, S., Jin, X., Li, S., & Du, T. (2015). A new Cretaceous Metatherian mammal from Henan, China. *PeerJ*, *3*, e896.

Bi, S., Wang, Y., Guan, J., Sheng, X., & Meng, J. (2014). Three new Jurassic euharamiyidan species reinforce early divergence of mammals. *Nature*, *514*, 579–584.

Bisbal E, F. J. (1986). Food habits of some neotropical carnivores in Venezuela (Mammalia, Carnivora). *Mammalia*, *50*, 329–340.

Bloch, J. I., Silcox, M. T., Boyer, D. M., & Sargis, E. J. (2007). New Paleocene skeletons and the relationship of plesiadapiforms to crown-clade primates. *Proceedings of the National Academy of Sciences*, *104*, 1159–1164.

Bock, W. J., & Wahlert, G. (1965). Adaptation and the form–function complex. *Evolution*, *19*, 269–299.

Bonaparte, J. F., & Rougier, G. W. (1987). Mamiferos del Cretacico inferior de Patagonia. *IV Congreso Latinamericano de Paleontología*, *1*, 343–359.

Bond, W. J., & Scott, A. C. (2010). Fire and the spread of flowering plants in the Cretaceous. *New Phytologist*, *188*, 1137–1150.

Bookstein, F. L. (1997). *Morphometric Tools for Landmark Data: Geometry and Biology*. Cambridge University Press, Cambridge.

Bothma, J. D. P. (1966). Notes on the stomach contents of certain Carnivora (Mammalia) from the Kalahari Gemsbok Park. *Koedoe, 9*, 37–39.

Boyce, C. K., Brodribb, T.J., Field, T. S., & Zwieniecki, M. A. (2009). Angiosperm leaf vein evolution was physiologically and environmentally transformative. *Proceedings of the Royal Society B, 276*, 1771–1776.

Boyer, D. M. (2008). Relief index of second mandibular molars is a correlate of diet among prosimian primates and other euarchontan mammals. *Journal of Human Evolution*, *55*, 1118–1137.

Boyer, D. M., Prasad, G. V., Krause, D. W., Godinot, M., Goswami, A., Verma, O., & Flynn, J. J. (2010). New postcrania of Deccanolestes from the Late Cretaceous of India and their bearing on the evolutionary and biogeographic history of euarchontan mammals. *Naturwissenschaften*, *97*, 365–377.

Brocklehurst, N., Ruta, M., Müller, J., & Fröbisch, J. (2015). Elevated extinction rates as a trigger for diversification rate shifts: early amniotes as a case study. *Scientific Reports*, *5*, 17104.

Brooke, A. P. (1994). Diet of the fishing bat, *Noctilio leporinus* (Chiroptera: Noctilionidae). *Journal of Mammalogy, 75*, 212–218.

Burnham, K. P., & Anderson, D. R. (2003). *Model selection and multimodel inference: a practical information-theoretic approach*. Springer, New York.

Butler, M. A., & King, A. A. (2004). Phylogenetic comparative analysis: a modeling approach for adaptive evolution. *The American Naturalist*, *164*, 683–695.

Butler, P. M. (1972). Some functional aspects of molar evolution. *Evolution, 26*, 474–483.

Butler, P. M. (1973). Molar wear facets of early Tertiary North American primates. *In* Montagna, W., & Zingeser, M.R., editors, *Craniofacial biology of primates*, *4th International Congress of Primatology, 3*, pages 1–27. Karger, Basel.

Byrne, H., et al. (2016). Phylogenetic relationships of the New World titi monkeys (*Callicebus*): first appraisal of taxonomy based on molecular evidence. *Frontiers in Zoology*, *13*, 10.

Carraway, L. N., Alexander, L. F., & Verts, B. J. (1993). *Scapanus townsendii*. *Mammalian Species*, *434*, 1–7.

Case, J. A., Goin, F. J., & Woodburne, M. O. (2004). "South American" marsupials from the Late Cretaceous of North America and the origin of marsupial cohorts. *Journal of Mammalian Evolution*, *11*, 223–255.

Charles-Dominique, P. (1974). Ecology and feeding behaviour of five sympatric lorisids in Gabon. *In* R. D. Martin, G. A. Doyle & A. C. Walker, editors, *Prosimian Biology*, pages 131–150. University of Pittsburgh Press, Pittsburgh, PA.

Chen, M., & Wilson, G. P. (2015). A multivariate approach to infer locomotor modes in Mesozoic mammals. *Paleobiology*, *41*, 280–312.

Chow, M., Chang, Y., Wang, B., & Ting, S. (1977). Paleocene mammalian fauna from the Nanxiong Basin, Guangdong. *Paleontologica Sinica, New Series C*, *20*, 1–100.

Cifelli, R. L. (1990). Cretaceous mammals of southern Utah. I. Marsupials from the Kaiparowits Formation (Judithian). *Journal of Vertebrate Paleontology*, *10*, 295–319.

Cifelli, R. L. (1990). Cretaceous mammals of southern Utah. IV. Eutherian mammals from the Wahweap (Aquilan) and Kaiparowits (Judithian) formations. *Journal of Vertebrate Paleontology*, *10*, 346–360.

Cifelli, R. L. (1993). Early Cretaceous mammal from North America and the evolution of marsupial dental characters. *Proceedings of the National Academy of Sciences, 90*, 9413–9416.

Cifelli, R. L. (1999). Tribosphenic mammal from the North American early Cretaceous. *Nature*, *401*, 363–366.

Cifelli, R. L. (2004). Chapter 5: Marsupial Mammals from the Albian-Cenomanian (Early-Late Cretaceous) Boundary, Utah. *Bulletin of the American Museum of Natural History*, 62–79.

Cifelli, R. L., & Davis, B. M. (2015). Tribosphenic mammals from the Lower Cretaceous Cloverly Formation of Montana and Wyoming. *Journal of Vertebrate Paleontology*, e920848.

Christensen, H. B. (2014). Similar associations of tooth microwear and morphology indicate similar diet across marsupial and placental mammals. *PloS One*, *9*, e102789.

Claude, J., Paradis, E., Tong, H., & Auffray, J. C. (2003). A geometric morphometric assessment of the effects of environment and cladogenesis on the evolution of the turtle shell. *Biological Journal of the Linnean Society*, *79*, 485–501.

Clauset, A., & Redner, S. (2009). Evolutionary model of species body mass diversification. *Physical Review Letters, 102*, 038103.

Cleary, G. P., Corner, L. A., O'Keeffe, J., & Marples, N. M. (2011). Diet of the European badger (*Meles meles*) in the Republic of Ireland: A comparison of results from an analysis of stomach contents and rectal faeces. *Mammalian Biology-Zeitschrift für Säugetierkunde, 76*, 470–475.

Clemens, W. A. (2002). Evolution of the mammalian fauna across the Cretaceous-Tertiary boundary in northeastern Montana and other areas of the Western Interior. *The Hell Creek Formation and the Cretaceous-Tertiary boundary in the northern Great Plains: Geological Society of America Special Paper*, *361*, 217–245.

Clemens, W. A. (2011). *Eoconodon* ("Triisodontidae," Mammalia) from the Early Paleocene (Puercan) of northeastern Montana, USA. *Palaeontologia Electronica*, *14*, 22A.

Clemens, W. A. (2017). *Procerberus* (Cimolestidae, Mammalia) from the Latest Cretaceous and Earliest Paleocene of the Northern Western Interior, USA. *PaleoBios*, *34*, 1–26.

Close, R. A., Friedman, M., Lloyd, G. T. & Benson, R. B. (2015). Evidence for a mid-Jurassic adaptive radiation in mammals. *Current Biology, 25*, 2137–2142.

Close, R. A., Davis, B. M., Walsh, S., Wolniewicz, A. S., Friedman, M., & Benson, R. B. (2016). A lower jaw of Palaeoxonodon from the Middle Jurassic of the Isle of Skye, Scotland, sheds new light on the diversity of British stem therians. *Palaeontology*, *59*, 155–169.

Coiffard, C., Gomez, B., Daviero-Gomez, V., & Dilcher, D. L. (2012). Rise to dominance of angiosperm pioneers in European Cretaceous environments. *Proceedings of the National Academy of Sciences*, *109*, 20955–20959.

Collinson, M. E., & Hooker, J. J. (1991). Fossil evidence of interactions between plants and plant-eating mammals. *Philosophical Transactions of the Royal Society of London B*, *333*, 197–208.

Conith, A. J., Imburgia, M. J., Crosby, A. J., & Dumont, E. R. (2016). The functional significance of morphological changes in the dentitions of early mammals. *Journal of the Royal Society Interface*, *13*, 20160713.

Cooper, C. E. (2011). *Myrmecobius fasciatus* (Dasyuromorphia: Myrmecobiidae). *Mammalian Species, 43*, 129–140.

Cooper, N., & Purvis, A. (2010). Body size evolution in mammals: complexity in tempo and mode. *The American Naturalist*, *175*, 727–738.

Cooper, N., Thomas, G. H., Venditti, C., Meade, A., & Freckleton, R. P. (2016). A cautionary note on the use of Ornstein Uhlenbeck models in macroevolutionary studies. *Biological Journal of the Linnean Society*, *118*, 64–77.

Cox, P. G., & Baverstock, H. (2016). Masticatory muscle anatomy and feeding efficiency of the American beaver, *Castor canadensis* (Rodentia, Castoridae). *Journal of Mammalian Evolution, 23*, 191–200.

Crampton, J. S., Beu, A. G., Cooper, R. A., Jones, C. M., Marshall, B., & Maxwell, P. A. (2003). Estimating the rock volume bias in paleobiodiversity studies. *Science, 301*, 358–360.

Crompton, A. W. (1963). The evolution of the mammalian jaw. *Evolution*, *17*, 431–439.

Crompton, A. W. (1971). The origin of the tribosphenic molar. *In* Kermack, D. M. & Kermack, K. A., editors, *Early Mammals*, pages 65–87. *Zoological Journal of the Linnean Society*.

Crompton, A. W. (1995). Masticatory function in nonmammalian cynodonts and early mammals. *In* Thomason, J. J., editor, *Functional Morphology in Vertebrate Paleontology*, pages 55–75. Cambridge University Press, Cambridge.

Crompton, A. W. (2011). Masticatory motor programs in Australian herbivorous mammals: diprotodontia. *Integrative and Comparative Biology, 51*, 271–281.

Crompton, A. W. & Hiiemae, K. (1970). Molar occlusion and mandibular movements during occlusion in the American opossum, *Didelphis marsupialis* L. *Zoological Journal of the Linnean Society, 49*, 21–47.

Crompton, A. W. & Jenkins, F. A., Jr. (1968). Molar occlusion in Late Triassic mammals. *Biological Reviews*, *43*, 427–458.

Crompton, A. W. & Kielan-Jaworowska, Z. (1978) Molar structure and occlusion in Cretaceous therian mammals. *In* Butler, P. M. & Joysey, K. A., editors, *Studies in the Development, Function and Evolution of Teeth*, pages 249–287, Academic Press.

Crompton, A. W. & Sita-Lumsden, A. (1970). Functional significance of the therian molar pattern. *Nature*, *227*, 197–199.

Crompton, A. W., & Parker, P. (1978). Evolution of the Mammalian Masticatory Apparatus: The fossil record shows how mammals evolved both complex chewing mechanisms and an effective middle ear, two structures that distinguish them from reptiles. *American Scientist, 66*, 192–201.

Crompton, A. W., & Hylander, W. L. (1986). Changes in mandibular function following the acquisition of a dentary-squamosal jaw articulation. *In* Hotton, N., III, MacLean, P. D., Roth, J. J., & Roth, E. C., editors, *The ecology and biology of mammal-like reptiles*, pages 263–282. Smithsonian Institution Press, Washington, D. C.

Crompton, A. W., Owerkowicz, T., & Skinner, J. (2010). Masticatory motor pattern in the koala (*Phascolarctos cinereus*): a comparison of jaw movements in marsupial and placental herbivores. *Journal of Experimental Zoology Part A: Ecological Genetics and Physiology, 313*, 564–578.

Damuth, J., & Janis, C. M. (2011). On the relationship between hypsodonty and feeding ecology in ungulate mammals, and its utility in palaeoecology. *Biological Reviews*, *86*, 733–758.

Darwin, C. (1859). *The origin of species by means of natural selection: or, the preservation of favored races in the struggle for life*. John Murray.

Dashzeveg, D. (1975). New primitive therian from the Early Cretaceous of Mongolia. *Nature, 256*, 402–403.

Dashzeveg, D., Dingus, L., Loope, D. B., Swisher III, C. C., Dulam, T., & Sweeney, M. R. (2005). New stratigraphic subdivision, depositional environment, and age estimate for the Upper Cretaceous Djadokhta Formation, southern Ulan Nur Basin, Mongolia. *American Museum Novitates*, *3498*, 1–31.

Davies, R. A. G., Botha, P., & Skinner, J. D. (1986). Diet selected by springbok *Antidorcas marsupialis* and Merino sheep *Ovis aries* during a Karoo drought. *Transactions of the Royal Society of South Africa 46*, 165–176.

Davis, B. M. (2007). A revision of "pediomyid" marsupials from the Late Cretaceous of North America. *Acta Palaeontologica Polonica*, *52*, 217–256.

Davis, B. M. (2011). Evolution of the tribosphenic molar pattern in early mammals, with comments on the "dual-origin" hypothesis. *Journal of Mammalian Evolution, 18*, 227–244.

Davis, B. M. (2012). Micro-computed tomography reveals a diversity of Peramuran mammals from the Purbeck Group (Berriasian) of England. *Palaeontology, 55*, 789–817.

Davis, B. M., & Cifelli, R. L. (2011). Reappraisal of the tribosphenidan mammals from the Trinity Group (Aptian-Albian) of Texas and Oklahoma. *Acta Palaeontologica Polonica*, *56*, 441–462.

Davis, B. M., Cifelli, R. L., & Cohen, J. E. (2016). First fossil mammals from the upper Cretaceous Eagle Formation (Santonian, Northern Montana, USA), and mammal diversity during the Aquilan North American Land Mammal Age. *Acta Palaeontologica Polonica, 67*, 101–126.

Davis, B. M., Cifelli, R. L., & Kielan-Jaworowska, Z. (2008). Earliest evidence of Deltatheroida (Mammalia: Metatheria) from the Early Cretaceous of North America. *In* Sargis, E. J., & Dagosto, M., editors, *Mammalian Evolutionary Morphology*, pages 3–24. Springer Netherlands.

Davis, J. L., Santana, S. E., Dumont, E. R., & Grosse, I. R. (2010). Predicting bite force in mammals: two-dimensional versus three-dimensional lever models. *Journal of Experimental Biology*, *213*, 1844–1851.

Davis, J. S. (2014). *Functional Morphology of Mastication in Musteloid Carnivorans*. PhD dissertation. Ohio University.

Davis, M., & Pineda-Munoz, S. (2016). The temporal scale of diet and dietary proxies. *Ecology and Evolution*, *6*, 1883–1897.

De Muizon, C. (1991). La fauna de mamiferos de Tiupampa (paleoceno inferior, formacion Santa Lucia), Bolivia. *Fósiles y facies de Bolivia. I Vertebrados, Revista Técnica YPFB*, *12*, 575–624.

De Muizon, C. (1998). *Mayulestes ferox*, a borhyaenoid (Metatheria, Mammalia) from the early Palaeocene of Bolivia. Phylogenetic and palaeobiologic implications. *Geodiversitas*, *20*, 19–142.

De Muizon, C., & Cifelli, R. L. (2000). The condylarths (archaic Ungulata, Mammalia) from the early Palaeocene of Tiupampa (Bolivia): implications on the origin of the South American ungulates. *Geodiversitas*, *22*, 47–150.

De Muizon, C., & Cifelli, R. L. (2001). A new basal "didelphoid" (Marsupialia, Mammalia) from the early Paleocene of Tiupampa (Bolivia). *Journal of Vertebrate Paleontology*, *21*, 87–97.

De Muizon, C., & Marshall, L. G. (1992). *Alcidedorbignya inopinata* (Mammalia: Pantodonta) from the early Paleocene of Bolivia; phylogenetic and paleobiogeographic implications. *Journal of Paleontology*, *66*, 499–520.

Dearing, M. D. (1996). Disparate determinants of summer and winter diet selection of a generalist herbivore, *Ochotona princeps*. *Oecologia, 108*, 467–478.

DeMar, R. & Barghusen, H. R. (1972). Mechanics and the evolution of the synapsid jaw. *Evolution, 26*, 622–637.

Diaz, G. B., Ojeda, R. A., Gallardo, M. H., & Giannoni, S. M. (2000). *Tympanoctomys barrerae. Mammalian Species*, *646*, 1–4.

Dickman, C. R. (1988). Age-related dietary change in the European hedgehog, *Erinaceus europaeus*. *Journal of Zoology, 215*, 1–14.

dos Reis M, Donoghue PC, Yang Z. (2014). Neither phylogenomic nor palaeontological data support a Palaeogene origin of placental mammals. *Biology Letters, 10*, 20131003.

dos Reis, M., Inoue, J., Hasegawa, M., Asher, R. J., Donoghue, P. C., & Yang, Z. (2012). Phylogenomic datasets provide both precision and accuracy in estimating the timescale of placental mammal phylogeny. *Proceedings of the Royal Society B*, *279*, 3491–3500.

Dötsch, C. (1986). Mastication in the musk shrew, *Suncus murinus* (Mammalia, Soricidae). *Journal of Morphology*, *189*, 25–43.

Dötsch, C. (1994). Function of the feeding apparatus in red-toothed and white-toothed shrews (Soricidae) using electromyography and cineradiography. *Advances in the Biology of Shrews*, 233–239.

Dubey, S., Salamin, N., Ohdachi, S. D., Barrière, P., & Vogel, P. (2007). Molecular phylogenetics of shrews (Mammalia: Soricidae) reveal timing of transcontinental colonizations. *Molecular Phylogenetics and Evolution, 44*, 126–137.

Dunham, K. M. (1980). The diet of impala *Aepyceros melampus* in the Sengwa Wildlife Research Area, Rhodesia. *Journal of Zoology, 192*, 41–57.

Eaton, J. G., & Cifelli, R. L. (2013). Review of Late Cretaceous Mammalian faunas of the Kaiparowits and Paunsaugunt plateaus, southwestern Utah. *At the Top of the Grand Staircase: The Late Cretaceous of Southern Utah. Indiana University Press, Bloomington*, 319–369.

Eaton, J. G. (2006). Santonian (Late Cretaceous) mammals from the John Henry Member of the Straight Cliffs Formation, Grand Staircase-Escalante National Monument, Utah. *Journal of Vertebrate Paleontology*, *26*, 446–460.

Eberle, J. J., & Lillegraven, J. A. (1998). A new important record of earliest Cenozoic mammalian history: geologic setting, Multituberculata, and Peradectia. *Rocky Mountain Geology*, *33*, 3–47.

Eberth, D. A., Badamgarav, D., & Currie, P. J. (2009). The Baruungoyot-Nemegt transition (Upper Cretaceous) at the Nemegt type area, Nemegt Basin, south central Mongolia. *Journal of the Paleontological Society of Korea, 25*, 1–15.

Eizirik, E., Murphy, W. J., Koepfli, K. P., Johnson, W. E., Dragoo, J. W., Wayne, R. K., & O'Brien, S. J. (2010). Pattern and timing of diversification of the mammalian order Carnivora inferred from multiple nuclear gene sequences. *Molecular Phylogenetics and Evolution*, *56*, 49–63.

Emmons, L. H. (1980). Ecology and resource partitioning among nine species of African rain forest squirrels. *Ecological Monographs, 50*, 31-54.

Ellis, B. A., Mills, J. N., Glass, G. E., McKee, K. T., Jr., Enria, D. A., & Childs, J. E. (1998). Dietary habits of the common rodents in an agroecosystem in Argentina. *Journal of Mammalogy 79*, 1203–1220.

Eriksson, O. (2014). Evolution of angiosperm seed disperser mutualisms: the timing of origins and their consequences for coevolutionary interactions between angiosperms and frugivores. *Biological Reviews of the Cambridge Philosophical Society, 91*, 168–186.

Evans, A. R., & Fortelius, M. (2008). Three-dimensional reconstruction of tooth relationships during carnivoran chewing. *Palaeontologia Electronica, 11*, 10A.

Evans, A. R., & Sanson, G. D. (1998). The effect of tooth shape on the breakdown of insects. *Journal of Zoology*, *246*, 391–400.

Evans, A. R. & Sanson, G. D. (2003). The tooth of perfection: functional and spatial constraints on mammalian tooth shape. *Biological Journal of the Linnean Society, 78*, 173–191.

Evans, A. R. & Sanson, G. D. (2006). Spatial and functional modeling of carnivore and insectivore molariform teeth. *Journal of Morphology, 267*, 649–662.

Evans, A. R., Wilson, G. P., Fortelius, M., & Jernvall, J. (2007). High-level similarity of dentitions in carnivorans and rodents. *Nature*, *445*, 78–81.

Fabre, P. H., Hautier, L., Dimitrov, D., & Douzery, E. J. (2012). A glimpse on the pattern of rodent diversification: a phylogenetic approach. *BMC Evolutionary Biology*, *12*, 88.

Fanti, F., Currie, P. J., & Badamgarav, D. (2012). New specimens of Nemegtomaia from the Baruungoyot and Nemegt formations (Late Cretaceous) of Mongolia. *PloS One*, *7*, e31330.

Feild, T. S., et al. (2011). Fossil evidence for Cretaceous escalation in angiosperm leaf vein evolution. *Proceedings of the National Academy of Sciences*, *108*, 8363–8366.

Fielden, L. J., Perrin, M. R., & Hickman, G. C. (1990). Feeding ecology and foraging behaviour of the Namib Desert golden mole, *Eremitalpa granti namibensis* Chrysochloridae. *Journal of Zoology, 220*, 367–389.

Figueirido, B., Janis, C. M., Pérez-Claros, J. A., De Renzi, M., & Palmqvist, P. (2012). Cenozoic climate change influences mammalian evolutionary dynamics. *Proceedings of the National Academy of Sciences*, *109*, 722–727.

Figueirido, B., Martín-Serra, A., Tseng, Z. J., & Janis, C. M. (2015). Habitat changes and changing predatory habits in North American fossil canids. *Nature Communications*, *6*, 7976.

Figueirido, B., Palmqvist, P., & Pérez-Claros, J. A. (2009). Ecomorphological correlates of craniodental variation in bears and paleobiological implications for extinct taxa: an approach based on geometric morphometrics. *Journal of Zoology*, *277*, 70–80.

Figueirido, B., Serrano-Alarcon, F. J., Slater, G. J., & Palmqvist, P. (2010). Shape at the cross-roads: homoplasy and history in the evolution of the carnivoran skull towards herbivory. *Journal of Evolutionary Biology*, *23*, 2579–2594.

Fish, D. R., & Mendel, F. C. (1982). Mandibular movement patterns relative to food types in common tree shrews (*Tupaia glis*). *American Journal of Physical Anthropology*, *58*, 255–269.

Flannery, T. F. (1994). *Possums of the world: a monograph of the Phalangeroidea.* GEO Productions, Sydney, Australia.

Fleming, T. H. (1979). Do tropical frugivores compete for food?. *American Zoologist, 19*, 1157–1172.

Foote, M. (1992). Rarefaction analysis of morphological and taxonomic diversity. *Paleobiology*, *18*, 1–16.

Foote, M. (1993). Discordance and concordance between morphological and taxonomic diversity. *Paleobiology*, *19*, 185–204.

Fox, R. C. (2015). A revision of the Late Cretaceous–Paleocene eutherian mammal Cimolestes Marsh, 1889. *Canadian Journal of Earth Sciences*, *52*, 1137–1149.

Fox, R. C., & Naylor, B. G. (2003). A Late Cretaceous taeniodont (Eutheria, Mammalia) from Alberta, Canada. *Neues Jahrbuch fur Geologie und Palaontologie-Abhandlungen*, *229*, 393.

Fox, R. C., & Scott, C. S. (2011). A new, early Puercan (earliest Paleocene) species of *Purgatorius* (Plesiadapiformes, Primates) from Saskatchewan, Canada. *Journal of Paleontology*, *85*, 537–548.

Fox, R. C., Scott, C. S., & Bryant, H. N. (2007). A new, unusual therian mammal from the Upper Cretaceous of Saskatchewan, Canada. *Cretaceous Research, 28*, 821–829.

Fox, R. C., Scott, C. S., & Buckley, G. A. (2015). A 'giant'purgatoriid (Plesiadapiformes) from the Paleocene of Montana, USA: mosaic evolution in the earliest primates. *Paleontology, 58*, 277–291.

Fox, R. C., Scott, C. S., & Rankin, B. D. (2010). Edworthia lerbekmoi, a new primitive paromomyid primate from the Torrejonian (early Paleocene) of Alberta, Canada. *Journal of Paleontology*, *84*, 868–878.

Funmilayo, O. (1979). Food consumption preferences and storage in the mole *Talpa europaea*. *Acta Theriologica, 24*, 379–390.

Gautier-Hion, A., Emmons, L. H., & Dubost, G. (1980). A comparison of the diets of three major groups of primary consumers of Gabon primates, squirrels and ruminants. *Oecologia, 45*, 182–189.

Gazin, C. L. (1941). The mammalian faunas of central Utah, with notes on the geology. *Proceedings of the United States National Museum, 91*, 1–53.

Gaetano, L. C., & Rougier, G. W. (2011). New materials of *Argentoconodon fariasorum* (Mammaliaformes, Triconodontidae) from the Jurassic of Argentina and its bearing on triconodont phylogeny. *Journal of Vertebrate Paleontology*, *31*, 829–843.

Gambaryan, P. P., & Kielan-Jaworowska, Z. (1995). Masticatory musculature of Asian taeniolabidoid multituberculate mammals. *Acta Palaeontologica Polonica*, *40*, 45–108.

Gelfo, J. N., Goin, F. J., Woodburne, M. O., & Muizon, C. D. (2009). Biochronological relationships of the earliest South American Paleogene mammalian faunas. *Palaeontology*, *52*, 251–269.

Gelfo, J. N., Ortiz-Jaureguizar, E., & Rougier, G. W. (2007). New remains and species of the 'condylarth' genus *Escribania* (Mammalia: Didolodontidae) from the Palaeocene of Patagonia, Argentina. *Earth and Environmental Science Transactions of the Royal Society of Edinburgh*, *98*, 127–138.

Gheerbrant, E., & Astibia, H. (1994). A new mammal from the Maastrichtian of Laño (Spanish Basque Country). *Sciences de la Terre et des Planètes*, *318*, 1125–1131.

Gibb, et al. (2015). Shotgun mitogenomics provides a reference phylogenetic framework and timescale for living xenarthrans. *Molecular Biology and Evolution*, *33*, 621–642.

Gill, P. G., Purnell, M. A., Crumpton, N., Brown, K. R., Gostling, N. J., Stampanoni, M., & Rayfield, E. J. (2014). Dietary specializations and diversity in feeding ecology of the earliest stem mammals. *Nature*, *512*, 303–305.

Gingerich, P. D. (1973). Molar occlusion and function in the Jurassic mammal *Docodon*. *Journal of Mammalogy*, *54*, 1008–1013.

Gingerich, P. D. (1980). Evolutionary patterns in early Cenozoic mammals. *Annual Review of Earth and Planetary Sciences*, *8*, 407–424.

Gingerich, P. D. (2006). Environment and evolution through the Paleocene–Eocene thermal maximum. *Trends in Ecology & Evolution*, *21*, 246-253.

Goin, F. J., et al. (2006). The earliest Tertiary therian mammal from South America. *Journal of Vertebrate Paleontology*, *26*, 505–510.

Goin, F. J., Woodburne, M. O., Zimicz, A. N., Martin, G. M., & Chornogubsky, L. (2016). Paleobiology and Adaptations of Paleogene Metatherians. In *A Brief History of South American Metatherians*, pages 185–208. Springer Netherlands.

Good, I. J. (1953). The population frequencies of species and the estimation of population parameters. *Biometrika, 40*, 237–264.

Gonçalves, F., Munin, R., Costa, P., & Fischer, E. (2007). Feeding habits of *Noctilio albiventris* (Noctilionidae) bats in the Pantanal, Brazil. *Acta Chiropterologica*, *9*, 535–538.

Goodwin, G.G. & Greenhall, A.M. (1961). A review of the bats of Trinidad and Tobago. *Bulletin of the American Museum of Natural History, 122*, 187–302.

Gould, S. J., & Eldredge, N. (1977). Punctuated equilibria: the tempo and mode of evolution reconsidered. *Paleobiology*, *3*, 115–151.

Gow, C. E. (1986). A new skull of *Megazostrodon* (Mammalia, Triconodonta) from the Elliot Formation (Lower Jurassic) of southern Africa. *Palaeontologia Africana, 26*, 13–23.

Gradstein, F. M., Ogg, J. G., Schmitz, M., & Ogg, G. (editors). (2012). *The Geologic Time Scale 2012*. Elsevier, Amsterdam.

Gray, G. G., & Simpson, C. D. (1980). *Ammotragus lervia*. *Mammalian Species*, *144*, 1–7.

Greegor, D. H., Jr. (1980). Diet of the little hairy armadillo, *Chaetophractus vellerosus*, of northwestern Argentina. *Journal of Mammalogy, 61*, 331–334.

Grossnickle, D. M. (2017). The evolutionary origin of jaw yaw in mammals. *Scientific Reports, 7*, 45094.

Grossnickle, D. M., & Newham, E. (2016). Therian mammals experience an ecomorphological radiation during the Late Cretaceous and selective extinction at the K–Pg boundary. *Proceedings of the Royal Society B*, *283*, 20160256.

Grossnickle, D. M., & Polly, P. D. (2013). Mammal disparity decreases during the Cretaceous angiosperm radiation. *Proceedings of the Royal Society B, 280*, 20132110.

Greaves, W. S. (1974). Functional implications of mammalian jaw joint position. *Forma et functio, 7*, 363–376.

Guillotin, M., Dubost, G., & Sabatier, D. (1994). Food choice and food competition among the three major primate species of French Guiana. *Journal of Zoology, 233*, 551–579.

Gunnell, G. F. (1989). Evolutionary history of Microsyopoidea (Mammalia, ?Primates) and the relationship between Plesiadapiformes and Primates. *University of Michigan Papers on Paleontology, 27,* 1–157.

Gunz, P., Mitteroecker, P., & Bookstein, F. L. (2005). Semilandmarks in three dimensions. *In* Slice, D. E., editor. *Modern morphometrics in physical anthropology*, pages 73–98. Springer US.

Hahn, G. (1969). Beiträge zur Fauna der Grube Guimarota Nr. 3. Die Multituberculata. *Palaeontographica Abteilung A*, *133*, 1–100.

Hahn, G., & Hahn, R. (1998). Neue Beobachtungen an Plagiaulacoidea (Multituberculata) des Ober-Juras 2. Zum Bau des Unterkiefers und des Gebisses bei Meketibolodon und bei Guimarotodon. *Berl Geowiss Abh E*, *28*, 9–37.

Hahus, S. C. & Smith, K. G. (1990). Food habits of *Blarina*, *Peromyscus*, and *Microtus* in relation to an emergence of periodical cicadas Magicicada. *Journal of Mammalogy, 71*, 249–252.

Hallett, J. G. (1978). *Parascalops breweri*. *Mammalian Species*, *98*, 1–4.

Halliday, T. J. D., & Goswami, A. (2016). Eutherian morphological disparity across the end-Cretaceous mass extinction. *Biological Journal of the Linnean Society*, *118*, 152–168.

Halliday, T. J. D., Upchurch, P. & Goswami, A. (2015). Resolving the relationships of Paleocene placental mammals. *Biological Reviews*, *92*, 521-550.

Halliday, T. J. D., Upchurch, P., & Goswami, A. (2016). Eutherians experienced elevated evolutionary rates in the immediate aftermath of the Cretaceous–Palaeogene mass extinction. *Proceedings of the Royal Society B*, 283, 20153026.

Hammer, Ø., Harper, D. A. T., & Ryan, P. D. (2008). PAST-palaeontological statistics, version 1.89. Paleontological Museum, University of Oslo, Noruega. http://folk.uio.no/ohammer/past/index.html.

Han, G., & Meng, J. (2016). A new spalacolestine mammal from the Early Cretaceous Jehol Biota and implications for the morphology, phylogeny, and palaeobiology of Laurasian 'symmetrodontans'. *Zoological Journal of the Linnean Society*, *178*, 343–380.

Hansen, T. F. (1997). Stabilizing selection and the comparative analysis of adaptation. *Evolution*, *51*, 1341–1351.

Harding, L. E. (2011). *Trachypithecus delacouri* (Primates: Cercopithecidae). *Mammalian Species, 43*, 118–128.

Harmon, L. J., et al. (2010). Early bursts of body size and shape evolution are rare in comparative data. *Evolution*, *64*, 2385–2396.

Hayssen, V. (2008). *Bradypus pygmaeus* (Pilosa: Bradypodidae). *Mammalian Species*, *812*, 1–4.

He, K., Shinohara, A., Helgen, K. M., Springer, M. S., Jiang, X. L., & Campbell, K. L. (2016). Talpid mole phylogeny unites shrew moles and illuminates overlooked cryptic species diversity. *Molecular Biology and Evolution*, *34*, 78–87.

Heaney, L. R., Tabaranza Jr, B. R., Rickart, E. A., Balete, D. S., & Ingle, N. R. (2006). The mammals of Mt. Kitanglad Nature Park, Mindanao, Philippines. *Fieldiana Zoology*, *112*, 1–63.

Heinrich, W. D. (1998). Late Jurassic mammals from Tendaguru, Tanzania, East Africa. *Journal of Mammalian Evolution*, *5*, 269–290.

Helgen, K. M., & Helgen, L. E. (2009). Biodiversity and Biogeography of the Moss-mice of New Guinea: A Taxonomic Revision of *Pseudohydromys* (Muridae: Murinae). *In* R. S. Voss, R. S., & Carleton, M. D., editors, *Systematic mammalogy: contributions in honor of Guy G. Musser*, pages 230–313. *Bulletin of the American Museum of Natural History 331*.

Helldin, J. O. (2000). Seasonal diet of pine marten *Martes martes* in southern boreal Sweden. *Acta Theriologica*, *45*, 409–420.

Hemming, C. F. (1972). The South Turkana Expedition: scientific papers. VIII. The ecology of South Turkana: a reconnaissance classification. *Geographical Journal, 138*, 15–40.

Henkel, S., & Krebs, B. (1977). Der erste Fund eines Säugetier-Skelettes aus der Jura-zeit. *Umschau in Wissenschaft und Technik*, *77*, 217–218.

Herring, S. W., & Herring, S. E. (1974). The superficial masseter and gape in mammals. *American Naturalist, 108*, 561–576.

Herring, S. W., & Scapino, R. P. (1973). Physiology of feeding in miniature pigs. *Journal of Morphology, 141*, 427–460.

Hicks, J. F., Fastovsky, D., Nichols, D. J. U., & Watabe, M. (2001). Magnetostratigraphic correlation of Late Cretaceous dinosaur-bearing localities in the Nemegt and Ulan Nuur basins, Gobi Desert, Mongolia. *Geological Society of America Program Abstracts A*, *323*.

Hiiemae, K. & Jenkins, F. A. (1969). The anatomy and internal architecture of the muscles of mastication in *Didelphis marsupialis*. *Postilla, 140*, 1–49.

Hockman, J. G., & Chapman, J. A. (1983). Comparative feeding habits of red foxes *Vulpes vulpes* and fray foxes *Urocyon cinereoargenteus* in Maryland. *American Midland Naturalist 110*, 276–285.

Homan, J. A., & Jones, J. K. (1975). *Monophyllus redmani*. *Mammalian Species*, *57*, 1–3.

Hoogland, J. L. (1996). *Cynomys ludovicianus*. *Mammalian Species*, *535*, 1–10.

Hu, Y. (1993). Two new genera of Anagalidae (Anagalida, Mammalia) from the Paleocene of Qianshan, Anhui and the phylogeny of anagalids. *Vertebrata PalAsiatica*, *31*, 153–182.

Hu, Y., Fox, R. C., Wang, Y., & Li, C. (2005A). A new spalacotheriid symmetrodont from the Early Cretaceous of northeastern China. *American Museum Novitates, 3475,* 1–20.

Hu, Y., Meng, J., Li, C., & Wang, Y. (2010). New basal eutherian mammal from the Early Cretaceous Jehol biota, Liaoning, China. *Proceedings of the Royal Society B*, *277*, 229–236.

Hu, Y., Meng, J., Wang, Y. & Li, C. (2005B). Large Mesozoic mammals fed on young dinosaurs. *Nature, 433*, 149–152.

Hu, Y., & Wang, Y. (2002). *Sinobaatar* gen. nov.: first multituberculate from the Jehol Biota of Liaoning, northeast China. *Chinese Science Bulletin*, *47*, 933–938.

Hu, Y., Wang, Y., Luo, Z.-X., & Li, C. (1997). A new symmetrodont mammal from China and its implications for mammalian evolution. *Nature*, *390*, 137–142.

Huang, X. S., & Zheng, J. J. (1999). A new tillodont from the Paleocene of Nanxiong Basin, Guangdong. *Vertebrata PalAsiatica*, *37*, 96–104.

Hunt, G. (2012). Measuring rates of phenotypic evolution and the inseparability of tempo and mode. *Paleobiology*, *38*, 351–373.

Hunter J. P. (1997). *Adaptive radiation of Early Paleocene ungulates*. PhD dissertation. State University of New York, Stony Brook.

Hunter, J. P., Hartman, J. H., & Krause, D. W. (1997). Mammals and mollusks across the Cretaceous-Tertiary boundary from Makoshika State Park and vicinity (Williston Basin), Montana. *Rocky Mountain Geology*, *32*, 61–114.

Hunter, J. P., & Jernvall, J. (1995). The hypocone as a key innovation in mammalian evolution. *Proceedings of the National Academy of Sciences*, *92*, 10718-10722.

Hurvich, C. M., & Tsai, C. L. (1989). Regression and time series model selection in small samples. *Biometrika*, *76*, 297–307.

Hylander, W. L. (1975). Incisor size and diet in anthropoids with special reference to Cercopithecidae. *Science*, *189*, 1095–1098.

Hylander, W. L. (2006). Functional anatomy and biomechanics of the masticatory apparatus. *In* Hylander, W. L., Laskin, J. L. & Greene, C. S., editors, *Temporomandibular disorders: an evidenced approach to diagnosis and treatment*, pages 3–34, Quintessence Publishing Company.

Iriarte-Diaz, J., Terhune, C. E., Taylor, A. B., & Ross, C. F. (2017). Functional correlates of the position of the axis of rotation of the mandible during chewing in non-human primates. *Zoology*, *124*, 106–118.

Jablonski, D. (1986). Background and mass extinctions: the alternation of macroevolutionary regimes. *Science*, *231*, 129–134.

Jackson, K. L., & Woolley, P. A. (1993). The diet of five species of New Guinean rodents. *Science in New Guinea*, *19*, 77–86.

Janis, C.M. (1988). An estimation of tooth volume and hypsodonty indices in ungulate mammals, and the correlation of these factors with dietary preferences. *In* Russell, D.E., Santoro, J.-P., Sigogneau-Russell, D., editors, *Teeth Revisited: Proceedings of the VIIth International Symposium on Dental Morphology, Paris, 1986*, pages 367–387. Me´moirs de Muse´e d'Histoire Naturelle, Paris, series C, Paris, France.

Janis, C. M. (1990). Correlation of cranial and dental variables with dietary preferences in mammals: a comparison of macropodoids and ungulates. *Memoirs of the Queensland Museum, 28*, 349–366.

Janis, C. M. (1995). Correlations between craniodental morphology and feeding behavior in ungulates: reciprocal illumination between living and fossil taxa. *In* Thomason, J. J., editor, *Functional Morphology in Vertebrate Paleontology*, pages 76–98. Cambridge University Press, Cambridge.

Janis, C. M. (2000). Patterns in the evolution of herbivory in large terrestrial mammals: the Paleogene of North America. In Sues, H.-D., editor, *Evolution of herbivory in terrestrial vertebrates,* pages 168–222. Cambridge University Press, Cambridge.

Jarvis, J. U., & Sherman, P. W. (2002). *Heterocephalus glaber*. *Mammalian Species*, *706*, 1–9.

Jenkins, F. A., Crompton, A. W. & Downs, W. R. (1983). Mesozoic mammals from Arizona: new evidence on mammalian evolution. *Science, 222*, 1233–1235.

Jenkins Jr, F. A., & Schaff, C. R. (1988). The Early Cretaceous mammal *Gobiconodon* (Mammalia, Triconodonta) from the Cloverly Formation in Montana. *Journal of Vertebrate Paleontology*, *8*, 1–24.

Jennings, M. R., & Rathbun, G. B. (2001). *Petrodromus tetradactylus*. *Mammalian Species*, *682*, 1–6.

Ji, Q., Luo, Z. X., Ji, S. A. (1999). A Chinese triconodont mammal and mosaic evolution of the mammalian skeleton. *Nature*, *398*, 326–330.

Ji, Q., Luo, Z. X., Yuan, C. X., & Tabrum, A. R. (2006). A swimming mammaliaform from the Middle Jurassic and ecomorphological diversification of early mammals. *Science*, *311*, 1123–1127.

Ji, Q., Luo, Z. X., Yuan, C. X., Wible, J. R., Zhang, J. P., & Georgi, J. A. (2002). The earliest known eutherian mammal. *Nature*, *416*, 816–822.

Ji, Q., Luo, Z. X., Zhang, X., Yuan, C. X. & Xu, L. (2009). Evolutionary development of the middle ear in Mesozoic therian mammals. *Science, 326*, 278–281.

Jiang, X., et al. (2011). Dinosaur-bearing strata and K/T boundary in the Luanchuan-Tantou Basin of western Henan Province, China. *Science China Earth Sciences*, *54*, 1149–1155.

Jones, K. E., et al. (2009). PanTHERIA: a species-level database of life history, ecology, and geography of extant and recently extinct mammals. *Ecology*, *90*, 2648–2648.

Jones, M. E., Rose, R. K., & Burnett, S. (2001). *Dasyurus maculatus*. *Mammalian Species*, *676*, 1–9.

Kallen, F. C., & Gans, C. (1972). Mastication in the little brown bat, *Myotis lucifugus*. *Journal of Morphology*, *136*, 385-420.

Kay, R. F. (1975). The functional adaptations of primate molar teeth. *American Journal of Physical Anthropology*, *43*, 195–215.

Kay, R. F. & Hiiemae, K. M. (1974). Jaw movement and tooth use in recent and fossil primates. *American Journal of Physical Anthropology, 40*, 227–256.

Kays, R. W. (1999). Food preferences of kinkajous (*Potos flavus*): a frugivorous carnivore. *Journal of mammalogy*, *80*, 589–599.

Kelly, T. S. (2014). Preliminary report on the mammals from Lane's Little Jaw Site Quarry: A latest Cretaceous (earliest Puercan?) local fauna, Hell Creek Formation, southeastern Montana. *Paludicola, 10*, 50–91.

Kerley, G. I. H. (1992). Trophic status of small mammals in the semi-arid Karoo, South Africa. *Journal of Zoology, 226*, 563–572.

Kielan-Jaworowska, Z., Cifelli, R. L., & Luo, Z. X. (2004). *Mammals from the age of dinosaurs: origins, evolution, and structure*. Columbia University Press, New York, NY.

Kielan-Jaworowska, Z. & Dashzeveg, D. (1989). Eutherian mammals from the Early Cretaceous of Mongolia. *Zoologica Scripta, 18*, 347–355.

Kielan-Jaworowska, Z., Eaton, J. G., & Bown, T. M. (1979). Theria of metatherian-eutherian grade. *In* Clemens, W. A., Kielan-Jaworowska, Z., & Lillegraven, J. A. *Mesozoic mammals: the first two-thirds of mammalian history*, pages 182–191. University of California Press, Berkeley.

Kimura, Y., Hawkins, M. T., McDonough, M. M., Jacobs, L. L., & Flynn, L. J. (2015). Corrected placement of *Mus-Rattus* fossil calibration forces precision in the molecular tree of rodents. *Scientific Reports*, *5,* 14444.

Kinzey, W. G., & Becker, M. (1983). Activity pattern of the masked titi monkey, *Callicebus personatus. Primates, 24*, 337–343.

Kirk, E. C., Lemelin, P., Hamrick, M. W., Boyer, D. M., & Bloch, J. I. (2008). Intrinsic hand proportions of euarchontans and other mammals: implications for the locomotor behavior of plesiadapiforms. *Journal of Human Evolution*, *55*, 278–299.

Klare, U., Kamler, J. F., & Macdonald, D. W. (2011). The bat-eared fox: a dietary specialist? *Mammalian Biology - Zeitschrift für Säugetierkunde, 76*, 646–650.

Koepfli, K. P., et al. (2008). Multigene phylogeny of the Mustelidae: resolving relationships, tempo and biogeographic history of a mammalian adaptive radiation. *BMC Biology*, *6*, 10.

Koontz, F. W. & Roeper, N. J. (1983). *Elephantulus rufescens*. *Mammalian Species*, *204*, 1–5.

Krause, D. W., & Gingerich, P. D. (1983). Mammalian fauna from Douglass Quarry, earliest Tiffanian (late Paleocene) of the eastern Crazy Mountain Basin, Montana. *Contributions from the Museum of Paleontology, The University of Michigan, 26*, 157-196.

Krause, D. W., et al. (2014). First cranial remains of a gondwanatherian mammal reveal remarkable mosaicism. *Nature*, *515*, 512–517.

Krebs, B. (1991). Das Skelett von Henkelotherium guimarotae gen. et sp. nov.(Eupantotheria, Mammalia) aus dem Oberen Jura von Portugal. *Selbstverlag Fachbereich Geowissenschaften, 133,* 1–110.

Krebs, B. (1993). Das Gebiss von Crusafontia (Eupantotheria, Mammalia)–Funde aus der Unter−Kreide von Galve und Uña (Spanien). *Berliner geowissenschaftliche Abhandlungen E*, *9*, 233–252.

Kunz, T. H. (1974). Feeding ecology of a temperate insectivorous bat (*Myotis velifer). Ecology*, *55*, 693–711.

Kusuhashi, N., Tsutsumi, Y., Saegusa, H., Horie, K., Ikeda, T., Yokoyama, K., & Shiraishi, K. (2013). A new Early Cretaceous eutherian mammal from the Sasayama Group, Hyogo, Japan. *Proceedings of the Royal Society B*, *280*, 20130142.

Labandeira, C. C., Johnson, K. R., & Wilf, P. (2002). Impact of the terminal Cretaceous event on plant–insect associations. *Proceedings of the National Academy of Sciences*, *99*, 2061–2066.

Labandeira, C. C., & Sepkoski, J. J. 1993 Insect diversity in the fossil record. *Science, 261*, 310–315.

Lack, J. B., & Van Den Bussche, R. A. (2010). Identifying the confounding factors in resolving phylogenetic relationships in Vespertilionidae. *Journal of Mammalogy*, *91*, 1435–1448.

Langham, N. (1983). Distribution and ecology of small mammals in three rain forest localities of Peninsula Malaysia with particular references to Kedah Peak. *Biotropica, 15*, 199–206.

Larivière, S., & Calzada, J. (2001). *Genetta genetta*. *Mammalian Species*, *680*, 1–6.

Lautenschlager, S., Gill, P., Luo, Z. X., Fagan, M. J., & Rayfield, E. J. (2017). Morphological evolution of the mammalian jaw adductor complex. *Biological Reviews*, *92*, 1910-1940.

Law, C. J., Young, C., & Mehta, R. S. (2016). Ontogenetic scaling of theoretical bite force in southern sea otters (*Enhydra lutris nereis*). *Physiological and Biochemical Zoology*, *89*, 347–363.

Lazagabaster, I. A., Rowan, J., Kamilar, J. M., & Reed, K. E. (2016). Evolution of craniodental correlates of diet in African Bovidae. *Journal of Mammalian Evolution*, *23*, 385–396.

Leirs, H., Verhagen, R., Verheyen, W., & Perrin, M. R. (1995). The biology of *Elephantulus brachyrhynchus* in natural miombo woodland in Tanzania. *Mammal Review, 25*, 45–49.

Leite, Y. L. R., Costa, L. P., & Stallings, J. R. (1996). Diet and vertical space use of three sympatric opossums in a Brazilian Atlantic forest reserve. *Journal of Tropical Ecology, 12*, 435–440.

Lidgard, S., & Crane, P. R. (1988). Quantitative analyses of the early angiosperm radiation. *Nature*, *331*, 344–346.

Lieberman, D. E., & Crompton, A. W. (2000). Why fuse the mandibular symphysis? A comparative analysis. *American Journal of Physical Anthropology*, *112*, 517–540.

Lillegraven, J. A., & Krusat, G. (1991). Cranio-mandibular anatomy of *Haldanodon exspectatus* (Docodonta; Mammalia) from the Late Jurassic of Portugal and its implications to the evolution of mammalian characters. *Rocky Mountain Geology*, *28*, 39–138.

Lima, E. M., & Ferrari, S. F. (2003). Diet of a free-ranging group of squirrel monkeys (*Saimiri sciureus*) in eastern Brazilian Amazonia. *Folia Primatologica, 74*(3), 150–158.

Liow, L. H. (2004). A test of Simpson's "rule of the survival of the relatively unspecialized" using fossil crinoids. *The American Naturalist*, *164*, 431-443.

Lloyd, G. T. (2012). A refined modelling approach to assess the influence of sampling on palaeobiodiversity curves: new support for declining Cretaceous dinosaur richness. *Biology Letters, 81,* 123–126.

Lloyd, G. T., et al. (2008). Dinosaurs and the Cretaceous terrestrial revolution. *Proceedings of the Royal Society B, 275*, 2483–2490.

Long, C. A. (1974). *Microsorex hoyi* and *Microsorex thompsoni*. *Mammalian Species*, *33*, 1–4.

Lopatin, A. V. (2006). Early Paleogene insectivore mammals of Asia and establishment of the major groups of Insectivora. *Paleontological Journal, 40*, S205–S405.

Lopatin, A. V., Maschenko, E. N., Averianov, A. O., Rezvyi, A. S., Skutschas, P. P., & Leshchinskiy, S. V. (2005). Early Cretaceous mammals from Western Siberia: 1. Tinodontidae. *Paleontological Journal*, *39*, 523-534.

Lucas, P., Constantino, P., Wood, B., & Lawn, B. (2008). Dental enamel as a dietary indicator in mammals. *BioEssays*, *30*, 374–385.

Lucas, P. W., et al. (2009). Indentation as a technique to assess the mechanical properties of fallback foods. *American Journal of Physical Anthropology*, *140*, 643–652.

Luo, Z. X. (2007). Transformation and diversification in early mammal evolution. *Nature, 450*, 1011–1019.

Luo, Z. X. (2011). Developmental patterns in Mesozoic evolution of mammal ears. *Annual Review of Ecology, Evolution, and Systematics, 42*, 355–380.

Luo, Z. X., Chen, P., Li, G. & Chen, M. (2007A). A new eutriconodont mammal and evolutionary development in early mammals. *Nature, 446*, 288–293.

Luo, Z. X., Crompton, A. W., & Sun, A. L. (2001). A new mammaliaform from the early Jurassic and evolution of mammalian characteristics. *Science*, *292*, 1535–1540.

Luo, Z. X., Gatesy, S. M., Jenkins, F. A., Amaral, W. W., & Shubin, N. H. (2015A). Mandibular and dental characteristics of Late Triassic mammaliaform Haramiyavia and their ramifications for basal mammal evolution. *Proceedings of the National Academy of Sciences*, *112*, E7101–E7109.

Luo, Z. X., Ji, Q., Wible, J. R., & Yuan, C. X. (2003). An Early Cretaceous tribosphenic mammal and metatherian evolution. *Science*, *302*, 1934–1940.

Luo, Z. X., Ji, Q., & Yuan, C. X. (2007B). Convergent dental adaptations in pseudo-tribosphenic and tribosphenic mammals. *Nature*, *450*, 93–97.

Luo, Z. X., Kielan-Jaworowska, Z. & Cifelli, R. L. (2002). In quest for a phylogeny of Mesozoic mammals. *Acta Palaeontologica Polonica, 47*, 1–78.

Luo, Z. X., Kielan-Jaworowska, Z., & Cifelli, R. L. (2004). Evolution of dental replacement in mammals. *Bulletin of Carnegie Museum of Natural History, 36*, 159–175.

Luo, Z. X., & Martin, T. (2007). Analysis of molar structure and phylogeny of docodont genera. *Bulletin of Carnegie Museum of Natural History*, 27–47.

Luo, Z. X., Meng, Q. J., Ji, Q., Liu, D., Zhang, Y. G., & Neander, A. I. (2015B). Evolutionary development in basal mammaliaforms as revealed by a docodontan. *Science*, *347*, 760–764.

Luo, Z. X., & Wible, J. R. (2005). A Late Jurassic digging mammal and early mammalian diversification. *Science*, *308*, 103–107.

Luo, Z. X., Yuan, C. X., Meng, Q. J. & Ji, Q. (2011) A Jurassic eutherian mammal and divergence of marsupials and placentals. *Nature, 476*, 442–445.

Lupia, R., Lidgard, S., & Crane, P. R. (1999). Comparing Palynological Abundance and Diversity: Implications for Biotic Replacement during the Cretaceous Angiosperm Radiation. *Paleobiology, 25*, 305–340.

MacIntyre, G. T. (1966). The Miacidae (Mammalia, Carnivora). Part 1. The systematics of *Ictidopappus* and *Protictis*. *Bulletin of the American Museum of Natural History, 131,* 115–210.

Maestri, R., Monteiro, L. R., Fornel, R., Upham, N. S., Patterson, B. D., & Freitas, T. R. O. (2017). The ecology of a continental evolutionary radiation: Is the radiation of sigmodontine rodents adaptive?. *Evolution*, *71*, 610–632.

Maestri, R., Patterson, B. D., Fornel, R., Monteiro, L. R., & Freitas, T. R. O. (2016). Diet, bite force and skull morphology in the generalist rodent morphotype. *Journal of Evolutionary Biology, 29*, 2191–2204.

Marshall, L. G. (1978). *Dromiciops australis*. *Mammalian Species*, *99*, 1–5.

Marshall, L. G., & De Muizon, C. (1995). Part II. The skull. *Pucadelphys andinus*, *165*, 21–90.

Martin, T. (1999). Dryolestidae (Dryolestoidea, Mammalia) aus dem Oberen Jura von Portugal. *Abhandlungen der Senckenbergischen Naturforschenden Gesellschaft, 550*, 1–119.

Martin, T., Buffetaut, E., & Tong, H. (2015). A Late Cretaceous eutherian mammal from southwestern France. *Paläontologische Zeitschrift*, *89*, 535-544.

Martin, T., Marugán-Lobón, J., Vullo, R., Martín-Abad, H., Luo, Z. X., & Buscalioni, A. D. (2015). A Cretaceous eutriconodont and integument evolution in early mammals. *Nature, 526*, 380–384.

Matthew, W. D. (1937). Paleocene faunas of the San Juan Basin, New Mexico. *American Philosophical Society, 30,* 1–510.

Maynard Smith, J. & Savage, R. J. G. (1959). The mechanics of mammalian jaws. *School Science Review, 141*, 289–301.

McKenna, D. D., Sequeira, A. S., Marvaldi, A. E., & Farrell, B. D. (2011). Temporal lags and overlap in the diversification of weevils and flowering plants: recent advances and prospects for additional resolution. *American Entomologist*, *57*, 54–55.

McKenna, M. C. (1975). Toward a phylogenetic classification of the Mammalia. *In* Luckett, W. P., & Szalay, F. S., editors, *Phylogeny of the Primates*, pages 21–46. Plenum Press, New York.

McKenna, M. C., Xue, X., & Zhou, M. (1984). *Prosarcodon lonanensis*, a new Paleocene micropternodontid palaeoryctoid insectivore from Asia. *American Museum Novitates*, *2780*, 1–17.

McNab, B. K. (1995). Energy expenditure and conservation in frugivorous and mixed-diet carnivorans. *Journal of Mammalogy, 76*, 206–222.

Meehan, T. J., & Wilson, R. W. (2002). New viverravids from the Torrejonian (middle Paleocene) of Kutz Canyon, New Mexico and the oldest skull of the Order Carnivora. *Journal of Paleontology*, *76*, 1091–1101.

Mellett, J. S. (1984). Autocclusal mechanisms in the carnivore dentition. *Australian Mammalogy, 8*, 233–238.

Meloro, C. (2011). Feeding habits of Plio-Pleistocene large carnivores as revealed by the mandibular geometry. *Journal of Vertebrate Paleontology*, *31*, 428–446.

Mendoza, M., Janis, C. M., & Palmqvist, P. (2002). Characterizing complex craniodental patterns related to feeding behaviour in ungulates: a multivariate approach. *Journal of Zoology*, *258*, 223–246.

Menegaz, R. A., Baier, D. B., Metzger, K. A., Herring, S. W. & Brainerd, E. L. (2015). XROMM analysis of tooth occlusion and temporomandibular joint kinematics during feeding in juvenile miniature pigs. *Journal of Experimental Biology, 218*, 2573–2584.

Meng, J., Hu, Y., Wang, Y. & Li, C. (2003). The ossified Meckel's cartilage and internal groove in Mesozoic mammaliaforms: implications to origin of the definitive mammalian middle ear. *Zoological Journal of the Linnean Society, 138*, 431–448.

Meng, J., Hu, Y., Wang, Y., Wang, X., & Li, C. (2006). A Mesozoic gliding mammal from northeastern China. *Nature*, *444*, 889–893.

Meng, J., Wang, Y., & Li, C. (2011). Transitional mammalian middle ear from a new Cretaceous Jehol eutriconodont. *Nature*, *472*, 181–185.

Meng, Q. J., Grossnickle, D. M., Liu, D., Zhang, Y. G., Neander, A. I., Ji, Q., & Luo, Z. X. (2017). New gliding mammaliaforms from the Jurassic. *Nature*, *548*, 291–296.

Meng, Q. J., Ji, Q., Zhang, Y. G., Liu, D., Grossnickle, D. M., & Luo, Z. X. (2015). An arboreal docodont from the Jurassic and mammaliaform ecological diversification. *Science*, *347*, 764–768.

Meredith, R. W., et al. (2011). Impacts of the Cretaceous Terrestrial Revolution and KPg extinction on mammal diversification. *Science*, *334*, 521–524.

Meredith, R. W., Westerman, M., Case, J. A., & Springer, M. S. (2008). A phylogeny and timescale for marsupial evolution based on sequences for five nuclear genes. *Journal of Mammalian Evolution, 15*, 1–36.

Meserve, P. L. (1981). Trophic Relationships among small mammals in a Chilean semiarid thorn scrub community. *Journal of Mammalogy, 62*, 304–314.

Meserve, P. L., Lang, B. K., & Patterson, B. D. (1988). Trophic relationships of small mammals in a Chilean temperate rainforest. *Journal of Mammalogy, 69*, 721–730.

Meserve, P. L., Martin, R. E., & Rodriguez, J. (1983). Feeding ecology of two Chilean caviomorphs in a central Mediterranean savanna. *Journal of Mammalogy, 64*, 322–325.

Mills, J. R. E. (1966). The functional occlusion of the teeth of Insectivora. *Zoological Journal of the Linnean Society, 46*, 1–25.

Mills, J. R. E. (1967). A comparison of lateral jaw movements in some mammals from wear facets on the teeth. *Archives of Oral Biology, 12*, 645–661.

Mitchell, J. S. (2015). Extant-only comparative methods fail to recover the disparity preserved in the bird fossil record. *Evolution*, *69*, 2414–2424.

Mitchell, J. S., & Makovicky, P. J. (2014). Low ecological disparity in Early Cretaceous birds. *Proceedings of the Royal Society B, 281*, 20140608.

Mitchell, J. S., Roopnarine, P. D., & Angielczyk, K. D. (2012). Late Cretaceous restructuring of terrestrial communities facilitated the end-Cretaceous mass extinction in North America. *Proceedings of the National Academy of Sciences, 109*, 18857–18861.

Mitchell, K. J., et al. (2014). Molecular phylogeny, biogeography, and habitat preference evolution of marsupials. *Molecular Biology and Evolution*, *31*, 2322–2330.

Mittermeier, R. A., et al. (2007). Primates in peril: the world's 25 most endangered primates, 2006–2008. *Primate Conservation*, *22*, 1–40.

Moczek, A. P., et al. (2011). The role of developmental plasticity in evolutionary innovation. *Proceedings of the Royal Society B*, *278*, 2705–2713.

Monadjem, A. (1997). Stomach contents of 19 species of small mammals from Swaziland. *South African Journal of Zoology, 32*, 23–26.

Monteiro, L. R., & Nogueira, M. R. (2011). Evolutionary patterns and processes in the radiation of phyllostomid bats. *BMC Evolutionary Biology*, *11*, 137.

Montellano-Ballesteros, M., & Fox, R. C. (2015). A new tribotherian (Mammalia, Boreosphenida) from the late Santonian to early Campanian upper Milk River Formation, Alberta. *Canadian Journal of Earth Sciences*, *52*, 77–83.

Montellano-Ballesteros, M., Fox, R. C., & Scott, C. S. (2013). Species composition of the Late Cretaceous eutherian mammal *Paranyctoides* Fox. *Canadian Journal of Earth Sciences*, *50*, 693–700.

Murphy, W. J., Eizirik, E., Johnson, W. E., Zhang, Y. P., Ryder, O. A., & O'brien, S. J. (2001). Molecular phylogenetics and the origins of placental mammals. *Nature*, *409*, 614-618.

Myers, P., Espinosa, R., Parr, C. S., Jones, T., Hammond, G. S., and Dewey, T. A. (2017). The Animal Diversity Web (online). Accessed at http://animaldiversity.org.

Nabavizadeh, A. (2016). Evolutionary trends in the jaw adductor mechanics of ornithischian dinosaurs. *The Anatomical Record*, *299*, 271–294.

Newham, E., Benson, R., Upchurch, P., & Goswami, A. (2014). Mesozoic mammaliaform diversity: The effect of sampling corrections on reconstructions of evolutionary dynamics. *Palaeogeography, Palaeoclimatology, Palaeoecology*, *412*, 32–44.

Newsome, A., Corbett, L., Catling, P., & Burt, R. (1983). The feeding ecology of the dingo. 1. Stomach contents from trapping in south-eastern Australia, and the non-target wildlife also caught in dingo traps. *Wildlife Research, 10*, 477–486.

Niemitz, C. (1979). Results of a field study on the western tarsier (*Tarsius bancanus borneanus* Horsfield, 1821) in Sarawak. *Sarawak Museum Journal, 27*, 171–228.

Nogueira, M. R., Peracchi, A. L., & Monteiro, L. R. (2009). Morphological correlates of bite force and diet in the skull and mandible of phyllostomid bats. *Functional Ecology*, *23*, 715–723.

Norconk, M. A. (1996). Seasonal variation in the diets of white-faced and bearded sakis (*Pithecia pithecia* and *Chiropotes satanas*) in Guri Lake, Venezuela. *In* M. A. Norconk, A. L. Rosenberger, & P. A. Garber, editors, *Adaptive radiations of Neotropical primates,* pages 403–423. Plenum Press, New York.

Novacek, M. J., Rougier, G. W., Wible, J. R., McKenna, M. C., Dashzeveg, D., & Horovitz, I. (1997). Epipubic bones in eutherian mammals from the Late Cretaceous of Mongolia. *Nature*, *389*, 483–486.

O'Leary, M. A., et al. (2013). The placental mammal ancestor and the post–K-Pg radiation of placentals. *Science*, *339*, 662–667.

O'Leary, M. A., Lucas, S. G., & Williamson, T. E. (2000). A new specimen of *Ankalagon* (Mammalia, Mesonychia) and evidence of sexual dimorphism in mesonychians. *Journal of Vertebrate Paleontology*, *20*, 387–393.

O'Meara, R. N., & Thompson, R. S. (2014). Were there miocene meridiolestidans? Assessing the phylogenetic placement of necrolestes patagonensis and the presence of a 40 million year meridiolestidan ghost lineage. *Journal of Mammalian Evolution*, *21*, 271–284.

O'Shea, T. J. (1991). *Xerus rutilus*. *Mammalian Species*, *370*, 1–5.

Olds, N., & Shoshani, J. (1982). *Procavia capensis*. *Mammalian Species*, *171*, 1–7.

Olsen, A. M. (2017). Feeding ecology is the primary driver of beak shape diversification in waterfowl. *Functional Ecology, 31*, 1985–1995.

Oprea, M., & Wilson, D. E. (2009). *Chiroderma doriae* (Chiroptera: Phyllostomidae). *Mammalian Species*, *816*, 1–7.

Oron, U. & Crompton, A. W. (1985). A cineradiographic and electromyographic study of mastication in Tenrec ecaudatus. *Journal of Morphology, 185,* 155–182.

Osborn, H. F. (1902). The law of adaptive radiation. *American Naturalist, 36*, 353–363.

Osborn, H. F. (1907). *Evolution of Mammalian Molar Teeth*. Macmillan, New York.

Osborn, H. F. (1929). The titanotheres of ancient Wyoming, Dakota, and Nebraska. Volumes I and II. *United States Geological Survey Monograph, 55*, 1–953.

Otálora-Ardila, A., Flores-Martínez, J. J., & Voigt, C. C. (2013). Marine and terrestrial food sources in the diet of the fish-eating myotis (*Myotis vivesi*). *Journal of Mammalogy, 94*, 1102–1110.

Pahl, L. I. (1987). Feeding-Behavior and Diet of the Common Ringtail Possum, *Pseudocheirus peregrinus*, in Eucalyptus Woodlands and *Leptospermum* Thickets in Southern Victoria. *Australian Journal of Zoology, 35*, 487–506.

Panciroli, E., Janis, C., Stockdale, M., & Martín-Serra, A. (2017). Correlates between calcaneal morphology and locomotion in extant and extinct carnivorous mammals. *Journal of Morphology, 278*, 1333–1353.

Paradis, E., Claude, J., & Strimmer, K. (2004). APE: analyses of phylogenetics and evolution in R language. *Bioinformatics*, *20*, 289–290.

Patterson, B. (1956). Early Cretaceous mammals and the evolution of mammalian molar teeth. *Fieldiana: Geology, 13*, 1–105.

Patterson, B. D., & Gallardo, M. H. (1987). *Rhyncholestes raphanurus*. *Mammalian Species*, *286*, 1–5.

Patterson, B. D., & Upham, N. S. (2014). A newly recognized family from the Horn of Africa, the Heterocephalidae (Rodentia: Ctenohystrica). *Zoological Journal of the Linnean Society, 172*, 942–963.

Patzkowsky, M. E. (1995). A hierarchical branching model of evolutionary radiations. *Paleobiology, 21*, 440–460.

Pavey, C. R., & Burwell, C. J. (1997). The diet of the diadem leaf-nosed bat *Hipposideros diadema*: confirmation of a morphologically-based prediction of carnivory. *Journal of Zoology*, *243*, 295–303.

Pennell, M. W., et al. (2014). geiger v2.0: an expanded suite of methods for fitting macroevolutionary models to phylogenetic trees. *Bioinformatics*, *30*, 2216–2218.

Peter, S. E., & Foote, M. (2001). Biodiversity in the Phanerozoic: a reinterpretation. *Paleobiology, 27*, 583–601.

Perrin, M. R., Dempster, E. R, & Downs, C. T. (1999). *Gerbillurus paeba*. *Mammalian Species*, *606*, 1–6.

Perrin, M. R., & Fielden, L. J. (1999). *Eremitalpa granti*. *Mammalian Species*, *629*, 1–4.

Petchey, O. L., & Gaston, K. J. (2006). Functional diversity: back to basics and looking forward. *Ecology letters*, *9*, 741–758.

Pfretzschner, H. U., Martin, T., Matzke, A. T., & Sun, G. (2005). A new docodont mammal from the Late Jurassic of the Junggar Basin in Northwest China. *Acta Palaeontologica Polonica, 50*, 799–808.

Pineda-Munoz, S., & Alroy, J. (2014). Dietary characterization of terrestrial mammals. *Proceedings of the Royal Society B*, *281*, 20141173.

Pineda-Munoz, S., Evans, A. R., & Alroy, J. (2016). The relationship between diet and body mass in terrestrial mammals. *Paleobiology*, *42*, 659–669.

Pineda-Munoz, S., Lazagabaster, I. A., Alroy, J., & Evans, A. R. (2017). Inferring diet from dental morphology in terrestrial mammals. *Methods in Ecology and Evolution*, *8*, 481–491.

Pinheiro, J., Bates, D., DebRoy, S., & Sarkar, D. (2016). nlme: linear and nonlinear mixed effects models. R package, version 3.1-128. http://CRAN.R-project.org/package=nlme.

Platt, R. N., Amman, B. R., Keith, M. S., Thompson, C. W., & Bradley, R. D. (2015). What Is *Peromyscus*? Evidence from nuclear and mitochondrial DNA sequences suggests the need for a new classification. *Journal of Mammalogy*, *96*, 708–719.

Polly, P. D., et al. (2011). History matters: ecometrics and integrative climate change biology. *Proceedings of the Royal Society B*, *278,* 1131–1140.

Polly, P. D. (2016). *Geometric morphometrics for Mathematica, version 12.0*. Department of Geological Sciences, Indiana University, Bloomington, IN.

Polly, P. D., Le Comber, S. C. & Burland, T. M. (2005). On the occlusal fit of tribosphenic molars: Are we underestimating species diversity in the Mesozoic? *Journal of Mammalian Evolution, 12*, 283–299.

Prasad, G. V. R., Verma, O., Sahni, A., Parmar, V., & Khosla, A. (2007). A Cretaceous hoofed mammal from India. *Science*, *318*, 937–937.

Price, S. A., & Hopkins, S. S. (2015). The macroevolutionary relationship between diet and body mass across mammals. *Biological Journal of the Linnean Society*, *115*, 173–184.

Price, S. A., Hopkins, S. S., Smith, K. K., & Roth, V. L. (2012). Tempo of trophic evolution and its impact on mammalian diversification. *Proceedings of the National Academy of Sciences, 109*, 7008–7012.

Prothero, D. R. (1981). New jurassic mammals from Como Bluff, Wyoming and the interrelationships of nontribosphenic Theria. *Bulletin of the American Museum of Natural History, 57*, 1040–1046.

Purnell, M. A., Crumpton, N., Gill, P. G., Jones, G., & Rayfield, E. J. (2013). Within-guild dietary discrimination from 3-D textural analysis of tooth microwear in insectivorous mammals. *Journal of Zoology*, *291*, 249–257.

R Core Team (2016). R: A language and environment for statistical computing. R Foundation for Statistical Computing, Vienna, Austria. https://www.R-project.org/.

Radinsky, L. B. (1968). A new approach to mammalian cranial analysis, illustrated by examples of prosimian primates. *Journal of Morphology*, *124*, 167–179.

Radinsky, L. B. (1981). Evolution of skull shape in carnivores: 1. Representative modern carnivores. *Biological journal of the Linnean society*, *15*, 369–388.

Ram, Y., & Ross, C. F. (2018). Evaluating the triplet hypothesis during rhythmic mastication in primates. *Journal of Experimental Biology*, *221*, jeb165985.

Ramírez-Chaves, H. E., Weisbecker, V., Wroe, S., & Phillips, M. J. (2016). Resolving the evolution of the mammalian middle ear using Bayesian inference. *Frontiers in Zoology, 13*, 39.

Rathbun, G. B. (1976). The ecology and social structure of the elephant-shrews *Rhynchocyon chrysopygus* Günther and *Elephantulus rufescens* Peters. PhD dissertation, University of Nairobi, Kenya.

Rauhut, O. W., Martin, T., Ortiz-Jaureguizar, E., & Puerta, P. (2002). A Jurassic mammal from South America. *Nature, 416*, 165–168.

Raup, D. M., & Gould, S. J. (1974). Stochastic simulation and evolution of morphology-towards a nomothetic paleontology. *Systematic Zoology, 23*, 305–322.

Redman, C. M., & Leighton, L. R. (2009). Multivariate faunal analyses of the Turonian Bissekty Formation: Variation in the degree of marine influence in temporally and spatially averaged fossil assemblages. *Palaios*, *24*, 18–26.

Reed, D. A., Iriarte-Diaz, J. & Diekwisch, T. G. H. (2016). A three dimensional free body analysis describing variation in the musculoskeletal configuration of the cynodont lower jaw. *Evolution & Development, 18*, 41–53.

Reichman, O. J. (1975). Relation of desert rodent diets to available resources. *Journal of Mammalogy*, *56*, 731–751.

Renne, P. R., et al. (2013). Time scales of critical events around the Cretaceous-Paleogene boundary. *Science*, *339*, 684–687.

Revell, L. J. (2010). Phylogenetic signal and linear regression on species data. *Methods in Ecology and Evolution*, *1*, 319–329.

Revell, L. J. (2012). phytools: an R package for phylogenetic comparative biology (and other things). *Methods in Ecology and Evolution*, *3*, 217–223.

Rich, T. H., Flannery, T. F., Trusler, P., Kool, L., Van Klaureren, N. A., & Vickers-Rich, P. (2001). A second tribosphenic mammal from the Mesozoic of Australia. *Records of the Queen Victoria Museum*, *110*, 1–9.

Rich, T. H., Flannery, T. F., Trusler, P., Kool, L., Van Klaveren, N. A., & Vickers-Rich, P. (2002). Evidence that monotremes and ausktribosphenids are not sistergroups. *Journal of Vertebrate Paleontology, 2*, 466–469.

Rich, T. H., Hopson, J. A., Gill, P. G., Trusler, P., Rogers-Davidson, S., Morton, S., Cifelli, R. L., Pickering, D., Kool, L., Siu, K. & Burgmann, F.A. (2016). The mandible and dentition of the Early Cretaceous monotreme *Teinolophos trusleri*. *Alcheringa: An Australasian Journal of Palaeontology*, 1–27.

Rich, T. H., Vickers-Rich, P., Constantine, A., Flannery, T. F., Kool, L., & van Klaveren, N. (1997). A tribosphenic mammal from the Mesozoic of Australia. *Science*, *278*, 1438–1442.

Rabosky, D. L. (2014). Automatic detection of key innovations, rate shifts, and diversity-dependence on phylogenetic trees. *PloS One*, *9*, e89543.

Rabosky, D. L. (2017). Phylogenetic tests for evolutionary innovation: the problematic link between key innovations and exceptional diversification. *Philosophical Transactions of the Royal Society B*, *372*, 20160417.

Rohlf, F. J. & Marcus, L. F. (1993). A revolution in morphometrics. *Trends in Ecology & Evolution, 8*, 129–132.

Rohlf, F. J. & Slice, D. (1990). Extensions of the Procrustes method for the optimal superimposition of landmarks. *Systematic Biology, 39*, 40–59.

Rook, D. L., Hunter, J. P., Pearson, D. A., & Bercovici, A. (2010). Lower jaw of the Early Paleocene mammal *Alveugena* and its interpretation as a transitional fossil. *Journal of Paleontology*, *84*, 1217–1225.

Rose, K. D. (2006). *The beginning of the age of mammals*. Johns Hopkins University Press, Baltimore.

Rosi, M. I., Cona, M. I., Roig, V. G., Massarini, A. I., & Verzi, D. H. (2005). *Ctenomys mendocinus*. *Mammalian Species*, *777*, 1–6.

Ross, C. F., Iriarte-Diaz, J., & Nunn, C. L. (2012). Innovative approaches to the relationship between diet and mandibular morphology in primates. *International Journal of Primatology, 33*, 632–660.

Rougier, G. W. (1993). *Vincelestes neuquenianus* Bonaparte (Mammalia, Theria) un primitivo mamífero del Cretácico Inferior de la Cuenca Neuquina. PhD dissertation.

Rougier, G. W., Apesteguía, S., & Gaetano, L. C. (2011). Highly specialized mammalian skulls from the Late Cretaceous of South America. *Nature*, *479*, 98–102.

Rougier, G. W., Davis, B. M., & Novacek, M. J. (2015A). A deltatheroidan mammal from the Upper Cretaceous Baynshiree Formation, eastern Mongolia. *Cretaceous Research*, *52*, 167-177.

Rougier, G. W., Martinelli, A. G., Forasiepi, A. M., & Novacek, M. J. (2007). New Jurassic mammals from Patagonia, Argentina: a reappraisal of australosphenidan morphology and interrelationships. *American Museum Novitates, 3566*, 1–54.

Rougier, G. W., Sheth, A. S., Carpenter, K., Appella-Guiscafre, L., & Davis, B. M. (2015B). A new species of *Docodon* (Mammaliaformes: Docodonta) from the Upper Jurassic Morrison Formation and a reassessment of selected craniodental characters in basal mammaliaforms. *Journal of Mammalian Evolution, 22*, 1–16.

Rougier, G. W., Wible, J. R., Beck, R. M., & Apesteguía, S. (2012). The Miocene mammal Necrolestes demonstrates the survival of a Mesozoic nontherian lineage into the late Cenozoic of South America. *Proceedings of the National Academy of Sciences, 109*, 20053–20058.

Rougier, G. W., Wible, J. R., & Novacek, M. J. (1998). Implications of *Deltatheridium* specimens for early marsupial history. *Nature*, *396*, 459.

Ruedi, M., et al. (2013). Molecular phylogenetic reconstructions identify East Asia as the cradle for the evolution of the cosmopolitan genus *Myotis* (Mammalia, Chiroptera). *Molecular Phylogenetics and Evolution*, *69*, 437–449.

Ruiz-Olmo, J., & López-Martín, J. M. (1996). Seasonal food of pine marten (*Martes martes* L., 1758) in a fir forest of Pyrenean mountains Northeastern Spain. *In* Mathias, M. L., Santos-Reis, M., Amori, G., Libois, R., Mitchell-Jones, A., & Saint-Girons, M.C., editors, *Proceedings of the 1st European Congress of Mammalogy*, pages 189–196. Lisbon, Portuga.

Ryder, J. A. (1878). On the mechanical genesis of tooth-forms. *Proceedings of the Academy of Natural Sciences of Philadelphia, 30*, 45–80.

Saarinen, J. J., et al. (2014). Patterns of maximum body size evolution in Cenozoic land mammals: eco-evolutionary processes and abiotic forcing. *Proceedings of the Royal Society B, 281*, 20132049.

Samuels, J. X. (2009). Cranial morphology and dietary habits of rodents. *Zoological Journal of the Linnean Society*, *156*, 864–888.

Santana, S. E., & Cheung, E. (2016). Go big or go fish: morphological specializations in carnivorous bats. *Proceedings of the Royal Society B*, *283*, 20160615.

Santos, M., Aguirre, L. F., Vázquez, L. B., & Ortega, J. (2003). *Phyllostomus hastatus. Mammalian Species, 722*, 1–6.

Sato, J. J., et al. (2016). Molecular phylogenetic analysis of nuclear genes suggests a Cenozoic over-water dispersal origin for the Cuban *Solenodon*. *Scientific Reports*, *6*, 31173.

Sato, Y., Mano, T., & Takatsuki, S. (2005). Stomach contents of brown bears *Ursus arctos* in Hokkaido, Japan. *Wildlife Biology, 11*, 133–144.

Scapino, R. (1981). Morphological investigation into functions of the jaw symphysis in carnivorans. *Journal of Morphology*, *167*, 339–375.

Schluter, D. (2000). *The ecology of adaptive radiation*. Oxford University Press, Oxford.

Schmidly, D. J. (1974). *Peromyscus attwateri*. *Mammalian Species, 48*, 1–3.

Schneider, C. A., Rasband, W. S., & Eliceiri, K. W. (2012). NIH Image to ImageJ: 25 years of image analysis. *Nature Methods*, *9*, 671–675.

Schoch, R. M. (1981). Taxonomy and Biostratigraphy of the Early Tertiary Taeniodonta (Mammalia: Eutheria). *Geological Society of America Bulletin*, *92*, 1982–2267.

Schoch, R. M., & Lucas, S. G. (1981). New conoryctines (Mammalia: Taeniodonta) from the Middle Paleocene (Torrejonian) of western North America. *Journal of Mammalogy*, *62*, 683–691.

Scott, W. B., & Jepsen, G. L. (1936). The mammalian fauna of the White River Oligocene: Part I. Insectivora and Carnivora. *Transactions of the American Philosophical Society*, *28*, 1–153.

Schultz, J. A. & Martin, T. (2011). Wear pattern and functional morphology of dryolestoid molars (Mammalia, Cladotheria). *Paläontologische Zeitschrift*, *85*, 269–285.

Schultz, J. A. & Martin, T. (2014). Function of pretribosphenic and tribosphenic mammalian molars inferred from 3D animation. *Naturwissenschaften, 101*, 771–781.

Scott, C. S. (2010). New cyriacotheriid pantodonts (Mammalia, Pantodonta) from the Paleocene of Alberta, Canada, and the relationships of Cyriacotheriidae. *Journal of Paleontology*, *84*, 197–215.

Scott, C. S., & Fox, R. C. (2005). Windows on the evolution of *Picrodus* (Plesiadapiformes: Primates): Morphology and relationships of a species complex from the Paleocene of Alberta. *Journal of Paleontology*, *79*, 635–657.

Scott, C. S., Fox, R. C., & Youzwyshyn, G. P. (2002). New earliest Tiffanian (late Paleocene) mammals from Cochrane 2, southwestern Alberta, Canada. *Acta Palaeontologica Polonica*, *47*, 691–704.

Scott, C. S., & Gardner, J. D. (2013). Summary of fossil vertebrate taxa named by Richard C. Fox, with an annotated list of taxa named between 1962 and 2012 and new photographs for non-mammalian therapsid and mammalian holotypes erected between 1968 and 1994. *Canadian Journal of Earth Sciences*, *50*, 213–234.

Scott, C. S., Spivak, D. N., & Sweet, A. R. (2013). First mammals from the Paleocene Porcupine Hills Formation of southwestern Alberta, Canada. *Canadian Journal of Earth Sciences*, *50*, 355–378.

Scott, W. B. (1940). The Mammalian Fauna of the White River Oligocene: Part IV. Artiodactyla. *Transactions of the American Philosophical Society*, *28*, 363–746.

Sidor, C. A. (2003). Evolutionary trends and the origin of the mammalian lower jaw. *Paleobiology, 29*, 605–640.

Silcox, M. T., & Williamson, T. E. (2012). New discoveries of early Paleocene (Torrejonian) primates from the Nacimiento Formation, San Juan Basin, New Mexico. *Journal of Human Evolution*, *63*, 805–833.

Simons, E. L. (1960). The Paleocene Pantodonta. *Transactions of the American Philosophical Society*, *50*, 3–99.

Simpson, G. G. (1925). Mesozoic Mammalia, II; *Tinodon* and its allies. *American Journal of Science*, *10,* 451–470.

Simpson, G. G. (1928). *A catalogue of the Mesozoic Mammalia in the Geological Department of the British Museum*. Trustees of the British Museum, London.

Simpson, G. G. (1929). American Mesozoic Mammalia. *Memoirs of the Peabody Museum of Yale University, 3*, 1–235.

Simpson, G. G. (1936). Studies of the earliest mammalian dentitions. *The Dental Cosmos, 78*, 791–800.

Simpson, G. G. (1936). A new fauna from the Fort Union of Montana. *American Museum Novitates*, *873*, 1–27.

Simpson, G. G. (1937). The beginning of the age of mammals. *Biological Reviews., 12*, 1-46.

Simpson, G. G. (1937). *The Fort Union of the Crazy Mountain field, Montana and its mammalian faunas*. U.S. National Museum Bulletin, *169*, 1-287.

Simpson, G. G. (1940). Studies on the earliest primates. *Bulletin of the American Museum of Natural History*, *77*, 185-212.

Simpson, G. G. (1944). *Tempo and mode in evolution*. Columbia University Press, New York City.

Slater, G. J. (2013) Phylogenetic evidence for a shift in the mode of mammalian body size evolution at the Cretaceous-Paleogene boundary. *Methods in Ecology and Evolution,* 4, 734–744.

Slater, G. J. (2015). Iterative adaptive radiations of fossil canids show no evidence for diversity-dependent trait evolution. *Proceedings of the National Academy of Sciences, 112*, 4897–4902.

Slater, G. J., Harmon, L. J., & Alfaro, M. E. (2012). Integrating fossils with molecular phylogenies improves inference of trait evolution. *Evolution*, *66*, 3931–3944.

Smit, H. A., Jansen van Vuuren, B., O'Brien, P. C. M., Ferguson-Smith, M., Yang, F., & Robinson, T. J. (2011). Phylogenetic relationships of elephant-shrews (Afrotheria, Macroscelididae). *Journal of Zoology, 284*, 133–143.

Smith, A. B., & McGowan, A. J. (2007). The shape of the Phanerozoic marine palaeodiversity curve: how much can be predicted from the sedimentary rock record of Western Europe?. *Palaeontology*, *50*, 765–774.

Smith, A. T., & Weston, M. L. (1990). *Ochotona princeps*. *Mammalian Species, 352*, 1–8.

Smith, F. A., et al. (2010). The evolution of maximum body size of terrestrial mammals. *Science*, *330*, 1216–1219.

Smith, F. A., & Lyons, S. K. (2011). How big should a mammal be? A macroecological look at mammalian body size over space and time. *Philosophical Transactions of the Royal Society of London B, 366*, 2364–2378.

Smits, P. D. (2015). Expected time-invariant effects of biological traits on mammal species duration. *Proceedings of the National Academy of Sciences*, *112*, 13015–13020.

Sokal, R. R. & Rohlf, F. J. (1995). *Biometry: the principles and practice of statistics in biological research. Third edition*. W. H. Freeman. New York, New York, USA.

Sowls, L. K. (1997). *Javelinas and other peccaries: their biology, management, and use.* Texas A&M University Press, College Station.

Sprain, C. J., Renne, P. R., Wilson, G. P., & Clemens, W. A. (2015). High-resolution chronostratigraphy of the terrestrial Cretaceous-Paleogene transition and recovery interval in the Hell Creek region, Montana. *Geological Society of America Bulletin*, *127*, 393–409.

Springer, M. S., et al. (2012). Macroevolutionary dynamics and historical biogeography of primate diversification inferred from a species supermatrix. *PloS One*, *7*, e49521.

St. Clair, E. M., Boyer, D. M., Bloch, J. I., & Krause, D. W. (2010). First records of a triisodontine mammal, *Goniacodon levisanus*, in the late Paleocene of the northern Great Plains, North America. *Journal of Vertebrate Paleontology*, *30*, 604–608.

Steppan, S. J., Adkins, R. M., & Anderson, J. (2004). Phylogeny and divergence-date estimates of rapid radiations in muroid rodents based on multiple nuclear genes. *Systematic Biology, 53*, 533–553.

Stern, D., Crompton, A. W. & Skobe, Z. (1989). Enamel ultrastructure and masticatory function in molars of the American opossum, *Didelphis virginiana*. *Zoological Journal of the Linnean Society, 95*, 311–334.

Storz, J. F., & Kunz, T. H. (1999). *Cynopterus sphinx*. *Mammalian Species*, *613*, 1–8

Stroud, J. T., & Losos, J. B. (2016). Ecological opportunity and adaptive radiation. *Annual Review of Ecology, Evolution, and Systematics*, *47*, 502-532.

Sullivan, J., Demboski, J. R., Bell, K. C., Hird, S., Sarver, B., Reid, N., & Good, J. M. (2014). Divergence with gene flow within the recent chipmunk radiation (*Tamias*). *Heredity*, *113*, 185–194.

Tabuce, R., Asher, R. J., & Lehmann, T. (2008). Afrotherian mammals: a review of current data. *Mammalia*, *72*, 2–14.

Tabuce, R., et al. (2013). New eutherian mammals from the Late Cretaceous of Aix-en-Provence Basin, southeastern France. *Zoological Journal of the Linnean Society*, *169*, 653–672.

Tapaltsyan, V., Eronen, J. T., Lawing, A. M., Sharir, A., Janis, C., Jernvall, J., & Klein, O. D. (2015). Continuously growing rodent molars result from a predictable quantitative evolutionary change over 50 million years. *Cell Reports*, *11*, 673-680.

Tarver, J. E. & Donoghue, P. C. (2011). The trouble with topology: phylogenies without fossils provide a revisionist perspective of evolutionary history in topological analyses of diversity. *Systematic Biology*, *60*, 700–712.

Taylor, W. A., Lindsey, P. A., & Skinner, J. D. (2002). The feeding ecology of the aardvark *Orycteropus afer*. *Journal of Arid Environments*, *50*, 135–152.

Tevis, L., Jr. (1953). Stomach contents of chipmunks and mantled squirrels in northeastern California. *Journal of Mammalogy, 34*, 316–324.

Thielen, D. R., Arends, A., Segnini, S., & Fariñas, M. (1997). Food availability and population dynamics of *Marmosa xerophila* Handley and Gordon 1979 (Marsupialia: Didelphidae). *Zoocriaderos, 2*, 1–15.

Ting, S. Y., et al. (2011). Asian early Paleogene chronology and mammalian faunal turnover events. *Vertebrata PalAsiatica*, *49*, 1–28.

Tobin, T. S., et al. (2012). Extinction patterns, δ^{18} O trends, and magnetostratigraphy from a southern high-latitude Cretaceous–Paleogene section: Links with Deccan volcanism. *Palaeogeography, Palaeoclimatology, Palaeoecology*, *350*, 180–188.

Tomiya, S. (2013). Body size and extinction risk in terrestrial mammals above the species level. *The American Naturalist*, *182*, E196–E214.

Torres-Mura, J. C., Lemus, M. L., & Contreras, L. C. (1989). Herbivorous specialization of the South American desert rodent *Tympanoctomys barrerae*. *Journal of Mammalogy, 70*, 646–648.

Trofimov, B. A., & Szalay, F. S. (1994). New Cretaceous marsupial from Mongolia and the early radiation of Metatheria. *Proceedings of the National Academy of Sciences*, *91*, 12569–12573.

Turnbull, W. D. (1970). Mammalian masticatory apparatus. *Fieldiana: Geology, 18*, 147–356.

Ungar, P. S., & Sponheimer, M. (2011). The diets of early hominins. *Science*, *334*, 190–193.

Urban, D. J., Anthwal, N., Luo, Z. X., Maier, J. A., Sadier, A., Tucker, A. S., & Sears, K. E. (2017). A new developmental mechanism for the separation of the mammalian middle ear ossicles from the jaw. *Proceedings of the Royal Society B, 284*, 20162416.

Van Valen, L. M. (1967). New Paleocene insectivores and insectivore classification. *Bulletin of the American Museum of Natural History, 135*, 221–284.

Van Valen, L. (1973). A new evolutionary law. *Evolutionary Theory*, *1*, 1-30.

Van Valkenburgh, B. (1988). Trophic diversity in past and present guilds of large predatory mammals. *Paleobiology*, *14*, 155–173.

Varty, N. (1990). Ecology of the small mammals in the riverine forests of the Jubba Valley, Southern Somalia. *Journal of Tropical Ecology, 6*, 179–189.

Vavrek, M. J. & Larsson, H. C. (2010). Low beta diversity of Maastrichtian dinosaurs of North America. *Proceedings of the National Academy of Science, 107*, 8265–8268.

Vernes, K. (1995). The diet of the red-legged pademelon *Thylogale stigmatica* (Gould) (Marsupialia: Macropodidae) in fragmented tropical rainforest, north Queensland, Australia. *Mammalia 59*, 517–526.

Vinyard, C. J., Williams, S. H., Wall, C. E., Johnson, K. R., & Hylander, W. L. (2005). Jaw-muscle electromyography during chewing in Belanger's treeshrews (Tupaia belangeri). *American Journal of Physical Anthropology*, *127*, 26–45.

Virgós, E., Llorente, M., & Cortésá, Y. (1999). Geographical variation in genet (*Genetta genetta* L.) diet: a literature review. *Mammal Review*, *29*, 117–126.

von Koenigswald, W., Anders, U., Engels, S., Schultz, J. A. & Kullmer, O. (2013). Jaw movement in fossil mammals: analysis, description and visualization. *Paläontologische Zeitschrift*, *87*, 141–159.

Voss, R. S., Gutiérrez, E. E., Solari, S., Rossi, R. V., & Jansa, S. A. (2014). Phylogenetic relationships of mouse opossums (Didelphidae, *Marmosa*) with a revised subgeneric classification and notes on sympatric diversity. *American Museum Novitates*, *3817*, 1–27.

Vullo, R., Gheerbrant, E., de Muizon, C., & Néraudeau, D. (2009). The oldest modern therian mammal from Europe and its bearing on stem marsupial paleobiogeography. *Proceedings of the National Academy of Sciences*, *106*, 19910–19915.

Wall, C. E., & Krause, D. W. (1992). A biomechanical analysis of the masticatory apparatus of Ptilodus (Multituberculata). *Journal of Vertebrate Paleontology*, *12*, 172–187.

Wang, X., & Zhai, R. (1995). *Carnilestes*, a new primitive lipotyphlan (Insectivora: Mammalia) from the early and middle Paleocene, Nanxiong Basin, China. *Journal of Vertebrate Paleontology*, *15*, 131–145.

Wang, Y., Hu, Y., Meng, J. & Li, C. (2001). An ossified Meckel's cartilage in two Cretaceous mammals and origin of the mammalian middle ear. *Science, 294*, 357–361.

Wang, Y., & Jin, X. (2004). A new Paleocene tillodont (Tillodontia, Mammalia) from Qianshan, Anhui, with a review of Paleocene tillodonts from China. *Vertebrata PalAsiatica*, *42*, 13–26.

Warton, D. I., & Hui, F. K. (2011). The arcsine is asinine: the analysis of proportions in ecology. *Ecology*, *92*, 3–10.

Weijs, W. A. (1994). Evolutionary approach of masticatory motor patterns in mammals. *In* Bels, V., Chardon, M. & Vandewalle, P., editors, *Biomechanics of Feeding in Vertebrates*, pages 281–320. Springer.

Westerman, M., Krajewski, C., Kear, B. P., Meehan, L., Meredith, R. W., Emerling, C. A., & Springer, M. S. (2016). Phylogenetic relationships of dasyuromorphian marsupials revisited. *Zoological Journal of the Linnean Society*, *176*, 686–701.

Whitaker, J. O., Jr. (1963). Food, habitat and parasites of the woodland jumping mouse in central New York. *Journal of Mammalogy, 44*, 316–321.

Whitaker, J. O., Jr. (1966). Food of *Mus musculus*, *Peromyscus maniculatus bairdi* and *Peromyscus leucopus* in Vigo County, Indiana. *Journal of Mammalogy, 47*, 473–486.

Whitten, J. E. J. (1981). Ecological separation of three diurnal squirrels in tropical rainforest on Siberut Island, Indonesia. *Journal of Zoology, 193*, 405–420.

Wible, J. R. (2008). On the cranial osteology of the Hispaniolan solenodon, *Solenodon paradoxus* Brandt, 1833 (Mammalia, Lipotyphla, Solenodontidae). *Annals of Carnegie Museum, 77*, 321–402.

Wible, J. R., Rougier, G. W., Novacek, M. J., & Asher, R. J. (2009). The eutherian mammal *Maelestes gobiensis* from the Late Cretaceous of Mongolia and the phylogeny of Cretaceous Eutheria. *Bulletin of the American Museum of Natural History*, *327*, 1–123.

Wilf, P., Labandeira, C. C., Johnson, K. R., & Ellis, B. (2006). Decoupled plant and insect diversity after the end-Cretaceous extinction. *Science*, *313*, 1112-1115.

Williams, S. H., Vinyard, C. J., Wall, C. E., Doherty, A. H., Crompton, A. W., & Hylander, W. L. (2011). A preliminary analysis of correlated evolution in mammalian chewing motor patterns. *Integrative and Comparative Biology, 51*, 247–259.

Williamson, T. E., Brusatte, S. L., Carr, T. D., Weil, A., & Standhardt, B. R. (2012). The phylogeny and evolution of Cretaceous–Palaeogene metatherians: cladistic analysis and description of new early Palaeocene specimens from the Nacimiento Formation, New Mexico. *Journal of Systematic Palaeontology*, *10*, 625–651.

Williamson, T. E., Brusatte, S. L., Secord, R., & Shelley, S. (2016). A new taeniolabidoid multituberculate (Mammalia) from the middle Puercan of the Nacimiento Formation, New Mexico, and a revision of taeniolabidoid systematics and phylogeny. *Zoological Journal of the Linnean Society*, *177*(1), 183-208.

Williamson, T. E., & Taylor, L. H. (2011). New species of *Peradectes* and *Swaindelphys* (Mammalia: Metatheria) from the Early Paleocene (Torrejonian) Nacimiento Formation, San Juan Basin, New Mexico, USA. *Palaeontologia Electronica*, *14*, 1–16.

Williamson, T. E., & Weil, A. (2011). A new Puercan (early Paleocene) hyopsodontid "condylarth" from New Mexico. *Acta Palaeontologica Polonica*, *56*, 247–255.

Williamson, T. E., Weil, A., & Standhardt, B. (2011). Cimolestids (Mammalia) from the early Paleocene (Puercan) of New Mexico. *Journal of Vertebrate Paleontology*, *31*, 162–180.

Wilson, D. E. (1971). Food habits of *Micronycteris hirsuta* (Chiroptera: Phyllostomidae). *Mammalia, 35*, 107–110.

Wilson, D. E. & Ruff, S. (1999). *The Smithsonian book of North American mammals*. Smithsonian Institution Press, Washington, DC, USA.

Wilson, G. P. (2013). Mammals across the K/Pg boundary in northeastern Montana, USA: dental morphology and body-size patterns reveal extinction selectivity and immigrant-fueled ecospace filling. *Paleobiology*, *39*, 429–469.

Wilson, G. P. (2014). Mammalian extinction, survival, and recovery dynamics across the Cretaceous-Paleogene boundary in northeastern Montana, USA. *Geological Society of America Special Papers*, *503*, 365–392.

Wilson, G. P., Dechesne, M., & Anderson, I. R. (2010). New latest Cretaceous mammals from northeastern Colorado with biochronologic and biogeographic implications. *Journal of Vertebrate Paleontology*, *30*, 499–520.

Wilson, G. P., Ekdale, E. G., Hoganson, J. W., Calede, J. J., & Vander Linden, A. (2016). A large carnivorous mammal from the Late Cretaceous and the North American origin of marsupials. *Nature Communications*, *7*, 13734.

Wilson, G. P., Evans, A. R., Corfe, I. J., Smits, P. D., Fortelius, M., & Jernvall, J. (2012). Adaptive radiation of multituberculate mammals before the extinction of dinosaurs. *Nature*, *483*, 457–460.

Wilson, G. P., & Riedel, J. A. (2010). New specimen reveals deltatheroidan affinities of the North American Late Cretaceous mammal *Nanocuris*. *Journal of Vertebrate Paleontology*, *30*, 872–884.

Winchester, J. M., Boyer, D. M., St Clair, E. M., Gosselin-Ildari, A. D., Cooke, S. B., & Ledogar, J. A. (2014). Dental topography of platyrrhines and prosimians: convergence and contrasts. *American Journal of Physical Anthropology*, *153*, 29–44.

Wing, S. L., & Tiffney, B. H. (1987). The reciprocal interaction of angiosperm evolution and tetrapod herbivory. *Review of Palaeobotany and Palynology*, *50*, 179-210.

Woodburne, M. O. (2004). *Late Cretaceous and Cenozoic mammals of North America: biostratigraphy and geochronology*. Columbia University Press, New York.

Workman, C., & Dung, L. V. (2009). The chemistry of eaten and uneaten leaves by Delacour's langurs (*Trachypithecus delacouri*) in Van Long Nature Reserve, Vietnam. *Vietnamese Journal of Primatology, 3*, 29–36.

Wu, J., Yonezawa, T., & Kishino, H. (2017). Rates of Molecular Evolution Suggest Natural History of Life History Traits and a Post-K-Pg Nocturnal Bottleneck of Placentals. *Current Biology*, *27*, 3025-3033.

Wydeven, P. R., & Dahlgren, R. B. (1982). A comparison of prairie dog stomach contents and feces using a microhistological technique. *Journal of Wildlife Management, 46*, 1104–1108.

Yamashita, N. (2008). Food physical properties and their relationship to morphology: the curious case of kily. *Primate Craniofacial Function and Biology*, 387–406.

Yuping, Z., & Yongsheng, T. (1981). New anagaloid mammals from Paleocene of South China. *Vertebrata PalAsiatica*, *19*, 133–144.

Yuan, C. X., Ji, Q., Meng, Q. J., Tabrum, A. R., & Luo, Z. X. (2013). Earliest evolution of multituberculate mammals revealed by a new Jurassic fossil. *Science*, *341*, 779–783.

Zan, S., Wood, C. B., Rougier, G. W., Jin, L., Chen, J., & Schaff, C. R. (2006). A new" middle" Cretaceous zalambdalestid mammal, from a new locality in Jilin Province, northeastern China. *Journal of the Paleontological Society of Korea*, *22*, 153–172.

Zelditch, M. L., Ye, J., Mitchell, J. S., & Swiderski, D. L. (2017). Rare ecomorphological convergence on a complex adaptive landscape: Body size and diet mediate evolution of jaw shape in squirrels (Sciuridae). *Evolution*, *71*, 633–649.

Zhang, F., Crompton, A. W., Luo, Z., & Schaff, C. R. (1998). Pattern of dental replacement of Sinoconodon and its implication for evolution of mammals. *Vertebrata Pal Asiatica*, *36*, 197–217.

Zheng, X., Bi, S., Wang, X., & Meng, J. (2013). A new arboreal haramiyid shows the diversity of crown mammals in the Jurassic period. *Nature*, *500*, 199–202.

Zhou, C. F., Wu, S., Martin, T., & Luo, Z. X. (2013). A Jurassic mammaliaform and the earliest mammalian evolutionary adaptations. *Nature*, *500*, 163–167.

Zhou, Y. B., Newman, C., Buesching, C. D., Zalewski, A., Kaneko, Y., Macdonald, D. W., & Xie, Z. Q. (2011). Diet of an opportunistically frugivorous carnivore, *Martes flavigula*, in subtropical forest. *Journal of Mammalogy*, *92*, 611–619.

APPENDIX A

Specimen information for the mammaliaform genera analyzed in Chapter 2. Additional notes concerning the specimens are provided in Appendix B. Abbreviations: EC, Early Cretaceous; EJ, Early Jurassic; LJ, Late Jurassic; LT, Late Triassic; MJ, Middle Jurassic.

Taxon	Image source and specimen(s)	Age
Stem Mammaliaforms		
Agilodocodon	Meng et al. (2015), BMNH001138A and B (reconstruction)	MJ
Arboroharamiya	Zheng et al. (2013), STM33-9 (reconstruction)	MJ or LJ
Castorocauda	Ji et al. (2006), JZMP 04-117 (reconstruction)	MJ
Docodon	Simpson (1929), YPM 11826 (reconstruction)	LJ
Docofossor	Luo et a. (2015B), BMNH131735A and B (reconstruction)	LJ
Dinnetherium	Jenkins et al. (1983), MCZ 20872	EJ
Hadrocodium	Luo et al. (2001), IVPP 8275	EJ
Haldanodon	Luo (2011), reconstruction based on multiple specimens, including those in Lillegraven & Krusat (1991)	LJ
Haramiyavia	Luo et al. (2015A), MCZ7/95A and B (reconstruction)	LT
Kuehneotherium	Gill et al. (2014), reconstruction based on multiple specimens	LT-EJ
Megazostrodon	Kielan-Jaworowska et al. (2004), reconstruction based on multiple specimens	EJ
Morganucodon	Gill et al. (2014), reconstruction based on multiple specimens	LT-EJ
Sinoconodon	Zhang et al. (1998), IVPP 4727	LT-EJ
Megaconus	Zhou et al. (2013), PMOL-AM00007A and B (reconstruction)	MJ
Xianshou	Bi et al. (2014), IVPP V16707A (reconstruction)	LJ
Australosphenidans		
Asfaltomylos	Rauhut et al. (2002), MPEF-PV1671	EJ
Bishops	Rich et al. (2001)	EC
Henosferus	Rougier et al. (2007), reconstruction based on multiple specimens	EJ
Pseudotribos	Luo et al. (2007B), CAGS040811 (reconstruction)	MJ
Teinolophos	Rich et al. (2016), MSC 148 (NMV P20823)	EC
Multituberculates		
Ctenacodon	Simpson (1929), YPM 11833 (reconstruction)	LJ-EC
Guimarotodon	Hahn & Hahn (1998), Nach V.J. 461-155 and IPFUB Gui Mam 143/76 (reconstruction)	LJ
Kuehneodon	Hahn (1969), V. J. 4-155 (reconstruction)	LJ
Meketibolodon	Hahn & Hahn (1998), IPFUB Gui Mam 89/76	LJ
Paulchoffatia	Hahn (1969), V. J. 1-155 (reconstruction)	LJ
Plagiaulax	Simpson (1929), reconstruction based on multiple specimens	MJ
Rugosodon	Yuan et al. (2013), BMNH1143A and B (reconstruction)	LJ
Sinobaatar	Hu & Wang (2002), IVPP V12517	EC
Zofiabaatar	Bakker & Carpenter (1990)	LJ
Eutriconodontans		
Amphilestes	Simpson (1928), reconstruction based on multiple specimens	MJ
Argentoconodon	Gaetano & Rougier (2011), reconstruction based largely on MPEF-PV2363	EJ
Gobiconodon	Jenkins & Schaff (1988), MCZ 19965	EC
Jeholodens	Ji et al. (1999), GMV 2139 (reconstruction)	EC
Liaoconodon	Meng et al. (2011), IVPP V16051 (reconstruction)	EC
Phascolotherium	Simpson (1928), reconstruction based on multiple specimens	MJ
Priacodon	Kielan-Jaworowska et al. (2004), reconstruction based on multiple specimens	LJ
Repenomamus	Wang et al. (2001), IVPP V12549	EC
Triconodon	Simpson (1928), reconstruction based on multiple specimens	EC
Trioracodon	Simpson (1928), reconstruction based on multiple specimens	LT-EJ
Volaticotherium	Meng et al. (2006), IVPP V14739 (reconstruction)	MJ

Yanoconodon	Luo et al. (2007A), reconstruction based on NJU-P06001A	EC
Spalacotherioids (& *Tinodontids*)		
Heishanlestes	Hu et al. (2005A), IVPP V 7480	EC
Lactodens	Han & Meng (2016), HG-M016	EC
Maotherium	Ji et al. (2009), HGM 41H-III-0321 (reconstruction)	EC
Spalacotherium	Kielan-Jaworowska et al. (2004)	EC
Tinodon	Simpson (1925), reconstruction based on multiple specimens	LJ-EC
Yermakia	Lopatin et al. (2005), PM TGU 16/7-22	EC
Zhangheotherium	Hu et al. (1997), IVPP V7466 (reconstruction)	EC
Dryolestoids		
Amblotherium	Simpson (1928), reconstruction based on multiple specimens	LJ-EC
Crusafontia	Krebs (1993), reconstruction based on multiple specimens	EC
Dryolestes	Martin (1999), Gui Mam 41/79	LJ
Henkelotherium	Luo (2007), reconstruction based on multiple specimens, including those in Henkel & Krebs (1977) and Krebs (1991)	LJ
Laolestes	Prothero (1981)	LJ-EC
Phascolestes	Simpson (1928), reconstruction based on multiple specimens	EC
Therians & close kin		
Amphitherium	Simpson (1928)	MJ
Eomaia	Ji et al. (2002), CAGS01-IG1-a and b (reconstruction)	EC
Juramaia	Luo et al. (2011), BMNH PM1143 (reconstruction)	MJ-LJ
Montanalestes	Cifelli (1999), OMNH 60793 (reconstruction)	EC
Peramus	Prothero (1981)	EC
Prokennalestes	Kielan-Jaworowska & Dashzeveg (1989), GI PST 10-6 (for AP analysis), GI PST 10-14b (for additional measurements)	EC
Sasayamamylos	Kusuhashi et al. (2013), MNHAH D1-030444	EC
Sinodelphys	Luo et al. (2003), CAGS00-IG03 (reconstruction)	EC
Tendagurutherium	Heinrich (1998), MB.Ma.46910	LJ
Other		
Vincelestes	Bonaparte & Rougier (1987)	EC
Fruitafossor	Luo & Wible (2005), LACM 150948 (reconstruction)	LJ

APPENDIX B

Jaw joint elevation, coronoid process (CP) elevation, and tooth row length of jaw specimens in Chapter 2 (see Appendix A). The values are ratios, calculated by dividing the measurements by the length of the jaw. Median values for groups are in bold and italics. Jaw joint and coronoid process elevation results are shown in Figure 2.5. In the notes column, "molar landmark" refers to the single landmark between the penultimate and ultimate molars (Fig. 2.4), and "APr shape analysis" refers to the geometric morphometrics analysis of the angular process (APr) region of the jaw (Figs. 2.3 and 2.4). Abbreviation: APr, angular process; CP, coronoid process.

Taxon	Jaw joint elevation	CP elevation	Tooth row length	Notes
Stem Mammaliaforms	***0.0493***	***0.2454***	***0.5808***	
Agilodocodon	0.1223	0.2458	0.6476	Part of the CP is drawn with a dashed line in the source image and is likely to represent an estimate of is shape.
Arboroharamiya	0.0370	0.3997	0.5121	
Castorocauda	0.0242	0.1425	0.6642	Part of the CP is drawn with a dashed line in the source image and is likely to represent an estimate of is shape.
Docodon	0.0265	0.2454	0.6702	*D. victor* specimen from Simpson (1929) was used for linear measurements but not for the APr shape analysis because the APr is likely incorrectly reconstructed (Rouger et al., 2015B). The *D. apoxys* specimen described by Rougier et al. (2015B) was used for the APr shape analysis.
Docofossor	0.0749	0.3508	0.5855	
Dinnetherium	0.0279	0.1447	0.6020	
Hadrocodium	0.0617	0.1965	0.5023	
Haldanodon	0.1264	0.3068	0.5668	
Haramiyavia	0.0828	0.2538	0.5648	
Kuehneotherium	0.0983	0.1879	0.6475	
Megazostrodon	0.0493	0.1427	0.6191	Part of the CP is drawn with a dashed line in the source image and is likely to represent an estimate of is shape.
Morganucodon	0.0834	0.2302	0.5808	
Sinoconodon	0.0283	0.2195	0.4843	A juvenile specimen (IVPP 4727) from Zhang et al. (1998) was used for jaw joint and tooth row measurements because more molars are present, but the adult specimen (IVPP 8688) appears to have similar dimensions.
Megaconus	0.0142	0.2519	0.5783	
Xianshou	0.0445	0.2543	0.4419	
Australosphenidans	***0.1179***	***0.2178***	***0.6462***	
Asfaltomylos	0.2118		0.5598	A portion of the APr is likely broken and in the incorrect position. I largely ignored the broken piece for the APr shape analysis. Jaw length is estimated because the anterior tip of the jaw is broken. The CP elevation is not measured because the CP is not fully preserved or reconstructed.

Bishops	0.1989		0.6324	Jaw length is estimated because anterior tip of jaw is broken. The CP elevation is not measured because the CP is not fully preserved or reconstructed.
Henosferus	0.0389	0.1988	0.6602	
Pseudotribos	0.0497	0.2369	0.6600	
Teinolophos	0.1179		0.7448	The CP elevation is not measured because the CP is not fully preserved or reconstructed.
Multituberculates	***-0.0156***	***0.2558***	***0.4822***	
Ctenacodon	0.0856	0.2574	0.4822	
Guimarotodon	-0.0422	0.3054	0.5358	
Kuehneodon	-0.0031		0.4590	Molar landmark location is estimated due to lack of molars. The CP elevation is not measured because the CP is not fully preserved or reconstructed.
Meketibolodon	0.0075	0.2283	0.4442	Part of the CP is drawn with a dashed line in the source image and is likely to represent an estimate of is shape.
Paulchoffatia	-0.0159		0.4907	Molar landmark location is estimated due to lack of molars. The CP elevation is not measured because the CP is not fully preserved or reconstructed.
Plagiaulax	0.0048	0.2692	0.4669	Molar landmark location is estimated due to lack of molars.
Rugosodon	-0.0860	0.1670	0.6464	
Sinobaatar	-0.0715	0.1720	0.6561	
Zofiabaatar	-0.0156	0.2558	0.4403	
Eutriconodontans	***-0.0174***	***0.2261***	***0.6340***	
Amphilestes	0.0263	0.2118	0.6798	
Argentoconodon	-0.0469	0.2449	0.7220	
Gobiconodon	-0.0462	0.2029	0.5308	
Jeholodens	0.0152	0.1230	0.7139	
Liaoconodon	0.0209	0.2891	0.6172	
Phascolotherium	0.0617	0.2426	0.5672	
Priacodon	-0.0087	0.2971	0.6586	
Repenomamus	-0.0379	0.2514	0.5350	
Triconodon	-0.0262	0.2335	0.5804	
Trioracodon	-0.0474	0.2186	0.6310	
Volaticotherium	-0.0586	0.1845	0.6370	
Yanoconodon	0.0150	0.2112	0.6448	
Spalacotherioids (& Tinodontids)	***0.0633***	***0.2215***	***0.6392***	
Heishanlestes	0.0633	0.2363	0.6392	Jaw length is estimated because anterior tip of jaw is broken.
Lactodens	0.0952	0.1854	0.6858	
Maotherium	0.0349	0.2015	0.5864	
Spalacotherium	0.1304	0.2401	0.6522	
Tinodon	0.0798	0.2215	0.6017	
Yermakia	0.0221	0.2370	0.6445	Not used in the APr shape analysis due to broken angular region. The jaw articulation point was estimated because the condylar process may be incomplete.
Zhangheotherium	-0.0042	0.1392	0.6123	
Dryolestoids	***0.1257***	***0.2515***	***0.6337***	
Amblotherium	0.0887	0.2196	0.6549	
Crusafontia	0.1056	0.2518	0.6709	
Dryolestes	0.1378	0.3167	0.5639	
Henkelotherium	0.1262	0.2512	0.6533	
Laolestes	0.1347	0.2469	0.6141	
Phascolestes	0.1252	0.2600	0.5868	
Therians & kin	***0.0680***	***0.2191***	***0.6069***	
Amphitherium	0.1064	0.2150	0.5962	

Eomaia	0.0480	0.2213	0.6675	
Juramaia	0.0693		0.6489	Some of the APr and condylar process shape was estimated by Luo et al. 2011. The coronoid elevation is not measured because the CP is not fully preserved or reconstructed.
Montanalestes	0.0985		0.6069	Jaw length is estimated because anterior tip of jaw is broken. The coronoid elevation is not measured because the CP is not fully preserved or reconstructed.
Peramus	0.0511	0.2191	0.5819	
Prokennalestes	0.0667	0.1341	0.5605	Jaw length is estimated because anterior tip of jaw appears broken. A small portion of the APr may also be broken.
Sasayamamylos	0.1133	0.3232	0.5876	
Sinodelphys	0.0636	0.1907	0.6781	Part of the CP is drawn with a dashed line in the source image and is likely to represent a shape estimate.
Tendagurutherium				Only used in the APr analysis because the anterior portion of the jaw is missing (and therefore jaw length cannot be measured or estimated).
Other				
Fruitafossor	0.1553	0.4217	0.5180	Not included with a mammal group due to questionable phylogenetic affinity and derived features. See text.
Vincelestes	0.1423	0.1821	0.5055	Not included with a mammal group due to questionable phylogenetic affinity and derived features. See text.

APPENDIX C

Measurements of mammaliaform and modern mammal jaws and skulls for Chapter 2. Average jaw measurements ('Jaw width to length') are used for determining the length and posterior width of the jaw models (Figs. 2.7 and 2.8). Average skull measurements are used to determine the estimated position of the muscle origins of the superficial masseter (SM) and medial pterygoid (MP) (see 2.3 Methods). Posterior jaw widths at the jaw joints are often estimated from the glenoid fossae of the skull (see 2.3 Methods). 'Pterygoid to pterygoid width' and 'zygoma to zygoma width' values are divided by the total jaw width at the jaw joints. Length measurements (i.e., 'anterior tip of jaw to pterygoid' and 'anterior tip of jaw to zygoma') are divided by the total jaw length. Thus, table values represent ratios of the measurements to the total width or length of the jaw. Values in bold and italics are averages (means) for each group, and overall means, medians, and standard deviations are given at the bottom. Field Museum of Natural History (FMNH) specimen numbers are provided for modern genera.

Taxon	MP origin location		SM origin location		
	Pterygoid to pterygoid width	**Anterior tip of jaw to pterygoid**	**Zygoma to zygoma width**	**Anterior tip of jaw to zygoma**	**Jaw width to length**
Fossil mammaliaforms (mean)	***0.2476***	***0.7417***	***0.8631***	***0.5383***	***0.6540***
Morganucodon (Kielan-Jaworowska et al. 2004)	0.3400	0.6235	0.7120	0.5134	0.6181
Sinoconodon (Zhang et al. 1998)	0.2733	0.7080	0.8109	0.5204	0.6551
Hadrocodium (Luo et al. 2001)	0.2887	0.7025	0.8017	0.5218	0.6741
Vincelestes (Rougier 1993)	0.2108	0.7525	0.8476	0.4495	0.6950
Mayulestes (de Muizon 1998)	0.1674	0.8616	1.0023	0.5700	0.6333
Asiatherium (Kielan-Jaworowska et al. 2004)	0.2053	0.8024	1.0041	0.6548	0.6482
Modern eutherians (mean)	***0.2446***	***0.8459***	***0.9966***	***0.5688***	***0.6002***
Amblysomus (FMNH165582)	0.1891	0.7703	0.7264	0.4363	0.8056
Chrysochloris (FMNH207280)	0.2356	0.7648	0.7737	0.5020	0.8698
Echinosorex (FMNH85105)	0.2451	0.8288	1.0602	0.6081	0.4253
Erinaceus (FMNH96345)	0.4140	0.8503	1.0740	0.5292	0.7125
Hylomys (FMNH32308)	0.3683	0.8642	0.8824	0.5836	0.6191
Solenodon (FMNH57320)	0.1527	0.8375	1.1782	0.5745	0.4558
Scutisorex (FMNH160178)	0.1724	0.8844	0.9009	0.5260	0.6831
Suncus (FMNH57608)	0.1005	0.8999	0.9308	0.4688	0.6374
Talpa (FMNH6449)	0.2006	0.8216	0.8382	0.5969	0.5377
Condylura (FMNH199405)	0.3329	0.8683	0.8962	0.6801	0.5134
Echinops (FMNH156189)	0.2023	0.8963	1.2650	0.5184	0.4479
Tenrec (FMNH172708)	0.2930	0.8359	1.2375	0.6324	0.2625
Ptilocercus (FMNH76855)	0.2523	0.7940	1.0547	0.5400	0.6848
Tupaia (FMNH32994)	0.2480	0.8589	1.0197	0.6092	0.6846
Vulpes (FMNH214921)	0.2848	0.8724	1.0468	0.6587	0.5275

Procyon (FMNH221769)	0.2772	0.8965	0.9544	0.5812	0.6706
Mustela (FMNH165361)	0.2599	0.8967	1.1233	0.5350	0.6900
Rhynchocyon (FMNH151213)	0.1737	0.7854	0.9771	0.6583	0.5757
Modern metatherians (mean)	***0.2198***	***0.8249***	***0.9686***	***0.5628***	***0.5721***
Caenolestes (FMNH124620)	0.2762	0.7965	0.8741	0.5066	0.6327
Lutreolina (FMNH136826)	0.1927	0.8663	0.9435	0.5080	0.5665
Chironectes (FMNH75093)	0.1891	0.8933	0.9841	0.5726	0.6169
Metachirus (FMNH69323)	0.1968	0.8842	0.9577	0.6341	0.5410
Dasyurus (FMNH 127358)	0.2229	0.8124	0.9350	0.5629	0.6060
Didelphis (FMNH 152106)	0.2471	0.7648	1.0888	0.5923	0.4512
Monodelphis (FMNH 20251)	0.2136	0.7569	0.9969	0.5631	0.5905
Overall mean	***0.2400***	***0.8193***	***0.9624***	***0.5611***	***0.6043***
Overall median	***0.2446***	***0.8359***	***0.9577***	***0.5631***	***0.6191***
Standard deviation	***0.0646***	***0.0669***	***0.1333***	***0.0606***	***0.1181***

APPENDIX D

Specimen summary table with dietary and body mass information for the modern species that are analyzed in Chapter 3. A majority of specimens were photographed at the Field Museum of Natural History (FMNH), and University of Michigan Museum of Zoology (UMMZ) specimen images were obtained via the Animal Diversity Web (ADW). Diet values represent the percentages of plant material consumed, and this data are based primarily off studies of stomach and fecal contents. Body mass data is from PanTHERIA (Jones et al. 2009) unless a separate source is noted in parentheses. Abbreviations: ADW, Animal Diversity Web; FMNH, Field Museum of Natural History; IU Zooarchaeology Lab, William R. Adams Zooarchaeology Laboratory at Indiana University; NMMH, Smithsonian National Museum of Natural History; UMMZ, University of Michigan Museum of Zoology.

Order Family	**Species (image source)**	**Diet as % plant (diet source)**	**Body mass (grams)**
Afrosoricida			
Chrysochloridae	*Eremitalpa granti* (FMNH 53075)	7 (Fielden et al. 1990, Perrin & Fielden 1999)	22.04
Tenrecidae	*Hemicentetes nigriceps* (FMNH 166132)	0 (ADW)	102.99
	Potamogale velox (FMNH 25973)	0 (ADW)	670.99
Artiodactyla			
Bovidae	*Aepyceros melampus* (FMNH 20659)	100 (Dunham 1980)	52591.69
	Ammotragus lervia (FMNH 55701)	100 (Gray and Simpson 1980)	94202.22
	Antidorcas marsupialis (FMNH 34494)	100 (Davies et al. 1986)	33571.24
	Cephalophus callipygus (FMNH 34289)	100 (Gautier-Hion et al. 1980)	19079.23
	Cephalophus dorsalis (FMNH 34288)	99.9 (Gautier-Hion et al. 1980)	20000
	Cephalophus leucogaster (FMNH 34291)	99.9 (Gautier-Hion et al. 1980)	13208.69
	Cephalophus nigrifrons (FMNH 26075)	99.9 (Gautier-Hion et al. 1980)	14676.33
	Cephalophus silvicultor (FMNH 34295)	99.9 (Gautier-Hion et al. 1980)	62006.6
	Philantomba monticola (FMNH 177241)	99.5 (Gautier-Hion et al. 1980)	4896.05
	Tragelaphus spekii (FMNH 60552)	100 (Gautier-Hion et al. 1980)	75554.25
Tayassuidae	*Tayassu pecari* (FMNH 49848)	100 (Sowls 1997)	31798.71
Tragulidae	*Hyemoschus aquaticus* (FMNH 34294)	99.8 (Gautier-Hion et al. 1980)	10850
Carnivora			
Canidae	*Canis lupus dingo* (FMNH 119851)	0 (Newsome et al. 1983)	14500 (ADW)
	Canis mesomelas (FMNH 85509)	2.4 (Bothma 1966)	8247.3
	Otocyon megalotis (FMNH 38190)	42.37 (Bothma 1966, Klare et al. 2011)	4098.12
	Urocyon cinereoargenteus (FMNH 199764)	50.42 (Hockman & Chapman 1983)	3833.71
	Vulpes lagopus (FMNH 74070)	0 (Anthony et al. 2000)	3584.37
	Vulpes vulpes (IU Zooarchaeology Lab)	14.72 (Hockman & Chapman 1983)	4820.36
Felidae	*Lynx rufus* (FMNH 44058)	0 (ADW)	6374.47
Herpestidae	*Helogale hirtula* (FMNH 140214)	0 (Hemming 1972)	484.63
Hyaenidae	*Crocuta crocuta* (FMNH 104021)	0 (ADW)	63369.98
Mustelidae	*Galictis vittata* (FMNH 123657)	0 (Bisbal E. 1986)	2600 (ADW)
	Martes martes (FMNH 84721)	14 (Helldin 2000)	1299.99
	Martes flavigula (FMNH 83085)	24.07 (Zhou et al. 2011)	2504.64
	Meles meles (FMNH 34192)	75.83 (Cleary et al. 2011)	11884.03
	Mustela nivalis (FMNH 20838)	0 (ADW)	78.45

Nandinidae	*Nandinia binotata* (FMNH 53868)	90 (McNab 1995)	2167.2
Phocidae	*Lobodon carcinophaga* (Adam 2005)	0 (Adam 2005)	224999.99
Procyonidae	*Procyon lotor* (IU Zooarchaeology Lab)	71 (Baker et al. 1945)	6373.72
	Potos flavus (FMNH 84240)	100 (Kays 1999)	2441.81
Ursidae	*Ursus arctos* (FMNH 25713)	85.34 (Sato et al. 2005)	196287.5
Viverridae	*Genetta genetta* (Larivière & Calzada 2001)	0 (Virgós et al. 1999)	1756.17
Chiroptera			
Hipposideridae	*Hipposideros diadema* (UMMZ 157091)	0 (Pavey & Burwell 1997)	46.9
Megadermatidae	*Lavia frons* (FMNH 104584)	0 (ADW)	23.8
Mormoopidae	*Pteronotus parnellii* (FMNH 180713)	0 (ADW)	19.59
Noctilionidae	*Noctilio leporinus* (UMMZ 124382)	0 (Brooke 1994)	29.93
	Noctilio albiventris (UMMZ 125762)	10* (Gonçalves et al. 2007)	31.46
Phyllostomidae	*Artibeus jamaicensis* (FMNH 30776)	75 (Fleming 1979)	43.63
	Artibeus obscurus (Nogueira et al. 2005)	95* (Nogueira et al. 2009)	35.91
	Chiroderma doriae (Oprea & Wilson 2009)	100 (Oprea & Wilson 2009)	19.9
	Vampyrodes caraccioli (Nogueira et al. 2005)	100 (Goodwin & Greenhall 1961)	35.89
	Micronycteris hirsute (UMMZ 125174)	8 (Wilson 1971)	12.89
	Micronycteris minuta (UMMZ 126729)	5* (Nogueira et al. 2009)	6.9
	Sturnira lilium (UMMZ 125869)	95* (Nogueira et al. 2009)	20.19
	Lophostoma silvicolum (UMMZ 122198)	90* (Nogueira et al. 2009)	32.29
	Phyllostomus hastatus (Santos et al. 2003)	43* (Nogueira et al. 2009)	91.44
	Phyllostomus elongates (UMMZ 160619)	10* (Nogueira et al. 2009)	41.75
	Erophylla sezekorni (UMMZ 97624)	67* (Nogueira et al. 2009)	15.87
	Monophyllus redmani (Homan & Jones 1975)	54* (Nogueira et al. 2009)	8.79
	Glossophaga soricina (UMMZ 126814)	81* (Nogueira et al. 2009)	9.97
	Carollia perspicillata (UMMZ 160691)	84* (Nogueira et al. 2009)	19.23
	Uroderma bilobatum (UMMZ 126764)	95* (Nogueira et al. 2009)	16.28
	Platyrrhinus lineatus (UMMZ 124324)	95* (Nogueira et al. 2009)	24.34
	Macrotus californicus (FMNH 83298)	0 (Wilson & Ruff 1999)	11.83
	Vampyrum spectrum (FMNH 58160)	0 (ADW)	171.61
Pteropodidae	*Acerodon jubatus* (FMNH 33705)	100 (ADW)	1087.04
	Cynopterus sphinx (Storz & Kunz 1999)	100 (Storz & Kunz 1999)	44.71
	Pteropus alecto (FMNH 119868)	100 (ADW)	610.13
Vespertilionidae	*Myotis lucifugus* (FMNH 5612)	0 (ADW)	7.8
	Myotis vivesi (UMMZ 76439)	0 (Otálora-Ardila et al. 2013)	25.63
	Myotis velifer (FMNH 8786)	0 (Kunz 1974)	9.82
	Nycticeius humeralis (FMNH 21907)	0 (ADW)	9.12
Dasyuromorphia			
Dasyuridae	*Dasyurus maculatus* (FMNH 160039)	0 (Jones et al. 2001)	3284.15
Thylacinidae	*Thylacinus cynocephalus* (FMNH 81522)	0 (ADW)	29999.99
Myrmecobiidae	*Myrmecobius fasciatus* (Cooper 2011)	0 (ADW)	511.44
Dermoptera			
Cynocephalidae	*Cynocephalus volans* (FMNH 87396)	100 (ADW)	1250
	Galeopterus variegates (FMNH 141132)	100 (ADW)	1112.2
Didelphimorphia			
Caluromyidae	*Caluromys philander* (FMNH 92027)	90 (Leite et al. 1996)	246.47
Didelphidae	*Marmosa demerarae (Micoureus d.)* (FMNH 69864)	19.9 (Leite et al. 1996)	102.28
	Marmosa xerophila (NMNH 443818)	18 (Thielen et al. 1997)	46.2
	Didelphis aurita (D. marsupialis a.) (FMNH 114722)	42.6 (Leite et al. 1996)	1105.88
Diprotodontia			
Burramyidae	*Cercartetus caudatus* (FMNH 128369)	0 (Flannery 1994)	23.05
Macropodidae	*Thylogale stigmatica* (FMNH 60887)	100 (Vernes 1995)	4511.47
	Macropus giganteus (FMNH 64612)	100 (ADW)	33409.89
Phascolarctidae	*Phascolarctos cinereus* (FMNH 112543)	100 (ADW)	6528.74
Pseudocheiridae	*Pseudocheirus peregrinus* (FMNH 134502)	100 (Pahl 1987)	895.22
Vombatidae	*Vombatus ursinus* (FMNH 49085)	100 (ADW)	26000
Eulipotyphla			

Erinaceidae	*Erinaceus europaeus* (FMNH 57398)	1 (Dickman 1988)	777.95
	Podogymnura truei (FMNH 56165)	0 (Heaney et al. 2006)	1,639.12
Soricidae	*Blarina brevicauda* (FMNH 105800)	3.2 (Hahus & Smith 1990)	18.56
	Crocidura flavescens (FMNH 10376)	6.7 (Monadjem 1997)	31.22
	Crocidura mariquensis (FMNH 83579)	0 (Monadjem 1997)	10.35
	Myosorex cafer (FMNH 165585)	25.2 (Monadjem 1997)	12.3
	Myosorex varius (FMNH 165589)	2.9 (Monadjem 1997)	11.68
	Sorex hoyi (FMNH 168604)	0 (Long 1974)	3.37
	Sorex palustris (FMNH 199391)	13 (Beneski and Stinson 1987)	13.07
Talpidae	*Parascalops breweri* (FMNH 199419)	16 (Hallett 1978)	51.11
	Scalopus aquaticus (FMNH 8227)	0 (ADW)	87.15
	Scapanus townsendii (FMNH 191513)	26.96 (Carraway et al. 1993)	135 (ADW)
	Talpa europaea (FMNH 6449)	0 (Funmilayo 1979)	87.53
Lagomorpha			
Leporidae	*Sylvilagus floridanus* (FMNH 7739)	100 (ADW)	1207.19
Ochotonidae	*Ochotona princeps* (Smith & Weston 1990)	100 (Dearing 1996)	157.63
Macroscelidea			
Macroscelididae	*Elephantulus brachyrhynchus* (FMNH 196582)	0 (Koontz & Roeper 1983, Leirs et al. 1995)	45.11
	Elephantulus rufescens (FMNH 153099)	37 (Hemming 1972)	52.78
	Macroscelides proboscideus (FMNH 121554)	2 (Kerley 1992)	38.64
	Petrodromus tetradactylus (Jennings & Rathbun 2001)	4.6 (Rathbun 1976)	201
Microbiotheria			
Microbio-theriidae	*Dromiciops gliroides* (Marshall 1978)	28.36 Meserve et al. 1988	25
Paucituberculata			
Caenolestidae	*Caenolestes fuliginosus* (FMNH 70842)	0.6 (Barkley & Whitaker 1984)	28.64
	Rhyncholestes raphanurus (Patterson & Gallardo 1987)	45.4 (Meserve 1981)	21.94
Pilosa			
Bradypodidae	*Bradypus pygmaeus* (Hayssen 2008)	100 (ADW)	3000 (ADW)
Primates			
Atelidae	*Alouatta seniculus* (FMNH 78455)	99.89 (Guillotin et al. 1994)	6398.31
	Ateles paniscus (FMNH 95500)	99.84 (Guillotin et al. 1994)	8697.25
Cebidae	*Cebus apella (Sapajus a.)* (FMNH 60751)	73.07 (Guillotin et al. 1994)	2758.38
	Saimiri sciureus (UMMZ 122657)	55.1 (Lima & Ferrari 2003)	749.47
Cercopithecidae	*Cercopithecus cephus* (FMNH 8774)	87.4 (Gautier-Hion et al. 1980)	3444.88
	Cercopithecus neglectus (FMNH 44281)	95.1 (Gautier-Hion et al. 1980)	5324.52
	Cercopithecus nictitans (FMNH 35139)	90.4 (Gautier-Hion et al. 1980)	5256.91
	Cercopithecus pogonias (FMNH 60184)	83.9 (Gautier-Hion et al. 1980)	3578.27
	Colobus guereza (FMNH 27046)	99.9 (Gautier-Hion et al. 1980)	9925.88
	Mandrillus sphinx (FMNH 135289)	96 (Gautier-Hion et al. 1980)	16685.06
	Miopithecus talapoin (FMNH 121359)	63.8 (Gautier-Hion et al. 1980)	1248.86
	Trachypithecus delacouri (Harding 2011)	100 (Workman & Dung 2009)	9850 (Nadler et al. 2003)
Galagidae	*Euoticus elegantulus* (FMNH 106571)	80 (Charles-Dominique 1974)	295.48
	Galago (Sciurocheirus) alleni (NMNH 084534)	74.49 (Charles-Dominique 1974)	266.03
	Galago demidoff (FMNH 81754)	29.29 (Charles-Dominique 1974)	66.04
Lorisidae	*Arctocebus calabarensis* (FMNH 99360)	14.14 (Charles-Dominique 1974)	258.01
	Perodicticus potto (FMNH 148987)	89.59 (Charles-Dominique 1974)	1081.81
	Loris lydekkerianus (L. tardigradus l.) (FMNH 82801)	4 (Nekaris & Rasmussen 2003)	254.06
Pitheciidae	*Callicebus personatus* (FMNH 52337)	100 (Kinzey & Becker 1983)	1390.8
	Cacajao calvus (FMNH 104590)	94.6 (Ayres 1989)	3421.04
	Chiropotes satanas (FMNH 46179)	87.6 (Norconk 1996)	2967.27
	Pithecia pithecia (UMMZ 98974)	97.17 (Norconk 1996)	1667.19
Tarsiidae	*Tarsius bancanus* (FMNH 76863)	0 (Niemitz 1979)	168.04

	Carlito syrichta (Tarsius s.) (UMMZ 95741)	0 (ADW)	115.91
Rodentia			
Caviidae	*Hydrochoerus hydrochaeris* (FMNH 34361)	100 (ADW)	48144.91
Heterocephalidae	*Heterocephalus glaber* (Jarvis & Sherman 2002)	100 (Jarvis & Sherman 2002)	39.36
Cricetidae	*Abrothrix longipilis* (FMNH 124023)	47.61 (Meserve et al. 1988)	38.86
	Abrothrix sanborni (FMNH 22722)	62.89 (Meserve et al. 1988)	24.7
	Akodon azarae (FMNH 29193)	46.82 (Ellis et al. 1998)	25.27
	Calomys laucha (FMNH 95142)	72.16 (Ellis et al. 1998)	14
	Calomys musculinus (FMNH 157316)	72.68 (Ellis et al. 1998)	20.2
	Geoxus valdivianus (FMNH 124062)	44.13 (Meserve et al. 1988)	30.8
	Irenomys tarsalis (FMNH 133144)	97.61 (Meserve et al. 1988)	43.15
	Loxodontomys micropus (FMNH 132656)	97.25 (Meserve et al. 1988)	70.76
	Microtus ochrogaster (FMNH 91173)	97.35 (Hahus and Smith 1990)	42.5
	Necromys obscurus (FMNH 35357)	56.93 (Ellis et al. 1998)	40.69
	Oligoryzomys flavescens (FMNH 162817)	58.43 (Ellis et al. 1998)	21.3
	Oligoryzomys longicaudatus (FMNH 22660)	85.72 (Meserve et al. 1988)	27.54
	Peromyscus attwateri (FMNH 137141)	68.96 (Schmidly 1974)	27.9
	Peromyscus leucopus (FMNH 201360)	62.29 (Whitaker 1966, Hahus & Smith 1990)	18.07
	Phyllotis darwini (FMNH 119491)	94.53 (Meserve 1981)	50.82
Heteromyidae	*Chaetodipus baileyi* (FMNH 52831)	91.1 (Reichman 1975)	28.44
	Chaetodipus intermedius (FMNH 47874)	83.8 (Reichman 1975)	14.94
	Perognathus amplus (FMNH 140707)	96.3 (Reichman 1975)	11.97
Muridae	*Acomys cahirinus* (FMNH 101313)	92.99 (Hemming 1972)	41.16
	Acomys dimidiatus (A. cahirinus d.) (FMNH 74602)	87 (Varty 1990)	90 (Nowak 1999)
	Aethomys chrysophilus (FMNH 171507)	95.8 (Monadjem 1997)	80.85
	Aethomys (Micaelamys) namaquensis (FMNH 28902)	100 (Langham 1983)	57.1
	Arvicanthis niloticus (FMNH 107013)	99.9 (Hemming 1972)	95.8
	Batomys salomonseni (FMNH 92825)	100 (Heaney et al. 2006)	185.76
	Gerbilliscus leucogaster (FMNH 27313)	75.1 (Monadjem 1997)	73.75
	Gerbilliscus robustus (FMNH 164073)	85.8 (Hemming 1972)	95.99
	Gerbillurus paeba (Perrin et al. 1999)	91.59 (Perrin et al. 1999)	25.91
	Grammomys dolichurus (FMNH 158661)	98 (Varty 1990)	41.85
	Lemniscomys rosalia (FMNH 158039)	100 (Monadjem 1997)	49.92
	Lorentzimys nouhuysi (NMNH 585615)	61.13 (Jackson & Woolley 1993)	14.44
	Mastomys natalensis (FMNH 153963)	90.5 (Langham 1983, Monadjem 1997)	41.85
	Maxomys surifer (FMNH 108963)	59.06 (Monadjem 1997)	150.48
	Mus minutoides (FMNH 177918)	91.19 (Langham 1983, Kerley 1992)	6.43
	Myotomys (Otomys) unisulcatus (NMNH 343785)	100 (Kerley 1992)	102.5
	Otomys angoniensis (FMNH 174177)	100 (Langham 1983)	100.64
	Otomys irroratus (FMNH 25801)	100 (Langham 1983)	114.45
	Pseudohydromys murinus (Helgen & Helgen 2009)	33.7 (Jackson & Woolley 1993)	16.79
	Pseudohydromys occidentalis (Helgen & Helgen 2009)	0.5 (Jackson & Woolley 1993)	21.9
	Rattus rattus (FMNH 122570)	99.6 (Langham 1983)	142.68
	Rhabdomys pumilio (FMNH 214824)	94.53 (Kerley 1992)	40.73
	Rhynchomys tapulao (Balete et al. 2007)	0 (Balete et al. 2007)	234.55**
	Taterillus harringtoni (FMNH 66751)	97.69 (Hemming 1972)	124.85***
Nesomyidae	*Dendromus mesomelas (nyasae)* (FMNH 144350)	98.7 (Langham 1983)	10.2
	Dendromus mystacalis (FMNH 159414)	83.8 (Langham 1983)	8.17
	Malacothrix typical (FMNH 38558)	88.2 (Kerley 1992)	17.02

	Saccostomus campestris (FMNH 36895)	100 (Langham 1983)	50.33
	Saccostomus mearnsi (FMNH 43448)	97 (Varty 1990)	64.91
	Steatomys pratensis (FMNH 81859)	100 (Langham 1983)	30.58
Ctenomyidae	*Ctenomys mendocinus* (Rosi et al. 2005)	100 (Torres-Mura et al. 1989)	178.44
Octodontidae	*Octodon degus* (FMNH 119647)	96.18 (Meserve et al. 1983)	203.27
	Tympanoctomys barrerae (Diaz et al. 2000)	100 (Torres-Mura et al. 1989)	86.02
Sciuridae	*Callosciurus melanogaster* (NMNH 252410)	36.08 (Whitten 1981)	296
	Callospermophilus lateralis (Spermophilus l.) (FMNH 4855)	91.99 (Tevis 1953)	175.1
	Cynomys ludovicianus (Hoogland 1996)	100 (Wydeven & Dahlgren 1982)	797.05
	Epixerus ebii (FMNH 62225)	98.4 (Emmons 1980, Gautier-Hion et al. 1980)	520.96
	Funisciurus anerythrus (FMNH 149420)		223.54
	Funisciurus pyrropus (FMNH 148995)	80.5 (Emmons 1980)	
		86.9 (Emmons 1980)	243.18
	Heliosciurus rufobrachium (FMNH 43560)	95.47 (Emmons 1980)	332.88
	Lariscus obscurus (L. insignis o.) (FMNH 43551)	78.22 (Whitten 1981)	241.19
	Myosciurus pumilio (FMNH 46996)	63.2 (Emmons 1980, Gautier-Hion et al. 1980)	16.44
	Paraxerus poensis (FMNH 8305)	88.85 (Emmons 1980, Gautier-Hion et al. 1980)	100
	Protoxerus stangeri (FMNH 223556)	99.68 (Emmons 1980, Gautier-Hion et al. 1980)	630.43
	Sundasciurus lowii (FMNH 76880)	59.79 (Whitten 1981)	84.99
	Tamias amoenus (FMNH 135218)	79.17 (Tevis 1953)	50.63
	Tamias quadrimaculatus (FMNH 7648)	93 (Tevis 1953)	83.62
	Tamias speciosus (Best et al. 1994)	84 (Tevis 1953)	60.83
	Tamias townsendii (FMNH 9000)	92 (Tevis 1953)	79.12
	Xerus rutilus (FMNH 153116)	95 (Hemming 1972, O'Shea 1991)	316.96
Dipodidae	*Napaeozapus insignis* (FMNH 200127)	81 (Whitaker 1963)	22.25
Scandentia			
Tupaiidae	*Tupaia glis* (FMNH 98462)	33.5 (Langham 1983)	132.43
Tubulindentata			
Orycteropodidae	*Orycteropus afer* (FMNH 99431)	0 (Taylor et al. 2002)	56175.2
Cingulata			
Dasypodidae	*Chaetophractus vellerosus* (FMNH 54352)	37.96 (Greegor 1980)	930.16
	Dasypus novemcinctus (FMNH 84244)	2.5 (Whitaker 1963)	3949.01
Hyracoidea			
Procaviidae	*Procavia capensis* (Olds & Shoshani 1982)	100 (ADW)	2952.48

*Diet data from Nogueira et al. (2009) and Gonçalves et al. (2007) are estimates based on dietary ranges provided in the sources.

**Body mass of *Rhynchomys tapulao* is based on that of a sister species, *R. soricoides*, which has skull dimensions that are very similar to that of *R. tapulo* (Balete et al. 2007). The body mass of *R. soricoides* is from PanTHERIA (Jones et al. 2009).

***Body mass of *Taterillus harringtoni* was estimated using a skull length measurement (36 mm) and a regression equation in Millien & Bovy (2010).

APPENDIX E

Jaw measurements of modern mammals from Chapter 3. The jaw measurement numbers correspond to those shown in Figure 3.1, and the measurements are described in Table 3.1. Measurements 1-12 are linear measurements that are measured in millimeters (mm). Measurement 13 is the joint-angular process (JAPr) angle (in degrees), which was used in evolutionary modeling analyses (Table 3.6, Fig. 3.4C). Species are in the same order as in Appendix D. See Appenidix D for taxonomic information and full species names.

	Jaw measurement												
Species	**1**	**2**	**3**	**4**	**5**	**6**	**7**	**8**	**9**	**10**	**11**	**12**	**13**
Eremitalpa g.	12.15	6.82	1.23	2.47	2.03	2.04	2.23	1.18	7.09	4.79	3.74	4.79	32.71
Hemicentetes n.	31.22	17.75	4.23	3.19	6.39	2.75	2.75	1.94	17.55	5.99	4.96	6.10	19.03
Potamogale v.	37.02	21.16	9.02	1.96	8.99	4.62	4.95	3.33	20.86	9.46	5.47	6.77	18.33
Aepyceros m.	215.17	125.47	58.31	41.23	74.07	31.42	23.23	10.77	130.51	37.65	55.91	76.72	31.93
Ammotragus l.	232.19	138.99	60.16	46.87	79.91	29.45	26.67	15.27	145.09	34.53	52.05	88.03	29.74
Antidorcas m.	177.56	108.19	53.33	53.74	86.77	19.68	21.29	8.64	119.49	33.52	50.10	78.27	33.75
Cephalophus c.	150.91	73.71	37.88	27.57	45.60	25.02	18.69	8.22	77.38	20.37	36.31	53.80	38.40
Cephalophus d.	138.71	72.12	36.77	32.35	53.91	22.72	20.04	8.47	77.72	22.19	41.83	56.23	39.10
Cephalophus l.	143.86	70.56	36.42	33.81	50.49	28.80	19.83	9.00	76.90	17.48	46.18	63.40	46.16
Cephalophus n.	133.28	62.02	33.36	25.95	45.17	19.23	15.49	7.94	66.14	19.11	33.91	45.31	38.13
Cephalophus s.	219.92	107.91	58.96	52.46	80.51	43.19	33.02	14.41	118.86	29.14	74.05	97.55	45.20
Philantomba m.	94.24	48.00	25.29	20.13	33.24	12.99	10.98	6.98	51.10	13.37	23.33	32.68	34.23
Tragelaphus s.	220.01	110.13	52.81	46.18	87.27	34.27	30.30	13.86	118.77	41.54	60.68	88.37	37.99
Tayassu p.	155.62	90.00	43.91	32.84	42.68	30.75	31.76	7.89	92.43	23.08	36.70	68.09	35.78
Hyemoschus a.	105.79	52.26	29.66	30.98	39.19	8.93	14.84	6.99	60.40	13.56	26.13	41.36	33.49
Canis lupus d.	140.84	80.42	32.38	10.44	36.10	18.80	21.11	11.19	79.26	30.75	24.17	30.11	19.96
Canis m.	113.84	63.59	29.44	9.08	28.77	12.75	14.39	10.21	62.23	24.21	16.40	22.43	19.11
Otocyon m.	90.67	55.66	23.77	9.69	21.93	8.24	10.63	5.85	55.02	15.51	13.40	19.55	17.69
Urocyon c.	89.26	52.64	22.78	9.66	24.65	7.73	11.00	6.58	52.49	17.41	12.97	18.29	17.81
Vulpes l.	84.18	44.92	19.08	8.61	23.58	6.66	12.09	6.38	44.80	17.19	12.71	16.14	17.10
Vulpes v.	98.13	54.43	20.98	12.31	30.65	5.09	14.25	7.84	55.43	22.64	12.42	18.67	15.04
Lynx r.	83.98	49.29	10.62	1.54	21.32	14.59	15.35	6.38	48.00	21.69	13.01	17.46	18.07
Helogale h.	34.26	19.49	7.28	3.34	10.21	3.72	5.64	2.82	19.18	9.18	5.75	7.27	18.72
Crocuta c.	163.59	86.33	27.39	2.21	46.54	28.79	36.41	15.29	83.84	47.99	25.08	30.41	18.85
Galictis v.	49.60	31.08	13.50	1.10	13.78	7.77	8.38	4.17	30.42	14.44	7.07	8.83	15.88
Martes m.	59.08	35.26	13.51	1.40	17.77	8.02	8.72	4.72	34.06	18.66	7.85	10.73	14.68
Martes f.	55.60	32.63	12.41	1.83	16.07	7.76	8.64	4.51	32.12	16.79	8.19	10.06	16.62
Meles m.	82.81	54.78	21.33	8.74	27.91	4.68	14.98	5.45	54.00	25.74	11.51	16.94	14.76
Mustela n.	21.74	13.62	5.81	0.09	7.10	3.09	3.67	2.07	13.16	7.59	3.42	5.25	12.94
Nandinia b.	81.23	46.16	10.82	6.82	25.49	9.80	14.95	3.81	46.63	22.90	14.45	17.72	18.24
Lobodon c.	180.62	130.89	51.27	17.13	37.82	21.85	29.60	13.40	130.91	31.03	36.25	47.16	15.26
Procyon l.	68.74	43.42	17.34	11.17	28.04	3.61	9.38	4.57	44.33	19.24	12.34	17.54	17.93
Potos f.	54.62	33.92	9.65	4.30	19.06	20.62	12.39	1.89	33.36	16.77	11.84	27.37	47.40
Ursus a.	226.33	151.93	64.62	19.15	74.57	25.01	44.19	12.16	150.24	67.67	30.27	50.73	14.57
Genetta g.	57.86	32.19	11.32	5.60	17.34	6.04	8.07	4.88	31.94	13.48	9.54	11.65	19.64
Hipposideros d.	19.52	14.02	7.50	2.35	5.41	1.98	3.25	2.04	14.12	5.04	3.06	4.33	16.57
Lavia f.	16.58	12.33	6.26	1.40	3.86	1.00	1.78	1.73	12.26	4.52	2.09	2.56	10.57
Pteronotus p.	15.23	10.86	6.12	3.90	2.92	0.00	2.44	1.47	11.34	3.66	2.82	3.65	16.69
Noctilio l.	17.86	14.69	7.86	3.70	4.23	2.19	3.46	2.02	14.81	4.23	3.41	6.38	20.97
Noctilio a.	14.01	11.50	5.94	3.14	3.37	2.11	2.84	1.39	11.51	3.47	3.07	5.49	23.99
Artibeus j.	18.56	14.59	6.61	1.56	5.43	3.40	3.11	1.39	14.29	5.56	3.62	5.17	19.50
Artibeus o.	16.99	12.43	5.18	1.19	4.34	2.77	2.28	1.79	12.22	5.28	2.81	4.56	18.91
Chiroderma d.	18.47	13.74	6.20	1.63	5.58	3.47	2.92	1.89	13.61	5.75	3.74	5.40	21.60
Vampyrodes c.	15.41	10.72	5.17	2.18	4.00	1.32	2.01	1.33	10.69	3.98	2.66	3.54	17.55

Micronycteris h.	11.56	8.19	4.09	1.14	2.19	1.10	1.37	1.14	8.12	2.73	1.82	2.29	15.09
Micronycteris m.	14.11	10.79	4.04	0.98	3.59	2.43	2.21	0.84	10.68	4.30	2.39	3.86	18.23
Sturnira l.	16.57	12.39	6.20	2.51	5.37	1.52	2.54	1.80	12.44	4.85	3.34	4.19	17.33
Lophostoma s.	27.97	19.90	9.51	3.03	8.72	3.28	4.18	2.81	19.91	8.35	5.39	6.46	17.81
Phyllostomus h.	18.39	13.85	7.06	2.23	5.06	2.45	2.55	2.13	13.77	4.92	3.58	4.88	18.60
Phyllostomus e.	15.86	12.08	5.01	0.75	2.75	1.98	1.74	0.73	11.95	3.63	2.43	2.88	12.90
Erophylla s.	12.67	8.56	3.36	2.32	2.59	0.04	1.64	0.55	8.73	3.05	1.94	2.20	13.74
Monophyllus r.	12.29	8.11	3.15	1.97	2.77	0.53	1.37	0.57	8.24	3.08	1.89	2.65	16.24
Glossophaga s.	15.13	11.12	4.64	1.07	3.72	0.62	1.98	1.00	10.77	4.15	2.49	3.24	16.11
Carollia p.	14.49	11.12	5.02	1.07	3.80	1.82	2.45	1.08	10.83	4.78	2.39	3.19	14.10
Uroderma b.	16.32	12.34	5.95	1.33	3.89	1.94	2.56	1.15	12.00	4.32	2.83	3.82	14.85
Platyrrhinus l.	14.30	10.04	5.41	2.11	4.17	0.76	1.39	1.70	10.13	3.35	2.00	2.90	15.94
Macrotus c.	33.83	24.04	11.46	1.37	5.74	5.16	4.75	4.20	23.63	8.91	5.35	6.77	15.62
Vampyrum s.	64.04	40.36	15.10	5.99	19.81	12.89	7.26	4.08	39.96	16.61	10.70	21.07	29.23
Acerodon j.	18.56	14.59	6.61	1.56	5.43	3.40	3.11	1.39	14.29	5.56	3.62	5.17	19.50
Cynopterus s.	26.42	17.26	4.37	3.15	9.55	4.07	3.63	1.27	17.48	6.61	4.62	8.36	23.39
Pteropus a.	49.22	30.68	10.76	3.45	11.98	8.36	5.85	2.32	30.22	9.79	7.47	14.49	23.81
Myotis l.	10.00	6.60	3.31	1.98	2.52	0.05	1.31	0.91	6.76	2.13	1.65	2.05	16.12
Myotis vi.	15.67	10.16	5.53	3.29	4.07	0.10	1.75	1.68	10.59	3.40	2.54	3.21	15.76
Myotis ve.	12.59	8.67	4.30	2.00	3.07	0.60	1.58	1.32	8.74	3.17	1.99	2.60	16.15
Nycticeius h.	10.74	8.07	3.82	2.61	3.14	0.03	1.69	1.11	8.31	2.98	2.18	2.65	16.65
Dasyurus m.	72.37	53.93	23.67	6.70	20.62	8.35	8.43	6.06	53.07	19.64	10.45	19.06	15.38
Thylacinus c.	153.46	108.38	47.24	8.51	34.24	17.50	17.50	12.32	106.25	31.62	18.72	40.06	13.64
Myrmecobius f.	43.05	22.80	10.00	5.58	9.04	3.66	4.09	1.35	23.05	3.93	8.37	9.61	22.39
Cynocephalus v.	50.77	28.91	12.66	2.16	6.75	17.10	7.88	3.58	27.81	9.94	14.17	20.20	42.97
Galeopterus v.	47.03	24.42	10.54	2.30	5.71	13.99	7.44	2.38	23.07	7.46	11.33	17.39	43.88
Caluromys p.	38.86	26.22	10.19	4.09	11.94	6.85	5.72	1.96	26.10	7.88	7.63	11.94	23.90
Marmosa d.	32.78	22.70	9.57	4.83	11.16	2.14	4.31	1.88	22.99	7.16	5.45	9.11	14.99
Marmosa x.	21.40	14.53	6.92	4.58	8.03	0.77	2.32	1.67	15.07	4.62	3.84	6.28	17.55
Didelphis a.	65.13	42.50	20.83	11.02	21.31	2.53	7.34	4.13	43.27	12.89	9.09	16.13	15.39
Cercartetus c.	15.77	12.71	5.57	1.67	5.92	3.82	2.94	1.24	12.55	4.55	4.89	5.82	25.25
Thylogale s.	64.10	46.45	22.16	20.84	31.58	7.36	11.62	4.42	49.99	16.16	17.36	31.92	27.63
Macropus g.	122.77	85.95	46.99	52.14	72.68	18.54	26.36	9.36	100.98	32.19	39.70	79.56	33.15
Phascolarctos c.	104.29	77.51	31.07	39.49	50.91	22.14	23.69	4.53	86.48	16.03	30.93	65.56	37.80
Pseudocheirus p.	37.16	31.13	16.55	7.98	16.29	7.38	7.95	2.46	31.54	10.94	13.34	15.67	26.40
Vombatus u.	113.62	80.86	38.94	26.58	36.46	18.29	27.79	5.00	83.08	19.38	30.15	48.45	24.76
Erinaceus e.	40.50	29.62	12.19	11.45	16.21	1.86	6.78	2.76	31.24	10.65	10.55	13.05	20.97
Podogymnura t.	28.90	18.69	8.25	4.56	7.89	0.72	3.00	2.06	19.02	5.54	4.88	5.85	16.44
Blarina b.	11.75	10.61	5.07	2.96	5.16	1.46	2.08	1.28	10.70	4.33	4.14	4.45	23.12
Crocidura f.	14.03	11.76	5.35	2.73	6.06	2.27	2.48	1.78	11.98	5.18	4.62	5.02	23.55
Crocidura m.	9.67	8.24	3.96	1.83	3.60	1.48	1.42	1.24	8.28	3.24	3.16	3.37	22.45
Myosorex c.	10.61	8.94	4.27	2.64	4.70	1.07	1.78	1.27	9.05	3.46	3.78	3.95	23.32
Myosorex v.	11.43	9.58	4.41	2.27	4.80	1.76	1.67	1.41	9.66	3.99	3.74	4.09	23.30
Sorex h.	7.56	6.01	3.16	1.35	2.76	0.95	0.86	0.93	6.10	2.09	2.39	2.48	21.85
Sorex p.	10.63	8.61	4.10	2.16	4.05	1.38	1.58	1.31	8.56	3.67	3.39	3.56	23.13
Parascalops b.	19.14	14.58	6.67	4.60	6.05	0.95	1.93	2.13	14.85	5.64	4.99	5.70	21.04
Scalopus a.	23.35	18.24	8.04	7.23	8.93	0.13	3.49	2.51	19.49	6.46	4.79	7.45	18.94
Scapanus t.	25.84	18.96	8.73	6.30	8.18	1.86	2.62	2.69	19.77	6.99	5.93	8.33	22.85
Talpa e.	20.66	14.39	6.37	4.81	6.25	0.74	2.06	1.75	14.85	5.81	4.87	5.55	20.52
Sylvilagus f.	50.76	28.70	8.16	16.36	11.45	15.59	13.06	2.29	28.79	7.31	22.53	33.91	62.26
Ochotona p.	20.91	13.73	6.22	13.44	7.02	4.68	6.41	2.27	18.82	7.29	13.94	18.36	50.37
Elephantulus b.	24.25	12.81	5.82	7.77	8.15	1.71	2.92	1.69	14.90	2.34	6.40	9.67	32.93
Elephantulus r.	24.35	13.21	4.21	8.11	8.94	2.49	3.30	1.38	14.79	2.34	6.97	11.03	37.58
Macroscelides p.	20.84	13.72	6.89	11.17	11.00	1.41	2.94	1.83	17.53	3.20	8.86	12.68	39.15
Petrodromus t.	41.21	27.11	10.96	11.52	12.60	5.74	5.17	2.90	28.99	5.31	12.18	18.18	34.08
Dromiciops g.	21.13	14.66	5.74	3.54	6.13	2.35	2.37	1.22	15.09	3.68	5.75	6.08	21.99
Caenolestes f.	20.60	15.40	6.79	4.35	7.53	0.96	2.53	1.12	15.65	4.96	4.69	5.75	18.93
Rhyncholestes r.	24.09	17.44	8.08	5.67	8.81	0.97	2.74	1.37	17.91	5.08	5.83	6.75	20.62
Bradypus p.	45.21	32.03	9.14	8.15	15.42	13.44	11.24	4.32	31.90	10.53	16.26	21.49	36.15
Alouatta s.	83.48	56.28	22.90	27.44	25.57	32.19	18.67	4.07	59.92	20.52	29.49	61.87	60.41
Ateles p.	73.44	50.04	15.19	13.88	19.48	25.07	18.00	3.19	50.36	17.56	25.96	42.00	44.79
Cebus a.	67.27	43.42	12.66	17.40	24.62	22.68	17.61	2.54	46.39	17.64	28.07	40.76	47.12

Saimiri s.	36.69	26.31	8.91	8.45	11.35	9.11	8.89	2.60	26.57	10.26	13.25	18.24	35.31
Cercopithecus c.	64.41	45.09	15.80	17.75	23.51	16.37	15.93	3.91	46.95	14.46	21.65	35.58	38.41
Cercopithecus ne.	80.43	55.09	20.13	19.21	26.26	16.46	20.17	4.86	57.11	18.29	20.08	39.28	30.57
Cercopithecus ni.	76.57	54.58	18.59	17.04	25.23	19.37	16.96	3.93	55.69	16.37	23.15	39.12	35.87
Cercopithecus p.	52.78	36.52	16.57	15.37	17.53	12.95	13.34	3.99	38.91	12.46	16.86	30.83	37.90
Colobus g.	81.07	56.47	23.21	22.36	24.87	19.66	21.37	6.01	59.80	22.01	27.28	44.62	35.33
Mandrillus s.	174.37	122.11	38.36	34.26	52.35	28.33	44.91	9.27	123.57	31.66	34.65	75.49	21.32
Miopithecus t.	39.67	28.24	11.09	9.70	12.82	8.53	10.17	2.47	28.59	10.13	14.24	18.81	31.07
Trachypithecus d.	64.45	47.56	20.75	19.89	25.18	30.15	20.36	5.06	48.31	12.94	26.68	51.66	59.76
Euoticus e.	27.95	20.53	7.58	3.64	8.59	5.84	4.54	1.80	20.69	5.52	7.49	10.05	26.22
Galago a.	30.43	25.27	11.90	5.54	10.30	4.38	4.09	1.92	25.31	5.25	7.49	10.01	24.23
Galago d.	19.78	14.77	5.90	3.25	7.54	3.25	3.37	1.19	14.98	4.68	4.47	6.71	23.65
Arctocebus c.	32.73	25.77	10.31	5.41	9.91	6.19	5.35	1.98	25.93	6.20	8.62	12.21	24.76
Perodicticus p.	41.08	31.55	10.61	5.21	14.61	11.29	7.83	2.18	31.58	11.55	12.03	17.17	30.31
Loris l.	25.16	19.39	9.71	3.34	6.53	4.10	4.49	2.29	19.06	4.89	4.90	8.54	20.83
Callicebus p.	42.18	29.81	11.17	12.00	17.29	17.27	11.38	2.37	31.13	7.83	18.56	31.13	56.90
Cacajao c.	42.95	28.77	11.81	10.96	13.60	10.16	10.44	2.87	30.10	7.10	11.22	23.74	35.42
Chiropotes s.	54.73	34.91	10.45	9.76	14.64	25.10	18.74	2.10	34.82	10.73	15.99	38.99	62.54
Pithecia p.	43.61	32.26	13.24	10.12	14.00	12.97	12.09	2.67	32.80	9.37	17.14	25.09	36.87
Tarsius b.	27.28	20.94	9.52	6.48	6.77	4.65	4.20	2.51	20.69	4.05	9.24	11.19	29.59
Carlito s.	23.26	18.61	8.26	5.47	6.01	4.45	3.82	2.35	17.92	3.47	7.95	10.05	30.71
Hydrochoerus h.	156.61	94.80	55.59	13.04	13.82	68.55	35.17	6.76	82.07	38.57	68.90	81.76	54.82
Heterocephalus g.	19.18	13.02	3.88	5.39	6.74	5.13	5.29	0.89	13.03	5.80	8.06	10.60	41.04
Abrothrix l.	13.44	10.22	4.16	2.52	3.14	2.64	2.70	0.72	10.12	2.96	4.56	5.24	27.72
Abrothrix s.	12.20	9.11	3.73	2.08	2.56	2.22	2.58	0.72	9.04	3.26	3.76	4.52	25.34
Akodon a.	12.16	9.31	4.13	2.38	3.09	2.93	3.10	0.69	9.08	2.44	4.42	5.57	30.94
Calomys l.	9.98	7.09	2.96	2.30	2.93	1.83	3.09	0.50	7.18	1.76	3.32	4.20	27.63
Calomys m.	12.01	8.72	3.36	3.62	4.24	2.31	3.64	0.68	8.99	2.33	4.75	5.91	31.90
Geoxus v.	14.16	10.79	3.41	2.74	3.01	2.70	2.38	0.59	10.19	3.05	4.91	5.67	29.89
Irenomys t.	13.86	10.76	4.90	3.62	3.64	2.79	3.76	0.85	10.73	3.88	5.29	6.93	28.68
Loxodontomys m.	16.03	12.26	5.38	5.72	5.45	2.13	4.80	1.11	12.38	4.14	6.35	8.23	31.77
Microtus o.	14.50	10.51	5.00	6.82	7.19	1.66	4.20	0.90	11.86	3.48	5.94	8.58	33.01
Necromys o.	14.75	11.23	4.81	3.58	4.17	3.36	3.77	0.79	11.06	3.78	5.60	7.14	32.25
Oligoryzomys f.	11.61	8.80	3.22	3.08	3.31	2.26	3.37	0.58	8.84	3.32	4.17	5.54	29.20
Oligoryzomys l.	12.16	9.11	3.56	3.42	3.65	2.31	3.74	0.63	9.17	3.55	4.38	5.84	29.37
Peromyscus a.	13.64	10.55	3.91	3.86	3.07	2.47	3.66	0.63	10.79	4.61	5.26	6.64	28.31
Peromyscus l.	12.93	10.07	3.73	3.40	3.06	2.12	3.34	0.68	10.09	4.13	4.68	5.73	26.39
Phyllotis d.	15.53	11.77	4.93	4.28	4.35	3.32	4.69	0.87	11.73	3.88	5.88	7.90	30.88
Chaetodipus b.	13.45	8.47	2.72	3.80	3.34	2.30	3.76	0.67	8.82	2.64	3.06	6.49	29.11
Chaetodipus i.	10.75	6.85	2.47	1.99	2.22	2.35	2.70	0.71	6.75	2.32	2.54	4.94	31.08
Perognathus a.	10.50	6.68	2.18	2.47	2.28	1.99	2.56	0.64	6.79	2.25	2.37	5.14	30.72
Acomys c.	15.68	11.64	4.16	2.36	2.73	4.12	3.47	0.77	11.11	3.60	5.57	6.68	32.22
Acomys d.	16.36	12.08	3.90	2.15	2.95	4.78	4.35	0.76	11.30	4.45	5.87	7.32	33.05
Aethomys c.	19.39	14.90	5.81	3.69	4.93	5.66	5.26	1.17	14.10	3.21	7.77	9.83	36.07
Aethomys n.	15.41	12.32	4.78	2.47	3.94	4.63	4.08	0.67	12.01	3.48	6.02	7.75	33.12
Arvicanthis n.	21.97	16.52	6.27	4.59	6.63	7.21	7.54	1.11	15.74	3.73	8.41	12.31	36.92
Batomys s.	22.22	17.16	7.91	4.49	4.22	5.95	5.90	1.33	16.48	6.23	8.49	10.95	33.49
Gerbilliscus l.	21.96	16.26	7.99	3.85	4.21	4.70	4.76	1.52	15.69	3.27	6.61	9.29	29.65
Gerbilliscus r.	29.53	21.66	7.49	5.84	4.62	6.56	7.42	1.69	21.11	6.72	9.24	13.38	29.94
Gerbillurus p.	15.77	12.30	4.90	3.41	3.29	5.08	3.99	0.97	12.16	3.49	6.20	9.77	41.18
Grammomys d.	16.86	12.49	4.35	2.75	4.33	5.09	4.38	1.00	11.84	3.23	6.45	8.31	36.38
Lemniscomys r.	18.25	13.83	6.13	2.53	3.90	6.01	4.53	1.08	13.40	3.41	6.54	9.19	36.92
Lorentzimys n.	10.39	7.49	2.06	1.59	1.87	3.25	3.10	0.35	7.17	3.27	4.25	5.22	35.74
Mastomys n.	16.26	11.83	4.41	2.61	3.53	4.58	3.83	0.93	11.25	2.03	6.38	7.21	34.55
Maxomys s.	22.07	16.36	5.98	4.60	5.41	5.15	5.62	1.11	16.17	4.76	7.19	10.56	31.06
Mus m.	10.04	7.46	3.19	1.61	2.21	2.30	2.00	0.62	7.21	2.37	3.65	4.20	30.16
Myotomys u.	22.26	16.90	7.28	5.00	6.77	6.54	6.10	1.52	17.11	5.85	8.11	12.24	36.70
Otomys a.	20.97	16.59	7.30	5.34	7.11	6.02	6.19	1.35	16.77	5.46	8.35	12.94	35.28
Otomys i.	21.37	16.34	7.96	4.81	6.54	6.69	6.11	1.37	16.54	4.72	8.45	12.69	38.18
Pseudohydromys m.	11.88	9.13	2.98	1.29	1.84	3.29	2.15	0.75	8.60	3.24	4.09	4.68	30.87
Pseudohydromys o.	12.40	9.14	2.89	1.59	2.24	3.42	2.40	0.55	8.81	4.19	4.81	5.43	33.75
Rattus r.	18.24	13.37	6.54	3.63	4.63	4.36	4.93	1.04	13.06	3.94	6.31	8.28	31.18

Rhabdomys p.	25.71	15.92	2.53	3.49	3.76	3.13	2.69	0.66	15.38	3.15	6.48	6.70	24.73
Rhynchomys t.	14.25	10.92	4.60	3.12	4.60	4.18	4.25	0.73	10.75	3.08	5.84	7.48	35.07
Taterillus h.	18.49	13.84	4.90	4.08	4.07	4.07	4.63	1.03	13.26	2.76	5.55	8.92	30.92
Dendromus me.	11.18	8.13	3.18	1.73	2.27	2.71	2.25	0.76	7.86	2.90	3.64	4.82	31.97
Dendromus my.	10.49	8.08	3.06	2.05	2.71	2.69	2.47	0.61	7.94	2.94	3.71	4.90	32.46
Malacothrix t.	12.70	9.35	3.05	0.98	1.81	3.99	2.83	1.02	8.87	3.35	3.35	5.60	34.03
Saccostomus c.	22.12	15.91	5.15	5.80	8.56	6.72	7.40	0.94	15.94	5.25	9.82	13.21	38.48
Saccostomus m.	24.29	17.62	6.65	6.42	9.80	6.91	6.59	1.26	17.25	6.91	11.10	13.41	40.53
Steatomys p.	16.26	12.19	4.16	2.68	4.19	4.62	3.74	0.91	11.96	3.10	6.06	7.56	34.01
Ctenomys m.	29.09	22.16	7.97	8.76	8.49	7.68	10.58	2.27	22.10	6.92	15.49	17.19	33.05
Octodon d.	24.34	16.83	6.54	5.54	5.13	5.12	6.10	1.28	16.21	5.64	10.56	11.65	32.80
Tympanoctomys b.	22.17	16.28	5.50	4.22	5.09	6.83	6.76	0.93	16.14	5.10	11.30	11.40	36.80
Callosciurus m.	31.81	22.04	7.33	6.24	7.76	10.53	8.13	1.32	21.56	8.28	12.07	18.14	44.93
Callospermophilus l.	25.93	17.06	6.44	4.47	7.33	6.70	5.85	1.50	16.84	4.86	7.08	12.39	37.20
Cynomys l.	39.50	26.15	11.58	4.65	8.66	15.03	9.87	4.03	24.24	8.79	14.60	21.50	50.48
Epixerus e.	40.14	27.08	8.17	6.70	10.69	13.96	11.50	1.60	26.51	10.31	16.42	22.26	42.75
Funisciurus a.	26.87	18.23	6.47	4.23	6.84	8.57	6.27	1.64	17.79	5.24	10.77	14.43	43.41
Funisciurus p.	27.68	18.30	6.22	3.14	5.10	8.50	5.84	1.43	17.62	3.97	9.87	13.41	41.56
Heliosciurus r.	29.78	21.47	7.50	5.90	8.43	11.14	8.11	1.50	21.14	6.01	14.00	17.67	45.56
Lariscus o.	29.42	19.54	6.61	5.67	7.71	4.16	7.35	1.42	19.34	6.44	10.52	15.80	41.22
Myosciurus p.	12.23	8.71	2.45	2.40	1.81	3.88	4.05	0.47	8.18	4.19	5.30	6.57	36.92
Paraxerus p.	19.15	13.43	4.50	4.03	6.08	5.84	4.42	0.99	13.35	2.88	7.07	10.67	42.57
Protoxerus s.	37.30	25.45	8.33	5.60	10.06	13.40	11.25	1.48	24.64	8.84	14.25	20.80	42.25
Sundasciurus l.	23.03	15.89	5.26	5.28	6.15	5.71	5.17	1.23	15.88	5.40	8.19	11.73	37.62
Tamias a.	17.87	11.86	3.57	3.01	4.95	5.89	3.95	0.81	11.66	4.33	5.39	9.50	44.88
Tamias q.	20.25	13.58	4.38	2.63	4.85	6.37	4.36	1.00	13.31	5.01	6.63	9.98	41.13
Tamias s.	18.61	12.25	4.04	2.03	3.92	6.61	4.29	0.91	11.70	4.67	6.50	9.42	44.97
Tamias t.	21.21	14.14	4.89	3.28	5.70	2.99	4.91	1.01	13.91	4.67	6.75	10.88	41.00
Xerus r.	30.66	21.48	8.26	5.05	6.43	9.54	7.38	2.18	21.20	6.95	10.50	15.15	39.40
Napaeozapus i.	11.65	8.72	3.78	2.04	3.14	3.38	3.02	0.69	8.49	2.79	3.81	6.06	36.33
Tupaia g.	32.24	20.64	9.26	5.31	9.33	3.44	3.62	2.58	21.16	4.63	6.94	8.84	23.12
Orycteropus a.	181.53	91.71	36.31	42.95	68.04	20.13	15.12	6.36	101.69	28.58	29.53	70.16	36.99
Chaetophractus v.	46.83	23.49	9.38	16.03	20.76	6.06	7.43	2.50	27.78	8.50	14.30	23.46	40.55
Dasypus n.	80.56	40.25	8.40	10.19	20.37	4.00	6.92	1.34	41.06	11.86	7.37	17.81	17.36
Procavia c.	66.18	42.43	24.56	24.04	25.48	27.18	17.50	5.55	47.25	17.55	23.59	51.82	62.25

APPENDIX F

Jaw-angular process (JAPr) angles, geologic ages, and dietary assignments for fossil species from Chapter 3. These data are displayed in Figure 3.5. See Table 3.1 (and Figure 3.1) for a description of the JAPr angle. First and last fossil appearances (i.e., FADs and LADs, respectively), are based on vetted information from the Paleobiology Database (www.paleobiodb.org) and Grossnickle and Newham (2016). The analysis on fossil JAPr angles (Fig. 3.5) does not include taxa younger than the Eocene-Oligocene boundary (i.e., 33.9 Ma). Thus, LADs for fossil ranges that are much younger than this and extend into the Miocene are simply recorded as 'Miocene' in the LAD column. Diets of fossil genera given in the Paleobiology Database are listed in the 'PBDB diet' column. Based on these diets, I assigned fossils to one of three dietary groups (carnivore, omnivore, or herbivore) for display in Figure 3.5. Cretaceous jaw images are mainly those used in Grossnickle and Polly (2013), and primary sources for Cenozoic jaw images are provided in Chapter 3. Abbreviations: c, carnivore; FAD, first appearance datum; JAPr, jaw-angular process; h, herbivore; LAD, last appearance datum; Ma, millions of years ago; o, omnivore; PBDB, Paleobiology Database.

Genus	JAPr angle	FAD (Ma)	LAD (Ma)	PBDB diet	Dietary group
Metatheria					
Alphadon	17.13	84.2	66	omnivore	o
Andinodelphys	15.077	66	64.6	omnivore	o
Asiatherium	21.039	78	72.1	omnivore	o
Callistoe	14.4	47.8	33.9	carnivore	c
*Didelphodon coyi**	18.34	72.1	66	durophage	c
*Didelphodon vorax**	12.4	72.1	66	durophage	c
Eodelphis	17.98	86.5	66	carnivore-durophage	c
Epidolops	20.009	59.2	50.3	omnivore	o
Mayulestes	18.223	66	64.6	omnivore	o
Pucadelphys	12.954	66	64.6	omnivore	o
Sinodelphys	15.689	131	126	insectivore	c
Eutheria					
Agriochoerus	40.485	40.4	Miocene	herbivore	h
Amphidozotherium	15.967	38	28.4	insectivore	c
Ankalagon	19.522	64.6	61.6	carnivore	c
Apatemys	18.668	56	33.9	herbivore	h
Apternodus	23.923	40.4	28.1	insectivore	c
Archaeomeryx	29.252	48.6	37.2	grazer-browser	h
Archaeonycteris	22.662	55.8	38	insectivore	c
Arctocyon	18.96	64.6	55.8	omnivore	o
Ardynictis	14.934	48.6	28.4	insectivore	c
Arsinoitherium	35.64	41	23.03	insectivore**	h**
Asioryctes	16.389	75	70	insectivore	c
Aspanlestes	17.48	89.8	78	insectivore	c
Barunlestes	23.861	75	70	insectivore	c
Barylambda	26.616	56.8	50.3	herbivore	h
Borisodon	17.197	93.9	89.8	insectivore	c
Brontops	43.04	37.2	33.9	browser	h
Bumbanius	18.937	58.7	48.6	insectivore	c

Caenolambda	33.783	64.6	50.3	herbivore	h
Cantius	23.201	56	40.4	omnivore	o
Carodnia	41.049	61.6	47.8	insectivore**	h**
Carpolestes	28.876	61.7	55.8	herbivore	h
Chronolestes	25.91	55.8	48.6	herbivore	h
Claenodon	21.439	64.6	56.8	omnivore	o
Conoryctes	30.121	64.6	61.7	omnivore-herbivore	o
Coryphodon	33.41	56.8	41.2	herbivore	h
Cylindrodon	39.845	40.4	33.9	herbivore	h
Daphoenus	17.54	40.4	Miocene	carnivore-omnivore	c
Daulestes	18.39	93.9	86.5	insectivore	c
Deltatherium	17.967	64.6	61.7	carnivore	c
Dinictis	21.17	37.2	28.1	carnivore	c
Dissacus	17.183	64.6	47.8	carnivore	c
Douglassciurus	39.389	37.2	30.8	granivore-frugivore	h
Duchesneodus	40.013	46.2	37.2	browser	h
Ectoconus	30.649	66	64.6	herbivore	h
Ectoganus	24.816	61.7	48.6	herbivore	h
Elomeryx	44.356	38	Miocene	browser	h
Eoconodon	22.58	66	64.6	omnivore	o
Eomaia	18.259	131	126	insectivore	c
Eosigale	32	61.7	58.7	insectivore	c
Eotitanops	36.87	56	41	browser	h
Eotylopus	36.914	40.4	33.9	browser	h
Eppsinycteris	15.476	56	47.8	insectivore	c
Erlikotherium	16.352	47.8	41	insectivore	c
Eumys	37.958	40.4	28.1	herbivore	h
Eusmilus	13.092	38	28.1	carnivore	c
Eutypomys	41.391	40.4	23.03	herbivore	h
Gervachoerus	38.028	47.8	33.9	grazer-browser	h
Haplobunodon	37.439	47.8	33.9	grazer-browser	h
Haplolambda	35.66	61.7	55.8	herbivore	h
Heptacodon	40.893	41	28.1	browser	h
Hesperocyon (Pseudocynodictis)	21.846	38	28.1	carnivore-omnivore	c
Hyaenodon	17.016	47.8	Miocene	carnivore	c
Hypertragulus	39.15	40.4	Miocene	frugivore	h
Hypisodus	43.092	37.2	33.9	grazer-browser	h
Icaronycteris	13.473	56.8	41	insectivore	c
Kennalestes	16.072	93.9	71	insectivore	c
Kopidodon	21.18	48.6	41	insectivore	c
Kulbeckia	16.95	93.9	83.6	insectivore	c
Lambdotherium	36.327	55.8	46.2	browser	h
Leptictidium	21.86	56	33.9	insectivore	c
Leptictis	27.682	40.4	28.1	insectivore-carnivore	c
Leptomeryx	46.047	37.2	23.03	frugivore	h
Leptoreodon	36.759	46.2	37.2	browser	h
Lophialetes	38.269	48.6	33.9	browser	h
Loxolophus	15.988	66	61.7	omnivore	o
Maelestes	20.472	75	71	insectivore	c
Megacerops	36.282	37.2	33.9	browser	h
Menops (Allops)	32.694	40.4	33.9	browser	h
Merycoidodon	42.623	37.2	Miocene	herbivore	h
Metamynodon	36.84	47.8	28.1	browser	h
Midiagnus	34.936	55.8	48.6	omnivore	o
Moeritherium	48.548	47.8	28.1	grazer-browser	h
Montanalestes	18.999	113	100.5	insectivore	c

Nimravus	22.665	38	28.1	carnivore	c
Notharctus	28.783	55.8	40.4	omnivore	o
Notopithecus	44.897	55.8	33.9	herbivore	h
Onychodectes	23.091	66	64.6	omnivore	o
Oxyaena	21.16	58.7	48.6	carnivore	c
Pachyaena	17.923	61.7	50.3	carnivore	c
Palaechthon	29.227	64.6	61.7	omnivore	o
Palaeogale	18.775	37.2	Miocene	carnivore-omnivore	c
Palaeolagus	51.029	37.2	Miocene	grazer-browser	h
Palaeonictis	20.499	56.8	48.6	carnivore	c
Palaeosinopa	23.039	61.7	46.2	piscivore-durophage	c
Palaeostylops (Gashatostylops)	33.613	58.7	55.8	herbivore	h
Palaeosyops	30.162	55.8	40.4	browser	h
Palaeotherium	48.184	47.8	28.1	frugivore-folivore	h
Pantolambda	35.666	64.6	61.6	herbivore	h
Paraceratherium	43.702	37.2	23.03	browser	h
Paramys	39.194	56.8	33.9	herbivore	h
Patriofelis	21.998	50.3	40.4	carnivore	c
Perchoerus	37.923	37.2	28.1	herbivore-omnivore	h
Periptychus	32.895	66	61.7	herbivore	h
Phenacodus	30.942	64.6	47.8	herbivore	h
Phosphatherium	32.455	56	47.8	grazer-browser	h
Plesiadapis	22.71	61.7	50.3	herbivore	h
Poebrotherium	35.724	37.2	28.1	browser	h
Praolestes	23.672	58.7	55.8	insectivore	c
Procerberus	18.55	69	61.7	insectivore	c
Prodiacodon	20.792	66	50.3	insectivore-carnivore	c
Prodinoceras	34.477	58.7	55.8	herbivore	h
Prokennalestes	17.388	120	113	insectivore	c
Prolimnocyon	23.712	58.7	46.2	carnivore	c
Propalaeanodon	17.282	61.7	56.8	insectivore	c
Propalaeotherium	34.211	48.6	33.9	folivore-frugivore	h
Protitanotherium	39.548	46.2	33.9	browser	h
Protoptychus	42.826	46.2	40.4	herbivore	h
Protoreodon	35.637	46.2	33.9	herbivore	h
Protungulatum	23.916	69	64.6	omnivore	o
Psittacotherium	19.834	64.6	56.8	herbivore	h
Sarkastodon	19.645	47.8	41	carnivore	c
Sasayamamylos	16.377	112	109	insectivore	c
Saxonella	25.654	61.7	56.8	herbivore	h
Sinclairella	16.167	40.4	30.8	herbivore	h
Sinonyx	15.115	61.7	55.8	carnivore	c
Sinopa	21.507	58.7	40.4	carnivore	c
Sthenodectes	43.014	46.2	40.4	browser	h
Stylinodon	31.933	55.8	40.4	herbivore	h
Telmatherium (Manteoceras)	39.456	50.3	37.2	browser	h
Tetonius	28.326	55.8	48.6	insectivore	c
Thomashuxleya	37.712	55.8	41	herbivore	h
Titanoides	24.835	61.7	55.8	herbivore	h
Trigonostylops	46.337	57	37.2	herbivore	h
Trogosus	32.392	55.8	41	herbivore	h
Tubulodon	25.513	55.8	46.2	insectivore	c
Uintatherium	29.649	55.8	41	herbivore	h
Utaetus	21.447	48.6	33.9	insectivore	c
Voltaia	17.476	58.7	55.8	insectivore	c
Wortmania	23.687	66	64.6	herbivore	h

Zalambdalestes	24.745	75	71	insectivore	c
Zhelestes	17.305	93.9	86.5	insectivore	c

* Analyses on JAPr angles of fossils were run at the genus level. However, JAPr angle results for *Didelphodon vorax* and *D. coyi* were considerably different, and therefore both were included in the analysis.

** Based on their body sizes, taxonomic classifications, and molar morphologies, *Carodnia* and *Arsinoitherium* are expected to be herbivores, and almost certainly are not insectivores (as labeled by the Paleobiology Database). Thus, I categorized these as herbivores instead of insectivores.

APPENDIX G

Occurrence and clade information for the genera examined in the morphological analyses of Chapter 4. Note that some genera were not included in all analyses, and taxonomic diversity analyses include additional taxa beyond those of the morphological analyses. The fossil occurrence dataset is available via Dryad (doi:10.5061/dryad.qk643). For disparity analyses of individual continents (Fig. 4.8B), European and Asian taxa were merged as Eurasian taxa. Rock formations (or locations) in parentheses were not included in the analysis of formation disparities. See text for ages of time bins. Mammal subgroup abbreviations: a. ungulate, archaic ungulate; carnivora., carnivoramorpha; plesiadap., plesiadapiform. Rock formation abbreviations: Ag, Aguja; Ai, Aitym; An, Antlers; Ar, Argilas de Aveiro; Be, Bear; BG, Baruungoyot; Bi, Bissekty; BP, Black Peaks; Cl, Cloverly; CM, Cedar Mountain; Co, Coalspur; De, Denver; Dj, Djadokhta; Dk, Dakota; DP, Dinosaur Park; Dz, Dzunbain; Ea, Eagle; Fe, Ferris; FH, Fox Hills; Fm, Frenchman; Fo, Foremost; Fl, Fruitland; FU, Fort Union; HC, Hell Creek; JR, Judith River; Ka, Kaiparowits; Kh, Khodzhakul; Ki, Kirtland; Ln, Lance; Lr, Laramie; Me, Mesaverde; MR, Milk River; Mu, Murtoi; Na, Nacimiento; NH, North Horn; Ol, Oldman; Pa, Paskapoo; PB, Polecat Bench; PH, Porcupine Hills; Ra, Ravenscrag; Sc, Scollard; Sh, Shanghu; SL, Santa Lucia; SM, St. Mary River; StC, Straight Cliffs; To, Tornillo; Tu, Tullock; Wa, Wahweap; Wanghudun, Wn.

Genus	Group (subgroup)	Continent	Rock formation(s)	Time bins
Acristotherium	Eutheria	Asia	(Yixian)	K1
Eomaia	Eutheria	Asia	(Yixian)	K1
Sinodelphys	Metatheria	Asia	(Yixian)	K1
Atokatheridium	Metatheria	N. America	An, Cl	K1, K2
Kielantherium	Stem Tribosphenida	Asia	Dz	K1
Murtoilestes	Eutheria	Asia	Mu	K1
Prokennalestes	Eutheria	Asia	Dz	K1
Slaughteria	Stem Tribosphenida	N. America	An	K1, K2
Holoclemensia	Stem Tribosphenida	N. America	An	K1, K2
Kermackia	Stem Tribosphenida	N. America	An	K1, K2
Oklatheridium	Metatheria	N. America	An, Cl	K1, K2
Bobolestes	Eutheria	Asia	Kh	K2
Kokopellia	Metatheria	N. America	CM	K3
Montanalestes	Eutheria	N. America	Cl	K2
Sasayamamylos	Eutheria	Asia	(Sasayama Group)	K2
Sinbadelphys	Metatheria	N. America	CM	K3
Pariadens	Metatheria	N. America	CM, Dk	K3
Sheikhdzheilia	Eutheria	Asia	Kh	K2, K3
Zhangolestes	Eutheria	Asia	(Quantou)	K3
Eozhelestes	Eutheria	Asia	Kh	K3
Arcantiodelphys	Metatheria	Europe		K3
Dakotadens	Metatheria	N. America	Dk	K3
Sorlestes	Eutheria	Asia	(Jobu)	K3

Borisodon	Eutheria	Asia	(Drill core near Ashchikol' Lake, Kazakstan)	K3
Kulbeckia	Eutheria	Asia	Bi, Ai, (Yalovach)	K3, K4
Bulaklestes	Eutheria	Asia	Bi	K3
Daulestes	Eutheria	Asia	Bi	K3
Uchkudukodon	Eutheria	Asia	Bi	K3
Sulestes	Metatheria	Asia	Bi	K3
Eoungulatum	Eutheria	Asia	Bi, Ai	K3, K4
Parazhelestes	Eutheria	Asia	Bi, Ai	K3, K4
Aspanlestes	Eutheria	Asia	Bi, Ai, (Darbasa)	K3-K5
Paranyctoides (quadrans)	Eutheria	Asia (See text)	Bi, Ai	K3, K4
Zhelestes	Eutheria	Asia	Bi, Ai	K3, K4
Eoalphadon	Metatheria	N. America	Dk, Wa	K3-K5
Anchistodelphys	Metatheria	N. America	StC, Wa	K3-K5
Alphadon	Metatheria	N. America, Europe	Dk, Wa, Ka, Me, JR, Ag, Ki, Fl, Ol, Ln, HC, FH, Sc, Fm, NH, Ar, SL, MR, StC, Ea, (Two Medicine)	K3-K7
Protalphadon	Metatheria	N. America	Dk, Wa, Me, Ln, HC, FH, Fe, Lr	K3-K7
Varalphadon	Metatheria	N. America	StC, MR, Wa, Ka, Ea	K4-K6
Picopsis	Stem Tribosphenida	N. America	StC, MR, Ka	K4-K6
Kennalestes	Eutheria	Asia	Bi, Dj	K3-K6
Zhalmouzia	Eutheria	Asia	(Bostobe)	K4
Tirotherium	Stem Tribosphenida	N. America	MR	K4
Iugomortiferum	Metatheria	N. America	Wa	K5
Potamotelses	Stem Tribosphenida	N. America	MR, StC	K4
Iqualadelphis	Metatheria	N. America	Wa, MR, Ka, Ea	K4-6
Aquiladelphis	Metatheria	N. America	Wa, MR, Ki, Ea	K4-7
Paranyctoides (sternbergi)	Eutheria	N. America (See text)	Wa, Ka, JR, DP, Ol, Ea	K4-7
Albertatherium	Metatheria	N. America	MR, StC, Ea	K4
Aenigmadelphys	Metatheria	N. America	Wa, Ka	K5, K6
Deltatheridium	Metatheria	Asia	Dj, BG, (Darbasa)	K5-K7
Eodelphis	Metatheria	N. America	MR, JR, DP, Ol, SM, Fo, StC	K4-K7
Pediomys	Metatheria	N. America (K5-K7), Europe (K7)	Wa, DP, Ln, Fr, Sc, HC, FH, Ra, Ar	K5-K7
Turgidodon	Metatheria	N. America	Wa, Ka, Me, JR, DP, Ol, Ag, Fo, Ln, Fr, Sc, HC, SM	K5-K7
Tsagandelta	Metatheria	Asia	(Baynshiree) Not in time-sliced analyses because age is too uncertain (see text).	
Lotheridium	Metatheria	Asia	(Qiupa) Age is uncertain. Designated K6 based on Jiang et al. (2011) and ages of non-mammalian taxa in Qiupa Formation.	K6
Ukhaatherium	Eutheria	Asia	Dj	K6
Asiatherium	Metatheria	Asia	Dj	K6
Asioryctes	Eutheria	Asia	BG	K7
Avitotherium	Eutheria	N. America	Ka	K6
Barunlestes	Eutheria	Asia	BG, Dj	K6, K7
Gallolestes	Eutheria	N. America	Ag, (El Gallo)	K6
Maelestes	Eutheria	Asia	Dj	K6
Zalambdalestes	Eutheria	Asia	Dj	K6
Paleomolops (=*Palaeomolops*)	Stem Tribosphenida	N. America	Ag	K6
Protolambda	Metatheria	N. America	JR, DP, Ol, Ln, HC, Fm, Sc, FH, Lr, NH	K6, K7

Didelphodon	Metatheria	N. America	Ln, HC, Fm, Sc, FH, SM, (Horseshoe Canyon, Wapiti, Marshalltown)	K6, K7
Leptalestes	Metatheria	N. America	JR, DP, Ol, Fl/Ki, Ln, HC, Fm, Sc, FH, NH, SM, Lr, Ea, StC	K4-K7
Batodon	Eutheria	N. America	JR, (Edmontan Group)	K6, K7
Gypsonictops	Eutheria	N. America	Ka, Me, JR, DP, Ol, Fl/Ki, Ln, HC, Fm, Sc, FH, SM, Fe, Ra, (Prince Creek)	K6, K7
Cimolestes	Eutheria	N. America (K6-D2), S. America (D1)	JR, Ol, Fl/Ki, Fo, Ln, HC, Sc, Fm, FH, Ra, Fe, SM, Be, SL, (Prince Creek)	K6-D2
Labes	Eutheria	Europe	(Calizas de Lychnus)	K6, K7
Lainodon	Eutheria	Europe	(Vitoria)	K6
Mistralestes	Eutheria	Europe	(Aix-en-Provence Basin)	K6
Valentinella	Eutheria	Europe	(Aix-en-Provence Basin)	K7
Altacreodus	Eutheria	N. America	Ln, Fm, Sc, HC	K7
Ambilestes	Eutheria	N. America	Sc, HC, Ra	K7
Scollardius	Eutheria	N. America	Fm, Sc, HC	K7
Schowalteria	Eutheria	N. America	Sc	K7
Glasbius	Metatheria	N. America	Ln, HC, Fm	K7
Nanocuris	Metatheria	N. America	Ln, Fm	K7
Nortedelphys	Metatheria	N. America	Ln, HC, Fm, Sc, Ra, Lr	K7
Protungulatum	Eutheria (A. ungulate)	N. America	HC, Ln, Be, Tu, Fm, Ra, Fe	K7, D1
Deccanolestes	Eutheria (Plesiadap.)	India	(Intertrappean)	K7
Leptacodon	Eutheria	Europe (K7-D2), N. America (D1-D2)	Ar, FU, Pa, Tu	K7-D2
Kharmerungulatum	Eutheria (A. ungulate)	India	(Intertrappean)	K7
Delphodon	Eutheria	N. America	Ln, FH	K7
Paleoungulatum	Eutheria (A. ungulate)	N. America	HC	K7
Roberthoffstetteria	Metatheria	S. America	SL	D1
Szalinia	Metatheria	S. America	SL	D1
Pucadelphys	Metatheria	S. America	SL	D1
Alcidedorbignya	Eutheria	S. America	SL	D1
Alveugena	Eutheria	N. America	Fe, FU	D1
Baioconodon	Eutheria (A. ungulate)	N. America	HC, Tu, FU, PB, Ra, De, Fe, Be, To	K7, D1
Betonnia	Eutheria	N. America	Na	D1
Carcinodon	Eutheria (A. ungulate)	N. America	Na, FU, Ra, Be	D1
Eoconodon	Eutheria (A. ungulate)	N. America	Na, Tu, FU, PB, Fe, Ra	D1
Onychodectes	Eutheria	N. America	Na, FU, NH	D1
Puercolestes	Eutheria	N. America	Na, Ra	D1
Wortmania	Eutheria	N. America	Na, Tu	D1
Mimatuta	Eutheria (A. ungulate)	N. America	HC, Tu, PB, Ra, Fe	D1
Pucanodus	Eutheria (A. ungulate)	S. America	SL	D1
Cocatherium	Metatheria	S. America	(Lefipán—Grenier Farm locality)	D1
Oxyacodon	Eutheria (A. ungulate)	N. America	Na, Tu, FU, NH, Ra, Fe, Be, De	D1
Conacodon	Eutheria (A. ungulate)	N. America	Na, NH, De, Fe	D1
Bryanictis	Eutheria (Carnivora.)	N. America	To, FU, Na, PH, PB	D1, D2
Ectoconus	Eutheria (A. ungulate)	N. America	Na, NH, De, Fe	D1
Maiorana	Eutheria (A. ungulate)	N. America	PB, Fe	D1
Hemithlaeus	Eutheria (A. ungulate)	N. America	Na, PB, Fe	D1
Allqokirus	Metatheria	S. America	SL	D1
Alticonus	Eutheria (A. ungulate)	N. America	De, Fe	D1
Ampliconus	Eutheria (A. ungulate)	N. America	De, Fe	D1
Andinodelphys	Metatheria	S. America	SL	D1
Andinodus	Eutheria (A. ungulate)	S. America	SL	D1

Bubogonia	Eutheria (A. ungulate)	N. America	Na, Ra	D1
Chacomylus	Eutheria (A. ungulate)	N. America	Na	D1
Choeroclaenus	Eutheria (A. ungulate)	N. America	Na	D1
Incadelphys	Metatheria	S. America	SL	D1
Khasia	Metatheria	S. America	SL	D1
Mayulestes	Metatheria	S. America	SL	D1
Mithrandir	Eutheria (A. ungulate)	N. America	Na, Fe	D1
Molinodus	Eutheria (A. ungulate)	S. America	SL	D1
Simoclaenus	Eutheria (A. ungulate)	S. America	SL	D1
Thylacodon	Metatheria	N. America	Na, HC, Tu, PB, De, Fe	D1
Tinuviel	Eutheria (A. ungulate)	N. America	Tu, FU	D1
Tiuclaenus	Eutheria (A. ungulate)	S. America	SL	D1
Tiulordia	Metatheria	S. America	SL	D1
Tiznatzinia	Eutheria (A. ungulate)	N. America	Na	D1
Carsioptychus	Eutheria (A. ungulate)	N. America	NH	D2
Peradectes	Metatheria	N. America, S. America	Na, Tu, PB, To, SL	D1, D2
Desmatoclaenus	Eutheria (A. ungulate)	N. America	Na, NH, Ra, De	D1, D2
Loxolophus	Eutheria (A. ungulate)	N. America	Na, FU, NH, Ra, Fe, Be, De	D1, D2
Oxyprimus	Eutheria (A. ungulate)	N. America	HC, Tu, PB, Ra, Fe, Be, De	D1, D2
Oxyclaenus	Eutheria (A. ungulate)	N. America	HC, Tu, PB, Ra, Fe, Be, De, NH, FU, Na, PB	D1, D2
Procerberus	Eutheria	N. America	HC, Tu, PB, Ra, Fe, Be, De, Pa	K7-D2
Prothryptacodon	Eutheria (A. ungulate)	N. America	Na, FU, PB, Pa, PH	D1, D2
Aphronorus	Eutheria	N. America	Tu, FU, NH, PB, PH, Co	D1, D2
Chriacus	Eutheria (A. ungulate)	N. America	Tu, Na, FU, NH, PB, Pa, PH	D1, D2
Prodiacodon	Eutheria	N. America	Tu, Ra, Na, FU, PB, Pa	D1, D2
Pararyctes	Eutheria	N. America	Tu, Co	D1, D2
Palaeictops	Eutheria	N. America	Tu, PB	D1, D2
Purgatorius	Eutheria (Plesiadap.)	N. America	Tu, Ra, Be	D1, D2
Litaletes	Eutheria (A. ungulate)	N. America	FU, NH, PB, Ra	D1, D2
Auraria	Eutheria (A. ungulate)	N. America	De	D1
Litomylus	Eutheria	N. America	Be, Ra, Na, FU, PB, Pa	D1, D2
Protictis	Eutheria (Carnivora.)	N. America	Na, FU, NH, PB, Pa, PH	D2
Haplaletes	Eutheria	N. America	Tu, NH, Na, FU, PB	D1, D2
Anisonchus	Eutheria (A. ungulate)	N. America	Tu, NH, Ra, Be, Na, FU, PB, De	D1, D2
Promioclaenus	Eutheria (A. ungulate)	Asia, N. America	NH, Na, To, FU, PB, Pa, PH, BP, Co, Sh	D1, D2
Haploconus	Eutheria (A. ungulate)	N. America	Na, FU, NH, To	D1, D2
Mixodectes	Eutheria	N. America	To, Na, FU	D1, D2
Periptychus	Eutheria (A. ungulate)	N. America	Na, FU, NH, To, BP, De, Fe	D1, D2
Plesiolestes	Eutheria (Plesiadap.)	N. America	To, Na, FU, NH, Pa, PH, PB	D1, D2
Protoselene	Eutheria (A. ungulate)	N. America	Fe, To, Na, NH	D1, D2
Ursolestes	Eutheria (Plesiadap.)	N. America	Be	D1
Swaindelphys	Metatheria	N. America	FU, Na	D2
Acmeodon	Eutheria	N. America	Na, FU, PB, NH	D2
Ankalagon	Eutheria (A. ungulate)	N. America	Na	D2
Bessoecetor	Eutheria	N. America	FU, PB, Pa, PH	D2
Caenolambda	Eutheria	N. America	PB, BP	D2
Colpoclaenus	Eutheria (A. ungulate)	N. America	Na, Co, Pa	D2
Conoryctella	Eutheria	N. America	Na, NH	D2
Conoryctes	Eutheria	N. America	Na	D2
Coriphagus	Eutheria	N. America	Na, FU, PB	D2
Deltatherium	Eutheria (A. ungulate)	N. America	Na	D2
Deuterogonodon	Eutheria (A. ungulate)	N. America	Na, FU	D2
Gelastops	Eutheria	N. America	Tu, FU, PB, Pa, To	D2

Goniacodon	Eutheria (A. ungulate)	N. America	Na, FU, NH, PH, PB	D2
Huerfanodon	Eutheria	N. America	Na, FU, PB	D2
Leptonysson	Eutheria	N. America	FU	D2
Mimotricentes	Eutheria (A. ungulate)	N. America	Na, FU, PB, NH	D2
Myrmecoboides	Eutheria	N. America	FU, NH	D2
Paleotomus	Eutheria	N. America	FU, BP, Pa	D2
Pantolambda	Eutheria	N. America	Na, FU	D2
Pentacodon	Eutheria	N. America	Na	D2
Presbytherium	Eutheria	N. America	Pa	D2
Psittacotherium	Eutheria	N. America	Na, FU	D2
Triisodon	Eutheria (A. ungulate)	N. America	Na	D2
Arctocyon	Eutheria (A. ungulate)	Europe, N. America	Na, FU, PB, PH	D2
Thryptacodon	Eutheria (A. ungulate)	N. America	FU, PB	D2
Simpsonictis	Eutheria (Carnivora.)	N. America	FU, PB, Co	D2
Elpidophorus	Eutheria (Plesiadap.)	N. America	Pa, PH, FU	D2
Phenacodus	Eutheria (A. ungulate)	N. America	BP	D2
Anasazia	Eutheria (Plesiadap.)	N. America	Na	D2
Ectocion	Eutheria (A. ungulate)	N. America	FU	D2
Edworthia	Eutheria (Plesiadap.)	N. America	Pa	D2
Elphidotarsius	Eutheria (Plesiadap.)	N. America	FU	D2
Escavadodon	Eutheria (Carnivora.)	N. America	Na	D2
Eudaemonema	Eutheria	N. America	FU, PB, PH	D2
Ictidopappus	Eutheria (Carnivora.)	N. America	FU	D2
Ignacius	Eutheria (Plesiadap.)	N. America	Pa, PH, PB	D2
Jepsenella	Eutheria	N. America	FU, PB, PH	D2
Mioclaenus	Eutheria (A. ungulate)	N. America	Na	D2
Palaechthon	Eutheria (Plesiadap.)	N. America	Na, FU	D2
Palenochtha	Eutheria (Plesiadap.)	N. America	FU, PB, PH	D2
Paromomys	Eutheria (Plesiadap.)	N. America	Na, FU, NH, PB	D2
Picrodus	Eutheria (Plesiadap.)	N. America	FU, PB, Pa	D2
Torrejonia	Eutheria (Plesiadap.)	N. America	Na	D2
Premnoides	Eutheria (Plesiadap.)	N. America	FU, PB	D2
Pronothodectes	Eutheria (Plesiadap.)	N. America	FU, PB, Pa, PH	D2
Tetraclaenodon	Eutheria (A. ungulate)	N. America	Na, FU, PB, PH	D2
Astigale	Eutheria	Asia	Sh, Wn	D2
Carnilestes	Eutheria	Asia	Sh	D2
Dysnoetodon	Eutheria	Asia	Sh	D2
Prosarcodon	Eutheria	Asia	(Fangou)	D2
Linnania	Eutheria	Asia	Sh, (Fangou)	D2
Bemalambda	Eutheria	Asia	Sh	D2
Palasiodon	Eutheria (A. ungulate)	Asia	Sh	D2
Yuodon	Eutheria (A. ungulate)	Asia	Sh	D2
Escribania	Eutheria (A. ungulate)	S. America	(Salamanca)	D2
Dissacus	Eutheria (A. ungulate)	N. America	Na, FU, Sh	D2
Huananius	Eutheria	Asia	Sh	D2
Hukoutherium	Eutheria (A. ungulate)	Asia	Sh	D2
Benaius	Eutheria	Asia	Wn	D2
Eosigale	Eutheria	Asia	Wn	D2

APPENDIX H

Information and sources for the molars used in the morphometric analyses of Chapter 4. The species listed in the first column are the particular species chosen to represent the genera of the analyses. The image source for the GM analyses is also the source for the molar length and cusp heights-to-molar length ratios unless specified in Appendix I. Photographs of specimens were taken at the Field Museum of Natural History (FMNH), New Mexico Museum of Natural History and Science (NMMNH), Sam Noble Oklahoma Museum of Natural History (OMNH), University of California Museum of Paleontology (UCMP), and the Burke Museum of Natural History and Culture.

Species	Image source and specimen	Notes
Acristotherium yanensis	Hu et al. (2010), IVPP V15004	Not in GM analysis (no occlusal view in source).
Eomaia scansoria	Ji et al. (2002), CAGS01-IG1-a, b	Not in GM analysis (no occlusal view in source).
Sinodelphys szalayi	Luo et al. (2003), CAGS00-IG03	Not in GM analysis (no occlusal view in source).
Atokatheridium boreni	Davis et al. (2008), OMNH 61624	Molar is "m?" according to source. Paraconid and metaconid are chipped, so landmark locations are estimated.
Kielantherium gobiensis	Davis et al. (2008), after Dashzeveg (1975)	Molar image used for the GM is a drawing from Davis et al. (2008) that is likely based on PIN No. 3101-32 in Dashzeveg (1975).
Murtoilestes abramovi	Averianov & Skutschas (2001), ZIN 34994	m3 was used (instead of preferred m2). Paraconid and metaconid are chipped, so landmark locations are estimated.
Prokennalestes trofimovi	Photograph of OMNH 71501	
Slaughteria eruptens	Davis & Cifelli (2011), OMNH 63726	m2 was used but it is unclear as to whether this is the penultimate molar.
Holoclemensia texana	Photograph of PM 1005	
Kermackia texana	Davis & Cifelli (2011), PM 1245	Paraconid and metaconid are chipped, so landmark locations are estimated. Molar is "m?" according to source.
Oklatheridium sp.	Davis & Cifelli (2011), PM 965	Molar is labeled "m?" by source.
Bobolestes zenge	Averianov & Archibald (2005), CCMGE 7/12176	Paraconid is chipped, so landmark location is estimated.
Kokopellia juddi	Photograph of OMNH 26361	
Montanalestes keeblerorum	Photograph of OMNH 60793 (cast)	
Sasayamamylos kawaii	Kusuhashi et al. (2013), MNHAH D1-030444	
Sinbadelphys schmidti	Cifelli (2004), OMNH 33074	Hypoconulid and entoconid are chipped, so landmark locations are estimated.
Pariadens mckennai	Cifelli (2004), OMNH 33971	Molar is m2 or 3 according to source. Hypoconulid and entoconid are chipped, and landmark locations are estimated with help of m4 (OMNH 33072).
Sheikhdzheilia rezvyii	Averianov & Archibald (2005), ZIN 88438	m1 was used (instead of preferred m2).

Zhangolestes sp.	Zan et al. (2006), Ya2.24.i	Not in GM analysis due to lack of occlusal image or poor preservation.
Eozhelestes mangit	Averianov & Archibald (2005), CCMGE 26/12176	m1 was used (instead of preferred m2).
Arcantiodelphys marchandi	Vullo et al. (2009), MNHN CCH2 & MNHN CCH3 (composite)	The molar image is a composite and is "m?."
Dakotadens morrowi	Photograph of MNA V6023	The molar is "m?."
Sorlestes budan	Kielan-Jaworowska et al. (2004)	
Borisodon kara	Archibald & Averianov (2012), CCMGE 106/12455	
Kulbeckia kulbecke	Archibald & Averianov (2003), URBAC 98-2	
Bulaklestes kezbe	Archibald & Averianov (2006), URBAC 03−94	
Daulestes inobservabilis	Archibald & Averianov (2006), URBAC 03−88	Paraconid is chipped, so landmark location is estimated.
Uchkudukodon nessovi	Archibald & Averianov (2006), URBAC 04−181	Metaconid is chipped, so landmark location is estimated.
Sulestes karakshi	Averianov et al. (2010), URBAC 04-169	
Eoungulatum kudukensis	Archibald & Averianov (2012), URBAC 06–42	
Parazhelestes robustus	Archibald & Averianov (2012), URBAC 97–05	
Aspanlestes aptap	Archibald & Averianov (2012), CCMGE 4/12176	
Paranyctoides quadrans	Averianov & Archibald (2013B), URBAC 03−215	Molar is "m?" according to source. *P. quadrans* used for Asia and *P. sternbergi* used for N. America (see text).
Zhelestes temirkazyk	Archibald & Averianov (2012), URBAC 04–309	
Eoalphadon clemensi	Photograph of OMNH 49433	
Anchistodelphys archibaldi	Photograph of NMMNH C-697 (cast of MNA V4545)	
Alphadon perexiqus	Photograph of UCMP 165096 (cast of OMNH 25181)	
Protalphadon lulli	Photograph of UCMP 125084	
Varalphadon wahweapensis	Photograph of OMNH 20536	
Picopsis sp.	Eaton (2006), UMNH 12801	Molar is "m?" according to source. Protoconid is broken, so landmark location is estimated.
Kennalestes gobiensis	Photograph of ZPAL MgM-I/3 (cast)	
Zhalmouzia bazhanovi	Averianov et al. (2012), ZIN 100639	
Tirotherium aptum	Montellano-Ballesteros & Fox (2015), UALVP 29423	Molar is "m?" according to source, but based on discussion by the source authors this specimen is likely a penultimate molar.
Iugomortiferum thoringtoni	Photograph of OMNH 20705	Molar is labeled "m?" by source.
Potamotelses sp.	Eaton (2006), UMNH VP 12788	
Iqualadelphis lactea	Cifelli (1990), OMNH 20531	Several cusps are chipped, so landmark locations for the cusps were estimated.
Aquiladelphis minor	Davis (2007), UALVP 5531	
Paranyctoides sternbergi	Montellano-Ballesteros et al. (2013), UALVP 14825	*P. quadrans* used for Asia and *P. sternbergi* used for N. America (see text).
Albertatherium primus	Davis et al. (2016), OMNH 66380	
Aenigmadelphys archeri	Photograph of OMNH 20531	
Deltatheridium praetrituberculare	Photograph of PSS-MAE 132	

Eodelphis browni	Photograph of UA 7002	
Pediomys elegans	Davis (2007), OMNH 64266	Only found in Europe in Maastrichtian (K7) so only included in this time bin for Eurasian results.
Turgidodon russelli	Photograph of OMNH 63149	Molar is "m?" according to source.
Tsagandelta dashzevegi	Rougier et al. (2015A), PSS-MAE 629	Not included in time-sliced morphological analyses because age is too questionable (see text) and m3 is not available. m2 was used (instead of preferred m3) for GM, but m3 was used for molar length.
Lotheridium mengi	Bi et al. (2015), ZMNH M9032	Several cusps are chipped and landmark locations are estimated using m2 cusps.
Ukhaatherium nessovi	Novacek et al. (1997), PSS-MAE 102	Not in GM analysis (no occlusal view in source).
Asiatherium reshetovi	Trofimov & Szalay (1994), PIN no. 3907	
Asioryctes nemegtensis	Photograph of ZPAL MgM-I/134 (cast)	
Avitotherium utahensis	Cifelli (1990), OMNH 20424	Several cusps are chipped, so landmark locations for the cusps were estimated. Molar is "m?" according to source.
Barunlestes butleri	Photograph of ZPAL MgM-I/135	Several cusps are chipped, so landmark locations for the cusps were estimated.
Gallolestes pachymandibularis	Kielan-Jaworowska et al. (2004)	
Maelestes gobiensis	Wible et al. (2009), PSS-MAE 607	
Zalambdalestes lechei	Photograph of ZPAL MgM-I/14 (cast)	
Paleomolops langstoni	Photograph of OMNH 25161	*Palaeomolops* is a synonym.
Protolambda florencae	Davis (2007), UALVP 27268	
Didelphodon vorax	Photograph of UCMP 52290	
Leptalestes cooki	Photograph of OMNH 63573	Metaconid is missing, so landmark location is estimated.
Batodon tenuis	Photograph of UCMP 150071	
Gypsonictops illuminatus	Photograph of UCMP 170870	
Cimolestes stirtoni	Photograph of UCMP 170833	Labeled "*Cimolestes incisus/stirtoni,*" but likely *C. stirtoni* based on molar length.
Labes garimondi	Martin et al. (2014), GAR 007 (cast)	The molar is m1 or m2.
Lainodon orueetxebarriai	Gheerbrant & Astibia (1994), L1AT 1	Poor preservation, so not in GM analysis
Mistralestes arcensis	Tabuce et al. (2013), MHNAix-PV.2008.1.1	Poor preservation, so not in GM analysis
Valentinella vitrollense	Tabuce et al. (2013), UP-VLP-10-01	Poor preservation, so not in GM analysis
Altacreodus magnus	Photograph of UCMP 107747 (cast)	
Ambilestes cerberoides	Fox (2015), UALVP 2255	
Scollardius propalaeoryctes	Photograph of UCMP 107744	
Schowalteria clemensi	Fox & Naylor (2003)	Not in GM analysis due to severe wear.
Glasbius intricatus	Davis (2007), AMNH 58759	
Nanocuris improvida	Wilson & Riedel (2010), DMNH 55343	
Nortedelphys jasoni	Case et al. (2004), UCMP 46319	*N. jasoni* is treated as synonymous with *N. intermedius* and *Alphadon jasoni*.
Protungulatum gorgun	Photograph of UCMP 35987 (cast)	
Deccanolestes hislopi	Photograph of N046 (cast)	
Leptacodon jepseni	Photograph of UCMP 45949	Metaconid and paraconid cusps are broken, so landmark locations are estimated.
Kharmerungulatum vanvaleni	Prasad et al. (2007), VPL/JU/IM/31	The molar is m1 or m2. Cusps are worn, so cusp landmark locations are estimated.

?Delphodon praenuntius	Simpson (1929)	Not in GM analysis (no occlusal view in source).
Paleoungulatum	Kelly (2014), LACM 157265	
Roberthoffstetteria nationalgeographica	Photograph of UCMP 192067 (cast of MNHN VIL99 or 100)	
Szalinia gracilis	De Muizon & Cifelli (2001), MHNC 8350	
Pucadelphys andinus	Marshall & De Muizon (1995), YPFB Pal 6109 and 6473 (composite)	
Alcidedorbignya inopinata	De Muizon & Marshall (1992), MHNC P 1211	
Alveugena carbonensis	Rook et al. (2010), PTRM 14000	
Baioconodon nordicus	Photograph of NMMNH C-556 (cast of PU 16720)	
Betonnia tsosia	Williamson et al. (2011), NMMNH P-44352	Metaconid is missing, so landmark location is estimated.
Carcinodon sp.	Photograph of NMMNH P-47556	Several cusps are worn, so landmark locations for the cusps are estimated.
Eoconodon hutchisoni	Clemens (2011), UCMP 156117	
Onychodectes tisonensis	Photograph of NMMNH P-63948	
Puercolestes simpsoni	Williamson et al. (2011), NMMNH P-47312	
Wortmania otariidens	Schoch (1981), UK 12998	Molar image used for the GM may be from a different specimen.
Mimatuta sp.	Photograph of UCMP 116526	
Pucanodus gagnieri	De Muizon & Cifelli (2000), MHNC 1265 (cast)	
Cocatherium lefipanum	Goin et al. (2006), LIEB-PV 1001	Cusps are worn, so cusp landmark locations are estimated.
Oxyacodon agapetillus	Photograph of NMMNH C-519 (cast of AMNH 3557)	
Conacodon entoconus	Photograph of AMNH 3470 (cast)	
Bryanictis microlestes	Simpson (1937), USNM 9301	m1 was used instead of m2 because it is the penultimate molar in this genus.
Ectoconus ditrigonus	Photograph of AMNH 16491 (cast)	
Maiorana noctiluca	Photograph of UCMP 125042 (cast)	
Hemithlaeus kowalevskianus	Photograph of NMMNH C-491 (cast of AMNH 3556)	Several cusps are worn, so landmark locations for the cusps were estimated.
Allqokirus australis	Photograph of UCMP 192044 (cast of YPFB 6190)	Molar is “m?” according to source.
Alticonus gazini	Photograph of NMMNH C-567 (cast of UCM 34895)	
Ampliconus antoni	Eberle & Lillegraven (1998), UW 26200	
Andinodelphys cochabambensis	Photograph of UCMP 192048 (cast of YPFB 6194)	
Andinodus boliviensis	De Muizon & Cifelli (2000), YPFB Pal 6120 (cast)	
Bubogonia saskia	Scott & Gardner (2013), UALVP 15105	
Chacomylus sladei	Williamson & Weil (2011), NMMNH P-44345	
Choeroclaenus turgidunculus	Photograph of NMMNH C-4693 (cast of NMMNH P-15164)	
Incadelphys antiquus	Photograph of UCMP 192049 (cast of YPFB 6251)	Molar is labeled “m3” in source but is likely m2 (the source labels lower molars starting with m2, not m1).
Khasia tiupampina	Photograph of UCMP 192051 (cast of YPFB 6134)	Molar is “m?”

Mayulestes ferox	De Muizon (1998), MHNC 1249	
Mithrandir gillianus	Photograph of NMMNH C-427 (cast of AMNH 16461)	Metaconid is worn, so landmark location is estimated.
Molinodus suarezi	Photograph of UCMP 192057 (cast of YPFB 6113)	
Simoclaenus sylvaticus	De Muizon & Cifelli (2000), MHNC 8332 (cast)	Several cusps are worn, so landmark locations were estimated.
Thylacodon pusillus	Williamson et al. (2012), NMMNH P-47322	
Tinuviel eurydice	Hunter et al. (1997), MOR 807	Several cusps are worn, so landmark locations were estimated.
Tiuclaenus cotasi	De Muizon & Cifelli (2000), MHNC 1255 (cast)	
Tiulordia floresi	De Muizon (1991), YPFB Pal 6191	Molar is labeled "m3" in source but is likely m2 (the source labels lower molars starting with m2, not m1). Paraconid is missing, so landmark location is estimated.
Tiznatzinia vanderhoofi	Photograph of NMMNH C-313 (cast of AMNH 27700)	
Carsioptychus hamaxitus	Gazin (1941), USNM 16195	
Peradectes coprexeches	Williamson & Taylor (2011), NMMNH P-59545	
Desmatoclaenus protogonoides	Photograph of NMMNH P-8625	
Loxolophus priscus	Photograph of AMNH 3108 (cast)	
Oxyprimus erikseni	Photograph of UCMP 132315	
Oxyclaenus cuspidatus	Photograph of AMNH 794 (cast)	
Procerberus formicarum	Photograph of UCMP 150003	Metaconid is broken, and thus the landmark location is estimated.
Prothryptacodon sp. cf *P. furens*	Scott et al. (2013), TMP 2010.097.0115	
Aphronorus fraudator	Scott et al. (2013), TMP 2010.097.0082	Several cusps are worn, and thus landmark locations were estimated.
Chriacus calenaneus	Photograph of NMMNH P-5393 (cast UMVP 1472)	
Prodiacodon puercensis	Photograph of NMMNH C-1322 (cast of AMNH 16748)	
Pararyctes rutherfordi	Scott et al. (2002), UALVP 45095	
Palaeictops bridgeri	Photograph of AMNH 56032 (cast)	
Purgatorius coracis	Fox & Scott (2011), UALVP 51012	
Litaletes mantiensis	Photograph of AMNH 88341 (cast of KMNH 7852)	
Auraria urbana	Photograph of NMMNH C-444 (cast of UCM 34935)	
Litomylus dissentaneus	Photograph of AMNH 87543 (cast)	
Protictis simpsoni	Photograph of NMMNH P-67474	m1 used instead of m2 because it is the penultimate molar in this genus.
Haplaletes disceptatrix	Simpson (1937), USNM 9500	
Anisonchus sectorius	Photograph of AMNH 3527 (cast)	
Promioclaenus acolytus	Photograph of UCMP 63761 (cast of KU 9626)	
Haploconus angustus	Photograph of NMMNH C-479 (cast of UALP 10777)	
Mixodectes crassiusculus	Photograph of NMMNH C-1107 (cast of AMNH 3087)	
Periptychus carinidens	Photograph of UCMP 30006 (cast)	

Plesiolestes wilsoni	Photograph of NMMNH C-4723 (cast of NMMNH P-19650)	
Protoselene opisthacus	Photograph of NMMNH P-21503	
Ursolestes perpetior	Fox et al. (2015), UMMP 100258	
Swaindelphys encinensis	Williamson & Taylor (2011), NMMNH P-1972	Molar is m2 or m3.
Acmeodon secans	Photograph of NMMNH C-1153 (cast of AMNH 100369)	
Ankalagon saurognathus	Photograph of AMNH 766 (cast)	Talonid cusps very reduced or not present, so their landmark locations are estimated.
Bessoecetor septentrionalis	Simpson (1936), AMNH 33810	
Caenolambda jepseni	Simons (1960), PU 14863	Several cusps are worn, so landmark locations are estimated.
Colpoclaenus procyonoides	Photograph of AMNH 16552 (cast)	
Conoryctella pattersoni	Photograph of NMMNH P-25014	
Conoryctes comma	Photograph of NMMNH P-41519	
Coriphagus montanus	Photograph of NMMNH C-1064 (cast of AMNH 35907)	
Deltatherium fundaminis	Photograph of NMMNH C-1731 (cast of UALP 10596)	Protoconid is broken, so landmark location is estimated.
Deuterogonodon noletil	Photograph of NMMNH P-18942	
Gelastops parcus	Simpson (1937), USNM 9601	USNM 9850 used for lateral measurements.
Goniacodon levisanus	Photograph of NMMNH P-51327	
Huerfanodon polecatensis	Schoch (1981), PU 14178	Lateral image quality too poor for accurate height measurements.
Leptonysson basiliscus	Van Valen (1967), AMNH 35295	Protoconid is broken, and thus the landmark location is estimated.
Mimotricentes subtrigonus	Photograph of NMMNH P-19953	
Myrmecoboides montanensis	Simpson (1937), USNM 8037	
Paleotomus milleri	Photograph of NMMNH C-1078 (cast of AMNH 100644)	
Pantolambda intermedius	Simpson (1937), USNM 8384	
Pentacodon occultus	Photograph of NMMNH C-1100 (cast of AMNH 16592)	
Presbytherium rhodorugatus	Scott (2010), UALVP 46606	
Psittacotherium multifragum	Photograph of NMMNH P-16230	
Triisodon sp.	Photograph of NMMNH P-47812	
Arctocyon ferox	Photograph of UCMP 126136 (cast of AMNH 2456)	Landmark locations based in part on Scott et al. (2013) (TMP 2010.097.0004).
Thryptacodon sp.	Photograph of UW 7421	
Simpsonictis tenuis	MacIntyre (1966), AMNH 35348	
Elpidophorus minor	Photograph of NMMNH C-2860 (cast of PU 14201)	
Phenacodus bisonensis	Krause & Gingerich (1983), PU 14634	
cf. *Anasazia williamsoni*	Silcox & Williamson (2012), NMMNH P-64312	
Ectocion collinus	Simpson (1937), USNM 6166	
Edworthia lerbekmoi	Fox et al. (2010), UALVP 50989	
Elphidotarsius florencae	Photograph of NMMNH C-1463 (cast of PU 14282	
Escavadodon zygus	Photograph of NMMNH C-4655 (cast of NMMNH P-2489)	Metaconid is broken, so landmark location is estimated.
Eudaemonema bohachae	Scott et al. (2013), TMP 2011.090.0005	
Ictidopappus mustelinus	Simpson (1937), USNM 9296	m1 was used instead of m2 because it is the penultimate molar in this genus.

Ignacius clarkforkensis	Bloch et al. (2007), UM 108210	Several cusps are worn, so landmark locations for the cusps are estimated.
Jepsenella praepropera	Simpson (1940), AMNH 35292	
Mioclaenus turgidus	Photograph of NMMNH C-4699 (cast of NMMNH P-15865)	
Palaechthon woodi	Silcox & Williamson (2012), NMMNH P-58837	
Palenochtha minor	Gunnell (1989), YPM-PU 1946	
Paromomys libedianus	Silcox & Williamson (2012), NMMNH P-40531	
Picrodus calgariensis	Scott & Fox (2005), UALVP 43294	
Torrejonia wilsoni	Silcox & Williamson (2012),NMMNH P-53909	
Premnoides douglassi	Gunnell (1989), YPM-PU 14802 & YPM-PU 1979 (composite)	
Pronothodectes matthewi	Scott et al. (2013), TMP 2011.090.0002	
Tetraclaenodon puercensis	Photograph of PM36690 (cast of AMNH16653)	
Astigale nanxiongensis	Yuping & Yongsheng (1981), IVPP V5215	
Carnilestes palaeoasiaticus	Wang & Zhai (1995), IVPP V10488	m1 was used instead of m2 because it is the penultimate molar in this genus.
Dysnoetodon minuta	Photograph of UCMP V5837 (cast of IVPP 73150)	Several cusps are worn, so landmark locations for the cusps are estimated.
Prosarcodon lonanensis	McKenna et al. (1984), WNUG 78ShOO1	m1 was used instead of m2 because it is the penultimate molar in this genus.
Linnania lofoensis	Chow et al. (1977), IVPP V4234	
Bemalambda nanhsiungensis	Chow et al. (1977), IVPP V4158	
Palasiodon siurenensis	Chow et al. (1977), IVPP V4235	
Yuodon protoselenoides	Chow et al. (1977), IVPP V4236	Several worn/missing cusps, so landmark locations for the cusps are estimated.
Escribania chubutensis	Gelfo et al. (2007), MPEF-PV 1860	
Dissacus navajovius	Photograph of NMMNH C-1238 (cast of AMNH 3356)	Talonid cusps very reduced or not present, so their landmark locations were estimated.
Huananius youngi	Huang & Zheng (1999), IVPP V11700	Not in GM analysis (no occlusal view in source).
Hukoutherium ambigum	Chow et al. (1977), IVPP V4233	Not in GM analysis (no occlusal view in source).
Benaius qianshuiensis	Wang & Jin (2004), IVPP V13806	Hypoconid is worn, so landmark location is estimated.
Eosigale gujingensis	Hu (1993), V7425	Multiple cusps are worn, so some cusp landmark locations are estimated.

APPENDIX I

Molar lengths and cusp heights-to-molar length ratios for the early therians of Chapter 4. Measurements and ratios are of the penultimate molar unless specified in Appendix H. Note that molar lengths of some taxa are averages of multiple specimens. Species names in bold signify species that were included in the GM analysis. Unless specified, the sources for lateral images and/or molar lengths are those given in Appendix H. Abbreviations: mm, millimeters; m, lower molar; Tr, trigonid; Ta, talonid.

Species used in analyses	(Tr+Ta) /Length	Tr/ Length	Length (mm)	Notes
Acristotherium yanensis	0.76	0.58	1.3	Trigonid height estimated using additional molars of molar row.
Eomaia scansoria	1.354	1.128	1.53	
Sinodelphys szalayi	1.004	0.844	1.41	
Atokatheridium boreni	0.672	0.594	1.3	Molar is "m?" according to source. Paraconid and metaconid are chipped, so trigonid height is estimated.
Kielantherium gobiensis	0.877	0.830	1.32	
Murtoilestes abramovi			2.08	m3 was used (instead of preferred m2); Too poorly preserved for height measurements.
Prokennalestes trofimovi	0.805	0.671	1.67	
Slaughteria eruptens	0.922	0.813	1.23	m2 used but it is unclear if this is penultimate molar.
Holoclemensia texana	1.140	0.799	1.91	
Kermackia texana	0.804	0.625	1.25	Molar is "m?" according to the source.
***Oklatheridium* sp.**	0.929	0.751	1.77	Molar is labeled "m?" by source.
Bobolestes zenge	1.045	0.770	1.5	
Kokopellia juddi	0.821	0.668	2.46	
Montanalestes keeblerorum	0.996	0.779	1.39	
Sasayamamylos kawaii	0.850	0.625	1.8	
Sinbadelphys schmidti	0.653	0.521	1.51	
Pariadens mckennai	0.853	0.636	3.31	Molar is m2 or 3 according to the source.
Sheikhdzheilia rezvyii	0.686	0.532	1.68	m1 was used (instead of preferred m2). m2 length estimated from alveolus and talonid.
Zhangolestes sp.			2.12	Too poorly preserved for cusp height measurements.
Eozhelestes mangit	0.771	0.604	2.2	m1 was used (instead of preferred m2).
Arcantiodelphys marchandi			2.2	Molar image is a composite and is "m?." Molar length estimated using composite image. No height measurements because no lateral image.
Dakotadens morrowi	0.560	0.425	2.74	Molar is "m?."
Sorlestes budan			2.6	Too poorly preserved for height measurements (and image is oblique). Molar length calculated from source image and scale bar.
Borisodon kara	0.688	0.449	2.22	
Kulbeckia kulbecke	0.599	0.421	1.9	
Bulaklestes kezbe	0.884	0.617	1.53	
Daulestes inobservabilis	0.906	0.661	1.35	
Uchkudukodon nessovi	0.814	0.658	1.14	
Sulestes karakshi	0.764	0.674	2.7	

Eoungulatum kudukensis	0.560	0.396	2.94	
Parazhelestes robustus	0.638	0.448	2.74	
Aspanlestes aptap	0.545	0.364	2.12	
Paranyctoides quadrans	0.523	0.392	1.6	Molar is "m?" according to the source. *P. quadrans* used for Asia and *P. sternbergi* used for N. America (see text).
Zhelestes temirkazyk	0.602	0.444	2.42	
Eoalphadon clemensi	0.733	0.560	1.85	
Anchistodelphys archibaldi	0.895	0.668	1.60	
Alphadon perexiqus	0.900	0.628	1.82	
Protalphadon lulli	0.671	0.555	1.44	
Varalphadon wahweapensis	0.787	0.603	2.12	Too poorly preserved for height measurements. Cusp heights-to-molar length ratios based on OMNH 66388 (Davis et al., 2016).
***Picopsis* sp.**			1.22	Molar is "m?" according to the source. Too poorly preserved for height measurements.
Kennalestes gobiensis	1.077	0.824	1.78	
Zhalmouzia bazhanovi	0.551	0.393	1.8	
Tirotherium aptum	0.506	0.381	2.7	Molar is "m?" according to source, but based on discussion by the authors this specimen is likely a penultimate molar.
Iugomortiferum thoringtoni	0.498	0.320	2.57	Molar is labeled "m?" by source.
***Potamotelses* sp.**	0.665	0.554	2.8	
Iqualadelphis lactea	0.618	0.444	1.46	
Aquiladelphis minor	0.520	0.411	1.97	m2 used for height measurements because the protoconid of m3 is worn or broken. Molar length calculated from source image and scale bar.
Paranyctoides sternbergi	0.599	0.474	1.35	Molar length calculated from source image and scale bar. *P. quadrans* used for Asia and *P. sternbergi* used for N. America (see text).
Albertatherium primus			2.14	Specimen is too poorly preserved for height measurements.
Aenigmadelphys archeri	1.040	0.717	1.55	
Deltatheridium praetrituberculare	0.768	0.109	3.07	
Eodelphis browni	0.632	0.447	3.89	
Pediomys elegans	0.643	0.446	2.26	
Turgidodon russelli	0.598	0.435	2.83	Molar is "m?" according to source.
Tsagandelta dashzevegi	0.645	0.603	2.6	Not included in time-sliced analyses because the age is too questionable (see text) and m3 not available.
Lotheridium mengi	0.729	0.655	4.4	
Ukhaatherium nessovi	0.779	0.691	1.77	Molar length calculated from source image and scale bar.
Asiatherium reshetovi	0.679	0.446	1.84	
Asioryctes nemegtensis	1.028	0.952	1.72	
Avitotherium utahensis			2.01	Molar is "m?" according to source. Specimen is too poorly preserved for height measurements.
Barunlestes butleri	0.837	0.721	1.86	
Gallolestes pachymandibularis	0.568	0.438	3.0	Molar length calculated from source image and scale bar.
Maelestes gobiensis	0.853	0.638	1.85	
Zalambdalestes lechei	0.779	0.635	2.50	
Paleomolops langstoni	0.547	0.379	2.06	*Palaeomolops* is a synonym.
Protolambda florencae	0.594	0.396	5.07	Molar length calculated from source image and scale bar.
Didelphodon vorax	0.618	0.491	6.68	
Leptalestes cooki	0.618	0.471	2.27	

Batodon tenuis	1.335	1.060	1.57	
Gypsonictops illuminatus	0.651	0.507	2.38	
Cimolestes stirtoni	0.760	0.668	4.15	
Labes garimondi	0.615	0.439	1.26	The molar is m1 or m2.
Lainodon orueetxebarriai			2.7	
Mistralestes			2.84	Specimen is too poorly preserved for height measurements.
Valentinella			4.45	Molar length based on roots. Specimen is too poorly preserved for height measurements.
Altacreodus magnus	1.062	0.927	5.09	
Ambilestes cerberoides	0.945	0.788	3.56	
Scollardius propalaeoryctes	1.146	0.971	2.60	
Schowalteria clemensi			5.0	
Glasbius intricatus	0.506	0.343	1.95	
Nanocuris improvida			4.6	Trigonid is too poorly preserved for height measurements.
Nortedelphys jasoni	0.618	0.431	2.3	*N. jasoni* treated as synonymous with *N. intermedius* and *Alphadon jasoni*.
Protungulatum gorgun	0.591	0.401	5.27	
Deccanolestes hislopi	0.704	0.540	1.47	
Leptacodon jepseni	0.754	0.501	1.14	
Kharmerungulatum vanvaleni			2.35	Molar is m1 or m2. Molar length calculated from source image and scale bar. Cusps are too worn for accurate height measurements.
?Delphodon praenuntius	0.521	0.320	4.6	
Paleoungulatum hooleyi	0.376	0.279	4.0	Due to slightly chipped or worn cusps, cusp height measurements were based partially on m1.
Roberthoffstetteria nationalgeographica	0.269	0.189	3.13	
Szalinia gracilis	0.909	0.665	1.35	
Pucadelphys andinus	0.630	0.518	1.90	Molar length is mean of ten specimens.
Alcidedorbignya inopinata	0.434	0.379	5.37	Molar length is mean of MHNC P 1211 and seven additional specimens.
Alveugena carbonensis	0.764	0.597	5.83	
Baioconodon nordicus	0.412	0.278	6.23	
Betonnia tsosia	0.720	0.606	2.4	
***Carcinodon* sp.**	0.366	0.266	5.98	
Eoconodon hutchisoni	0.454	0.335	9.6	Molar length is mean of UCMP 156117 and three additional specimens.
Onychodectes tisonensis	0.360	0.242	6.4	
Puercolestes simpsoni	0.958	0.825	3.9	
Wortmania otariidens	0.210	0.138	8.3	
***Mimatuta* sp.**	0.498	0.367	4.52	
Pucanodus gagnieri	0.549	0.333	2.64	
Cocatherium lefipanum			2.9	Cusps are too worn for accurate height measurements.
Oxyacodon agapetillus	0.669	0.448	3.08	
Conacodon entoconus	0.425	0.345	5.36	
Bryanictis microlestes	0.892	0.740	4.66	m1 used instead of m2 because it is penultimate molar in this genus. Molar length is mean of USNM 9301 and seven specimens.
Ectoconus ditrigonus	0.294	0.167	10.44	
Maiorana noctiluca	0.597	0.436	3.15	
Hemithlaeus kowalevskianus			5.42	Cusps are too worn for accurate height measurements.
Allqokirus australis	0.690	0.537	4.19	Molar is “m?” according to the source.
Alticonus gazini	0.531	0.408	4.64	
Ampliconus antoni	0.449	0.343	6.38	

Andinodelphys cochabambensis	0.647	0.500	2.61	
Andinodus boliviensis	0.234	0.199	4.94	Molar length is mean of YPFB Pal 6120 and MHNC 1241.
Bubogonia saskia	0.508	0.386	7.5	Molar length calculated from source image and scale bar.
Chacomylus sladei	0.517	0.383	2.6	
Choeroclaenus turgidunculus	0.443	0.253	4.11	
Incadelphys antiquus	0.767	0.546	1.6	Molar is labeled "m3" in source but is likely homologous to m2's of this study (the source labels lower molars starting with m2 instead of m1).
Khasia tiupampina	0.624	0.469	1.80	The molar is "m?."
Mayulestes ferox	0.892	0.699	3.36	
Mithrandir gillianus	0.602	0.403	5.52	
Molinodus suarezi	0.488	0.266	3.99	
Simoclaenus sylvaticus	0.281	0.177	4.45	
Thylacodon pusillus	0.597	0.464	2.50	
Tinuviel eurydice			4.4	Cusps are too worn for accurate height measurements.
Tiuclaenus cotasi	0.630	0.385	2.76	Molar length is the mean of MHNC 1255 and four additional specimens.
Tiulordia floresi	0.802	0.604	1.4	Molar is labeled "m3" in source but is likely homologous to m2's of this study (the source labels lower molars starting with m2 instead of m1).
Tiznatzinia vanderhoofi	0.534	0.333	3.73	
Carsioptychus hamaxitus	0.294	0.228	8.0	
Peradectes coprexeches	0.689	0.598	1.55	
Desmatoclaenus protogonoides	0.377	0.216	8.75	
Loxolophus priscus	0.331	0.209	6.77	
Oxyprimus erikseni	0.497	0.394	3.44	
Oxyclaenus cuspidatus	0.553	0.408	6.18	
Procerberus formicarum	0.878	0.670	2.94	
Prothryptacodon* sp. cf *P. furens	0.464	0.339	4.8	
Aphronorus fraudator	0.557	0.389	2.7	
Chriacus calenaneus	0.703	0.473	6.5	Molar length calculated from source image and scale bar.
Prodiacodon puercensis	0.836	0.651	3.35	
Pararyctes rutherfordi	0.875	0.656	1.85	Molar length is mean of UALVP 45095 and one additional specimen.
Palaeictops bridgeri	0.583	0.439	3.54	
Purgatorius coracis	0.690	0.553	2.0	
Litaletes mantiensis	0.444	0.330	6.20	
Auraria urbana	0.371	0.271	6.67	
Litomylus dissentaneus	0.456	0.256	3.28	
Protictis simpsoni	0.868	0.803	8.65	Molar length from Meehan & Wilson (2002) (KUVP 7800). m1 used instead of m2 because it is penultimate molar in this genus.
Haplaletes disceptatrix	0.425	0.242	2.65	Molar length is mean of USNM 9500 and five specimens.
Anisonchus sectorius	0.511	0.368	5.25	
Promioclaenus acolytus	0.463	0.323	4.04	
Haploconus angustus	0.513	0.362	4.83	NMMNH C-480 (cast of AMNH 101102) used for height measurements.
Mixodectes crassiusculus	0.683	0.426	6.7	
Periptychus carinidens	0.406	0.255	11.55	
Plesiolestes wilsoni	0.481	0.374	3.43	
Protoselene opisthacus	0.465	0.289	4.6	
Ursolestes perpetior	0.566	0.422	1.55	
Swaindelphys encinensis	0.620	0.472	2.49	Molar is m2 or m3.
Acmeodon secans	0.622	0.519	3.54	

Ankalagon saurognathus	0.594	0.446	21.7	Molar length from O'Leary et al. (2000) (AMNH 2454).
Bessoecetor septentrionalis	0.717	0.505	2.3	
Caenolambda jepseni	0.435	0.324	20.0	
Colpoclaenus procyonoides	0.321	0.261	8.87	
Conoryctella pattersoni	0.397	0.261	8.0	Molar length from Schoch & Lucas (1981) (UNM B-1258).
Conoryctes comma	0.471	0.295	10.5	
Coriphagus montanus	0.452	0.356	2.93	
Deltatherium fundaminis	0.601	0.429	7.14	
Deuterogonodon noletil	0.382	0.247	12.6	Molar length from Simpson (1937) (USNM 6160).
Gelastops parcus	0.981	0.742	3.0	USNM 9850 used for lateral measurements.
Goniacodon levisanus	0.477	0.380	7.7	Molar length from St. Clair et al. (2010) (UM 51392).
Huerfanodon polecatensis			11.1	Lateral image quality too poor for accurate height measurements.
Leptonysson basiliscus	1.077	0.824	3.4	
Mimotricentes subtrigonus	0.474	0.301	6.56	
Myrmecoboides montanensis	0.629	0.393	2.3	
Paleotomus milleri	0.911	0.696	3.86	
Pantolambda intermedius	0.365	0.238	14.8	
Pentacodon occultus	0.445	0.358	5.05	
Presbytherium rhodorugatus	0.702	0.446	8.05	
Psittacotherium multifragum	0.711	0.490	9.2	
***Triisodon* sp.**	0.628	0.412	15.6	Molar length from St. Clair et al. (2010) (AMNH 3352).
Arctocyon ferox	0.309	0.180	12.12	
***Thryptacodon* sp.**	0.279	0.179	5.53	
Simpsonictis tenuis	1.256	1.067	2.85	Molar length is mean of AMNH 35348 and AMNH 35349.
Elpidophorus minor	0.657	0.387	3.07	
Phenacodus bisonensis	0.336	0.217	9.67	Molar length is mean of PU 14634 and two specimens.
cf. ***Anasazia williamsoni***	0.497	0.387	2.8	Molar length is mean of NMMNH P-64312 and two specimens.
Ectocion collinus	0.442	0.280	7.0	
Edworthia lerbekmoi	0.470	0.398	1.5	
Elphidotarsius florencae	0.465	0.396	1.43	
Escavadodon zygus	0.859	0.667	2.78	
Eudaemonema bohachae	0.480	0.355	3.9	
Ictidopappus mustelinus	0.694	0.611	3.8	m1 used instead of m2 because it is penultimate molar in this genus.
Ignacius clarkforkensis	0.396	0.371	2.57	
Jepsenella praepropera	0.898	0.810	1.6	
Mioclaenus turgidus	0.314	0.158	6.8	
Palaechthon woodi	0.548	0.427	1.6	Molar length is mean of NMMNH P-58837 and 17 specimens.
Palenochtha minor	0.403	0.317	1.8	
Paromomys libedianus	0.321	0.258	3.11	
Picrodus calgariensis	0.537	0.426	1.7	
Torrejonia wilsoni	0.420	0.311	3.3	Molar length is mean of NMMNH P-53909 and ten specimens.
Premnoides douglassi	0.553	0.458	2.1	
Pronothodectes matthewi	0.504	0.361	2.3	
Tetraclaenodon puercensis	0.376	0.218	8.17	
Astigale nanxiongensis			3.7	No height measurements because no lateral image.
Carnilestes palaeoasiaticus	0.558	0.432	2.6	m1 used instead of m2 because it is penultimate molar in this genus.
Dysnoetodon minuta	0.530	0.409	3.12	
Prosarcodon lonanensis	1.100	0.985	2.18	m1 used instead of m2 because it is penultimate molar in this genus.
Linnania lofoensis	0.537	0.446	3.4	
Bemalambda nanhsiungensis			11.3	Molar length is mean of IVPP V4158 and nine additional specimens.

				No height measurements because no lateral image.
Palasiodon siurenensis			4.24	No height measurements because no lateral image.
Yuodon protoselenoides			5	No height measurements because no lateral image.
Escribania chubutensis			8.16	No height measurements because no lateral image.
Dissacus navajovius	0.668	0.531	13.85	
Huananius youngi	0.540	0.438	4.7	
Hukoutherium ambigum	0.602	0.383	20.4	
Benaius qianshuiensis	0.517	0.447	4.98	
Eosigale gujingensis			3.6	Cusps are too worn for accurate height measurements.